Function and expression of the human immunoreceptor NKp65 on innate lymphocytes

Dissertation

zur Erlangung des Doktorgrades

der Naturwissenschaften

Vorgelegt am Fachbereich

Biochemie, Chemie und Pharmazie

der Johann Wolfgang Goethe-Universität

in Frankfurt am Main

von

Ines Kühnel

aus Frankfurt am Main

Frankfurt am Main, 2020

(D30)

Vom Fachbereich Biochemie, Chemie und Pharmazie der Johann Wolfgang Goethe-Universität Frankfurt als Dissertation angenommen.

Dekan:

Prof. Dr. Clemens Glaubitz

1. Gutachter:

Prof. Dr. Robert Tampé

2. Gutachter:

Prof. Dr. Rolf Marschalek

Datum der Disputation:

03.02.2021

Results and parts of this work are included in a submitted manuscript:

Kühnel I*, Vogler I*, Leibelt S., Born C, Neuss S, Spreu J, Boenig H, Buerger C, Döring C, Steinle A, Selective expression of the activating receptor NKp65 demarcates human ILC3 from mature NK cells. ***In revision*** (Journal of Experimental Medicine).

**shared first authorship*

Contents

Declaration

Except where stated otherwise by reference or acknowledgment, the work presented was generated by myself under the supervision of Prof. Dr. Alexander Steinle during my doctoral studies. All contributions from colleagues are explicitly referenced in the thesis. Material obtained in the context of collaborative research is listed below:

Monoclonal anti-NKp65 antibodies OMAR1 and 12C10 were generated by Dr. Isabel Vogler, Steinle laboratory, Institute for Molecular Medicine, Goethe-University, Frankfurt.

Luciferase reporter plasmids (constructs -351, -145, -61 and -32) were cloned by Dr. Björn Bauer, Steinle laboratory, Institute for Molecular Medicine, Goethe-University, Frankfurt.

Figure 39: Cell sorting was done by Praveen Mathoor, Brüne laboratory, Institute of Biochemistry I, Faculty of Medicine, Goethe-University, Frankfurt. Preparation and staining of cells were performed by myself.
Figure 47: Data shown in this figure was generated by Dr. Björn Bauer, Steinle laboratory, Institute for Molecular Medicine, Goethe-University, Frankfurt. Assembly of the figure was done by myself.
Figure 48: Luciferase assays were performed by myself using luciferase reporter plasmids generated by Dr. Björn Bauer, Steinle laboratory, Institute for Molecular Medicine, Goethe-University, Frankfurt.
Figure 49: Data was generated by Dr. Isabel Vogler and Dr. Stefan Leibelt, Steinle laboratory, Institute for Molecular Medicine, Goethe-University, Frankfurt. Assembly of the figure was done by myself.

The following parts of the thesis have been included in a submitted manuscript:

Section	**Figure**	**Manuscript**
4.1.2, 4.2.1, 4.2.2, 4.4.3, 4.5.1	Figure 16C, Figure 17A, Figure 18, Figure 19, Figure 20A, Figure 22, Figure 23, Figure 26, Figure 39, Figure 40, Figure 42B/C, Figure 43B	Kühnel *et al.* (***in revision***)

Zusammenfassung

Eine erstmalig vor circa zehn Jahren beschriebene Gruppe angeborener lymphoider Zellen (*innate lymphoid cells*, ILC) ist wichtiger Akteur des angeborenen Immunsystems und Gegenstand aktueller Forschung (Klose and Artis, 2020; Vivier et al., 2018). ILC spielen eine essenzielle Rolle bei der Abwehr von Pathogenen und in der Aufrechterhaltung der Gewebshomöostase. Die Gruppe der ILC besteht aus den bereits intensiv erforschten zytotoxischen Natürlichen Killer (NK) Zellen sowie ILC1, ILC2 und ILC3. Aufgrund ihres Zytokinprofils und der Expression von für Differenzierung und Funktion relevanter Transkriptionsfaktoren (TF), werden ILC auch als die angeborenen Gegenspieler der T Zellen angesehen. NK Zellen entsprechen dabei den zytotoxischen CD8 T Zellen, während ILC1, ILC2 und ILC3 den $CD4^+$ T Helfer-1 (Th1), Th2 und Th17 Zellen entsprechen (Diefenbach et al., 2014; Spits et al., 2013; Sun and Lanier, 2011). Im Gegensatz zu den adaptiven T Zellen, exprimieren ILC jedoch keine antigenspezifischen Rezeptoren. Weiterhin zirkulieren sie nicht kontinuierlich im Blutkreislauf, sondern werden als Gewebe-ständige (*tissue resident*) Zellen beschrieben. Ansässig im Gewebe, können ILC schnell auf Veränderungen der Umgebung reagieren und initiieren eine Immunantwort, die häufig mit der Sezernierung großer Mengen an Zytokinen einhergeht, lange bevor die adaptive Immunität einsetzt (Artis and Spits, 2015; Colonna, 2018; Mjosberg and Spits, 2016; Vivier et al., 2018).

ILC weisen auch innerhalb ihrer Subklasse eine hohe Heterogenität auf. Die Zuweisung zu einer bestimmten Untergruppe ist daher meist nicht ausschließlich anhand eines Merkmals möglich, sondern erfolgt durch die gleichzeitige Analyse mehrerer Faktoren. Darunter zählen die Analyse des Zytokinprofils sowie die verschiedener, intrazellulär und oberflächenexprimierter Moleküle, so genannter „Marker“. Allen ILC ist gemein, dass sie keine charakteristischen Oberflächenmarker anderer hämatopoetischer Entwicklungslinien, so genannte *lineage*-Marker (lin) exprimieren. Darunter fallen die Marker von T Zellen (*cluster of differentiation* (CD) 3), B Zellen (CD19) und Monozyten (CD14) (Simoni and Newell, 2018). NK Zellen kennzeichnen sich zusätzlich typischerweise durch die Expression des TF Eomesodermin (EOMES) und der Oberflächenmarker CD56, CD94, CD16, NKp80 sowie den Natürlichen Zytotoxizitätsrezeptoren (*natural cytotoxicity receptors*, NCR) NKp30, NKp46 und NKp44 (Moretta et al., 2001; Vitale et al., 2001). NK Zellen vermitteln weiterhin Zytotoxizität und sezernieren Interferon gamma (IFN-γ) als Antwort auf die Stimulation mit den Interleukinen (IL)-12 und IL-18 (Montaldo et al., 2016). Im Gegensatz zu den NK Zellen, exprimieren alle Helfer-ILC (ILC1, ILC2 und ILC3) den IL-7 Rezeptor (IL-7R). ILC1 werden

weitestgehend durch die Expression des TF *T-box expressed in T cells* (T-bet) sowie das Fehlen spezifischer Marker der anderen Subklassen beschrieben und gelten als der nicht zytotoxische Gegenspieler der NK Zellen. Die Abgrenzung der ILC2 erfolgt hauptsächlich durch den TF GATA-3, die Expression des Prostaglandin D2 Rezeptors (*chemotractant receptor homologuos molecule expressed on Th2 cells*, CRTH2) und ihre Immunantwort auf die Stimulation mit IL-33 und IL-25 in Form von Sezernierung der Zytokine IL-5, IL-13 and IL-9. Zellen der Gruppe der *RAR-related orphan receptor gamma-t* (RORγt) exprimierenden ILC3 reagieren auf die Stimulation mit IL-1β und IL-23 mit der Sekretion von IL-17 und IL-22 (Montaldo et al., 2016). Innerhalb der Gruppe der ILC3 wird weiterhin zwischen den „Lymphoid-Tissue-inducer" (LTi) Zellen und den NCR^+ oder NCR^- ILC3 unterschieden. Die Subklasse der NCR^-/NCR^+ ILC3 zeichnet sich dabei vor allem durch die Expression des Oberflächenmarkers CD117 aus, wohingegen LTi Zellen meist durch die zusätzliche Expression des C-C-Chemokin Rezeptors 6 (CCR6) charakterisiert werden (Melo-Gonzalez and Hepworth, 2017). Obwohl ILC durch die beschriebenen Marker formal in die einzelnen Subklassen unterteilt werden können, wird ihre Klassifizierung durch die hohe Heterogenität auch innerhalb der einzelnen Untergruppen erschwert. Zusätzlich haben ILC keinen starren Phänotyp, sondern weisen sich durch die Eigenschaft der sogenannten Plastizität aus. Diese beschreibt einen Vorgang, bei dem ILC durch bestimmte Umwelteinflüsse den Phänotyp bezüglich der Zytokinproduktion und funktionelle Eigenschaften einer anderen Untergruppe annehmen (Bal et al., 2020). Trotzdem wurde in einigen Studien ein Zusammenhang zwischen unterschiedlichen Autoimmun- und chronischen Entzündungs-Krankheiten und einer Veränderung der Verteilung und Funktion der ILC Untergruppen hergestellt (Dzopalic et al., 2019). Für die weitere Forschung auf diesem Gebiet sind Marker, durch deren alleinige Analyse eine spezifische Charakterisierung der Zellen erfolgen kann, ein essenzielles Hilfsmittel. Bisher sind solche Marker jedoch kaum bekannt. Die Etablierung solcher Marker würde nicht nur zur einfacheren Detektion der ILC beitragen, sondern könnte auch die Erforschung ihrer Entstehung erleichtern.

In der vorliegenden Arbeit wird NKp65 als ein Marker für ILC3 eingeführt. NKp65 ist ein C-Typ Lektin-ähnlicher Rezeptor (CTLR), der im Natürlichen Killer Gen Komplex (*natural killer gene complex*, NKC) durch das Gen *KLRF*2 codiert wird (Spreu et al., 2010). Durch die detaillierte durchflusszytometrische Analyse der Oberflächenexpression von NKp65 mit Hilfe eines in einer vorangegangenen Studie durch Dr. Isabel Vogler (Steinle et al., 2016) generierten Antikörpers, wurde dessen spezifische Expression auf humanen ILC3 gezeigt. Im Rahmen dieser Arbeit wurde ein besonderes Augenmerk auf die Unterscheidung der Entwicklungspfade der NK Zellen und ILC3 gelegt. Dafür wurden zum einen primäre humane Zellen *ex vivo*

analysiert und zum anderen eine *in vitro*-Differenzierungsmethode etabliert, bei der durch Hilfe von speziellen Fütterzellen (*feeder*-Zellen) und dem Zusatz verschiedener Zytokine aus $CD34^+$ hämatopoetischen Stammzellen (*hematopoietic stem cells*, HSC) NKp65 exprimierende ILC generiert werden konnten. Mit Hilfe dieser Methoden, wurde zunächst die bereits in vorangegangenen Studien angedeutete physiologische Expression von NKp65 auf humanen tonsillären ILC3 bestätigt (Steinle et al., 2016). Die durchflusszytometrische Analyse der NKp65 Expression tonsillärer ILC3 mehrerer Spender zeigte dabei eine inter-individuell verschieden ausgeprägte NKp65 Oberflächenexpression. Diese ist möglicherweise auf unterschiedliche Entzündungsstadien der Tonsillen oder das Vorhandensein von Einzelnukleotid-Polymorphismen zurückzuführen, da weder Alter noch Geschlecht einen signifikanten Einfluss zeigten. Das Vorkommen NKp65 exprimierender Zellen in der humanen Haut, in der auch der Ligand von NKp65, das Keratinozyten assoziierte C-Typ Lektin (KACL) exprimiert wird (Bauer et al., 2015; Spreu et al., 2010), wurde ebenfalls bestätigt und schafft eine Basis für die Erforschung eines möglichen Zusammenhangs dieses Rezeptor-Liganden Paares mit Autoimmunerkrankungen der Haut. Besonders interessant könnte dies in Zusammenhang mit der Erforschung der Psoriasis sein, da eine Akkumulierung von NCR^+ ILC3 in der Haut von Psoriasis Patient*innen bereits beschrieben wurde (Teunissen et al., 2014; Villanova et al., 2014). Durchflusszytometrische Analysen ergaben weiterhin, dass NKp65 nicht von ILC1, ILC2 oder NK Zellen exprimiert wird. Von besonderem Interesse ist in diesem Zusammenhang außerdem, dass reife NK Zellen NKp80 – ein dem NKp65 nah verwandtes Protein, das ebenfalls im NKC codiert wird – exprimieren. Die Expression von NKp80 wird dabei in einem sechs-Stufen Modell der NK Zellentwicklung als Marker für reife NK Zellen beschrieben und ist mit der Expression von Perforin und Zytotoxizität assoziiert (Freud et al., 2016). Neben klassischen $ROR\gamma t^+$ ILC3, wird NKp65 auch von einem physiologisch vorkommenden Typ von Zellen exprimiert, der sich durch die Expression der typischen ILC3 Marker CD117 und CD127 auszeichnet, jedoch auch die NK Zellen assoziierten Marker CD94 und CD56 exprimiert. Dieser Zelltyp wird in dem von Freud et al. postulierten Modell der NK Zellentwicklung der $NKp80^-$ Stufe 4a (S4a) zugeordnet (Freud et al., 2016). Auf Grund der Expression einer Vielzahl von Markern, die mit einem ILC3 Charakter assoziiert sind, wird dessen Zuordnung in den von Freud et al. postulierten linearen Verlauf der NK Zellentwicklung in einigen Studien angezweifelt (Satoh-Takayama et al., 2010; Vonarbourg and Diefenbach, 2012; Vonarbourg et al., 2010). Als wahrscheinlicher gilt, dass die Hochregulation von NK Zell Markern eine Folge der Plastizität von ILC3 darstellt (Cella et al., 2010; Raykova et al., 2017). Die NKp65 Expression dieser Zellen, welche in der vorliegenden Arbeit als Marker für ILC3

beschrieben wird, unterstützt diese These. Des Weiteren konnte gezeigt werden, dass *in vitro* generierte NKp65^{+}CD94^{+} S4a Zellen in Abhängigkeit des Notch Signalweges in NKp80 exprimierende NK Zellen differenzieren. Die Hochregulation von NKp80 in diesem Differenzierungsprozess ist dabei von einer Herabregulation von NKp65 begleitet, die in einer jeweils exklusiven Expression der beiden Marker resultiert. Für weitere Studien der NK Zellentwicklung könnte daher die hier gezeigte jeweils exklusive Expression von NKp65 auf ILC3 und NKp80 auf NK Zellen dienen.

Um einen Einblick in die physiologische Relevanz des CTLR NKp65 zu erlangen, wurden funktionelle Analysen durchgeführt. Dabei zeigte sich, dass NKp65 – exprimiert auf *in vitro* generierten ILC – Zytotoxizität gegenüber KACL exprimierender Zielzellen vermittelt. Eine Abhängigkeit der NKp65-KACL Interaktion wurde dabei durch die Blockade mit einem spezifischen anti-KACL Antikörper gezeigt, der nachweislich die Interaktion zwischen NKp65 und KACL verhindert (Bauer et al., 2015).

Der zweite Teil dieser Arbeit behandelt die Regulation der NKp65 Expression. Diesbezüglich wurden sowohl die transkriptionelle als auch die post-transkriptionelle Regulation untersucht. Die transkriptionelle Regulation wurde dabei anhand von Luciferase-Assays analysiert. Dafür wurden Reportervektoren generiert, in denen die DNA-Sequenz der Luciferase *downstream* der endogenen Promoter Sequenz des für NKp65 codierenden Gens KLRF2 integriert ist. Nach Transfektion dieser Reportervektoren in NK-92MI Zellen, die endogen NKp65 exprimieren (Spreu et al., 2010), ermöglicht die Messung der Luciferase-Aktivität direkte Rückschlüsse auf die Promoter-Aktivität. Durch sukzessive 5‘-Verkürzung der Promoter-Sequenz konnten zwei aktivierende Bereiche identifiziert werden, denen durch computerbasierte Analysen verschiedene potenzielle Transkriptionsfaktor-Bindungsstellen (TFBs) zugeordnet werden konnten. Einige der so identifizierten TFBs, sind mit dem IL-7 Signalweg assoziiert, darunter der Transkriptionsfaktor *signal transducers and activators of transcription* 5 (STAT5), der an dem durch IL-7 induzierten Janus Kinase (JAK)/STAT Signalweg beteiligt ist (Jiang et al., 2005). Die direkte Bindung von STAT5 an die vorhergesagte TFB im KLRF2 Promoter konnte mit Hilfe von Präzipitations-Assays und eine funktionelle Relevanz durch gezielte Mutation der Bindestelle gezeigt werden. Die Mutation zweier Nukleotide innerhalb der vorhergesagten STAT5 Bindestelle führte dabei zu einer signifikanten Reduktion der KLRF2 Promoter-Aktivität. Darüber hinaus führte die Stimulation primärer NKp65^{+} ILC3 mit einem STAT5-Inhibitor zu einer Reduktion der NKp65 Oberflächenexpression sowie einer reduzierten Anzahl von Transkripten. Dies stellt eine wichtige Verbindung zwischen der ILC3-spezifischen Expression von NKp65 und der IL-7

abhängigen Entwicklung und Homöostase dieser Zellen dar (Vonarbourg and Diefenbach, 2012). Da STAT5 ein weit verbreiteter Transkriptionsfaktor ist, NKp65 jedoch zelltypspezifisch exprimiert wird, erscheint eine alleinige Regulation der NKp65 Expression durch STAT5 unwahrscheinlich. Ein weiterer aktivierender Bereich im KLRF2 Promoter zeigte zwei Bindungsstellen für so genannte Forkhead Proteine, deren Einfluss auf die Promoter-Aktivität jedoch im Rahmen dieser Arbeit nicht genauer untersucht wurde. Zukünftige Analysen eines potenziellen Einflusses von Forkhead Proteinen könnten daher weiteren Einblick in die Regulation der NKp65 Expression geben.

Zuletzt wurde die post-transkriptionelle Regulation von NKp65 untersucht. Dabei zeigte sich, dass NKp65 auf der Zelloberfläche proteolytisch gespalten wird. Dieser als „Shedding" bezeichnete Prozess konnte durch die Inkubation mit dem Metalloprotease Inhibitor Batimastat verhindert werden, was einen Rückschluss auf eine Beteiligung von Metalloproteasen an der proteolytischen Spaltung von NKp65 zulässt (Rasmussen and McCann, 1997). Zusätzlich konnte gezeigt werden, dass Shedding durch die Bindung des Liganden KACL gefördert wird. Dabei wird – nach Inkubation NKp65 exprimierender Effektoren mit $KACL^+$ Zielzellen – die Ektodomäne von NKp65 auf die KACL exprimierende Zellen übertragen. Dies weist darauf hin, dass die proteolytische Spaltung von NKp65 während des Zell-Zell Kontaktes erfolgt. Eine physiologische Relevanz dieses Prozesses wurde bereits für CD16 beschrieben. Exprimiert auf NK Zellen, wird CD16 nach der Bindung von Zielzellen ebenfalls durch Metalloproteasen gespalten. Dies erwies sich als essenziell für die Trennung von NK Zelle und Zielzelle und ermöglicht NK Zellen weitere Zielzellen in einem Prozess, der als „serial killing" bezeichnet wird, abzutöten (Srpan et al., 2018). Ob dieser Mechanismus auch für das Shedding von NKp65 eine Rolle spielt, wurde in dieser Arbeit jedoch nicht adressiert.

Insgesamt konnte in dieser Arbeit die spezifische Expression von NKp65 auf ILC3, einem seltenen Subtyp humaner angeborener Immunzellen, gezeigt werden. Die exklusive Expression von NKp65 auf diesem Zelltyp ist besonders nützlich zur Unterscheidung von ILC3 und phänotypisch ähnlichen NK Zell Vorläufern und könnte weiterführend zu einem besseren Verständnis der NK Zellentwicklung beitragen. Die Regulation der NKp65 Expression durch den Transkriptionsfaktor STAT5 stellt zudem eine interessante Verbindung zwischen der spezifischen Expression von NKp65 auf ILC3 und deren IL-7 abhängiger Entwicklung und Homöostase her. Die beobachtete durch NKp65 vermittelte Zytotoxizität gegenüber KACL exprimierender Zellen, weist darüber hinaus auf eine mögliche Relevanz dieses genetisch verknüpften Rezeptor-Liganden Paares bei der gewebespezifischen Immunüberwachung hin.

Summary

In the past decade, tissue-resident innate lymphoid cells (ILC) have become a central field of immunological research. ILC are a family of innate immune cells comprising cytotoxic Natural Killer (NK) cells and the non-cytotoxic helper like ILC1, ILC2 and ILC3. They mirror the functions and phenotypes of T cells, but do not require rearranged antigen-specific receptors for their rapid response to signals from injured or infected tissue. As potent cytokine producers being enriched in mucosal tissue, ILC play an essential role in tissue maintenance and regulating immunity to chronic inflammation and infection (Vivier et al., 2018). Although heterogeneity and plasticity of ILC complicates their classification, the pathophysiology of a broad variety of autoimmune and chronic inflammatory diseases have been associated with dysregulations in ILC subset distribution and functions (Dzopalic et al., 2019). This highlights their importance in human health and disease and accounts for the need for markers unambiguously describing the different ILC subtypes. This work introduces NKp65, a C-type lectin-like receptor (CTLR) encoded in the natural killer gene complex by the *KLRF2* gene, as an exclusive marker for human ILC3. NKp65 expression especially discerns ILC3-like NK cell precursor from mature NK cells which express the NKp65-relative NKp80. Moreover, flow cytometric analysis of NKp65 expression aids in the demarcation of natural cytotoxicity receptor (NCR) expressing ILC3, from the closely related but functionally distinct RORγt^+ LTi cells and NCR^- ILC3. This work further provides insights into NK cell development by *in vitro* differentiation studies in which NKp65 expressing cells are generated in presence of OP9 feeder cells and cytokines to support development. In such cultures, NKp65 expressing *in vitro* ILC (ivILC) acquire NKp80 expression in a Notch-dependent manner indicating their differentiation into mature NK cells. Acquisition of NK cell phenotypic markers is accompanied by NKp65 downregulation which leads to the mutually exclusive expression of NKp80 on NK cells and NKp65 on ILC3-like cells. Further insights are provided into the functional consequences of NKp65 engagement by its cognate high affinity ligand ‘keratinocyte-associated C-type lectin’ (KACL) which is selectively expressed on human keratinocytes (Bauer et al., 2015; Spreu et al., 2010). Expressed on ivILC, NKp65 mediates killing of KACL expressing target cells, suggesting that NKp65-KACL interaction promotes cellular cytotoxicity. In this context, the observed metalloproteinase dependent shedding of NKp65 might play a role in the termination of the cellular interaction. The findings on the regulation of NKp65 expression demonstrate the presence of a functional STAT5 response element in the KLRF2 promoter endowing a transcriptional control of NKp65 expression by IL-7 signaling. This provides an interesting link

between the dependency of ILC3 on IL-7 signaling for their maintenance and the specific expression of NKp65 on these cells.

In summary, this study provides new insights into the physiologic expression of the CTLR NKp65 on human ILC3. The dependency of NKp65 surface expression on sustained STAT5 signaling provided by IL-7 underlines the connection of NKp65 expression and an ILC3 phenotype which might contribute to promote future research in discerning the interspersed pathways of ILC3 and NK cell development. The tissue and cell specific expression of NKp65 on ILC3 and its ligand KACL on keratinocytes of the human skin further suggests an important role of this genetically coupled receptor-ligand pair in tissue specific immunosurveillance.

1. Introduction

1.1 Principles of the immune system

The human immune system is a highly complex defense mechanism which protects the human body against harmful environmental influences such as bacteria, fungi, viruses or parasites. Besides these external challenges, the immune system is also capable of recognizing malignantly transformed cells of the own body and of distinguishing them from healthy cells. The essential tasks for an effective protection of the individuum against diseases are immunological recognition, elimination of the infection by immune effector functions, immune regulation and generation of an immunological memory. After the first contact with an infectious agent an initial defense is provided by physical and chemical barriers, such as antimicrobial proteins secreted on mucosal surface. Pathogens that pass this barrier are exposed to a high number of different cells and non-cellular factors of the immune system mediating their recognition and elimination. The immune system can be divided into two parts, the innate and the adaptive immune system. The innate immune system is operating rapidly after exposure to an infectious organism or pathogen, while the second line of defense, the adaptive immune system, takes several hours to days to develop (Murphy et al., 2012).

1.1.1 Cells of the immune system

The cells of the immune system originate from the bone marrow, where they develop from hematopoietic stem cells (HSC). To guard the peripheral tissues, they then migrate to circulate the blood or a specialized system of vessels, organs and tissues called the lymphatic system. The multipotent HSC can give rise to all blood cells including leucocytes of the myeloid and lymphoid lineage.

Cells of the myeloid lineage comprise monocytes and the more mature macrophages, mast cells, dendritic cells as well as the group of granulocytes containing neutrophils, eosinophils and basophils. They contribute to immunity by engulfing and destroying pathogens in a process called phagocytosis, by secretion of effector proteins and by the presentation of antigens to cells of the adaptive immune system. They are therefore characterized as the bridge between innate and adaptive immunity. The lymphoid lineage includes T cells, B cells and the group of innate lymphocytes. T cells are further distinguished into cytotoxic CD8 T cells and CD4 helper T cells (Murphy et al., 2012). Likewise, the group of innate lymphoid cells (ILC) comprises cytotoxic natural killer (NK) cells and the helper-like ILC which are based on their cytokine-profile further subdivided into ILC1, ILC2 and ILC3 (Vivier et al., 2018). Whereas T and B

cells belong to the adaptive immune system, cells of the myeloid lineage and ILC are assigned to the innate immune system regarding their lack of somatically recombined antigen receptors.

1.1.2 Innate immunity

The innate immune system relies on the recognition of particular types of molecules, called pathogen-associated molecular pattern (PAMP) that are common to many pathogens but absent in the host. Additionally, cells of the innate immune system can detect endogenous ligands on stressed or malignantly transformed cells. Cells of the innate immune system recognize PAMPs by germline-encoded pattern recognition receptors (PRRs) such as toll-like receptors (TLRs), leading to innate immune responses roughly classified into events of phagocytosis and inflammation. Besides the recognition and direct elimination of pathogens, the innate immune system crucially contributes to immunity by the delivery of danger signals to the adaptive arm of the immune system via antigen presentation and cytokine secretion. Innate immune responses are typically rapid and triggered without the characteristics of adaptive immunity e.g. antigen-specificity and immunological memory (Murphy et al., 2012). However, with regard to immunological memory, there are some reports demonstrating memory responses of NK cells and ILC challenging this paradigm (Wang et al., 2019).

1.2 Innate lymphoid cells

Innate lymphocytes comprise cytotoxic NK cells and tissue-resident ILC that are subgrouped according to their cytokine and transcription factor expression profiles into ILC1, ILC2, and ILC3. ILC1 are dependent on the transcription factor T-bet and secrete IFN-γ upon stimulation with IL-12 and IL-18. ILC2 produce IL-4, IL-5, and IL-13 when exposed to IL-25 and IL-33 and are marked by the expression of GATA-3, whereas RORγt expressing ILC3 produce IL-17 and/or IL-22 when activated with IL-1β and IL-23 (Artis and Spits, 2015; Colonna, 2018; Vivier et al., 2018). The functional specialization and developmental programs of the different ILC subsets resemble those recognized in $CD4^+$ T helper cell subsets. Therefore, ILC1, ILC2 and ILC3 are considered the innate counterparts of Th1, Th2 and Th17 cells, whereas NK cells are resembling $CD8^+$ cytotoxic T cells (Diefenbach et al., 2014; Sun and Lanier, 2011). Except for NK cells, all ILC are tissue resident cells which enables them to quickly respond to tissue stress and inflammation and underlines their critical role in regulating tissue homeostasis or repair during injury and infection. The past decade has provided plenty of data regarding the characterization of ILC subsets via surface markers or transcription factor

profiles. The most commonly used markers to discern the different subsets of human ILC are summarized in Table 1.

Table 1: Main phenotypic markers characterizing the different human ILC subsets.
W, weak expression; nd, not determined; +/-, expression is detected in some, but not all cells; a, expressed only on activated NK cells. The table was adapted from (Vivier et al., 2018) and (Killig et al., 2014).

	NK	ILC1	ILC2	LTi	NCR$^-$ILC3	NCR$^+$ILC3
CD127 (IL-7Rα)	-/+	+/-	+	+	+	+
CD161 (NK1.1)	+/-	+	+	+/-	+	+
ST2 (IL-33R)	+/-	-	+/-	nd	nd	-
IL-17Rβ (IL-25R)	-	-	+	-	nd	-
CD294 (CRTH2)	-	-	+	-	-	-
CD117 (c-kit)	-/w	-	+/-	+	+	+
CD69	w	+/-	nd	nd	nd	nd
CD196 (CCR6)	-	+/-	+/-	+	+/-	+/-
CD335 (NKp46)	+	-	-	-	-/w	w/+
CD336 (NKp44)	a	-	-	-/w	-	+
IL23R	+/-	+/-	-/w	+	+	+
IL1R	+/-	+	w	+	+	+
CD314 (NKG2D)	+	nd	nd	-	-/w	-/w
KIR	+/-	-	-	-	-	-
CD94	+/-	-	-	-	-	-
Perforin	+	-	-	-	-	-
CD56	+	-	-	-/w	+/-	+/-
CD16	+/-	-	-	-	-	-
NKp80	+	-	nd	nd	-	-
T-bet	+	+	-	-	-	-
EOMES	+	+/-	-	-	-	-
RORγt	-	-/w	-/w	+	+	+
GATA3	-/w	-/w	+	-/w	-/w	-/w
AhR	-/w	w	+	+	+	+

1.2.1 NK cells

NK cells are generally defined as CD3$^-$CD56$^+$ cytotoxic innate lymphocytes that can detect and eliminate virus infected and malignantly transformed cells (Vivier et al., 2008; Waldhauer and Steinle, 2008). In contrast to T and B cells, NK cells distinguish stressed cells from normal cells via an array of germline-encoded recognition receptors. Besides their capacity to kill a broad variety of target cells, NK cells also shape immune responses by secretion of cytokines and chemokines engaged by the interaction with DCs, T cells, macrophages or endothelial cells (Vivier et al., 2008). The two major subsets of NK cells can be categorized based on the expression of CD56 and CD16 into CD56^{dim}CD16$^+$ and CD56^{bright}CD16$^-$ cells. The vast majority of NK cells circulating the peripheral blood (PB) are CD56^{dim}CD16$^+$ and respond to

contacts with ligand expressing target cells by cytotoxicity and the secretion of cytokines and chemokines (Fauriat et al., 2010). Their expression of the Fc receptor CD16 further allows for antibody-dependent cellular cytotoxicity (ADCC). In contrast, $CD56^{bright}CD16^{-}$ NK cells are mainly located in tissues and preferentially respond to soluble factors, such as IL-12 and IL-18 by chemokine and cytokine production (Cooper et al., 2001).

NK cell effector functions are tightly regulated by an interplay of activating and inhibitory receptors that recognize different ligands and allow NK cells to discriminate target cells from healthy 'self' cells. Thereby, not only one single NK cell receptor dictates whether NK cells are activated to kill target cells. Instead, synergistic signals from different NK cell receptors are integrated (Long et al., 2013; Vivier et al., 2004).

Inhibitory NK cell receptors are characterized by carrying immunoreceptor tyrosine-based inhibition motifs (ITIM) in their cytosolic tail (Burshtyn et al., 1996). Most of the inhibitory NK cell receptors are specific for major histocompatibility class (MHC) I molecules and are members of the killer immunoglobulin-like receptor (KIR) or Ly49 family in humans and mice, respectively (Parham, 2005). Therefore, NK cells can sense the downregulation of MHC class I expression which is a classical escape mechanism of virus infected or malignantly transformed cells to evade the recognition by the cells of the adaptive immune system (Garcia-Lora et al., 2003). This 'missing self' recognition initially described by Kärre et al. is accompanied by a loss of inhibitory signals which in concert with activating signals can lead to NK cell activation (Ljunggren and Karre, 1985; Waldhauer and Steinle, 2008) (Figure 1). Inhibitory receptors for self MHC class I molecules are not only delivering 'missing self' signals but are also involved in a process called NK cell 'licensing' or 'education'. Accordingly, only NK cells that express receptors for self MHC class I molecules are functional whereas the remaining are either deleted or anergic (Anfossi et al., 2006; Kim et al., 2005). The 'missing self' theory failed to explain that NK cells kill certain MHC class I-sufficient tumor cells and spare MHC class I-deficient autologous cells (e.g. human erythrocytes). These phenomena can be explained by the observation that malignantly transformed or virus infected cells are recognized by NK cells via activating receptors by a mechanism called 'induced self' (Bauer et al., 1999; Diefenbach and Raulet, 2001) (Figure 1). The major receptors responsible for NK cell triggering are the natural cytotoxicity receptors (NCR) NKp46, NKp30 and NKp44 and the C-type lectin-like receptor (CTLR) NKG2D. The ligands for activating receptors are upregulated or *de novo* expressed on stressed healthy cells, or on malignant cells upon tumor transformation or viral infection (Bottino et al., 2005).

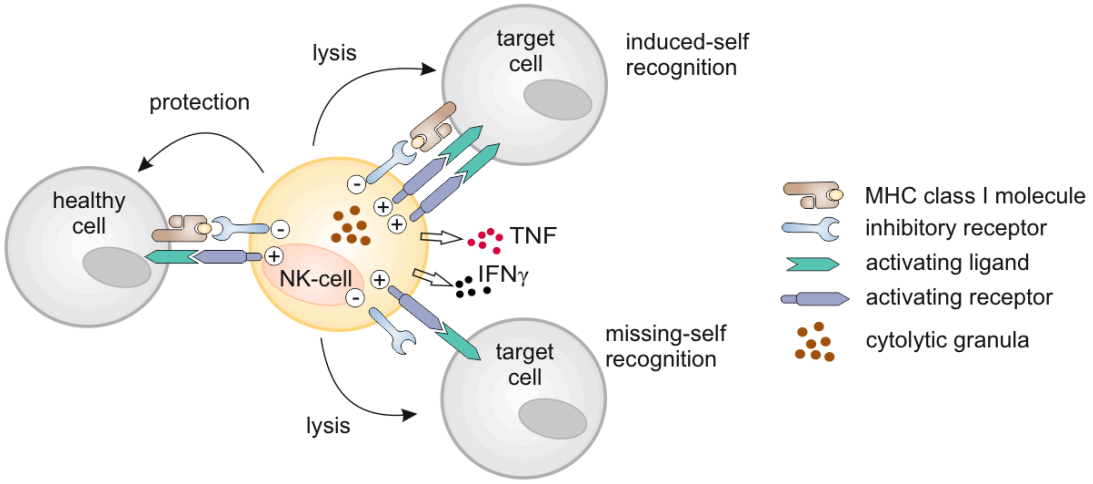

Figure 1: The activation of NK cells is determined by the balance of inhibitory and activating signals. Healthy cells are protected from natural killer (NK) cell killing by the expression of MHC class I molecules that stimulate inhibitory NK cell receptors. As a result of virus infection or malignant transformation cells can lose expression of MHC class I molecules which results in a loss of inhibitory signals and consequently activation of NK cells and target cell lysis (missing-self recognition). Infection or transformation can also lead to an upregulation of activating ligands which stimulate activating NK cell receptors and outbalance constitutive inhibitory signals. Adapted from (Raulet and Vance, 2006).

Altogether, the activation of NK cells depends on a tightly regulated balance between inhibitory and activating signals. Interactions of NK cells and healthy cells expressing NK cell inhibiting MHC class I molecules and no or few activating ligands results in NK cell quiescence. In contrast, malignant cells with reduced MHC class I levels and increased expression of activating NK ligands stimulate NK cell responses (Lanier, 2005) (Figure 1).

NK cell cytotoxicity is mediated via two distinct pathways, the release of cytotoxic granules containing perforin and granzymes, or the induction of death receptor-mediated apoptosis. The latter mechanism is unleashed by the expression of the death receptor ligands TNF-related apoptosis-inducing ligand (TRAIL) and/or Fas ligand (FasL) by NK cells which engage their respective receptors TRAIL-R1/R2 or CD95/Fas on the surface of diseased cells (Prager and Watzl, 2019). In resting NK cells, perforin and granzymes are stored in cytoplasmic secretory lysosomes that are released via exocytosis upon NK cell activation in a highly regulated and ordered process (Mace et al., 2014). This multi-step process is initiated by the contact between effector and target cell, leading to the formation of an immunological synapse (IS) (Davis et al., 1999). Signals originating from the receptor-ligand interactions within the IS lead to reorganization of the actin cytoskeleton finally resulting in fusion of the lytic granules with the plasma membrane and the release of perforin and granzymes into the IS. With the help of perforin, granzymes are delivered into the target cell in which they initiate apoptosis by cleaving, among others, caspase-3 (Andrade et al., 1998; Law et al., 2010; Mace et al., 2014). Whereas granzyme/perforin mediated killing is a rapid process, the death receptor mediated

cytotoxicity occurs much slower (Li et al., 2014). Death receptor activation induces the formation of the so-called death-inducing signaling complex, composing the activated receptor, adapter proteins and initiator procaspases-8-10 (Medema et al., 1997). Activation of caspase-8 (casp-8) and -10 results in a caspase cascade which ultimately leads to apoptosis (Peter and Krammer, 2003).

1.2.2 ILC1

ILC1 are IFN-γ producing cells that depend on the transcription factor T-bet, but not EOMES. The definition of ILC1 is complicated due to the lack of lineage defining markers and the reported plasticity amongst ILC1 and ILC2 or ILC3 (Vivier et al., 2018). Additionally, ILC1 share most of their functions and phenotypic markers with NK cells and particularly in humans, cells with a mixed NK cell and ILC1 phenotype have been observed (Spits et al., 2016). Initially, ILC1 were distinguished from NK cells by the absence of cytotoxicity, but recently cytotoxic activity has also been reported for ILC1, although to a lesser extent than in NK cells. Additionally, neither CD127 (IL-7Rα) nor EOMES are markers unambiguously defining ILC1 or NK cells. CD127 is usually expressed on all helper-like ILC but not expressed by mature NK cells. However, a $CD127^{low/-}CD103^{+}$ intraepithelial ILC1 subset has been described as has been CD127 expression on some human and mouse NK cells (Fathman et al., 2011; Freud et al., 2016). Although EOMES is expressed by most of human and mouse NK cells, a highly cytotoxic subset of $CD3^{-}CD56^{low}CD16^{+}$ NK cells show very low or no expression of EOMES. Additionally, ILC1 which are conventionally $EOMES^{-}$, can upregulate EOMES in certain tissues. Therefore, also the presence or absence of EOMES does not strictly distinguish NK cells from ILC1. Emerging data, showing that ILC1 and NK cells from different tissues have overlapping but different characteristics, further complicates their distinction (Spits et al., 2016). However, ILC1 differentiation is dependent on T-bet but not EOMES and therefore clearly distinct from NK cell development (Klose et al., 2014).

The first indication of ILC1 in mice was the description of a thymic NK cell like subset expressing CD127 and GATA3 (Vosshenrich et al., 2006), which is now considered ILC1 (Vivier et al., 2018). Besides thymic ILC1, three other ILC1 subsets have been described in mice all expressing NKp46 and NK1.1 and comprising $CD160^{+}$ intraepithelial ILC1 (Fuchs et al., 2013), hepatic ILC1 (Takeda et al., 2005) and $CD127^{-}$ salivary gland ILC1 (Cortez et al., 2014). Human ILC1 have been described in mucosal associated tissues such as tonsils and gut (Bernink et al., 2013; Fuchs et al., 2013), in the endometrium and decidua (Vacca et al., 2015), in the liver (Marquardt et al., 2015) and in the skin (Villanova et al., 2014). ILC1 described in

these tissues demonstrate a high heterogeneity ranging from cytotoxic ILC1 subsets with pronounced NK cell character to cytokine producing ILC1 with classical ILC features. The most extensively and best characterized T-bet$^+$ ILC1 population are intraepithelial ILC1 which are IL-7Rα^- and express CD103, CD56, CD94 and NKp44 as well as perforin and EOMES (Fuchs et al., 2013). Human CD103$^+$ intraepithelial ILC1 are the counterpart of mouse CD160$^+$ILC1 which were shown to develop independently from conventional splenic NK cells in IL-15R$\alpha^{-/-}$ mice. Therefore, although sharing many phenotypic markers with NK cells, intraepithelial ILC are considered a unique ILC1 subset different from NK cells (Fuchs et al., 2013). Another well characterized subset of ILC1 was found to be enriched in inflamed human tonsils and intestine and is marked by the expression of CD127 and T-bet. Conversely, other than intraepithelial ILC1, they strongly differ from NK cells by the lack of CD56, CD94, EOMES and perforin expression (Bernink et al., 2013).

All ILC subsets can adapt to the surrounding microenvironment by changing their phenotypes and functional profiles. This plasticity has also been observed for ILC1 which can derive from ILC3 after stimulation with proinflammatory cytokines. These so called exILC3 have been described in mice and in humans and derive from ILC3 by downregulation of RORγt accompanied by upregulation of T-bet which leads to the capacity of IFN-γ production (Bernink et al., 2013; Vonarbourg et al., 2010).

The prototypic function of ILC1 is the secretion of the proinflammatory cytokine IFN-γ which plays an important role in host defense against intracellular pathogens. Intestinal ILC1 contribute to protective responses against *Clostridium difficile* (Abt et al., 2015) and *Toxoplasma gondii* (Klose et al., 2014) infection (Figure 2, left). Although important during antimicrobial immune responses, exaggerated or prolonged cytokine production by ILC1 can also induce chronic inflammation and autoimmunity. The inflamed intestinal tissue of patients suffering from Crohn's disease harbors large numbers of ILC1, suggesting their contribution to inflammatory pathology (Bernink et al., 2013; Fuchs et al., 2013) (Figure 2, right). Additionally, ILC1 derived IFN-γ drives systemic inflammation in different mouse models of induced colitis (Bernink et al., 2013; Fuchs et al., 2013; Uhlig et al., 2006).

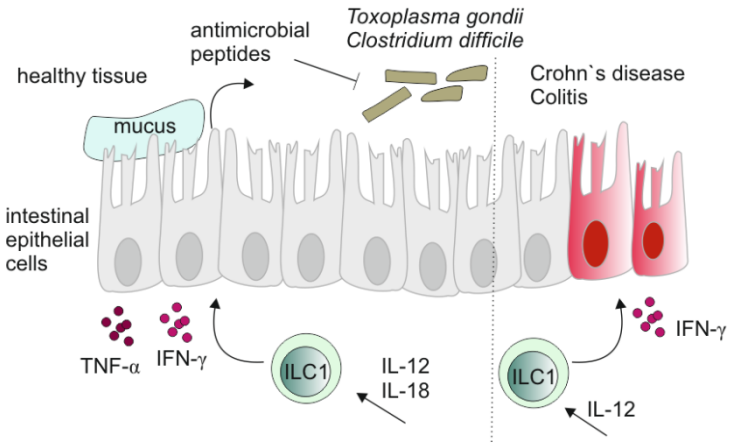

Figure 2: ILC1 in maintenance of intestinal homeostasis and chronic inflammation.
In healthy mucosa (left) ILC1 contribute to tissue homeostasis and immunity against intracellular pathogens such as *Toxoplasma gondii* or *Clostridium difficile*. Upon infection, IL-12 and IL-18 produced by dendritic cells and macrophages stimulates IFN-γ and TNF-α production by ILC1. These cytokines induce the secretion of antimicrobial peptides, stimulate mucus production by goblet cells and lead to activation of phagocytes. Altogether these processes induced by the stimulation of ILC1 promote tissue integrity and defense against pathogens. During chronic intestinal inflammation upon inflammatory bowel diseases such as Crohn's disease or colitis (right), alterations in the microflora and excessive levels of cytokines like IL-12 and IL-18 lead to an accumulation and activation of ILC1 stimulating massive production of IFN-γ. Excessive levels of IFN-γ consequently lead to chronic inflammation and tissue damage. Adapted from (Hazenberg and Spits, 2014).

1.2.3 ILC2

ILC2 express the signature transcription factor GATA3 and produce the type-2 cytokines IL-5, IL-9 and IL-13 in response to IL-25, IL-33 and thymic stromal lymphopoietin (TSLP). They are important regulators of anti-helminthic immunity and lung tissue homeostasis and contribute to the pathogenesis of allergic inflammation (Walker and McKenzie, 2013). ILC2 were first described as IL-25 responsive, lin^- cells in the spleen and lung of $Rag2^{-/-}$ mice (Fort et al., 2001; Hurst et al., 2002). More recently, ILC2 have been characterized extensively and are now phenotypically demarcated by the expression of ICOS, Sca1, CD127, CD25, ST2 (IL-33 receptor) and CRTH2 (Walker and McKenzie, 2013). In humans ILC2 are enriched in adipose tissue (Brestoff et al., 2015; Moro et al., 2010) and at barrier surfaces such as skin (Teunissen et al., 2014), lung (Mjosberg et al., 2011; Wojno et al., 2015) and intestine, but have also been described in PB (Mjosberg et al., 2011) and the liver (Jeffery et al., 2017).

Also, ILC2 adapt their phenotype in response to their microenvironment. As shown for ILC3, IL-12 drives functional plasticity of ILC2 which is manifested in the upregulation of T-bet expression and gain of the capacity to produce IFN-γ. These phenotypic alterations were shown *in vitro* but also in *ex vivo* ILC2 from intestinal samples of Crohn's disease patients (Lim et al., 2016).

As a source of the type 2 cytokines IL-5, IL-9 and IL-13 ILC2 play a pivotal role in the expulsion of helminth parasites as e.g. shown for *Nippostronylus brasiliensis* (Turner et al., 2013) or *Trichuris muris* (Wilhelm et al., 2016) in mice (Figure 3, left). Additionally, ILC2 can contribute to wound healing and tissue remodeling after influenza virus infection (Monticelli et al., 2011). These protective functions are mainly mediated by the production of the epidermal growth factor family member amphiregulin (AREG) (Zaiss et al., 2006). Although being essential for the repulsion of helminth and contributing to wound healing and tissue remodeling, a detrimental role for ILC2 has been suggested in the context of atopic diseases including atopic dermatitis, allergic rhinitis and allergic asthma. Increased numbers of ILC2 were detected in the bronchoalveolar lavage (Liu et al., 2015), the nasal polyps (Mjosberg et al., 2011) and skin lesions (Kim et al., 2013; Salimi et al., 2013) of patients suffering from allergic asthma, rhinosinusitis and atopic dermatitis, respectively. The exaggerated production of type 2 cytokines promotes eosinophil homeostasis and infiltration, secretion of IgE by B cells and causes hyperplasia of goblet cells which leads to increased inflammation and overproduction of mucus (Mindt et al., 2018) (Figure 3, right).

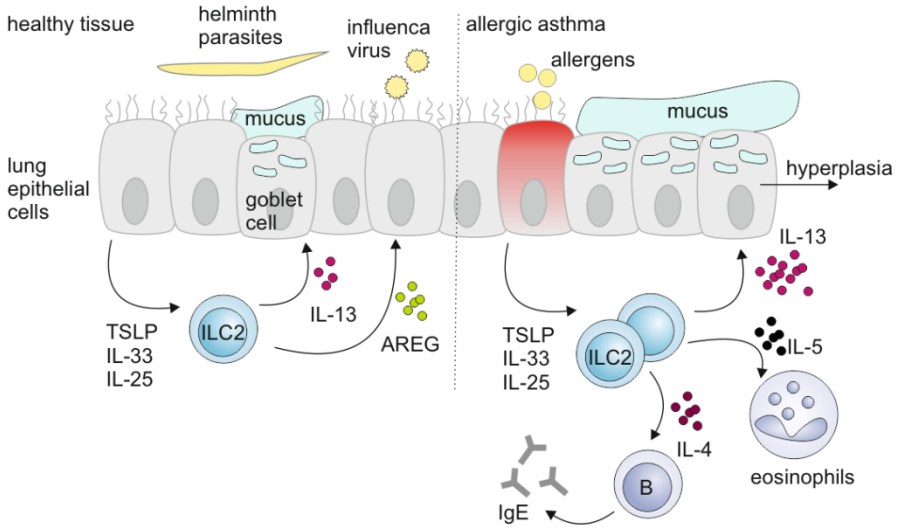

Figure 3: ILC2 responses against extracellular pathogens and their role in allergic asthma.
ILC2 play a crucial role in the protection against large extracellular parasites and allergens. During infection by parasites or viruses (left), lung epithelial cells produce TSLP, IL-33 and IL-25. These alarmin cytokines stimulate Th2 cytokine (IL-5, IL-9 and IL-13) and amphiregulin (AREG) secretion by ILC2. Th2 cytokines promote mucus production by goblet cells and the activation of other immune cells to eliminate parasites, whereas the epidermal growth factor ligand AREG causes epithelial remodeling during viral infection. Exaggerated production of Th2 cytokines during allergic asthma (right) causes eosinophil infiltration, IgE secretion by B cells as well as hyperplasia of goblet cells which results in inflammation of the lung epithelium and overproduction of mucus. Adapted from (Hazenberg and Spits, 2014) and (Mindt et al., 2018).

1.2.4 ILC3

Group 3 ILC express RORγt and respond to IL-1β and IL-23 by producing the signature cytokines IL-17 and/or IL-22. The group of RORγt expressing ILC is heterogenous and includes fetal lymphoid tissue-inducer (LTi) cells and postnatally developing ILC3, both defined as $CD127^+CD117^+$ cells. The latter are further dissected into NCR^+ and NCR^- ILC3, based on the expression of the NCR NKp44 in humans and NKp46 in mice. Whereas LTi cells were shown to be essential for the prenatal development of lymph nodes (LN) and Peyer's patches (PP), postnatally developing ILC3 are involved in the defense against extracellular pathogens, regulation of inflammatory processes and epithelial tissue homeostasis (Killig et al., 2014). ILC3 mainly reside in the human tonsil and the lamina propria (LP) of the intestine (Cella et al., 2009), but were also found in the spleen (Magri et al., 2014), the endometrium and decidua (Vacca et al., 2015), skin (Teunissen et al., 2014; Villanova et al., 2014), and lung (Kim et al., 2014).

$ROR\gamma t^+$ IL-22 producing ILC3 were initially termed NK-22 and first described as $lin^-CD56^+NKp44^+$ cells in human tonsils and Peyer's patches (Cella et al., 2009). More recent studies on tonsillar ILC3 revealed that they are homogenously $CD117^+CD127^+$ but differ in expression of NKp44 and CD56. Although the vast majority of tonsillar ILC3 was identified as $lin^-CD56^+NKp44^+$, RORC transcripts, the gene encoding for RORγt, were also detected in $CD56^-NKp44^+$ and $CD56^+NKp44^-$ cells, underlining their classification as ILC3. The different subsets of ILC3 differ in their capacity of cytokine production. While in humans IL-22 expression is strictly confined to $NKp44^+$ILC3, in mice IL-22 is preferentially expressed by $NKp46^-$ILC3 (Sawa et al., 2011). In contrast to $CD56^-NKp44^-$ILC3 derived from fetal LN and gut lamina propria of patients with Crohn's disease which produce IL-17, tonsillar ILC3 are devoid of IL-17 expression (Geremia et al., 2011; Hoorweg et al., 2012). The cytokine expression profile of ILC3 is also shaped by their microenvironment. In mice, the transition of IL-22 producing ILC3 into IFN-γ producing cells was observed in the intestine upon inflammatory conditions. Acquiring the capacity to produce IFN-γ is accompanied by phenotypic change into ILC1, e.g. downregulation of RORγt and upregulation of T-bet (Klose et al., 2013; Vonarbourg et al., 2010). The plasticity of ILC3 to ILC1 has also been observed in the human intestine in patients with Crohn's disease. While under homeostatic conditions the frequency of ILC1 in the human intestine is low (Simoni et al., 2017), in inflamed areas of patients with Crohn's disease numbers of ILC1 are markedly increased at the expense of ILC3 (Bernink et al., 2015; Bernink et al., 2013; Li et al., 2017). This suggests a conversion of ILC3 into ILC1 in an inflammatory microenvironment. Consistent with this notion, *in vitro*

stimulation of ILC3 with proinflammatory cytokines such as IL-2, IL-12 and IL-15 also leads to plasticity towards IFN-γ producing cells (Cella et al., 2010; Raykova et al., 2017). Besides the conversion into ILC1, ILC3 were also found to acquire a NK cell like phenotype upon stimulation with type 1 cytokines *in vitro*. In this regard IL-12 and IL-15 stimulation of NKp44$^+$ILC3 from human tonsils was shown to promote differentiation of EOMES$^+$CD94$^+$ cells and to induce cytolytic activity (Raykova et al., 2017).

During embryogenesis and the fetal period, LTi cells facilitate the formation of lymphoid organs such as lymph nodes and Peyer's patches (Buettner and Lochner, 2016). The organogenesis is promoted by factors including IL-7, SCF and TSLP which induce LTα1β2 expression by LTi cells enabling their interaction with mesenchymal cells. This decisive interaction leads to the secretion of different chemokines which attract adaptive lymphocytes and further facilitates the formation of the lymphoid organs (van de Pavert and Mebius, 2010). The postnatally developed ILC3 mainly reside at mucosal sites where they are involved in innate immune responses to extracellular bacteria, the containment of intestinal commensals and the renewal of epithelial cells. In the gut, ILC3-derived IL-22 stimulates IL-10, antimicrobial peptide and mucus production by epithelial cells as well as their proliferation (Cella et al., 2009). Additionally, presentation of microbial antigens to gut CD4$^+$ T cells by MHC class II expressing NCR$^-$ILC3 was shown to suppress the microbiota-specific proinflammatory T cell responses (Figure 4, left). IL-22 production by ILC3 was further shown to protect intestinal stem cells from damage caused by irradiation, genotoxic stress, or chemotherapy and to restore tissue injury during DSS induced colitis. In the inflamed tissue of patients suffering from Crohn's disease the proportion of NKp44$^+$ ILC3 is strongly decreased. This is most likely caused by their transdifferentiation into IFN-γ producing ILC1 (or ex ILC3) which is promoted by IL-12 produced by CD14$^+$ DCs. The presence of proinflammatory cytokines within these tissues therefore causes a phenotypic shift from protective IL-22 producing ILC3 to inflammatory IFN-γ producing ILC1 thereby perpetuating the disease (Figure 4, middle) (Klose and Artis, 2020). Whereas NKp44$^+$ILC3 have a protective role in the intestine, the accumulation of NCR$^+$ILC3 in lesional and nonlesional skin and PB of psoriasis patients suggests an implication of these cells in disease pathogenesis (Teunissen et al., 2014) (Figure 4, right). This is supported by studies in mice unraveling a causal link between ILC3 activation and skin pathology (Keren et al., 2018; Pantelyushin et al., 2012).

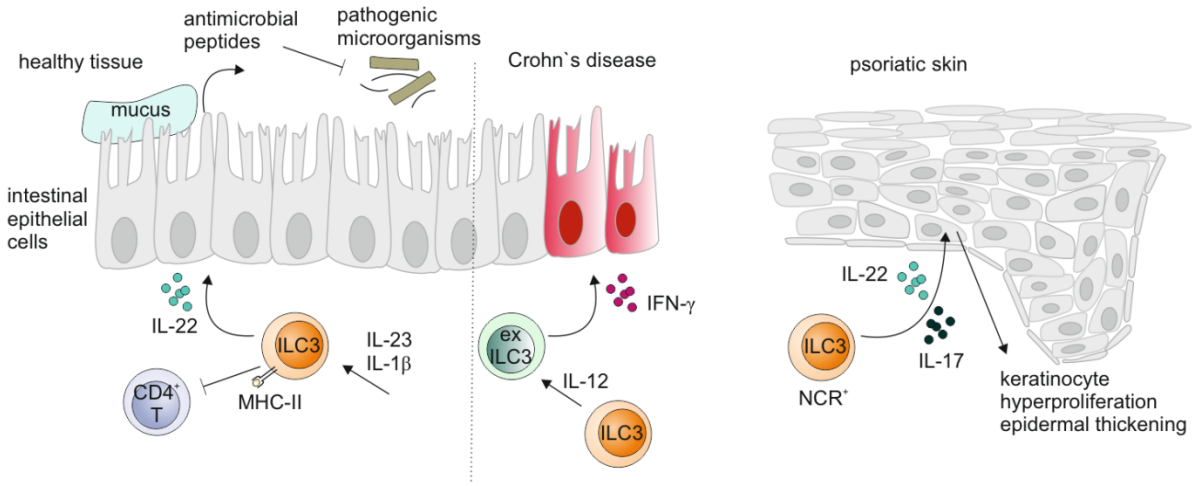

Figure 4: ILC3 in maintenance of tissue homeostasis and occurrence in disease.
ILC3 reside at mucosal sites such as the intestine where they contribute to the innate immune response against extracellular bacteria and the maintenance of barrier integrity by stimulating the renewal of epithelial cells (left). Encountering pathogen leads to the production of IL-1β and IL-23 by macrophages which stimulates IL-22 secretion by ILC3. ILC3-derived IL-22 leads to the production of IL-10, antimicrobial peptides and mucus by epithelial cells as well as their proliferation. Additionally, the presentation of microbial peptides to $CD4^+$ T cells by ILC3 suppresses microbiota-specific proinflammatory T cell responses. During chronic intestinal inflammation, elevated levels of IL-12 cause a phenotypic shift of the protective IL-22 producing ILC3 into IFN-γ producing exILC3 which promote severe inflammation and tissue damage (middle). In psoriatic skin (right), accumulation of natural cytotoxicity receptor (NCR) expressing ILC3 contribute to disease progression by secretion of elevated levels of IL-22 and IL-17 which causes keratinocyte hyperproliferation and epidermal thickening. Adapted from (Hazenberg and Spits, 2014).

1.2.5 ILCs and the lack of precise markers

Markers solely delineating a certain cell type are useful tools as they allow for a precise detection and might also facilitate a therapeutic enrichment or depletion of rare cells. However, in the field of ILC research such markers are still missing and cells are mainly defined by a combination of several markers that are also shared with other cell types (Vivier et al., 2018). In general, ILC are characterized by the lack of rearranged antigen receptors, their lymphoid morphology and the lack of major surface markers of other immune cell types (designated as lineage markers) such as CD3, CD14, CD19, and CD34. Due to their expression of CD127, the IL-7Rα chain, helper like ILC (ILC1, ILC2 and ILC3) were initially defined as lin^-CD127^+ cells (Spits et al., 2013). However, CD127 is also expressed on immature B cells (Clark et al., 2014), T cells and certain subsets of NK cells (Kang and Coles, 2012). Since certain stimuli can cause the downregulation or internalization of lineage markers as for example shown for CD3 expression on activated T cells (Valitutti et al., 1995), the definition of ILCs as lin^-CD127^+ cells is not always sufficient (Trabanelli et al., 2018). Additionally, the recent discovery of several subsets of helper like ILC that are $CD127^{dim}$ or $CD127^-$ controverts this definition (Dadi et al., 2016; Fuchs et al., 2013; Mora-Velandia et al., 2017). Not only distinguishing ILC from cells

of other lineages is complicated, but also the demarcation of the different ILC subsets. Whereas ILC2 can be distinguished by the expression of CRTH2, ILC1 are so far mostly defined by the lack of the markers CRTH2, CD117 and CD56 (Vivier et al., 2018). Especially complicated is the demarcation of NK cell precursor and ILC3, since most of the markers used to define ILC3 such as CD161, CD117, CD127 or NKp44 are also expressed by at least some subsets of NK cell precursor (Freud et al., 2016; Trabanelli et al., 2018). Moreover, the close relation of ILC3 and LTi cells complicates their distinction. In mice, LTi cells selectively express the C-C chemokine receptor type 6 (CCR6) and are additionally marked by the expression of CD4 and lack of the NCR NKp46 (Killig et al., 2014). In humans, CCR6 is expressed on almost all ILC3 and therefore not considered a selective marker for LTi cells (Roan et al., 2016). Additionally, human LTi cells lack CD4 expression and heterogeneously express the NCR NKp44 (Killig et al., 2014; Shikhagaie et al., 2017). In a more recent work, Neuropilin 1 (NRP1) has been introduced as a marker for LTi cells which despite its expression on plasmacytoid DC, naïve T cells and a subset of $CD4^+$ T follicular helper cells, might contribute to the distinction of LTi cells from postnatal ILC3 (Shikhagaie et al., 2017).

1.2.6 Development of innate lymphoid cells

ILC development is a highly complicated and orchestrated process which is regulated by a plethora of transcription factors, cytokines and environmental signals (Serafini et al., 2015). All ILC derive from the multipotent common lymphoid progenitor (CLP), which can also give rise to the lymphocytes of the adaptive immune system. In an initial simplified model of murine ILC development it was assumed that ILC development proceeds from the CLP and traverses the α-lymphoid progenitor (α-LP) and the early innate lymphoid progenitor (EILP) stages in a process which is critically dependent on the transcription factors nuclear factor IL-3 regulated protein (NFIL3), T cell factor 1 (Tcf-1) and the inhibitor of DNA binding 2 (Id2). The development of helper-like ILC1, ILC2 and ILC3 was thought to diverge from NK cell development at the EILP stage which can give rise to the $Id2^+$ ILC committed common helper innate lymphoid cell precursor (CHILP) and the $Id2^-$ NK cell restricted NK progenitor (NKP) (Klose and Diefenbach, 2014). However, two recently published studies using polychromic transcription factor reporter mice and single-cell gene expression analysis, revised the current model of ILC development (Walker et al., 2019; Xu et al., 2019). Both groups could show that also the $Id2^+$ CHILP can give rise to NK cells and rebutted its helper-like ILC commitment. Also, other transcription factors associated with helper-like ILC commitment such as PLZF (Constantinides et al., 2014; Diefenbach et al., 2014) were shown to be compatible with NK

cell development. The earliest branch point was suggested for ILC3 and especially CCR6$^+$ LTi-like cells which emerged from Id2$^+$PLZF$^-$ ILC progenitor (ILCP) by upregulation of RORγt, whereas upregulation of PLZF was accompanied by a decline of ILC3 potential. However, although to a lesser extent also the Id2$^+$PLZF$^+$ILCPs could give rise to RORγt$^+$ILC3. Strict lineage commitment was only observed for ILC2 development that clearly delineates from ILC1/ILC3 and NK cell development by upregulation of Bcl11b. Altogether, these data support a model in which EILPs give rise to Id2$^+$ ILCPs which represent a pool of related but heterogenous helper-like ILC and NK cell precursors. Rigid delineation of lineages so far was only shown for ILC2 and occurs much later in development than previously thought (Walker et al., 2019; Xu et al., 2019) (Figure 5).

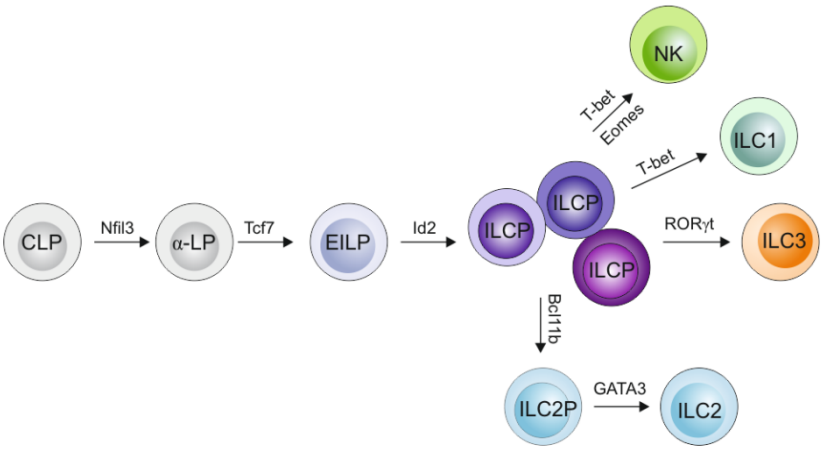

Figure 5: Development of murine innate lymphoid cells.
Murine ILC develop from the CLP traversing the α-LP and the EILP which gives rise to a pool of ILCP. ILCP in turn can develop into the ILC2 restricted ILC2 precursor (ILC2P) by upregulation of Bcl11b or to NK cells, ILC1 or ILC3 by upregulation of Eomes, T-bet or RORγt, respectively. Developmental transitions are indicated by solid black arrows. Abbreviations: α-LP, α-lymphoid progenitor; Bcl11b, B cell lymphoma/leukemia 11B; CLP, common lymphoid progenitor; EILP early innate lymphoid progenitor; Eomes, Eomesodermin; GATA3, GATA binding protein 3; Id2, inhibitor of DNA binding 2; ILC, innate lymphoid cells; ILCP, ILC progenitors; NFIL3, Nuclear factor IL-3 regulated protein; RORγt, Retinoic acid receptor-related orphan receptor gamma t; T-bet, T-box transcription factor TBX21; Tcf-1, T cell factor 1. Adapted from (Guia and Narni-Mancinelli, 2020) and (Walker et al., 2019).

Whereas for studies in mice fate mapping or knock out of certain genes facilitates the elucidation of developmental trajectory, studying human ILC development is much more complicated. However, also human ILC development starts from the CLP and traverses several stages with increasing lineage commitment (Figure 6). The human CLP is mostly defined as CD34$^+$ and by the lack of lineage markers expressed on mature blood cells such as CD2, CD3, CD14, CD19, CD56, CD66b and CD235 (Juelke and Romagnani, 2016). Analyses of human ILC development are mainly based on *in vitro* studies using total CD34$^+$ progenitors isolated from umbilical cord blood (CB), thymus, BM, PB or tonsils. In secondary lymphoid tissues

such as tonsils and lymph nodes, NK cell and helper ILC development traverses the early tonsil progenitor (ETP) stages 1 ($CD34^+CD10^+CD117^-$) and 2 ($CD34^+CD10^+CD117^+$) which differ in their expression of CD117. Although both, ETP1 and ETP2, are multipotent precursors which can also give rise to T cells and DCs, ETP2s were shown to have greater ILC-differentiation potential (Freud et al., 2006). The earliest committed common innate lymphoid progenitor (CILP) discovered so far is phenotypically described as $CD34^+CD117^+$IL-$1R1^+$ (Scoville et al., 2019). CILPs in turn give rise to the functionally similar $CD34^-CD117^+$ pan-ILC precursors (ILCPs). After the ILCP stage ILC2 development branches from a common NK cell and ILC3 developmental pathway (Figure 6). This has also been reported for mouse ILC development in which restricted ILC2 precursor diverge from a mixed population of ILC1, ILC3 and NK cell precursor by expression of Bcl11b (Figure 5) (Walker et al., 2019; Xu et al., 2019). In humans, a $CD56^+CD34^-CD117^+$ restricted ILC precursor (rILCP) that can generate NK cells and ILC3 but not ILC2 has been described (Chen et al., 2018). Therefore, in mice as well as in humans NK cells and ILC3 share a common developmental pathway different from ILC2. Of note, due to the rarity of ILC1 in healthy human tissue, analysis of their developmental trajectory is complicated. However, based on analyses in mice, it is assumed that they also derive from the rILCP (Guia and Narni-Mancinelli, 2020). The ILC3/NK cell prone rILCPs are marked by the expression of CD56. On human ILC3 CD56 is bimodally expressed and therefore not necessarily required for their development, suggesting that ILC3 can also directly arise from $CD56^-$ILCPs (Figure 6). In contrast, CD56 is expressed by the majority of NK cells and was shown to play an important role in the formation of a developmental synapse between stromal cells and immature NK cells during NK cell maturation (Mace et al., 2016). However, $CD56^+$ILCPs can develop into $CD117^+$ILC3 or $CD117^+$NK cells which can transdifferentiate but also can give rise to fully mature ILC3 or NK cells, respectively (Chen et al., 2018). Whereas the trajectory of final ILC3 maturation is largely unknown, the stages of final NK cell maturation have been studied intensively and are highlighted in the next section.

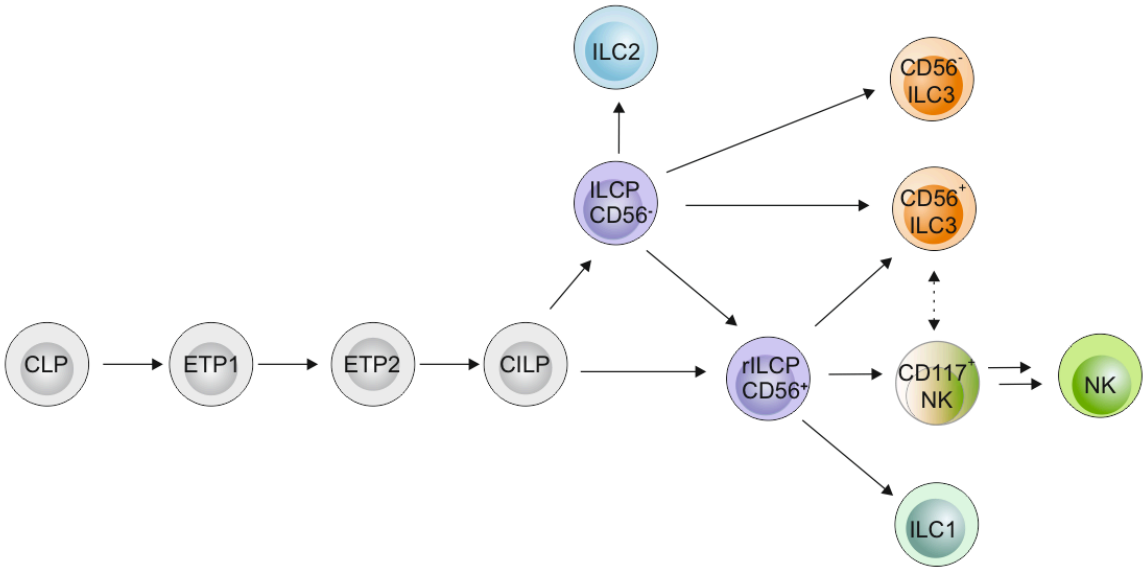

Figure 6: Development of human innate lymphoid cells.
Schematic depiction of the development of human ILC1, ILC2, ILC3 and NK cells in secondary lymphoid tissues from the CLP via diverse developmental intermediates. Black arrows symbolize developmental transitions between the indicated populations, the dashed arrow represents transdifferentiation between CD117^{+} NK cells and CD117^{+} ILC3. Abbreviations: CLP, common lymphoid progenitor; ETP, early tonsil progenitor: CILP, common innate lymphoid progenitor; ILCP, innate lymphoid cell progenitor; ILC, innate lymphoid cells. Adapted from (Guia and Narni-Mancinelli, 2020).

1.2.6.1 NK cell maturation

The bone marrow was considered the main side of human NK cell development until NK cell developmental intermediates were found to be enriched in secondary lymphoid tissues (SLTs) such as spleen, tonsils and LNs (Freud and Caligiuri, 2006). Intense analyses of these developmental intermediates led to a model proposed by Caligiuri and colleagues in which NK cell development traverses six developmental stages with increasing lineage restriction (Figure 7) (Chen et al., 2018; Freud et al., 2016). The early stages parallel those described for ILC development. However, with regard to NK cell development, ETP1s are defined as stage1 NK cells, whereas ETP2s and CILPs represent the stages 2a and 2b. The following stages 3a (ILCP) and 3b (rILCP) are marked by downregulation of CD34, phenotypically overlap with ILC3 and differ in their expression of CD56. From the NK cell/ILC3 restricted stage 3b, NK cell development proceeds into the stage 4a by upregulation of CD94 expression. Cells in stage 4a still show ILC3-associated features such as expression of RORγt, AHR, CD117 and CD127 as well as production of IL-22. The expression of NKp80 on stage 4b cells, strongly correlates with the acquisition of NK cell features such as cytotoxic potential, capability of IFN-γ production and EOMES expression. NKp80 therefore demarcates NK cell precursors with ILC3 features from bona fide NK cells. Cells in stage 4b which represent the CD56^{bright} NK cell subset give rise to stage 5 cells, marked by downregulation of CD94 and acquisition of CD16 and KIR

expression. Stage 5 NK cells parallel the CD56^{dim} NK cell subsets and can terminally mature into stage 6 cells which are characterized by CD57 expression (Chen et al., 2018; Freud et al., 2016).

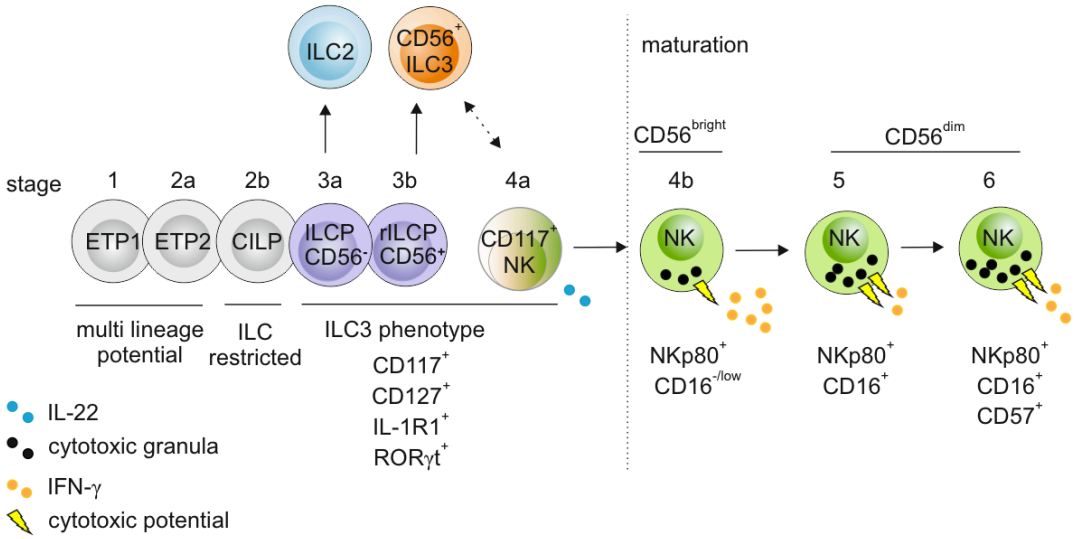

Figure 7: Six stages of human NK cell development in secondary lymphoid tissues (SLTs).
NK cell developmental trajectory from ETP1 to the most mature stage 6 NK cells. Early stages of NK cell development which can also give rise to ILC1, ILC2 and ILC3 (left), differ from the final stages of NK cell maturation (right) by the expression of NKp80. Abbreviations: ETP, early tonsil progenitor; CILP, common innate lymphocyte progenitor; ILCP, innate lymphoid cell progenitor; ILC, innate lymphoid cell. Adapted from (Freud et al., 2016) and (Chen et al., 2018).

1.3 Interleukin-7 and its role in ILC development

As described in the previous section, the development and maintenance of innate lymphoid cells is orchestrated by an interplay of various transcription factors, cytokines and other environmental cues. The cytokine milieu which is determined by the availability of soluble and cell-associated factors within the circulation or certain tissues, severely shapes ILC biology. Produced by the stromal cells of the bone marrow, different cytokines influence the early development of all ILC from the CLP. Cytokines that share the common γ-chain (γc) in their receptor complexes such as IL-2, IL-4, IL-7, IL-9, IL-15 and IL-21 facilitate the development of all ILC subsets (Xu and Di Santo, 2013). Supporting this notion, mice lacking γc are severely deficient in all ILC subsets as are humans that suffer from severe combined immunodeficiency disease (SCID) due to mutation of *IL2RG* or the gene encoding Janus family tyrosine kinase (JAK) 3, the downstream signaling kinase of γc dependent cytokines (Vely et al., 2016). Mouse models with a deficiency in genes encoding for a specific cytokine or cytokine receptor chain revealed that ILC2 and ILC3 development and maintenance mainly relies on IL-7, whereas NK

cells and ILC1 depend on IL-15 (Huntington, 2014; Vonarbourg and Diefenbach, 2012). In humans, a mutation with loss of function in *IL7R*, the gene coding for IL-7Rα, causes SCID which is manifested by the absence of T cells and RORγt^{+} ILC3, whereas B cells and NK cells develop normally (Lai et al., 1997; Puel et al., 1998; Vonarbourg et al., 2010).

The impact of IL-7 on ILC development was first reported for LTi cells which are defective in IL-7$^{-/-}$ and IL-7Rα$^{-/-}$ mice resulting in impaired genesis and architecture of secondary lymphoid organs (Vonarbourg and Diefenbach, 2012). Moreover, numbers of ILC2 and ILC3 are significantly reduced in mice deficient for IL-7 or IL-7Rα, whereas numbers of NK cells and ILC1 remained unaffected. Due to the compensatory role of thymic stromal lymphopoietin (TSLP), which also signals via the IL-7Rα, defects are greatest in IL-7Rα$^{-/-}$ mice. However, IL-7Rα is not strictly required for the development of ILC, as shown by the persistence of residual ILC in the small intestinal lamina propria (siLP) of IL-7Rα$^{-/-}$ mice. This persistence is attributed to the compensatory effects of IL-15, since mice defective for both, IL-7Rα and IL-15, lack residual ILC. Whereas IL-7Rα$^{-/-}$ mice have normal numbers of NK cells, deletion of IL-15 leads to greatly reduced numbers of NK cells which are even more reduced in mice with a combined knock out of IL-7Rα and IL-15. The supportive role of IL-7 for NK cell development is tissue dependent and most pronounced at sites that harbor IL-7Rα expressing NK cells. ILC1 were shown to be synergistically controlled by IL-7 and IL-15, since a critical reduction in ILC1 numbers was only observed in IL-7Rα$^{-/-}$IL-15$^{-/-}$ mice. IL-7 is not only important for the development and maintenance of ILC but also impacts their effector functions. Especially IL-22 production by RORγt^{+} ILC3 depends on IL-7 signaling as IL-7 counteracts the transition of RORγt^{+} IL-22 producing ILC3 into RORγt^{-} IFN-γ producing cells upon IL-12 and IL-15 stimulation by stabilizing RORγt expression (Vonarbourg et al., 2010). Additionally, in concert with retinoic acid (RA), IL-7 enhances the expression of α4β7 and selectin ligands in ILC3 thereby supporting their homing to gut associated tissue (Ruiter et al., 2015).

1.3.1 *In vivo* sources of IL-7

Although since its first description in 1988 a number of studies aimed to identify the cellular sources of IL-7, especially in humans a precise identification is still complicated due to its scarce expression and the lack of appropriate reagents (Kim et al., 2011). In mice, the establishment of different IL-7 reporter mice allowed for the identification of thymic stroma cells as the main source of IL-7 expression but also demonstrated IL-7 expression in lymph nodes (LN) and non-lymphoid sides such as the intestine, lung, liver and skin. Within these

tissues it is believed that IL-7 is constantly expressed by stromal and epithelial cells mainly being unaffected by extrinsic stimuli (Mazzucchelli and Durum, 2007). However, some reports have also demonstrated that IL-7 expression can be induced upon certain inflammatory stimuli (Roye et al., 1998; Sawa et al., 2009; Shalapour et al., 2010; Takashima et al., 1995; Tang et al., 1997). In humans, IL-7 expression has been reported in tonsillar germinal centers, keratinocytes, intestinal epithelial cells, follicular dendritic cells, vascular cells, peripheral DCs and platelets (Kim et al., 2011).

Interestingly, although IL-7 is considered a secreted and constitutively expressed cytokine, serum levels in healthy human individuals are rather low, ranging from 2 to 8 pg/ml (Lundstrom et al., 2012). Therefore, IL-7 is considered to be consumed locally. The main regulators of IL-7 abundance *in vivo* are IL-7Rα expressing hematopoietic cells, although IL-7 production is restricted to radioresistant non-hematopoietic cells. These observations led to a widely accepted consumption model in which IL-7 is constitutively produced by stromal and epithelial cells and homeostatic levels are controlled by the amount that is scavenged by IL-7Rα expressing cells. Although clearly outnumbered by T cells, among the IL-7Rα expressing cells ILC3 were shown to be the main consumer of IL-7 which is mainly due to a less pronounced downregulation of IL-7Rα upon IL-7 stimulation in ILC3 (Martin et al., 2017).

1.3.2 IL-7 signaling

The IL-7 receptor is a heterodimer composed of the IL-7Rα chain and the common γ-chain (γc). While IL-7Rα is associated with the JAK 1 (Rodig et al., 1998), the γc is associated with JAK3 (Suzuki et al., 2000). Binding of IL-7 to the IL-7Rα chain leads to recruitment of the γc, causing proximity of their intracellular domains bearing the respective JAKs. This induces transphosphorylation of JAK3 and JAK1, which potentiates their intrinsic kinase activity and subsequently leads to receptor phosphorylation (Figure 8). The phosphorylation of tyrosine 449 (Y449) of the IL-7Rα chain creates a docking site for signal transducers and activators of transcription 5 (STAT5) molecules, which bind to the phosphorylated receptor via their Src homology domain 2 (SH2) (Jiang et al., 2005). Receptor-bound STAT5 molecules are then phosphorylated by the associated JAKs, leading to their dimerization and translocation to the nucleus where they bind to the DNA and modulate the expression of certain genes.

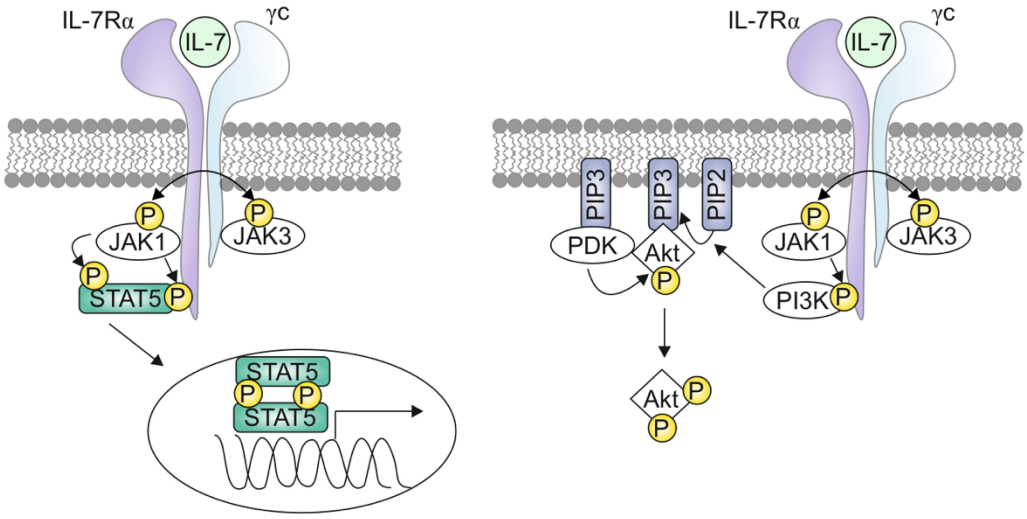

Figure 8: IL-7 receptor signaling pathways.
Upon binding of IL-7 the components of the IL-7 receptor, the IL-7 receptor α-chain (IL-7Rα) and the common γ-chain (γc) assemble which leads to transphosphorylation of the receptor-associated Janus family tyrosine kinases (JAK) 1 and JAK3. The resultant activation of JAK1 and JAK3 leads to phosphorylation of IL-7Rα thereby creating a docking site for STAT5 molecules (left) or phosphatidylinositol-3 kinase (PI3K) (right). Subsequent phosphorylation of STAT5 leads to disassembly from the receptor, dimerization and translocation to the nucleus where STAT5 can bind to the DNA and regulate the expression of several genes. In the PI3K pathway (right), binding of PI3K to the phosphorylated receptor leads to an allosteric activation, allowing for production of phosphatidylinositol-3, 4, 5-triphosphate (PIP3) by phosphorylation of phosphatidylinositol-4, 5-biphosphate (PIP2). PIP3 recruits the protein kinase B (Akt) and phosphoinositide-dependent protein kinase 1 (PDK1) to the plasma membrane. The resulting proximity of the kinases enables the phosphorylation of Akt which can now translocate to the cytosol or the nucleus and phosphorylate cellular proteins resulting in the regulation of diverse biological processes. Adapted from (Palmer et al., 2008).

Besides the JAK/STAT5 pathway, IL-7 can also signal via the phosphatidylinositol-3 kinase (PI3K) pathway (Figure 8). PI3K is a lipid kinase, characterized by its ability to phosphorylate inositol phospholipids. Like STAT5, PI3K also binds to the phosphorylated Y449 residue of the IL-7Rα chain which leads to allosteric activation of its catalytic subunit (Hunter, 2000). Recruitment of PI3K to the membrane results in the production of phosphatidylinositol-3, 4, 5-triphosphate (PIP3) by phosphorylation of phosphatidylinositol-4, 5-biphosphate (PIP2). Bound to the inner lipid bilayer of the plasma membrane, PIP3 promotes the accumulation of protein kinases harboring Pleckstrin Homology (PH)-domains such as protein kinase B (Akt) and phosphoinositide-dependent protein kinase 1 (PDK1) at the cell membrane (Cantley, 2002). This results in close vicinity of PDK1 to Akt, allowing for PDK1-dependent phosphorylation of Akt at T308. Additional phosphorylation of Akt at S473 further increases its activity by stabilizing its activated conformational state (Yang et al., 2002). Following activation at the plasma membrane, Akt can translocate to the nucleus or the cytosol where it phosphorylates cellular proteins thereby regulating cell metabolism, survival and apoptosis, differentiation as well as proliferation (Brazil et al., 2004).

1.4 Promoter and *cis*-regulatory elements

The regulation of gene expression at transcriptional level is a key control point for many cellular processes and mainly directed by promoters that encompass specific binding sites for proteins promoting the initiation and regulation of transcription, the so called *cis*-elements. The promoter is defined as the DNA region upstream of the transcription start site (TSS) with the key function to bind and correctly position the transcription initiation complex consisting of the RNA-polymerase and several transcription factors. This is achieved by the integrated action of several *cis*-regulatory elements that are distributed over the different promoter-compartments including the distal, the proximal and the core promoter (Figure 9).

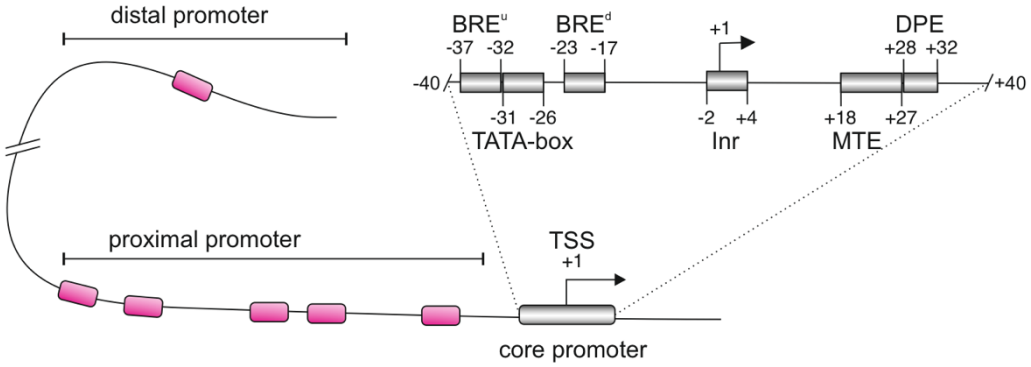

Figure 9: Schematic representation of an eukaryotic promoter with major core promoter elements.
The promoter of a certain gene contains several binding sites for regulatory proteins, the *cis*-regulatory elements (pink boxes). These are distributed along the different promoter components, the distal, the proximal and the core promoter. The distal promoter can be located up to many kilobases (kb) upstream of the transcriptional start site (TSS), whereas proximal promoter elements usually extend to less than 1kb. The core promoter is located +/- 40 base pairs (bp) around the TSS and can include different core promoter elements, such as the TATA-box, the downstream or upstream TFIIB recognition elements (BRE^d, BRE^u), the initiator (Inr), the Inr dependent motif ten element (MTE) or the downstream core element (DCE) (depicted as grey boxes). Adapted from (Maston et al., 2006) and (Lenhard et al., 2012).

The core promoter classically spans the region from -40 to +40 base pairs (bps) around the TSS (+1) and contains essential *cis*-regulatory elements that serve as docking sites for the basal transcription machinery (Dikstein, 2011). The first described and best characterized core promoter element is the TATA-box (Lifton et al., 1978). Although once thought to be a universal element, the TATA-box is only present in up to 35% of human genes (Dikstein, 2011). The TATA-box can cooperate with one or more other binding elements such as downstream or upstream TFIIB recognition elements (BRE^d, BRE^u), the downstream core element (DCE) or the initiator (Inr). Whereas BRE$^{d/u}$ as well as DCE are dependent on the presence of the TATA-box, the Inr is also functional in promoters that lack the TATA-box. These so-called TATA-less promoters show enrichment of functional Inr and the Inr dependent motif ten element

(MTE) and downstream promoter element (DPE). An important aspect of core promoter elements is their synergistic nature, which is in some cases critically dependent on a strict spacing (Burke and Kadonaga, 1997; Lim et al., 2004).

Proximal and distal promoter elements can be located a couple of hundred or even up to many kilo base pairs upstream of the TSS. They contain *cis*-regulatory elements such as enhancers, silencers and insulators (Lee and Young, 2000). These DNA sequences allow for the binding of specific transcription factors (TF) to the DNA, that can induce changes in the chromatin structure, directly recruit the RNA polymerase or accessory factors that promote or inhibit specific phases of transcription (Blackwood and Kadonaga, 1998; Lee and Young, 2000; Malik and Roeder, 2000).

1.5 Diversity of NK cell receptors

Functional responses of NK cells are regulated by a broad variety of germline-encoded activating and inhibitory NK cell receptors (NKRs). Most NKRs belong to either the immunoglobulin (Ig)-family which is encoded in the leukocyte receptor complex (LRC; human chromosome 19) or the C-type lectin-like superfamily (CLSF) which is genetically clustered in the natural killer gene complex (NKC; human chromosome 12) (Kelley et al., 2005; Yokoyama and Plougastel, 2003). The most prominent members of the Ig-family are the NCRs NKp46, NKp44 and NKp30, the group of KIRs and the family of signaling lymphocytic activation molecules (SLAM) (Lanier, 1998; Waldhauer and Steinle, 2008; Yokoyama and Plougastel, 2003). The CLSF includes C-type lectin-like receptors such as NKG2D, CD94/NKG2x, the murine Ly49 receptors and the members of the NKRP1 family including the prototypic mouse NKRP1 receptor Nkrp1c (NK1.1) and the human homologues LLT1, NKp80 and NKp65. Both, the Ig-family and the CLSF family comprise inhibitory and activating receptors as well as receptors that bind to MHC-I or MHC-I-like glycoproteins and receptors that bind to certain viral-, bacterial-, parasite-derived, or cellular ligands (Kruse et al., 2014; Vogler and Steinle, 2011).

1.5.1 The natural killer gene complex (NKC)

The importance of the NKC is highlighted by its conservation among diverse species and the fact that most of the proteins encoded in this genomic region are involved in NK cell recognition, activation and inhibition and NK cell mediated host defense (Yokoyama and Plougastel, 2003). As mentioned earlier the NKC encodes for proteins of the CLSF. Based on

their overall domain organization proteins of the CLSF are classified into 14 groups, all characterized by the possession of at least one C-type lectin-like domain (CTLD). Although the most common CTLD function is Ca^{2+} dependent carbohydrate binding, many CTLDs have lost this function and evolved to specifically interact with certain proteins (Drickamer and Fadden, 2002). These Ca^{2+} independent CTLDs are assigned to group V of the CLSF, the C-type lectin-like receptors (CTLR) (Drickamer and Fadden, 2002; Yokoyama and Plougastel, 2003; Zelensky and Gready, 2005). Among the CTLRs encoded in the NKC only a small number is not expressed on NK cells, such as the members of the Dectin-1 superfamily including C-type lectin-domain family member 1 (CLEC1), CLEC2, LOX-1 and Dectin-1. Whereas LOX-1 is mainly expressed by vascular-rich tissues, CLEC1, CLEC2 and Dectin-1 are expressed by endothelial cells and hematopoietic subpopulations (of mainly the myeloid lineage) including DCs, macrophages and neutrophils (Yokoyama and Plougastel, 2003). These CTLRs are classified as CLEC proteins whereas the CTLRs expressed by NK cells are designated as killer cell lectin-like receptors (KLRs).

1.5.2 NKC encoded KLRs and their ligands

Based on their respective ligands, the KLRs can be divided into two groups either recognizing MHC class I or MHC class I-like molecules or structurally related CTLRs belonging to the CLEC2 subfamily (Figure 10).

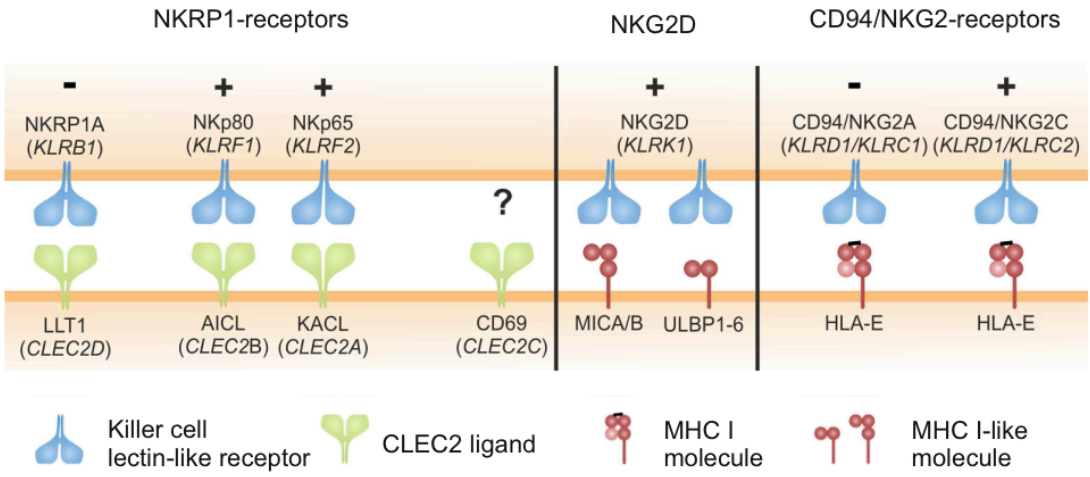

Figure 10: Human killer cell lectin-like receptors and their ligands.
NK cell receptors encoded in the human natural killer gene complex and their respective ligands. The receptors of the NKRP1-family NKRP1A, NKp80 and NKp65 engage their genetically linked C-type lectin-like ligands of the CLEC2-superfamily LLT1, AICL and KACL, respectively (left). The activating receptor NKG2D binds to different MHC class I like molecules of the MIC and ULBP family (middle), whereas the family of CD94/NKG2x-receptors bind classical MHC class I complexes composed of the heavy chain, the β2-microglobulin and a peptide (right). Genes are depicted in *italics*, + indicate activating and – inhibiting functions of the respective receptor-ligand interaction. Adapted from (Bartel et al., 2013).

The most prominent member of the KLRs recognizing MHC class-I like molecules is NKG2D (KLRK1), an activating receptor that binds the MHC class I chain-related proteins A and B (MICA/B) (Bauer et al., 1999) and the members of the family of UL16 binding proteins (ULBP) which are both upregulated upon cellular stress (Raulet et al., 2013; Steinle et al., 2001; Waldhauer and Steinle, 2008). Examples for MHC class-I binding NKRs are the heterodimeric CD94/NKG2x and the murine Ly49 receptors (Orr and Lanier, 2011; Yokoyama and Plougastel, 2003).

The second class of KLRs which are binding to CLEC proteins are clustered in a different region of the NKC and contains the members of the NKRP1 subfamily (Figure 10). One outstanding characteristic of this receptor family is that the genes encoding for their structurally related CLEC2 ligands are genetically interspersed amongst the NKRP1 genes (Carlyle et al., 2008; Vogler and Steinle, 2011) (Figure 11). The first member of the NKRP1 receptor family to be discovered was the mouse activating receptor Nkrp1c (NK1.1) which is widely used as a marker to identify NK cells in C57BL/6 mice (Glimcher et al., 1977). Whereas the ligand for Nkrp1c still remains elusive, it is established that other members of the murine NKRP1 family (Nkrp1d, Nkrp1g and NKrp1f) bind to the C-type lectin-related (Clr) molecules (Clr-b, -c, -d, -f, -g) (Carlyle et al., 2008). The family of human NKRP1 receptors comprises the inhibitory NKRP1A (CD161) and the activating receptors NKp80 and NKp65, encoded by the *KLRB1*, *KLRF1* and *KLRF2* locus, respectively. As for the mouse NKRP1 receptors, they also bind to genetically linked CLEC2 molecules, with NKRP1A ligating the lectin-like transcript 1 (LLT1; encoded by the *CLEC2D* locus), NKp65 binding the keratinocyte associated C-type lectin (KACL; *CLEC2A*) and NKp80 the activation-induced C-type lectin (AICL; *CLEC2B*) (Vogler and Steinle, 2011) (Figure 11).

Figure 11: The NKC region encoding for genetically linked C-type lectin-like receptor/ligand pairs.
The telomeric region of the human natural killer gene complex (NKC) on chromosome 12 is depicted as a black line with the genes (*italics*) encoding NKRP1A, LLT1, NKp80, AICL, NKp65 and KACL shown true to scale. Arrows indicate transcriptional orientation and dashed lines highlight receptor/ligand pairs. Adapted from (Bartel et al., 2013).

Whereas NKRP1A is described as the human homolog of the mouse inhibitory Nkrp1 receptors (Lanier et al., 1994), no murine homologues of NKp80 and NKp65 have been

reported. The only member of the CLEC2 ligand family that is conserved between humans and rodents is CD69 (*CLEC2C*). To date, the receptor for CD69 has not been identified, but it is well-known that CD69 is rapidly upregulated upon lymphocyte stimulation (Sancho et al., 2005).

1.5.2.1 The receptor ligand pair NKp80 and AICL

The CTLR NKp80 was first described as an activating receptor expressed on virtually all NK cells and a minor subset of $CD56^+$ T cells (Vitale et al., 2001). Later on, NKp80 expression was also detected on certain γδ T cells (Welte et al., 2006) and the $NKp80^+$ T cells were further characterized as memory effector T cells (Kuttruff et al., 2009). Recently Caligiuri and colleagues defined NKp80 as a marker for NK cell maturation in human secondary lymphoid tissue. They could show that in NK cell development, NKp80 expression strongly correlates with acquisition of NK effector functions. Being first expressed on stage 4b cells, a maturation state corresponding to the $CD56^{bright}$ cells in human peripheral blood, NKp80 clearly demarcates mature IFN-γ producing NK cells, from immature IL-22 producing ILC3-like stages (Freud et al., 2016). Expressed on T cells, NKp80 also marks a highly reactive subset of $CD8^+$ memory effector T cells with an inflammatory NK-like phenotype (Welte et al., 2006).

The genetically linked ligand for NKp80 is AICL. In the NKC, receptor (*KLRF1*) and ligand (*CLEC2B*) are encoded in a head to tail orientation in close proximity to each other. AICL is expressed on myeloid cells such as macrophages, granulocytes and activated monocytes (Welte et al., 2006). Interestingly, AICL surface expression is also inducible on NK cells. In resting NK cells, AICL is stored intracellularly and colocalized with the Golgi complex. Intracellular retention of AICL was shown to be dependent on the glycosylation status of its one atypical and three conventional N-glycosylation sites (Neuss et al., 2018). Stimulation of NK cells with IL-12 and IL-18 leads to AICL surface trafficking which is accompanied by downregulation of NKp80 and their conversion into memory-like cells (Cooper et al., 2009; Welte et al., 2006). This renders monokine activated NK cells susceptible to NKp80-mediated cytolysis by autologous NK cells and highlights the role of NKp80-AICL interaction in the autonomous regulation of NK cell responses (Figure 12). The crosstalk between NKp80 expressing NK cells and AICL expressing myeloid cells not only leads to cytolysis of the myeloid cells but also activates cytokine production in both, the NK cells and the myeloid cells. Therefore, the NKp80-AICL interaction also contributes to the control of immunoregulatory processes at sites of inflammation (Welte et al., 2006).

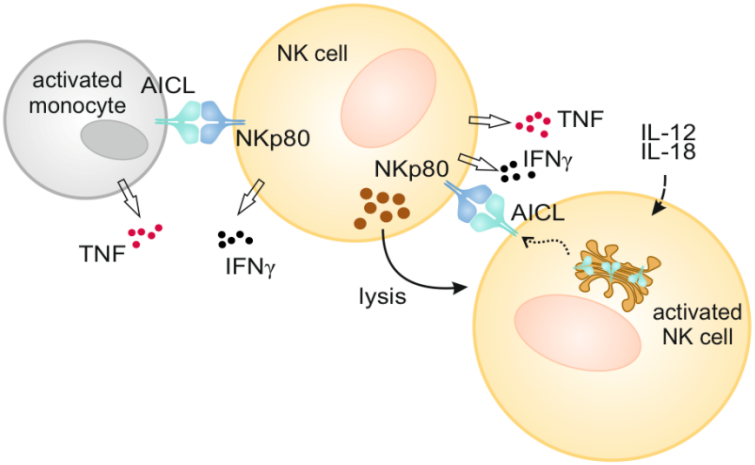

Figure 12: Functional consequences of NK cell activation by NKp80-AICL interaction.
The crosstalk of activated monocytes and NK cells by NKp80-AICL interaction leads to cell activation resulting in TNF and INF-γ production (left). Monokine stimulation of NK cells (right) leads to surface trafficking of AICL, which in resting NK cells is stored in the Golgi apparatus. This renders monokine stimulated NK cells susceptible to cytolysis by NKp80 expressing bystander NK cells. Adapted from (Bartel et al., 2013).

1.5.2.2 The receptor ligand pair NKp65 and KACL

NKp65 is a C-type lectin-like receptor encoded by the *KLRF2* locus in the NKC. In contrast to its close relative NKp80, NKp65 is expressed as a non-disulfide-linked homodimer on the human NK cell line NK-92, whereas human primary NK cells are devoid of NKp65 (Spreu et al., 2010; Steinle et al., 2016). After the first description of NKp65 expression on NK-92 cells in 2010, its physiological expression remained elusive until Vogler et al. could detect NKp65 expression on a minor subset of ILC, subsequently identified as ILC3 (Steinle et al., 2016) (Figure 13). In this preliminary study two NKp65 specific antibodies were generated, designated OMAR1 and 12C10. Using OMAR1, NKp65 was first detected on a small population of cytokine-activated NK cell enriched, $NKp44^+$ peripheral blood mononuclear cells (PBMC) (Figure 13A). Comparative transcriptional profiling of FACSorted $NKp65^+NKp44^+$ and $NKp65^-NKp44^+$ cells revealed that $NKp65^+$ cells express enhanced levels of ILC3 markers such as c-kit (CD117), IL-1 receptor (IL1R1) and the TF AHR, while classical NK markers (KIRs, CD16) were underrepresented (Figure 13B). Further, in a qPCR-based screen of various human tissues, KLRF2 transcripts were mainly detected in tissues known to be fairly rich sources of ILC3 such as tonsils, placenta and small intestine (Figure 13C) (Doisne et al., 2015; Simoni et al., 2017). Overall, the levels of KLRF2 transcripts were shown to be scarce, which is well in line with the known sparsity of ILC3. The surface expression of NKp65 on bona fide ILC3 was finally shown for human tonsillar cells, characterized by typical ILC3 surface markers and OMAR1 (Figure 13D).

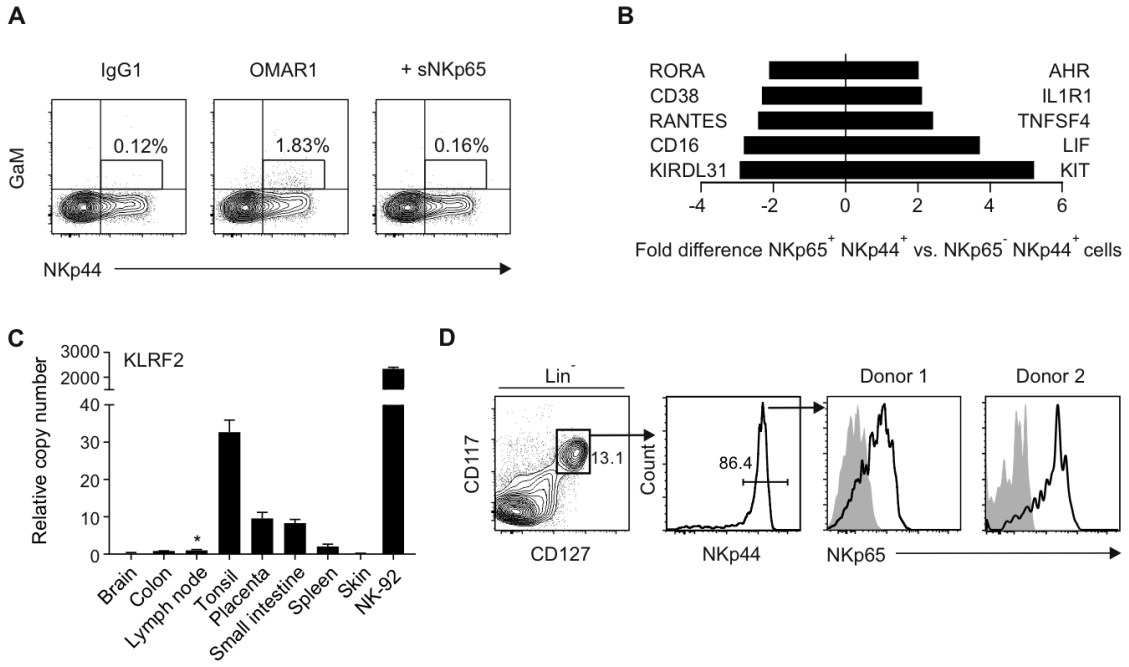

Figure 13: NKp65 expression by human ILC3.
A, PBMC enriched for NK cells by magnetic-activated cell sorting (MACS) purification and cultured for four days with IL-2, IL-12, and IL-18, were subsequently analyzed by flow cytometry for surface expression of NKp65 using the NKp65 specific antibody OMAR1 on cytokine-activated (i.e. $NKp44^+$) cells (**A**, middle panel). For control, cells were stained with an isotype control (**A**, left) or with OMAR1 pre-incubated with sNKp65 (**A**, right). Gates were set for $DAPI^-CD3^-$ cells. **B**, Differential gene expression averaged from microarray data of FACS-purified $NKp65^+NKp44^+$ versus $NKp65^-NKp44^+$ blood lymphocytes activated as in (**A**). **C**, Abundance of KLRF2 transcripts in various human tissues. Copy numbers of KLRF2 transcripts were determined by qPCR, normalized, and set relative to samples marked with an asterisk. For comparison, KLRF2 transcript levels of NK-92 cells are included. Data are shown as means of triplicates ± s.d.. **D**, $Lin^-CD117^+CD127^+NKp44^+$ lymphocytes from human tonsils analyzed for NKp65 surface expression using OMAR1-bio plus SA-APC (black line). Data shown in this figure were generated by Dr. Isabel Vogler, Steinle laboratory.

1.5.2.3 The high affinity interaction of NKp65 and KACL

NKp65 binds to its ligand KACL with extraordinary high affinity (K_D ~ 1-10 nM) (Li et al., 2013; Spreu et al., 2010). In contrast to other ligands of NKRP1 receptors which are mainly expressed by hematopoietic cells, KACL is specifically expressed on keratinocytes in the human skin (Spreu et al., 2007). Expressed on NK-92 cells, NKp65 stimulation results in cytotoxicity and the secretion of cytokines and is therefore considered an activating receptor (Spreu et al., 2010) (Figure 14). The physiological expression of NKp65 on human ILC3 that mainly reside in barrier tissues and the restricted expression of KACL on human keratinocytes suggests a role of the NKp65-KACL interaction for skin immunobiology. However, the functional consequences of triggering NKp65 on ILC3 remain elusive.

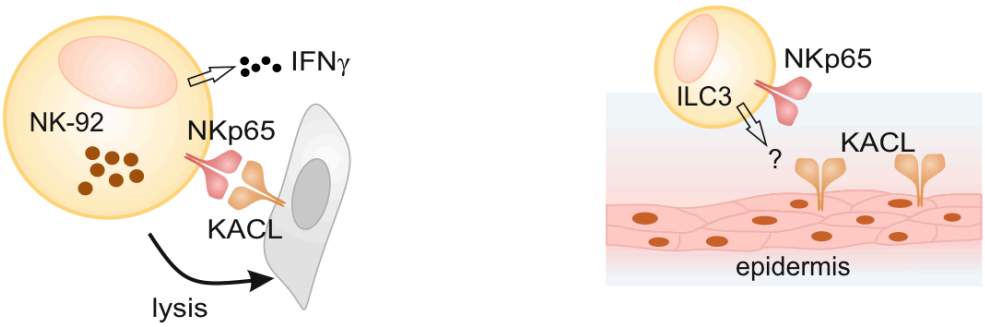

Figure 14: Functional consequences of the high affinity NKp65-KACL interaction.
Engagement of NKp65 expressed on NK-92 cells by KACL-bearing target cells stimulates cytotoxicity and INF-γ secretion (left). Physiologically, the expression of NKp65 on ILC3 and of KACL on human keratinocytes indicates a role for this receptor ligand pair in skin immunobiology. However, the functional consequences of triggering NKp65 in a physiological context are so far undefined. Adapted from (Bartel et al., 2013).

The effector functions of NKp65 depend on a tyrosine residue which is embedded in the hemi-immunoreceptor tyrosine-based activation motif (hemITAM) in its cytosolic tail (Bauer et al., 2017; Spreu et al., 2010). HemITAMs consist of a single tyrosine signaling unit (YxxL) and a triacidic motif with the consensus sequence DEDGYxxL (Bauer and Steinle, 2017). The hemITAM sequence in NKp65 (NEDGYxxL) differs from those of other CTLRs like Dectin-1 and CLEC2 (DEDGYxxL) in one amino acid in the triacidic motif. However, upon engagement by antibodies or KACL dimers, the hemITAM-embedded tyrosine 7 is phosphorylated and initiates a signaling pathway depending on Syk, which has also been reported for CLEC2 and Dectin-1. Syk phosphorylation is critically involved in the activation of NKp65 expressing cells although, in contrast to Dectin-1 and CLEC2 which directly recruit Syk, a physical association of Syk with the NKp65 hemITAM could not be shown (Bauer et al., 2017).

The structure of the soluble ectodomain NKp65-KACL complex displays a butterfly-shaped tetrameric assembly in which each subunit of the homodimeric KACL engages one NKp65 molecule (Figure 15) (Li et al., 2013). Although there is evidence that also NKp65 assembles to non-disulfide-linked homodimers (Spreu et al., 2010), no crystallographically related dimer interface was identified for NKp65 (Li et al., 2013). In contrast, KACL is present as a homodimer, structurally resembling other CLEC2 molecules such as CD69 (Natarajan et al., 2000). The mainly hydrophobic NKp65-KACL interface includes 17 hydrogen bonds and is characterized by a high shape complementary. The crystal structure further shows that NKp65 uses 20 residues to bind to 16 KACL residues.

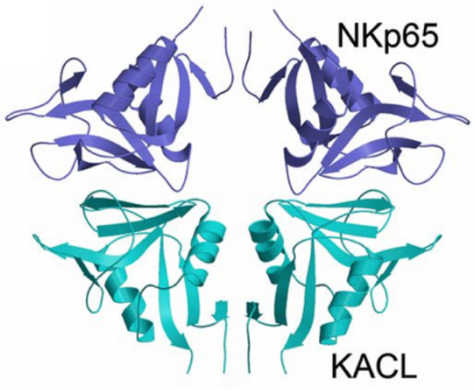

Figure 15: Structure of the soluble ectodomain NKp65-KACL complex.
Ribbon representation of two NKp65 monomers (purple) bound to one KACL homodimer (cyan) (Li et al., 2013).

Based on the crystallographical analysis Li et al. defined the amino acids F148, R158, F160, I161 and D162 in the KACL protein as essential for NKp65 binding. A more detailed study using non-conservative substitutions of these specific sites revealed that the amino acids R158 and I161 are critically involved in recognition of KACL by NKp65 expressing cells. It was further shown that glycosylation of the three putative N-glycosylation sites of KACL does not influence NKp65 binding (Bauer et al., 2015).

1.6 Scope and objectives

NKp65 was first described in 2010 as an activating receptor expressed on the NK cell line NK-92 (Spreu et al., 2010). Since then, its physiologic expression remained elusive until the generation of a specific antibody allowed for its detection on ILC3, a recently discovered subset of innate lymphocytes. The tissue-residency of ILC (Turner and Gasteiger, 2018) coincided with the skin-restricted expression of KACL (Bauer et al., 2015; Spreu et al., 2010), the high affinity ligand of NKp65, suggests a role of this genetically linked receptor ligand pair in tissue-specific immunosurveillance. However, whereas the expression of KACL on differentiating keratinocytes of the human skin is well described, the expression of NKp65 on ILC3 needs further investigation.

Hence, the physiologic expression of NKp65 was studied in more detail within in this work. First, the ILC3 character of NKp65 expressing cells was verified by detailed flow cytometric analyses, demonstrating the lack of NKp65 expression on any other subset of ILC including ILC1, ILC2, NK cells and LTi cells. Furthermore, the role of NKp65 expressing cells in the trajectory of NK cell development was analyzed by flow cytometric analyses of *ex vivo* human tonsillar cells. To support the *ex vivo* data and to monitor ILC development over time, NKp65 expressing cells were generated from $CD34^+$ hematopoietic stem cells in an optimized *in vitro* differentiation system with OP9 feeder cells and cytokines. Additionally, the consequences of the high affinity NKp65-KACL interaction were addressed in functional studies.

To contribute to a better understanding of the highly restricted expression of NKp65, its regulation on transcriptional and post-transcriptional level was studied in the second part of this work. Transcriptional regulation was assessed by studying the promoter of KLRF2, the gene encoding for NKp65. Therefore, computational prediction of putative binding sites was combined with functional studies using a luciferase reporter system. Lastly, post-transcriptional regulation was analyzed by incubation of NKp65 expressing cells with different cell stimulating agents, inhibitors or KACL expressing cells.

2. Material

2.1 Apparatus and consumables

Table 2: Apparatus and consumables.

Name	Company
Amicon® Ultra Centrifugal Filters	Merck (Darmstadt, DE)
BD FACS Canto II	BD Biosciences (Franklin Lakes, NJ)
CASY TT Cellcounter	OLS OMNI Life Sciences (Bremen, DE)
Fusion SL image acquisition system	Vilber Lourmat (Eberhardzell, DE)
Gene Pulser Xcell electroporation system	Bio-Rad (Hercules, CA)
gentleMACS Dissociator	Miltenyi (Bergisch-Gladbach, DE)
Multiscan™ Mikrotiterplate-Photometer	ThermoFisher Scientific (Waltham, MA)
Luciferase assay plates	PerkinElmer (Waltham, MA)
MicroBeta^2 Microplate Counter	PerkinElmer (Waltham, MA)
Mini Gel Tank	ThermoFisher Scientific (Waltham, MA)
Mini-PROTEAN Tetra Cell (gel electrophoresis)	Bio-Rad (Hercules, CA)
NanoPhotometer	Implen (München, DE)
Novex Tris-Glycine Mini Gels 16%	ThermoFisher Scientific (Waltham, MA)
Nunc MaxiSorp flat-bottom plates	ThermoFisher Scientific (Waltham, MA)
PVDF membrane	ThermoFisher Scientific (Waltham, MA)
QuantStudio 3 Real-Time-PCR-System	ThermoFisher Scientific (Waltham, MA)
SemiDry blotting apparatus	Cti GmbH (Idstein, DE)
Slide-A-Lyzer Dialysis Cassette	ThermoFisher Scientific (Waltham, MA)
SpeedVac vacuum concentrator	ThermoFisher Scientific (Waltham, MA)
Thermocycler peqSTAR 96 Universal Grade	PEQLAB (Erlangen, DE)
Thermocycler Primus 25	PEQLAB (Erlangen, DE)

2.2 Buffers and solutions

Table 3: Buffers and solutions for SDS-PAGE and immunoblotting.

Name	Ingredients/Company
Blocking solution	1x TBS 5% w/v skim milk powder 0.1% Tween-20
Laemmli sample buffer reducing (6x)	400 µl Laemmli sample buffer (6x) 100 µl β-Mercaptoethanol 100%
Laemmli sample buffer (6x)	375 mM Tris pH 6.8 30% v/v glycerol 6% w/v SDS 0.015% w/v Bromphenol blue
Novex™ SDS sample buffer (2x)	ThermoFisher Scientific (Waltham, MA)
Novex™ SDS running buffer (10x)	ThermoFisher Scientific (Waltham, MA)
NP-40 Lysis buffer	50 mM Trizma® base 150 mM NaCl 1% v/v NP-40 pH 8 at RT
Protein buffer (10x)	250 mM Trizma® base 1920 mM glycine
Resolving gel buffer	1.5 M Trizma® base pH 8.6 at RT

Name	Ingredients/Company
Stacking gel buffer	1 M Trizma® base pH 6.8 at RT
SDS running buffer (1x)	1x Proteinbuffer 0.1% w/v SDS
TBS (10x)	100 mM Trizma® base 1500 mM NaCl pH 7.5 at RT
TBST (1x)	1x TBS 0.1% Tween-20
Transfer buffer (1x)	1x protein buffer 20% v/v methanol

Table 4: Buffers and solutions for molecular cloning.

Name	Ingredients
DNA sample buffer (10x)	1x TAE 30% v/v glycerol 0.25% Orange G
LB agar with antibiotics	LB agar 100 µg/ml ampicillin or 50 µg/ml kanamycin
LB medium with antibiotics	LB medium 100 µg/ml ampicillin or 50 µl/ml kanamycin
LB agar	LB medium 1.5% agar
TAE (50x)	2 M Trizma® base 0.05 M EDTA pH 8.0 5.7% v/v Acetic acid pH 8.5 at RT

Table 5: Buffers and solutions for ELISA.

Name	Company
Blocking solution	1x PBS 15% BSA
PBS (10x)	2 g/l KCl 2 g/l KH_2PO_4 80 g/l NaCl 11.5 g/l Na_2HPO_4
PBST (1x)	1x PBS 0.05% v/v Tween-20

Table 6: Buffers and solutions for flow cytometry and MACS® cell separation.

Name	Ingredients
FACS buffer	1x PBS 2% v/v FCS 2 mM EDTA 0.01% w/v sodium azide
MACS buffer	1x PBS

Name	Ingredients
	0.5% BSA, sterile 30% 2.5 mM EDTA
Saponin buffer	1x PBS 0.5% w/v BSA 0.1% w/v saponin 0.01% w/v sodium azide

2.3 Reagents

Unless stated otherwise, standard chemicals and reagents were obtained from ThermoFisher Scientific, Merck, Sigma-Aldrich, Carl Roth or AppliChem. Only noteworthy chemicals, reagents and kits are listed below.

Table 7: Reagents.

Name	Company
3X FLAG Peptide	Sigma-Aldrich (St. Louis, MO)
β-Mercaptoethanol	AppliChem (Darmstadt, DE)
Ampicillin	MP Biomedicals (Santa Ana, CA)
Batimastat (BB94)	Sigma-Aldrich (St. Louis, MO)
Concanamycin-A	Sigma-Aldrich (St. Louis, MO)
Cytofix/Cytoperm™	BD Bioscience (Franklin Lakes, NJ)
CellTrace™ Far Red	Thermo Fisher Scientific (Waltham, MA)
DAPI	AppliChem (Darmstadt, DE)
DMSO	ThermoFisher Scientific (Waltham, MA)
dNTPs	ThermoFisher Scientific (Waltham, MA)
Ethanolamine	AppliChem (Darmstadt, DE)
Ficoll Paque Plus	GE Healthcare (Buckinghamshire, UK)
Fixable Viability Dye eFluor450	eBioscience (San Diego, CA)
Fixable Viability Dye eFluor506	
GolgiStop™	BD Bioscience (Franklin Lakes, NJ)
HRP Juice Plus	PJK (Kleinbittersdorf, DE)
Ionomycin	Sigma-Aldrich (St. Louis, MO)
Kanamycin	MP Biomedicals (Santa Ana, CA)
Mini-PROTEAN 4-20% TGX Gel	BioRad (Hercules, CA)
PageRuler™ Prestained Protein Ladder	ThermoFisher Scientific (Waltham, MA)
Phorbol 12-myristate 13-acetate (PMA)	Sigma-Aldrich (St. Louis, MO)
PI3K Inhibitor (Ly294002)	Cayman Chemical (Ann Arbor, MI)
Pierce™ Protein A IgG Binding Buffer	Sigma-Aldrich (St. Louis, MO)
Protease Inhibitor Cocktail (cOmplete™)	Roche (Basel, CHE)
Random Primer	NEB (Ipswich, UK)
Spectra™ Multicolor Low Range Protein Ladder	ThermoFisher Scientific (Waltham, MA)
STAT5 Inhibitor, CAS 285986-31-4	Merck (Darmstadt, DE)
SYBR Green	Sigma-Aldrich (St. Louis, MO)
SYTOX green	ThermoFisher Scientific (Waltham, MA)
TMB Microwell Peroxidase Substrate System	Seracare (Milford, MA)
Trypsin-EDTA solution	Sigma-Aldrich (St. Louis, MO)
Z-IETD-FMK caspase-8 inhibitor	Abcam (Cambridge, UK)

2.4 Oligonucleotides

Table 8: Oligonucleotides for molecular cloning.

Name	Sequence
F2 Prom UTR S2 rev	CTCTTCAAATGTCTAATGTCTTATTATC
KLRF2promdel_3.1_fw	GGAATTCGAGCTCTAGACATTTGTTCTGTTTGTTTAG
KLRF2promdel_3.2_fw	GGAATTCGAGCTCAGACATGAAGGAAGGAATTATG
KLRF2promdel_3.3_fw	GGAATTCGAGCTCCGCACACAAGTGGCAGGAAC
KLRF2promdel_5_fw	GGAATTCGAGCTCGCCAGATATTAACAAGCTTATATCC
KLRF2promdel_6_fw	GGAATTCGAGCTCTCCTGTGTGGTTTTAGACATCTGTGTCTG
KLRF2prom_core_fw	GGAATTCGAGCTCAGTAAATTTTGACTATTTTTGGCCTTCC
KLRF2prom_mdel_1_fw	GCCTAACTGGCCGGTACCTGAGCTCGCTAGCCTCGAGGATATCAAG TCCCAAATAACAAAATTGCTATTTTAACTTTTTTAATTTGAATTTTT ATTTAC
KLRF2prom_mdel_1_rev	CTTTTATAATAAAGTAAGAGAAAAAATAAAATAAAACAAATAATC TACAGAACAAATGTCTAGGTAAATAAAAATTCAAATT
KLRF2prom_mdel_2_fw	GGTACCTGAGCTCGCTAGCCTCGAGGATATCAAGTCCCAAATAACA AAATTGCTATTTTAACTTTTTTAATTTGAATTTTTATTTACCTAG
KLRF2prom_mdel2_rev	CTTTTATAATAAAGTAAGAGAAAAAATAAAATAAAACAAATAAAA ACAAACAGAACAAATGTCTAGGTAAATAAAAATTCA
KLRF2prom_mdel_3_fw	GTACCTGAGCTCGCTAGCCTCGAGGATATCAAGTCCCAAATAACAA AATTGCTATTTTAACTTTTTTAATTTGAATTTTTATTTACCTAGACAT TTG
KLRF2prom_mdel_3_rev	CATGTCTTTTATAATAAAGTAAGAGAAAAAATAAAATAAAAAATC TCTAAACAAACAGAACAAATGTCTAGGTAAATAA
KLRF2prom_mdel_4_fw	TCGCTAGCCTCGAGGATATCAAGTCCCAAATAACAAAATTGCTATT TTAACTTTTTTAATTTGAATTTTTATTTACCTAGACATTTGTTCTG
KLRF2prom_mdel_4_rev	CTTCCTTCATGTCTTTTATAATAAAGTAAGAGAAAAAATAAAACAA ATAATCTCTAAACAAACAGAACAAATGTCTAGGTA
KLRF2prom_mdel_5_fw	AGCTCGCTAGCCTCGAGGATATCAAGTCCCAAATAACAAAATTGCT ATTTTAACTTTTTTAATTTGAATTTTTATTTACCTAGACATTTGTTCT GTTTG
KLRF2prom_mdel_5_rev	CCTTCCTTCATGTCTTTTATAATAAAGTAAGAGAAAAAAAAAACAA ATAATCTCTAAACAAACAGAACAAATGTCTA
STAT5mut1_fw	ACACAGAATTGTAGCCAGATATTAA
STAT5mut1_rev	TTTTCAAGGTAAAGGTAGCTAGTG
pGL4.10luc2ATGfw	ATGGAAGATGCCAAAAACATTAAG
pGL4.10 SacI rev	TTGATATCCTCGAGGCTAGC

Table 9: Oligonucleotides for quantitative RT-PCR.

Name	Sequence
18S_fw	CGGCTACCACATCCAAGGAA
18S_rev	GCTGGAATTACCGCGGCT
KLRF2_fw	TGAGCTGGAGTTCATACAGAACA
KLRF2_rev	TGTCATCAGTTGGTCCAATCACT

Table 10: Oligonucleotides for pulldown assays.

Name	Sequence
STAT5_bio_fw	(Biotin)CTTGAAATTCACAGAATTGTAGC
STAT5_bio_rev	(Biotin)GCTACAATTCTGTGAATTTCAAG
STAT5_fw	CTTGAAATTCACAGAATTGTAGC
STAT5_rev	GCTACAATTCTGTGAATTTCAAG
STAT5_mut1_bio_fw	(Biotin)CTTGAAAAACACAGAATTGTAGC
STAT5_mut1_bio_rev	(Biotin)GCTACAATTCTGTGTTTTTCAAG
STAT5_mut1_fw	CTTGAAAAACACAGAATTGTAGC
STAT5_mut1_rev	GCTACAATTCTGTGTTTTTCAAG
STAT5_mut2_bio_fw	(Biotin)CTTGAAATTCACACTTTTGTAGC
STAT5_mut2_bio_rev	(Biotin)GCTACAAAAGTGTGAATTTCAAG
STAT5_mut2_fw	CTTGAAATTCACACTTTTGTAGC
STAT5_mut2_rev	GCTACAAAAGTGTGAATTTCAAG

2.5 Antibodies

Table 11: Primary antibodies.
Antibodies were used for flow cytometry, unless stated otherwise. Other applications: immunoblotting (IB), immunoprecipitation (IP). Antibodies produced in the laboratory of Prof. Dr. Steinle are indicated by the abbreviation IMM (Institute for Molecular Medicine).

Target	Clone	Conjugation	Isotype (species)	Application	Company
CD3	UCHT1	FITC	IgG1 (mouse)	1:100	Biolegend (San Diego, CA)
		PB			
CD14	HCD14	FITC	IgG1 (mouse)	1:100	Biolegend (San Diego, CA)
		PB			
CD16	3G8	APC	IgG1 (mouse)	1:100	Biolegend (San Diego, CA)
CD19	HIB19	FITC	IgG1 (mouse)	1:100	Biolegend (San Diego, CA)
		PB			
CD34	AC136	APC	IgG2a (mouse)	1:100	Miltenyi (Bergisch-Gladbach, DE)
	581	FITC	IgG1 (mouse)		Biolegend (San Diego, CA)
		PB			
CD34/CD45	8G12/2D1	PE/FITC	IgG1 (mouse)	1:25	BD Bioscience (San Jose, CA)
CD45-RA	REA562	PerCp-Vio700	IgG1 (rec. human)	1:300	Miltenyi (Bergisch-Gladbach, DE)
CD56	HCD56	APC-Cy7	IgG1 (mouse)	1:300	Biolegend (San Diego, CA)
CD94	DX22	FITC	IgG1 (mouse)	1:100	Biolegend (San Diego, CA)
		PE			
	HP-3D9	PerCp-Cy5.5		1:350	BD Bioscience (San Jose, CA)
CD117	104D2	PE-Cy7	IgG1 (mouse)	1:200	eBioscience (San Diego, CA)
CD127	A019D5	APC	IgG1 (mouse)	1:100	Biolegend (San Diego, CA)
		Bv510		1:25	
CD196	G034E3	PerCp-Cy5.5	IgG1 (mouse)	1:100	Biolegend (San Diego, CA)

Target	Clone	Conjugation	Isotype (species)	Application	Company
CD294	BM16	APC-Cy7	IgG2b (mouse)	1:50	Biolegend (San Diego, CA)
CD336 (NKp44)	P44-8	APC	IgG1 (mouse)	1:100	Biolegend (San Diego, CA)
	2.29	PE			Miltenyi (Bergisch-Gladbach, DE)
		Viobright FITC			
EOMES	WD1928	FITC	IgG1 (mouse)	1:50	eBioscience (San Diego, CA)
		PE-Cy7		1:100	
FLAG	M2	-	IgG1 (mouse)	5 µg/mL (IB, IP)	Sigma-Aldrich (St. Louis, MO)
		biotin			
GATA3	REA174	APC	IgG1 (rec. human)	1:50	Miltenyi (Bergisch-Gladbach, DE)
GM-CSF	BVD2-21C11	APC	IgG2a (rat)	1:100	Biolegend (San Diego, CA)
IFN-γ	B27	FITC	IgG1 (mouse)	1:250	BD Bioscience (San Jose, CA)
IL1R1	polyclonal	FITC	(goat)	1:50	R&D Systems (Minneapolis, CA)
IL-22	11URT1	PE-Cy7	IgG1 (mouse)	1:100	eBioscience (San Diego, CA)
KACL	OMA1	-	IgG2a (mouse)	10 µg/mL	IMM (Bauer et al., 2015)
	OMA6				IMM (Bauer et al., 2015)
NKp65	OMAR1	-	IgG1 (mouse)	10 µg/mL	IMM
		biotin			
	12C10	-			
NKp80	5D12	-	IgG1 (mouse)	10 µg/mL	IMM (Welte et al., 2006)
		FITC			
RORγt	REA278	PE	IgG1 (rec. human)	1:100	Miltenyi (Bergisch-Gladbach, DE)
STAT5	C17	-	IgG1 (rabbit)	10 µg/mL (IB)	Santa Cruz (Dallas, TX)
T-bet	4B10	Alexa Fluor 647	IgG1 (mouse)	1:100	Biolegend (San Diego, CA)

Table 12: Isotype controls.

Isotype controls used for flow cytometry or production of F(ab')$_2$ fragment control. Isotype control antibodies produced in the laboratory of Prof. Dr. Steinle are indicated by the abbreviation IMM (Institute for Molecular Medicine).

Target	Clone	Conjugation	Isotype (species)	Company
anti-NP	N1G9	-	IgG1 (mouse)	IMM
		biotin		
anti-NP	S43-10	-	IgG2a (mouse)	IMM

Table 13: Secondary antibodies.

Antibodies were used for flow cytometry, unless stated otherwise. Other applications: immunoblotting (IB), immunoprecipitation (IP).

Target	Isotype	Conjugation	Species	Application	Company
Mouse IgG	IgG	APC	Goat	1:300	Jackson ImmunoResearch (Newmarket, UK)
Mouse IgG + IgM	IgG	HRP	Goat	1:10000 (IB)	Jackson ImmunoResearch (Newmarket, UK)
Mouse IgG (H+L)	IgG $F(ab')_2$	PE	Goat	1:300	Jackson ImmunoResearch (Newmarket, UK)
Rabbit IgG (light chain specific)	IgG	HRP	Mouse	1:10000 (IB)	Jackson ImmunoResearch (Newmarket, UK)

2.6 Microbeads and kits

Table 14: Microbeads and kits

Name	Company
Anti-APC MicroBeads	Miltenyi (Bergisch-Gladbach, DE)
Anti-FITC MicroBeads	Miltenyi (Bergisch-Gladbach, DE)
Anti-PE MicroBeads	Miltenyi (Bergisch-Gladbach, DE)
M2 magnetic beads	Sigma-Aldrich (St. Louis, MO)
Streptavidin magnetic beads	ThermoFisher Scientific (Waltham, MA)
CD34 MicroBead Kit, human	Miltenyi (Bergisch-Gladbach, DE)
Dual-Glo Luciferase Assay System	Promega (Fitchburg, WI)
Foxp3/Transcription Factor Staining Buffer Set	eBioscience (San Diego, CA)
Pierce™ Protein A Agarose	ThermoFisher Scientific (Waltham, MA)
QIAGEN Plasmid Mini, Midi or Maxi Kit	QIAGEN (Hilden, DE)
QIAquick PCR Purification Kit	
QIAquick Gel Extraction Kit	
RNAqueous-Micro Isolation Kit	ThermoFisher Scientific (Waltham, MA)

2.7 Cytokines and recombinant proteins

Table 15: Cytokines and recombinant proteins.
Recombinant proteins produced in the laboratory of Prof. Dr. Steinle are indicated by the abbreviation IMM (Institute for Molecular Medicine).

Name	Company
Human IgG	Sigma-Aldrich (St. Louis, MO)
Soluble NKp65	IMM
Human Flt3-Ligand	Miltenyi (Bergisch-Gladbach, DE)
Human IL-1β	R&D Systems (Minneapolis, CA)
Human IL-7	Miltenyi (Bergisch-Gladbach, DE)
Human IL-12	R&D Systems (Minneapolis, CA)
Human IL-15	Miltenyi (Bergisch-Gladbach, DE)
Human IL-18	R&D Systems (Minneapolis, CA)
Human IL-23	R&D Systems (Minneapolis, CA)
Human SCF	Miltenyi (Bergisch-Gladbach, DE)
Streptavidin APC	Jackson ImmunoResearch (Newmarket, UK)
Streptavidin BV421	
Streptavidin PE	

2.8 Media and supplements

Table 16: Media and supplements.

Name	Company
Ascorbic acid	Sigma-Aldrich (St. Louis, MO)
DMEM high Glucose	Sigma-Aldrich (St. Louis, MO)
Fetal Calf Serum	Biochrom (Berlin, DE)
Ham's F-12 Nutrient Mix	ThermoFisher Scientific (Waltham, MA)
IMDM	Sigma-Aldrich (St. Louis, MO)
Horse Serum	Sigma-Aldrich (St. Louis, MO)
Human Serum	Sigma-Aldrich (St. Louis, MO)
L-glutamine solution (200 mM)	Sigma-Aldrich (St. Louis, MO)
MEM α, GlutaMAX™ Supplement	ThermoFisher Scientific (Waltham, MA)
Non-Essential Amino Acids	Sigma-Aldrich (St. Louis, MO)
Penicillin/Streptomycin (100X)	Sigma-Aldrich (St. Louis, MO)
Puromycin	AppliChem (Darmstadt, DE)
RPMI	Sigma-Aldrich (St. Louis, MO)
Sodium Pyruvate (100 mM)	Sigma-Aldrich (St. Louis, MO)
Sodium Selenite	Sigma-Aldrich (St. Louis, MO)

2.9 Enzymes

Table 17: Enzymes.

Name	Company
Collagenase D	Roche (Basel, CHE)
Dispase II	Sigma-Aldrich (St. Louis, MO)
DNAse I	Promega (Fitchburg, WI)
DNAse I (sterile)	Roche (Basel, CHE)
M-MLV reverse Transkriptase (H-)	Promega (Fitchburg, WI)
PNGaseF	NEB (Ipswich, UK)
Phusion-Polymerase	NEB (Ipswich, UK)
Restriction endonucleases	NEB (Ipswich, UK)
Shrimp Alkaline Phosphatase (rSAP)	NEB (Ipswich, UK)
T4 DNA Ligase	ThermoFisher Scientific (Waltham, MA)
Taq-Polymerase	NEB (Ipswich, UK)

2.10 Plasmids

Table 18: Plasmids.

Name	Resistance gene		Company
	prokaryotic	eukaryotic	
pGL4.10[luc2]	Ampicillin	-	Promega (Fitchburg, WI)
pIRES2-eGFP	Kanamycin	Neomycin	Clontech (Mountain View, CA)
pMXsIP	Ampicillin	Puromycin	Toshio Kitamura, University of Tokyo (Kitamura, 1998)
pRL-SV40	Ampicillin	-	Promega (Fitchburg, WI)

2.11 Bacterial strains

Table 19: Bacterial strains.

Name	Company
Escherichia coli DH5α	ThermoFisher Scientific (Waltham, MA)
Escherichia coli Top10	ThermoFisher Scientific (Waltham, MA)
Escherichia coli XL1-Blue	Agilent Technologies (Santa Clara, CA)

2.12 Cell lines

Table 20: Cell lines.

Name	Characteristics
CEM	acute lymphoblastic leukemia cell line
NKR	acute lymphoblastic leukemia cell line
NK-92MI	malignant non-Hodgkin's lymphoma cell line ectopic IL-2 expression
U937	histiocytic lymphoma cell line
OP9	mouse stroma cells

3. Methods

3.1 Cell culture methods

U937 cells were cultured in RPMI-1640 medium supplemented with 10% FCS, 1% penicillin/streptomycin (P/S) and 1% L-glutamine. NK-92MI cells were cultured in IMDM medium containing 10% FCS, 10% horse serum, 1% P/S and 1% L-glutamine. For NK-92MI/NKp65 cells (Spreu et al 2010) medium was additionally supplemented with 5 µg/ml puromycin. NKR and CEM transductants (mock or KACL) (Neuss et al., 2018) were cultured in RPMI medium supplemented with 10% FCS, 1% P/S, 1% L-glutamine and 0.6 µg/ml puromycin. BM-derived stroma cell lines OP9-mock, OP9-DLL1 and OP9-DLL4 (Schmitt and Zuniga-Pflucker, 2002) were maintained in MEMα GlutaMAX medium supplemented with 20% FCS and 1% P/S. All cells were cultured at 37°C and 5% CO_2.

3.2 Human cell isolation and culture

3.2.1 Isolation of mononuclear cells from human tonsils

Surgical samples of human tonsils were obtained from the Department of Otorhinolaryngology, University Hospital Frankfurt am Main, with approval of the local Ethics Committee. Tonsils were cut in small pieces, enzymatically digested with 0.5 mg/ml Collagenase D (Roche) and 3,000 U/ml DNAse I (Roche) at 37°C, and mechanically disrupted using a gentleMACS Dissociator. Cell suspension was passed over a 100 µm cell strainer and mononuclear cells (MNC) were isolated by density gradient centrifugation using Ficoll® Paque Plus following the manufacturer's instructions.

3.2.2 Isolation of human PBMC from buffy coats

Buffy coats were obtained from the DRK Blutspendedienst. Human PBMC were isolated from buffy coats by density gradient centrifugation using Ficoll® Paque Plus following the manufacturer's instructions. Briefly, buffy coats were diluted with PBS and carefully layered on Ficoll® Paque Plus. After centrifugation at 400 x g for 30 min at 20°C the lymphocyte layer was collected and washed three times with PBS.

3.2.3 Isolation of lymphocytes from human skin

Skin samples of juvenile foreskin were obtained from the Department of Pediatric Surgery, University Hospital Frankfurt am Main, with approval of the local Ethics Committee. Foreskin

was sectioned into small pieces containing epidermal and dermal tissue. The sectioned tissue was subsequently enzymatically digested with 0.3% w/v Dispase II in PBS. After 16 h digestion, the epidermal layer was removed from the underlying dermal tissue. The dermal tissue was incubated with 0.5 mg/ml Collagenase D and 3,000 U/ml DNAse I for 30 min at 37°C prior to mechanical disruption using a gentleMACS Dissociator.

3.2.4 Magnetic-activated cell sorting (MACS) of NKp44$^+$ILC3

Tonsillar MNC (3.2.1) were suspended in MACS buffer and stained with anti-NKp44-PE or anti-NKp44-APC for 20 min at 4°C. After washing twice with MACS buffer, stained cells were enriched using anti-PE or anti-APC microbeads and MACS technology according to the manufacturer's instructions. Enriched cells were subsequently cultured in RPMI medium supplemented with 10% FCS, 1% P/S, 1% L-glutamine, 1% non-essential amino acids, and 50 ng/ml IL-7 as indicated.

3.3 *In vitro* differentiation of innate lymphocytes

In order to differentiate human innate lymphocytes from CD34$^+$ hematopoietic stem and progenitor cells (HSPC), OP9 cocultures were performed. One day before start of the coculture, OP9-mock cells were seeded in 24-well plates (2.5x10^4 c/well). Human CD34$^+$ HSPC were enriched from G-CSF-mobilized healthy donor apheresis samples using MACS CD34 microBeads after Ficoll density gradient centrifugation. Purified CD34$^+$ HSPC (>90% purity) were suspended in HSC medium (DMEM and Ham's F-12 medium (2:1 mixture) supplemented with 10% heat-inactivated human AB sera (Sigma-Aldrich), 1% P/S, 1% L-glutamine, 25 µM of β-Mercaptoethanol, 20 µg/ml of ascorbic acid, and 0.05 µg/ml of sodium selenite) and seeded on a monolayer of subconfluent OP9-mock cells (5-7x10^3 c/well). Human recombinant IL-7 (20 ng/ml), IL-15 (10 ng/ml), SCF (20 ng/ml), and Flt3-L (10 ng/ml) were added as indicated and cells cultivated for up to nine weeks with a weekly transfer to a fresh monolayer of feeder cells (OP9-mock or OP9-DLL1 as indicated) in fresh cytokine-containing medium. For cell sorting ivILC were generated on OP9-mock feeder cells and harvested after 28 days in culture. Cells were sorted on a FACS Aria III (BD Biosciences). NKp65$^+$ cells were subsequently cultured on OP9-mock, OP9-DLL1, or OP9-DLL4 cells for five days.

3.4 Methods in protein biochemistry

3.4.1 Preparation of culture supernatants and cell lysates

Supernatants of cultured, cocultured or PMA/Ionomycin stimulated cells (3.5.6) were prepared by successive centrifugation. First, cells were precipitated at 1,600 rpm for 3 min and used for the preparation of cell lysates. The supernatants were transferred into a fresh reaction tube and cleared by centrifugation at 13,000 rpm for 15 min at 4°C. Subsequently the samples were filtered through a 0.2 µm syringe filter and supplemented with cOmplete™ Protease Inhibitor Cocktail.

The remaining cell precipitate from the first centrifugation step was washed twice with PBS prior to cell lysis for 20 min on ice using NP40 lysis buffer. Cell lysates were cleared by centrifugation at 13,000 rpm for 5 min at 4°C.

3.4.2 Enzymatic deglycosylation of proteins with PNGaseF

For deglycosylation of proteins that were previously enriched from lysates or culture supernatants by immunoprecipitation as described in 3.4.3, samples were treated with PNGaseF according to the manufacturer's instructions for 2 h at 37°C. The reaction was stopped by adding 2x Novex™ Tris-Glycine SDS sample buffer and incubation at 95°C for 5 min.

3.4.3 Immunoprecipitation

For immunoprecipitation of FLAG-tagged NKp65 from culture supernatants or cell lysates, anti-FLAG M2 magnetic beads were washed two times with TBST and added to cleared culture supernatants or lysates (described in 3.4.1). After incubation for 3 h at 4°C on a rotator, beads were washed four times with TBST and proteins eluted by incubation with 150 µg/ml 3x FLAG peptide in 10% TBS for 30 min at 4°C. The sample volume was reduced to 20 µl using a SpeedVac vacuum concentrator and proteins were deglycosylated by PNGaseF treatment (3.4.2) prior to immunoblot analysis (3.4.5).

3.4.4 SDS-Polyacrylamide Gel Electrophoresis (SDS-PAGE)

Deglycosylated samples from immunoprecipitations (3.4.3) were fractionated by SDS-PAGE using 16% Novex Tris-Glycine Mini Gels in a Mini Gel Tank with Novex SDS Tris-Glycine running buffer (125 V, 90 min). Spectra™ Multicolor Low Range Protein Ladder was used as size standard.

Samples from STAT5 pulldown assays (3.5.4) were fractionated by SDS-PAGE using 15% polyacrylamide gels with stacking and separation gel.

3.4.5 Immunoblotting

For immunoblot analysis, samples fractionated by SDS-PAGE (3.4.4) were transferred to PVDF membranes by semi-dry blotting. Membranes were blocked by incubating 5% milk powder dissolved in 0.1% TBST for 1 h at RT. NKp65 was detected via its FLAG tag by incubation with anti-FLAG M2 mAb (10 µg/ml) followed by HRP-conjugated Goat anti-mouse antibody (1:10,000). For detection of STAT5, membranes were incubated with anti-STAT5 antibodies followed by incubation with HRP-conjugated mouse anti-rabbit antibodies (1:10,000). Membranes were developed by HRP-juice PLUS.

3.4.6 ELISA

For the sandwich ELISA of soluble NKp65 (sNKp65) two NKp65 specific mAbs OMAR1 and 12C10 were used that were produced by Dr. Isabel Vogler (Steinle laboratory) in a preliminary study. The capture mAb 12C10 (2 µg/ml in PBS) was immobilized to plates over night at 4°C. Plates were then blocked by addition of 100 µL 15% bovine serum albumin (BSA) for 2 h at 37°C and washed. Afterwards, the standard (recombinant sNKp65 in 7.5% BSA-PBS) and the cleared cell culture supernatants or cell lysates (prepared as described in 3.4.1 and diluted 1:2 in 7.5% BSA-PBS) were added and the plates incubated for 2 h at 37°C. After incubation, plates were washed and bound sNKp65 was detected with biotinylated mAb OMAR1 (1 µg/ml in 7.5% BSA-PBS) by 2 h incubation at 37°C. After washing, horseradish peroxidase (HRP)-conjugated streptavidin (diluted 1:4,000 in 3.75% BSA-PBS) was added for 1 h at 37°C. Plates were then washed and developed using the TMB peroxidase substrate system. HRP activity was stopped by adding 1 M phosphoric acid and the absorbance was measured at 450 nm.

3.4.7 Preparation of F(ab')$_2$ Fragments

F(ab')$_2$ fragments of the anti-KACL antibody OMA1 and the control IgG2a were generated by digestion with pepsin (200 mg/g IgG) in 0.1 M glycine buffer (pH 4.0) at 37°C. Digestion was stopped after 8 h by adjusting the pH to 7.0 by adding 1 M NaOH. F(ab')$_2$ fragments were purified using Pierce™ Protein-A Agarose. Therefore, a column was packed with resin slurry, following equilibration by adding binding buffer (Pierce™ Protein A IgG Binding Buffer) and allowing the solution to drain through the column. After diluting the digested antibody sample 1:1 with binding buffer, the sample was applied to the column and allowed to flow into the resin prior to washing the column by applying binding buffer. As the solution drains, all fractions were collected since they include the F(ab')$_2$ fragments, while the Fc part remains bound to the

column. After elution of the Fc fragments by adding elution buffer (0.1 M glycine, pH 3), the column was regenerated by adding neutralization buffer (1 M Tris, pH 8). After equilibration of the column by adding binding buffer, the $F(ab')_2$ fragment containing fraction was added again to the column and the procedure repeated. After this second purification step, $F(ab')_2$ fragments were dialyzed against PBS using a Slide-A-Lyzer Dialysis Cassette and subsequently concentrated to 1 mg/ml using Amicon® Ultra Centrifugal Filters, following the manufacturer's instructions. The purity of the $F(ab')_2$ fragments was verified by SDS-PAGE and Coomassie staining.

3.5 Functional *in vitro* assays

3.5.1 Intracellular cytokine detection assay

In order to investigate the cytokine response of *in vitro*-generated ILC (ivILC), ivILC were harvested after 41 days in culture as described in (3.3.). Collected cells were washed twice with PBS and cultured for 4.5 h at 37°C in RPMI medium supplemented with 10% FCS, 1% L-glutamine, 1% P/S and either IL-1β and IL-23 (both 10 ng/ml), IL-12 and IL-18 (both 5 ng/ml) or PMA (25 ng/ml) and Ionomycin (1 µM) as indicated. Each condition was prepared in triplicates. After incubation, cells were washed twice with PBS and analyzed for intracellular cytokine expression by FACS (3.6.2).

3.5.2 Cytotoxicity assays

In vitro-generated ILC (ivILC) (day 30 to 50 of culture) were co-cultured with U937 or NKR-KACL cells in presence of 10 µg/ml mAb OMA1 $F(ab')_2$ fragments or an isotype control at E:T ratios ranging from 0.5:1 to 2:1. Prior to coculture, target cells were labeled with Celltracer™ Far Red, according to the manufacturer's protocol. As indicated, in some assays NKR cells or ivILC were pre-incubated for 30 min at 37°C with 10 µM Z-IETD-FMK or 50 nM Concanamycin-A, respectively. After 15 h co-culture at 37°C, Far Red$^+$ cells were counted using a FACSCanto™ II (BD Biosciences). To determine % cytotoxicity, counts of all remaining Far Red$^+$ target cells in co-cultures were divided by counts of all Far Red$^+$ target cells in parallel cultures without ivILC.

3.5.3 Luciferase assays

Prior to electroporation, $4x10^6$ NK-92MI cells were washed twice with PBS and suspended in 300 µL of IMDM medium. Cells were transferred into 4 mm electroporation cuvettes and

electroporated (200 V, 1150 µF) with 50 µg of pGL4.10-promoter-luciferase constructs containing the *KLRF2 p*romoter, mutations or deletions thereof or the empty vector as control and 5 µg pRLSV40. After incubation at room temperature for 10 min cells were transferred into 6-well plates containing 3 ml of IMDM medium supplemented with 10% FCS, 10% horse serum, 1% P/S and 1% L-glutamine. After incubation for 24 h luciferase activity was measured using the Dual-Glo Luciferase Reporter Assay System and a MicroBeta^2 luminescence counter according to the manufacturer's instructions.

3.5.4 STAT5 pulldown assay

A total of 1 mg of protein from whole cell lysates of NK-92MI cells was incubated with 100 pmol of biotin-labeled STAT5-binding DNA probes (Table 10) and incubated for 30 min at 4°C in 1 ml of DNA binding buffer (10 mM Tris/HCl pH 7.5, 60 mM KCl, 1 mM DTT, 1 µg/ml BSA, 10% glycerol, 25 µg/ml sonicated salmon sperm DNA). Pierce^{TM} Streptavidin Magnetic Beads were washed twice with TBST, added to the reaction mixture and incubated for 1 h at 4°C. After washing with TBST beads were resuspended in 6x reducing SDS sample buffer and incubated at 95°C for 10 min. After centrifugation, the supernatants were conducted to SDS-gel electrophoresis (3.4.4) and subsequent immunoblotting (3.4.5).

3.5.5 Inhibition of STAT5 and PI3-Kinase in tonsillar ILC

NKp44$^+$ ILC3, enriched from human tonsillar MNC (3.2.4) were incubated with 50 µM STAT5 inhibitor, 50 µM PI3-Kinase inhibitor (Ly294002) or equal volumes of DMSO for up to 16 h in RPMI-1640 medium supplemented with 10% FCS, 1% P/S, 1% L-glutamine and 20 ng/ml IL-7.

3.5.6 Cocultures and PMA/Ionomycin stimulation addressing NKp65 shedding

For coculture and stimulation experiments cells were cultured in RPMI medium supplemented with 10% FCS, 1% P/S and 1% L-glutamine. All stimulating reagents (PMA, Ionomycin and Batimastat) were dissolved in DMSO. Therefore, cells were incubated with equal volumes of DMSO in control experiments. All experiments were analyzed in triplicates.

For cocultures, equal numbers of NK-92MI/NKp65 and CEM/KACL or CEM/mock cells were incubated for 2 h at 37°C in presence or absence of 10 µM Batimastat (BB94), respectively. All samples were analyzed in triplicates. NK-92MI/NKp65 cells were stimulated with PMA (25 ng/ml) and Ionomycin (1 µM) (P/I) in presence or absence of 10 µM BB94 for 2 h at 37°C as indicated.

3.6 Flow cytometry

All surface and intracellular fluorescence stainings were analyzed on a FACSCanto™ II (BD Bioscience) and data analyzed using FlowJo software.

3.6.1 Surface fluorescence staining

Cells were incubated with the indicated mAb (10 µg/ml) for 30 min at 4°C. After washing, cell bound antibodies were stained with either fluorochrome-conjugated goat anti-mouse IgG antibodies or fluorochrome-conjugated streptavidin. In some experiments, cells were subsequently stained with fluorochrome-conjugated antibodies specific for human antigens. Dead cells were excluded from the analysis by staining with DAPI, fixable viability dye eFluor™ 450, fixable viability dye eFluor™ 506 or SYTOX green.

3.6.2 Intracellular fluorescence staining

To assess expression of intracellular cytokines, cells were washed twice with PBS and incubated with fixable viability dye eFluor™ 450 or fixable viability dye eFluor™ 506. After washing twice with FACS buffer, cells were fixed with Cytofix/Cytoperm according to the manufacturer's instructions and subsequently stained with cytokine-specific antibodies using saponin buffer. Transcription factor stainings with fluorochrome-conjugated antibodies against RORγt, EOMES, T-bet and GATA3 were done with the FoxP3 staining kit according to the manufacturer's protocol.

3.7 Methods in molecular biology

3.7.1 General cloning techniques

General cloning procedures were used according to the literature (Green et al., 2012). All kits and enzymes were used according to the manufacturer's recommendations. All primers used for polymerase chain reaction (PCR) are listed in Table 8 and were purchased from Sigma-Aldrich. After final amplification and purification, plasmids were analyzed by sequencing (SeqLab, Göttingen).

3.7.1.1 Cloning with restriction enzymes

Inserts were generated by PCR using the Phusion® DNA polymerase. Products were analyzed by running a sample of the reaction mixture on an agarose gel, following standard protocols. For purification of PCR products the QIAquick PCR purification Kit was used.

Vectors were purified after amplification using QIAGEN Plasmid Kits. Purified vectors and inserts were digested with appropriate digestion High-Fidelity HF® restriction enzymes. After digestion purification was done by running the reaction mixture on an agarose gel (1-3%) in TAE buffer. After cutting bands of interest, vector and insert were purified using the QIAquick Gel Extraction Kit. After vector dephosphorylation using rSAP (10 min at 37°C followed by inactivation at 65°C for 5 min) a ligation reaction was performed using T4 DNA ligase and a vector to insert ratio of 1:3. After ligation, 1 to 5 µl of the reaction mixture were transformed into DH5α, Top10 or XL1-blue (3.7.3).

3.7.1.2 Overlap extension PCR cloning

Overlap extension PCR cloning was done according to (Bryksin and Matsumura, 2010). In short, forward and reverse primer with an overlap of approximately 25 bps were PCR-amplified to generate the primer insert. This insert was then used as primer in a second PCR with circular plasmid template. Following restriction digest of the original plasmid by DpnI, overlap extension products were transformed into XL1-blue (3.7.3).

3.7.1.3 Site directed mutagenesis

Mutations were introduced by site-directed mutagenesis. Two complementary primers harboring the mutation were designed and used to amplify the whole vector by PCR. Therefore, the standard PCR procedure was changed using an annealing temperature of 55°C and 16 cycles. After restriction digest of the original plasmid using DpnI the plasmid was transformed into *E. coli* (3.7.3).

3.7.2 Generation of luciferase plasmids

As original vector the plasmid containing the KLRF2 promoter sequence (-351 to + 108 bps relative to the TSS) cloned in front of the luciferase gene within the pGL4.10[luc2] vector (generated by Dr. Björn Bauer, Steinle laboratory) was used. Using this vector, the plasmids utilized for luciferase assays (3.5.3) were generated by different cloning techniques. The primers used for each cloning procedure are listed in Table 8.

Generation of the 5' truncated constructs was achieved by cloning with restriction enzymes (3.7.1.1) using the primer pGL4.10 SacI rev as reverse primer and the respective forward primer KLRF2promdel_X_fw. Microdeletions were introduced by overlap extension PCR (3.7.1.2) with forward and reverse primer according to Table 8 as indicated and mutation of the STAT5 binding site was achieved by site directed mutagenesis (3.7.1.3) using the primer pair STAT5mut1_fw and STAT5mut1_rev.

3.7.3 Transformation of *E. coli*

100 µl of chemical competent bacteria were thawed on ice and incubated for additional 30 min with purified plasmid DNA (10 to 25 ng) or 1 to 5 µl of a ligation reaction. After heat shock at 42°C for 30 to 45 s cells were immediately placed on ice and incubated for 2 min prior to adding 100 to 200 µl LB media. Incubation at 37°C for 1 to 2 h was followed by plating cells onto an agarose plate with selective LB media containing antibiotics according to resistance. Clones were picked after over-night incubation at 37°C and used for inoculation of liquid cultures.

3.8 Quantitative RT-PCR

RNA was isolated using RNAqueous™-micro total RNA isolation kit followed by reverse transcription using M-MLV reverse transcriptase. cDNA was amplified with primer pairs specific for NKp65 and 18S rRNA (Table 9). Amplifications were performed on a QuantStudio 3 or StepOne Plus machine using SYBR-Green Master mix. Relative gene expression was calculated using the $\Delta\Delta C_T$ method.

3.9 Statistical analysis

Data are routinely shown as mean ± s.d.. Unless stated otherwise, statistical significance was determined by one-way Analysis of Variance (ANOVA) with Tukey's post test using GraphPad Prism 7.0. *P < 0.05; **P < 0.01; ***P < 0.001; ****P < 0.0001.

4. Results

4.1 Characterization of NKp65 expression on human innate lymphocytes

4.1.1 Inter-individual variability of NKp65 expression on human tonsillar ILC3

As stated in the introduction (1.5.2.2), in previous studies on this project Dr. Isabel Vogler generated an antibody against NKp65, designated as OMAR1. Using this monoclonal antibody (mAb) she could show physiological expression of NKp65 on NKp44^{+}ILC3 from human tonsils for the first time.

During the time course of the present study, NKp44^{+}ILC3 from tonsils of 20 human donors were purified by magnetic-activated cell sorting (MACS) technology and analyzed for NKp65 expression by flow cytometry using OMAR1 on a FACS Canto II with standardized settings, allowing for the comparison of specific fluorescence intensity (SFI) values across different experiments. In the flow cytometric analyses shown hereinafter cells are routinely pre-gated on singlets and lineage negative (lin^{-}), live cells (DAPI^{-}) with lineage referring to the markers CD3, CD14, CD19 and CD34 unless otherwise stated. The gating strategy is exemplarily shown for MACS-purified tonsillar NKp44^{+}ILC3 of one donor (Figure 16A). In the following figures pre-gating is indicated and plots of relevant markers are shown only. Flow cytometric analyses of NKp44^{+}ILC3 gated as shown in Figure 16A revealed a high variance in NKp65 surface expression between individuals as exemplarily shown for one donor with high, intermediate and low expression, respectively (Figure 16B). Compiled data of cytometric analyses of 20 different donors further emphasized the inter-individual variability of NKp65 surface expression with SFIs ranging from 0 to 186 (Figure 16C). Further analysis comparing gender and age revealed that NKp65 expression did not significantly differ between male and female individuals and did not correlate with the donor's age (Figure 16D and E). However, high expression of NKp65 (SFI > 90) was only observed for individuals older than 20 years (Figure 16E).

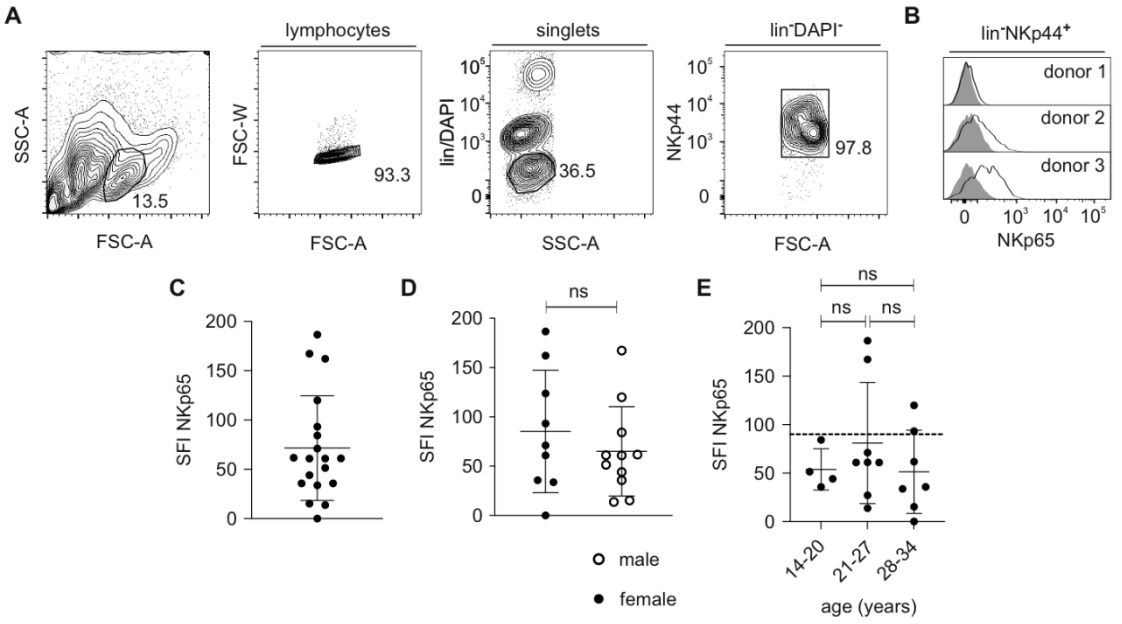

Figure 16: Inter-individual variability of NKp65 expression on human tonsillar ILC3.
Flow cytometric analyses of NKp65 expression assessed with OMAR1-bio plus SA-APC on MACS-purified NKp44$^+$ILC3 from human tonsils. **A**, Gating strategy for lineage- (lin$^-$)NKp44$^+$ILC3 (lin: CD3, CD14, CD19, CD34). **B**, Representative histograms of NKp65 expression (black lines) on NKp44$^+$ILC3 of three different donors gated as in (A). Shaded histograms represent control stainings with the respective isotype control (IgG1-bio). **C-E**, NKp65 expression (SFI) on lin-NKp44$^+$ cells of n = 20 different donors with mean ± s.d. and donors graded according to gender (**D**) or age (**E**). Statistical significance was analyzed by two-tailed unpaired Student`s t-test (**D**) or one-way ANOVA with Tukey's post hoc test (**E**) (ns, not significant).

4.1.2 NKp65 is not expressed by other subsets of innate lymphoid cells

4.1.2.1 NKp65 is not expressed by tonsillar ILC1, ILC2 and cNK cells

To emphasize the specificity of NKp65 surface expression by ILC3, tonsillar mononuclear cells (MNCs) of three independent human donors were analyzed by flow cytometry for NKp65 expression. The different subsets of innate lymphocytes were defined according to their phenotype based on surface markers of conventional NK cells (cNK) (lin$^-$CD127$^-$CD56$^+$), ILC1 (lin$^-$CD127$^+$CRTH2$^-$CD117$^-$CD94$^-$), ILC2 (lin$^-$CD127$^+$CRTH2$^+$) and ILC3 (lin$^-$ CD127$^+$CD117$^+$) (Figure 17A) (Mjosberg and Spits, 2016). Frequencies of lin$^-$ cells (0.6 ± 0.14 %) were reportedly low as were frequencies of ILC1 and ILC2, 0.8 ± 0.4% and 0.5 ± 0.4% of lin$^-$ cells, respectively. Also, in line with reports from the literature, ILC3 were the most frequent subset of CD127$^+$ tonsillar ILC among lin$^-$ cells (26 ± 6%) and NK cells made up for 43 ± 5% (Figure 17B) (Simoni et al., 2017). Of note, 30 ± 9% of lin$^-$ cells were not classified (Nd, not defined) by the surface markers used in the analysis. Analyzing NKp65 expression on these subsets confirmed marked NKp65 surface expression on ILC3, whereas other subsets of

tonsillar innate lymphocytes including ILC1, ILC2 and cNK cells were NKp65 negative (Figure 17C).

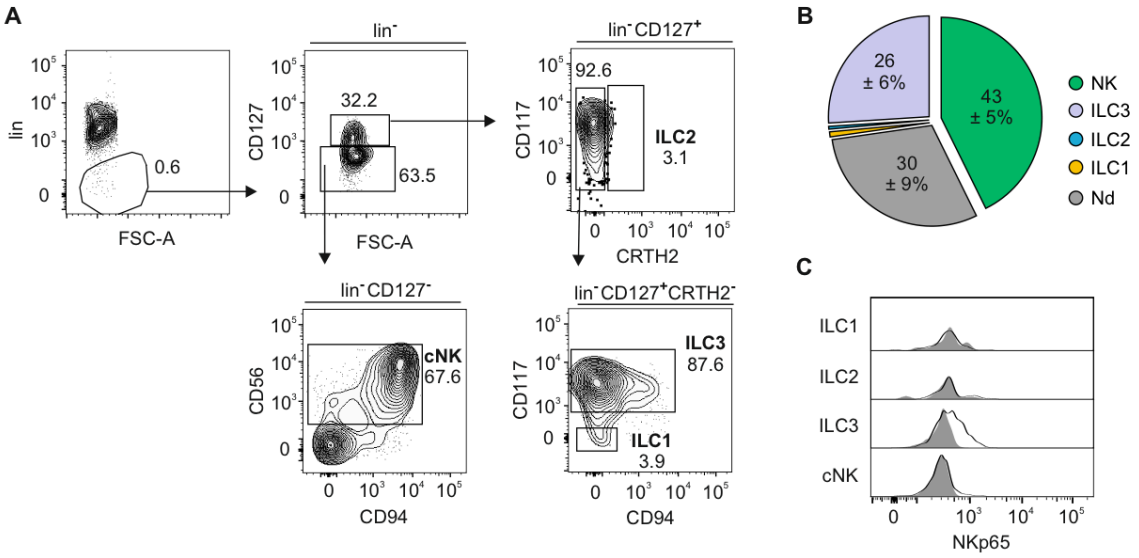

Figure 17: NKp65 expression hallmarks human tonsillar ILC3.
A-C, Flow cytometric analyses of tonsillar mononuclear cells (MNC) of three independent human donors. **A**, Representative flow cytometry analyses of human tonsillar MNC gated for ILC1 (lin$^-$CD127$^+$CRTH2$^-$CD117$^-$), ILC2 (lin$^-$CD127$^+$CRTH2$^+$), ILC3 (lin$^-$CD127$^+$CRTH2$^-$CD117$^+$) and cNK cells (lin$^-$CD127$^-$CD56$^+$). **B**, Compiled data of flow cytometric analyses of tonsillar cells gated as in **A**. Numbers indicate calculated frequencies (mean ± s.d.) of ILC1, ILC2, ILC3, NK and not defined (Nd) cells among the lin$^-$ population. **C**, NKp65 surface expression on ILC subsets gated as in **A** assessed with mAb OMAR1-bio plus SA-BV421 (solid line). Isotype control stainings are shown as shaded histograms.

Due to the fact that the different groups of ILC do share certain surface markers (Table 1), a more reliable method to distinguish ILC subsets is to combine the analysis of surface markers and signature transcription factors. Flow cytometric analyses of tonsillar MNC gated for lin$^-$CD127$^+$GATA3$^+$ ILC2, lin$^-$CD127$^+$RORγt$^+$ ILC3 and lin$^-$CD127$^-$EOMES$^+$ cNK cells (Figure 18A) not only confirmed the exclusive expression of NKp65 on ILC3, but also underlined the ILC3 character of NKp65$^+$ cells by verifying their expression of RORγt (Figure 18B). As already evidenced by the analysis of surface markers (Figure 17), EOMES$^+$ NK cells and GATA3$^+$ ILC2 were NKp65$^-$. Of note, frequencies of T-bet$^+$ ILC1 were extremely rare, complicating the analysis of NKp65 expression on this subset by intracellular staining. Therefore, the lack of NKp65 expression on ILC1 was only confirmed by the analysis based on surface stainings (Figure 17C).

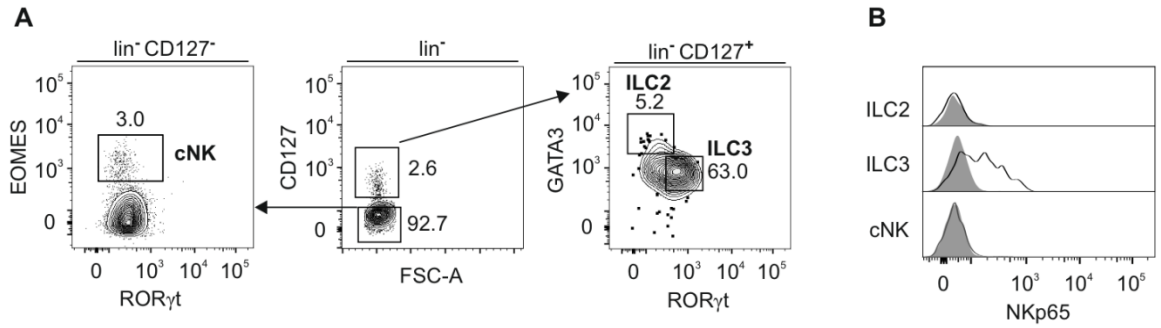

Figure 18: NKp65 is expressed by RORγt$^+$ lymphocytes.
Flow cytometric analyses of permeabilized human tonsillar mononuclear cells from one representative out of three independent donors. **A**, Gating strategy for the analysis of NKp65 surface expression on lin$^-$CD127$^-$Eomes$^+$ NK cells, lin$^-$CD127$^+$GATA3$^+$ ILC2 or lin$^-$CD127$^+$RORγt$^+$ ILC3. **B**, NKp65 expression on tonsillar ILC gated as in **A** assessed by OMAR1-bio plus SA-APC (black line). Respective isotype control stainings are shown as shaded histograms.

4.1.2.2 NKp65 hallmarks NCR$^+$ ILC3 whereas other RORγt$^+$ ILC3 subsets are NKp65 negative

ILC3 are a heterogenous group of RORγt expressing cells. They comprise natural cytotoxicity receptor (NCR) negative ILC3 including CCR6$^+$ LTi cells, and NCR$^+$ ILC3 (van de Pavert and Vivier, 2016). To unravel NKp65 expression on different types of ILC3, human tonsillar MNC were analyzed by flow cytometry following the phenotypic definition of NCR$^-$ or NCR$^+$ILC3 and LTi cells. By gating on lin$^-$CD127$^+$CD117$^+$ cells, the different ILC3 subsets were dissected by NKp44 and CCR6 expression as NKp44$^+$ ILC3 (NCR$^+$), NKp44$^-$CCR6$^-$ ILC3 (NCR$^-$) and NKp44$^-$CCR6$^+$ (LTi cells) (Figure 19A). While committed NCR$^+$ ILC3 markedly expressed NKp65, other RORγt-expressing innate lymphocytes such as LTi and NCR$^-$ ILC3-like precursor cells poorly expressed NKp65, if at all (Figure 19B).

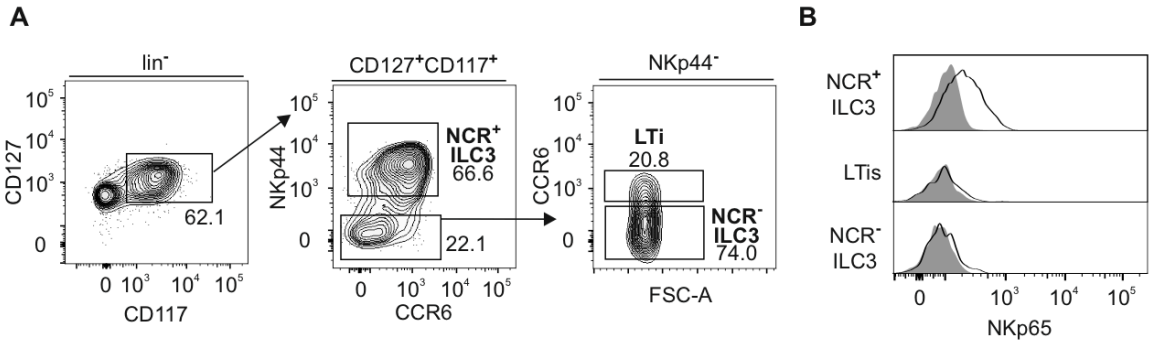

Figure 19: NKp65 expression on ILC3 subpopulations.
A, Gating strategy for flow cytometric analyses of human tonsillar ILC3. ILC3 were defined as lin$^-$CD127$^+$CD117$^+$ and the subpopulations discerned according to NKp44 and CCR6 expression as NKp44$^+$ (NCR$^+$) ILC3, NKp44$^-$CCR6$^-$(NCR$^-$) ILC3 and NKp44$^-$CCR6$^+$ LTi cells. **B**, Tonsillar mononuclear cells gated as in **A** were analyzed for NKp65 expression using OMAR1-bio plus SA-PE (black lines). Shaded histograms represent isotype control stainings. **A**, **B**, Data are representative for three independent analyses of tonsillar cells isolated from different human donors.

4.1.2.3 NKp65 is not detected on peripheral blood innate lymphocytes

The absence of NKp65 on other subsets of innate lymphocytes was also shown for ILC from peripheral blood mononuclear cells (PBMC) of healthy human donors, by flow cytometric analyses using OMAR1 (Figure 20). Distinguishing the different subsets of ILC according to their phenotypic expression of surface markers (Figure 20A) revealed that NKp65 could not be detected on any peripheral blood ILC subset, including ILC1, ILC2, NCR$^-$ ILC3 and cNK cells (Figure 20B). In contrary to the human tonsil which is fairly rich in NKp44$^+$ ILC3, frequencies of NKp44$^+$ ILC3 in the peripheral blood of healthy individuals are negligible, rationalizing the complete absence of NKp65$^+$ cells in the peripheral blood (Villanova et al., 2014) (Figure 20).

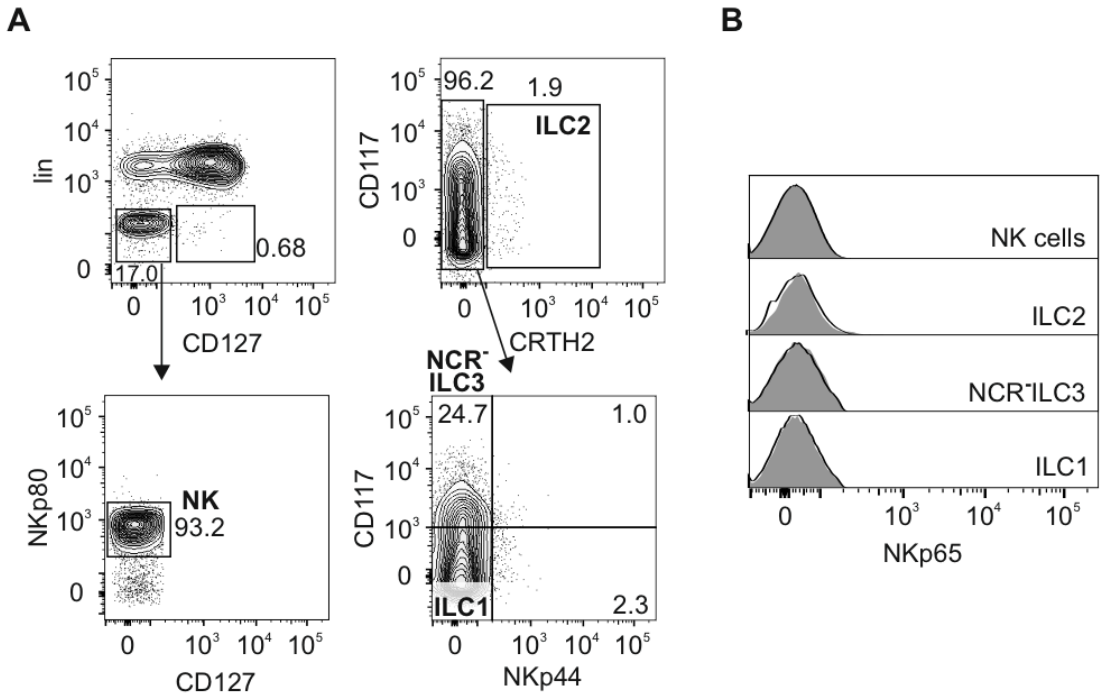

Figure 20: NKp65 is not detected on peripheral blood innate lymphocytes.
Flow cytometric analyses of human peripheral blood ILC for NKp65 surface expression. Representative data from analyses of six unrelated donors. **A**, Lin$^-$CD127$^+$ PBMC were gated for ILC2 (CRTH2$^+$), ILC1 (CRTH2$^-$CD117$^-$ NKp44$^-$) as well as NCR$^-$ ILC3 (CRTH2$^-$CD117$^+$NKp44$^-$) and lin$^-$CD127$^-$ PBMC were gated for NK cells (NKp80$^+$). **B**, NKp65 expression on cells gated as in **A** was analyzed using mAb OMAR1-bio plus SA-APC (solid line). Isotype control stainings are shown as shaded histograms.

4.2 NKp65 expression during NK cell development

A recent series of studies proposed a multi-stage developmental pathway of human NK cells and other innate lymphocytes mostly based on cytometric analyses of tonsillar lymphocytes (Chen et al., 2018; Freud et al., 2016; Freud et al., 2006). According to this model, innate lymphocytes develop from early tonsillar progenitors (ETP1: CD34$^+$, CD117$^-$, IL1R1$^-$ /

ETP2: CD34$^+$, CD117$^+$, IL1R1$^-$) via a common innate lymphocyte progenitor (CILP: CD34$^+$, CD117$^+$, IL1R1$^+$) into ILC3-like progenitor cells (stage 3: CD56$^+$, CD94$^-$, NKp80$^-$, RORγt$^+$; stage 4a: CD56$^+$, CD94$^+$, NKp80$^-$, RORγt$^+$) which ultimately differentiate into *bona fide* mature NK cells (stage 4b: CD56$^+$, CD94$^+$, NKp80$^+$, RORγt$^-$, EOMES$^+$) with NKp80 demarcating mature (stage 4b) NK cells from ILC3-like precursors. NKp80 is continuously expressed also in the more mature stages S5 and S6 that are additionally marked by CD16 expression (Figure 21) (Freud et al., 2016).

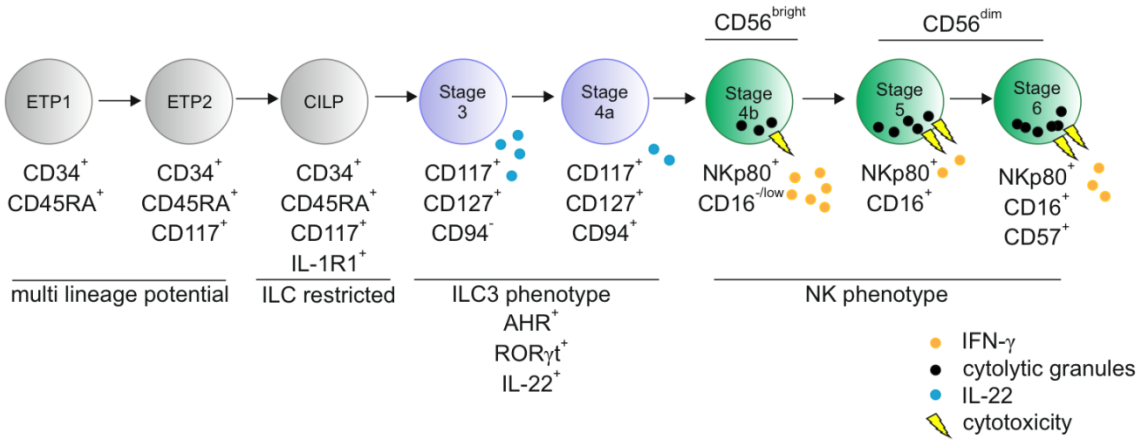

Figure 21: Model of natural killer cell development in secondary lymphoid tissues.
NK cell developmental trajectory from ETP1 to the most mature stage 6 cells according to the expression of CD34, CD117, CD94, NKp80, and CD16. Abbreviations: ETP, early tonsil progenitor; CILP, common innate lymphocyte progenitor; ILC, innate lymphoid cell; AHR, aryl hydrocarbon receptor. Adapted from (Freud et al., 2016).

4.2.1 NKp65 expression on human tonsillar NK cell precursors *ex vivo*

4.2.1.1 NKp65 is not detected on early tonsil progenitors

In order to unravel the role of NKp65 in NK cell development, NKp65 surface expression by various developmental stages of tonsillar innate lymphocytes was assessed by flow cytometry using mAb OMAR1. Dissecting tonsillar cells into the early progenitors with multi lineage potential (ETP1, ETP2) and the ILC committed CILP according to the expression of CD34, CD45-RA, CD117 and IL1-R1, revealed that NKp65 was not expressed by the early progenitors with multi lineage potential (ETP1, ETP2) and the ILC committed CILP (Figure 22).

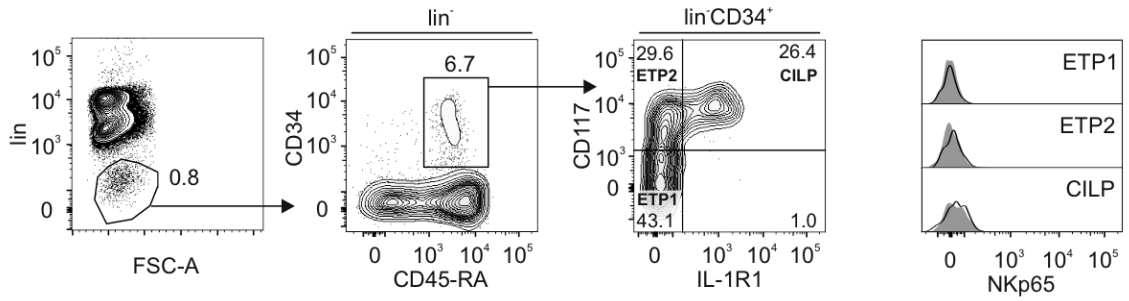

Figure 22: NKp65 is not detected on early tonsil progenitors (ETP).
Flow cytometric analyses of cells isolated from human tonsils. Cells were gated for lin$^-$CD34$^+$CD45-RA$^+$ and dissected into ETP1 (CD117$^-$IL-1R1$^-$), ETP2 (CD117+IL-1R1$^-$) and common innate lymphocyte progenitor (CILP, CD117$^+$IL-1R1$^+$) according to CD117 and IL-1R1 expression. NKp65 expression was analyzed using OMAR1-bio plus SA-PE (black lines). Shaded histograms show the respective isotype stainings (IgG1-bio plus SA-PE). One representative out of three donors analyzed in two independent experiments is shown.

4.2.1.2 NKp65 hallmarks NK cell developmental stages with ILC3-character

Flow cytometric analyses of more mature NK cell developmental stages (stage 3 to 5) dissected by the expression of CD117, CD94, NKp80 and CD16 revealed marked NKp65 expression only on the NKp80$^-$ stage 3 and 4a cells, well in line with their ILC3-character, whereas mature NKp80$^+$ stages 4b and 5 were NKp65$^-$ (Figure 23). Hence, NKp80 and NKp65, although genetically closely related, are mutually exclusively expressed by NK cells and ILC3-like cells, respectively. Of note, in the gating strategy based on the phenotypic definition used in this experiment, stage 3 NK cells are not distinguishable from *bona fide* ILC3. Therefore, it is possible that NKp65 expression on stage 3 cells, originates from ILC3 that are also included in the 'S3-gate'. Nevertheless, the expression of NKp65 on NK cell precursors is demonstrated by the NKp65$^+$ S4a subset, which clearly differs from ILC3 in expression of CD94.

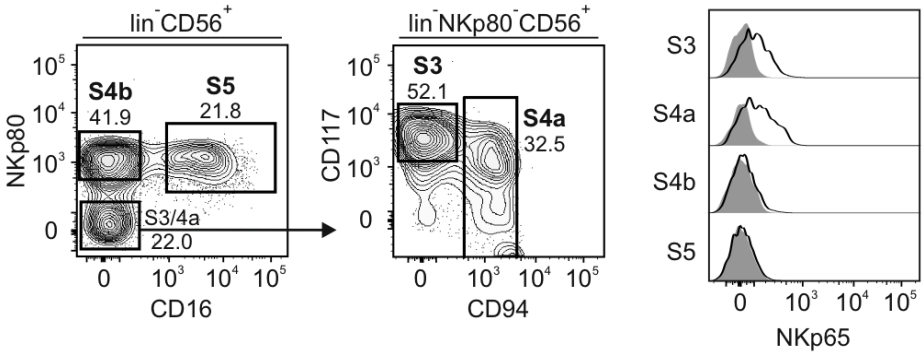

Figure 23: NKp65 is expressed on NK cell developmental stages with ILC3 character.
Flow cytometric analyses of human tonsillar lymphocytes gated for lin$^-$CD56$^+$ and stages S3, S4a, S4b, and S5, respectively, based on their expression of NKp80, CD16, CD117, and CD94 (Freud et al.). NKp65 expression was assessed with OMAR1-bio plus SA-PE (black line). Shown is one representative example out of four donors analyzed in two independent experiments. Shaded histograms represent respective isotype stainings.

4.2.1.3 NKp65 expression at the transition from NK cells to ILC3

In a more recent work, Freud and colleagues studied human NK cell development from tonsillar progenitors in more detail and in the context of the development of other ILC lineages (Chen et al., 2018). In this study ILC3 were demarcated from stage 3 NK cells by the expression of NKp44. The exclusion of ILC3 resulted in a refined definition of stage 3 NK cells with segregation into stages 3a and 3b which are mainly discerned by the expression of CD56 (Figure 24). Both stages were defined as lin$^-$CD34$^-$CD117$^+$ cells and by the lack of surface markers defining mature ILC2 (CRTH2$^+$), cNK cells (CD16$^+$, CD94$^+$, NKG2A$^+$, NKG2C$^+$, KIR2D$^+$, KIR3DL1-2$^+$ and NKp80$^+$) and ILC3 (NKp44$^+$). While the CD56$^-$ stage 3a cells demonstrated NK cell, ILC2 and ILC3 lineage differentiation potential, the CD56$^+$ stage 3b subset represented a physiologic pool of NK cell and ILC3 precursors, only (Chen et al., 2018) (Figure 24). Since ILC3 in human tonsils bimodally express CD56 (Glatzer et al., 2013; Hoorweg et al., 2012), they may also derive directly from CD56$^-$ stage 3a cells. In contrast, NK cells in human tissues usually constitutively express CD56 and a strong dependency of NK cell maturation on CD56 expression has been reported (Mace et al., 2016), indicating that fully mature NK cells traverse the CD56$^+$ stage 3b. Moreover, transdifferentiation between CD117$^+$ NK cells and ILC3 has been reported (Chen et al., 2018) (Figure 24).

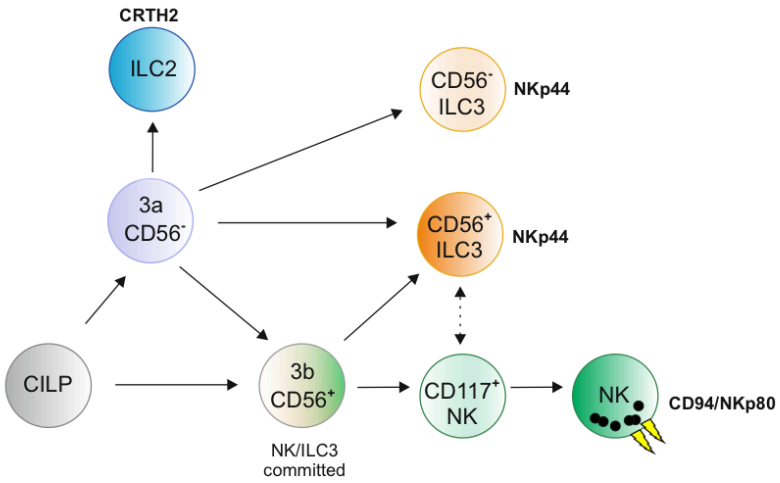

Figure 24: Model of human ILC development in tonsils.
Developmental trajectory from the common innate lymphocyte progenitor (CILP) into the different innate lymphoid cell (ILC) lineages ILC2, ILC3 and cNK cells via the CD56$^-$/CD56$^+$ stages 3a and 3b. Markers used to identify the finally mature cell subsets hereinafter are shown in bold type. Developmental transitions between the indicated populations are represented by solid black arrows, the dashed arrow represents transdifferentiation between CD117$^+$ NK cells and CD117$^+$ ILC3. Adapted from (Chen et al., 2018).

To investigate the expression of NKp65 on these precursors of ILC3 and NK cell development, tonsillar MNC were analyzed by flow cytometry and gated for the stages 3a and 3b as well as $CD56^+/CD56^-$ ILC3 and $CD117^+/CD117^-$ NK cells (Figure 25A). Analyses of NKp65 expression on these subsets revealed that the stages 3a and 3b express neglectable levels of NKp65, but repeatedly showed distinct expression of NKp65 on ILC3, both $CD56^+$ and $CD56^-$. Additionally, NKp65 was detected on $CD117^+$ (stage 4a) NK cells, whereas fully mature $CD117^-$ NK cells were $NKp65^-$ (Figure 25B). Comprehensive data of cytometric analyses of tonsillar ILC from three independent donors showed highest NKp65 expression (SFI) for ILC3 with no significant difference between the $CD56^-$ and $CD56^+$ subsets, as well as significantly less NKp65 expression on $CD117^+$ NK cells (S4a) and barely detectable levels on S3a, S3b and $CD117^-$ NK cells (Figure 25C). Hence, marked NKp65 expression precisely designated cells with ILC3 character.

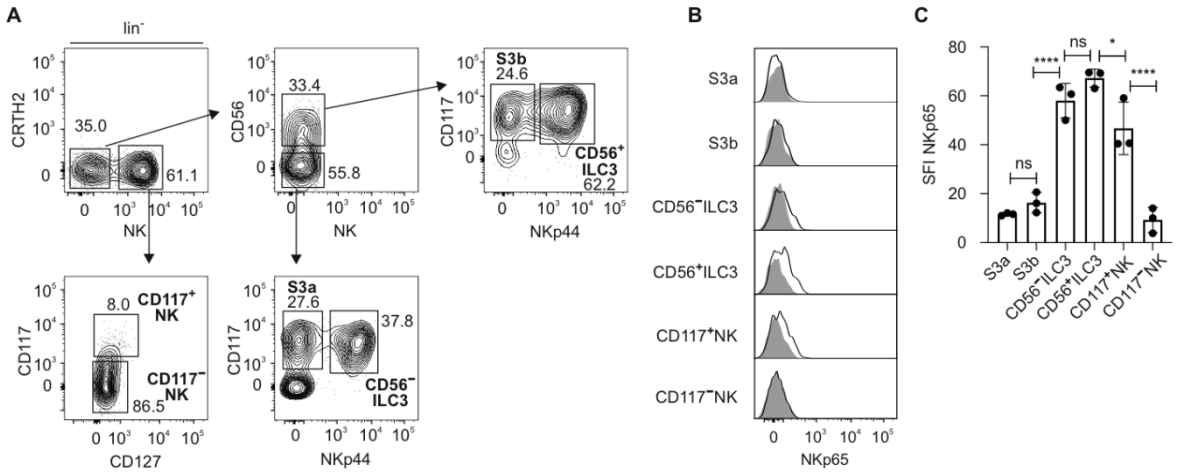

Figure 25: NKp65 expression segregates early ILC progenitors from ILC3-like cells.
A-C, Flow cytometric analyses of human tonsillar mononuclear cells. **A**, Gating strategy to discern the different developmental stages and mature cells according to their phenotypic definition, pre-gated for lin^-, live cells and shown for one representative out of three independent experiments. Cells were gated for stage 3a (S3a; $NK^-CRTH2^-NKp44^-CD56^-CD117^+$), S3b ($NK^-CRTH2^-NKp44^-CD56^+CD117^+$), $CD56^-/CD56^+$ ILC3 ($NK^-CRTH2^-NKp44^+$) and $CD117^-/CD117^+$ NK cells (NK^+CRTH2^-), respectively. Lineage (lin) refers to CD3, CD14, CD19 and CD34; NK refers to CD94 and NKp80. **B**, NKp65 expression was assessed on the different subsets gated as shown in **A** using OMAR1-bio plus SA-APC (black lines). Shaded histograms represent respective isotype control staining (IgG1-bio plus SA-APC). **C**, Compiled data of three independent analyses of tonsillar cells from three unrelated donors. Bars represent mean ± s.d. of NKp65 specific fluorescence intensity (SFI), each circle represents one donor. Statistical significance was calculated using one-way ANOVA with Tukey's post hoc test (ns, not significant, $*P < 0.05$, $****P < 0.0001$).

4.2.2 NKp65$^+$ S4a cells are present in human skin

As mentioned in the introduction, NKp65 expressing ILC3 were also detected in human skin (1.5.2.2). However, in this preliminary analysis stage 4a NK cells were not analyzed. Therefore, ILC derived from human juvenile foreskin were analyzed for NKp65 expression by flow cytometry using OMAR1, confirming NKp65 expression on ILC3, characterized as lin$^-$CD127$^+$CD117^{high}CD94$^-$ cells. Moreover, CD94$^+$ S4a NK cell precursors (lin$^-$CD127$^+$CD117^{int}CD94$^+$) which were detected among tonsillar ILC (Figure 23), were also present in human skin and markedly expressed NKp65 (Figure 26).

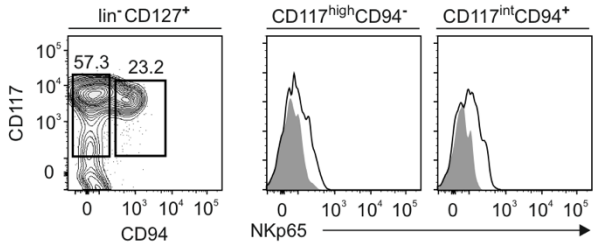

Figure 26: NKp65 is expressed on human skin ILC3 and ILC3-like cells.
Flow cytometric analysis of NKp65 expression on ILC3 (lin$^-$CD127$^+$CD117^{high}CD94$^-$) and ILC3-like stage 4a cells (lin$^-$CD127$^+$CD117^{int}CD94$^+$) among freshly isolated cells from dermis of juvenile foreskin. NKp65 expression was detected using OMAR1-bio + SA-PE (black line). Isotype control stainings are filled. Lineage markers (lin): CD3, CD14, CD19, CD34.

4.3 NKp65 expression on ILC precursors *in vitro*

To further characterize the expression of NKp65 during ILC development, NKp65-expressing cells were established by *in vitro*-differentiation from human CD34$^+$ hematopoietic stem and progenitor cells (HSPC). The following results are based on a preliminary study by Dr. Isabel Vogler who could show for the first time that NKp65 expressing cells develop from CD34-enriched cells from healthy human donors *in vitro* in cocultures with irradiated EL08.1D2 cells and cytokines as reported elsewhere (Ahn et al., 2013). The following experiments were done following this established protocol, except for the change to the more commonly used OP9-feeder cell system.

4.3.1 NKp65$^+$ cells differentiate *in vitro* from CD34$^+$ HSPC

Starting from CD34$^+$ HSPC that were MACS-purified to 97% purity from human PBMC (Figure 27A), development of ILC as well as NKp65 expression was monitored by weekly flow cytometric analyses using previously described markers to discern the different ILC subsets (Table 1). Analyses after seven days in culture revealed that among cells gated for different

developmental subsets (Figure 27B) including HSC ($CD34^+CD45\text{-}RA^-$), ETP ($CD34^+CD45\text{-}RA^+$), CILP ($CD34^+CD45\text{-}RA^+CD117^+$) and immature innate lymphocytes (iILC, $CD45\text{-}RA^+CD34^-CD56^-$), a small population of lin^-CD56^+ cells had acquired slight NKp65 expression, exclusively (Figure 27C).

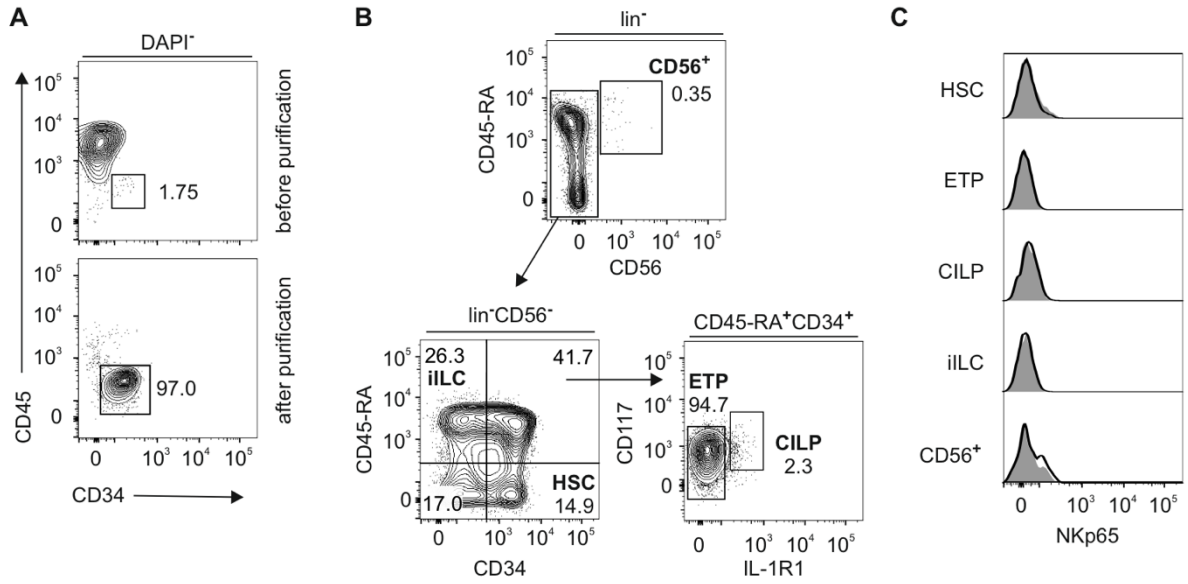

Figure 27: NKp65 expression first emerges on $CD56^+$ lymphocytes *in vitro*.
A, Purity of MACS-purified $CD34^+$ hematopoietic stem and progenitor cells (HSPC) determined by flow cytometric analyses of CD34 and CD45 expression before (upper panel) and after (lower panel) MACS-purification from human PBMC. **B**, **C**, Flow cytometric analyses of *in vitro* differentiated cells at day seven in culture. **B**, Cells (pre-gated for lin^-, live cells) were analyzed for CD45-RA, CD34, IL-1R1 and CD56 expression to dissect HSC ($CD34^+CD45\text{-}RA^-$), early tonsil progenitors (ETPs, $CD34^+CD45\text{-}RA^+IL\text{-}1R1^-$), common innate lymphocyte progenitor (CILP, $CD34^+CD45\text{-}RA^+IL\text{-}1R1^+$), immature innate lymphocytes (iILC, $CD34^-CD45\text{-}RA^+$) and $CD56^+$ lymphocytes. **C**, NKp65 expression was analyzed on subsets of early ILC development gated as in **B** using OMAR1-bio plus SA-PE (black lines). Shaded histograms represent isotype control stainings (IgG1-bio plus SA-PE).

In vitro innate lymphocyte (ivILC) maturation from $CD34^+$ HSPC into $CD56^+$ lymphocytes, exemplarily shown for one donor (Figure 28), was further assessed by monitoring the frequencies of $CD34^+$ cells, which constantly decreased from 58% at day seven to 6% at day 21. Downregulation of CD34 was accompanied by upregulation of CD56 (Figure 28A, B). Whereas at day seven frequencies of $CD56^+$ cells were less than 1%, at day 21 52% of the cells had acquired CD56 expression. During the time course of this analysis the lack of NKp65 expression on early $CD56^-$ precursors persisted (data not shown), whereas NKp65 expression on rapidly expanding $CD56^+$ lymphocytes increased (Figure 28C).

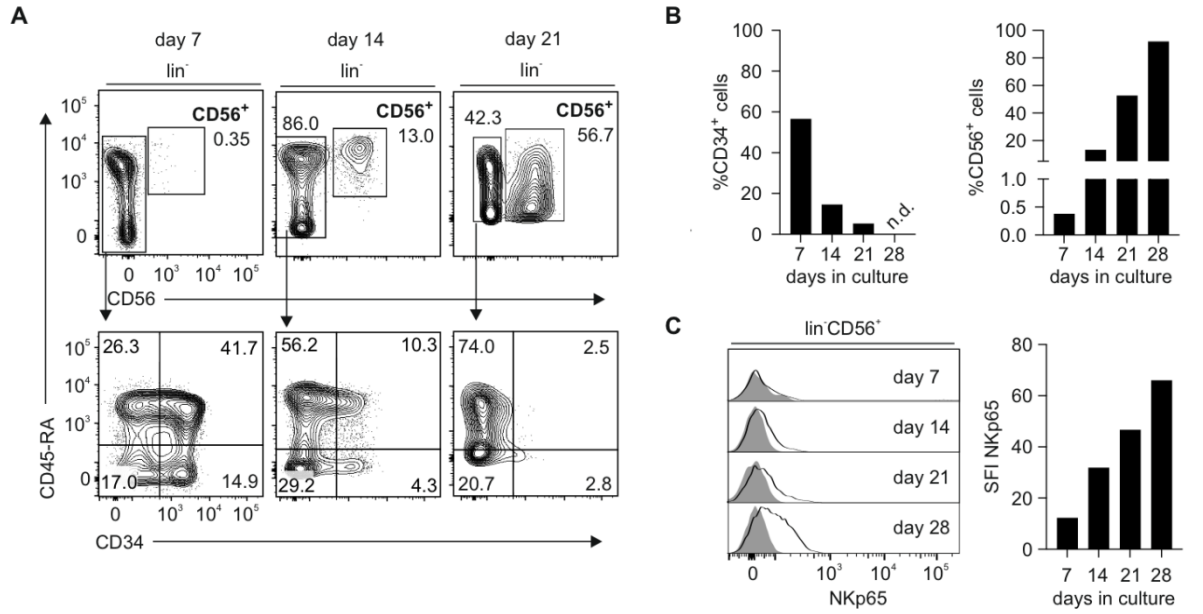

Figure 28: *In vitro* development of NKp65 expressing CD56$^+$ lymphocytes.
Representative flow cytometric analyses of i*n vitro* differentiated innate lymphocytes (ivILC) **A**, ivILC were analyzed for CD34, CD45-RA and CD56 expression at day 7, day 14 and day 21 in culture. **B**, Bar diagrams depict percentages of CD34$^+$ (left) and CD56$^+$ (right) cells at different time points analyzed as in **A** (n.d., not detected). **C**, Left, histograms of NKp65 expression on lin$^-$CD56$^+$ ivILC at day 7, 14, 21 and 28 in culture analyzed by OMAR1-bio plus SA-PE (black line) and isotype control stainings (shaded histograms). Right, respective bar diagram showing the specific fluorescence intensity (SFI) of NKp65 expression.

After 28 days in culture, the majority of cells represented CD56$^+$ innate lymphocytes. This rapid development into CD56$^+$ lymphocytes, exemplarily shown for two cohorts each including three donors, cultivated in parallel (Figure 29A), was consistent for all 45 donors analyzed.

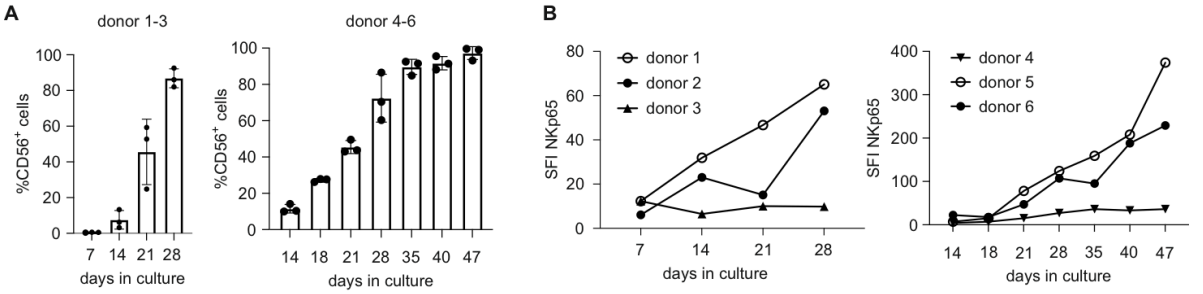

Figure 29: Inter-individual variability of NKp65 expression on *in vitro* differentiated innate lymphocytes (ivILC).
Flow cytometric analyses of cultured ivILC at different timepoints within day 7 to 28 or 14 to 47. ivILC were established from six donors in two experiments with three donors each. **A**, Percentages of CD56$^+$ cells among lin$^-$ live cells. Bars represent mean ± s.d., each circle represents one donor. **B**, NKp65 expression on lin$^-$CD56$^+$ ivILC shown as specific fluorescence intensity (SFI) over time, determined by OMAR1-bio plus SA-PE and respective isotype staining. Data shown are representative examples for a total of 45 donors analyzed.

Flow cytometric analyses of NKp65 expression on the CD56$^+$ cells revealed that although for most of the donors NKp65 expression increased with time in culture, the strength of

expression varied and some donors only sparsely expressed NKp65 within the time period of analysis (Figure 29B). This inter-individual variability of NKp65 expression was also observed in analyses of tonsillar ILC3 from 20 different donors (Figure 16).

4.3.1.1 NKp65 expression on ILC3-like cells can be recapitulated *in vitro*

Analyzing $CD56^+$ ivILC based on the definition of NK cell maturation stages used before (Figure 20), segregated the $CD56^+$ cells into two major subpopulations, $CD117^{high}CD94^-$ (stage S3) and $CD117^{int}CD94^+$ (stage S4a) cells that both markedly expressed NKp65 (Figure 30). In contrast, NKp65 expression on the minute populations of stages S4b and S5 was barely detectable. However, like tonsillar ILC (Figure 23), ivILC showed a mutually exclusive expression of NKp80 and NKp65 since mature NK cell stages S4b and S5, both marked by the expression of NKp80, were $NKp65^-$ (Figure 30).

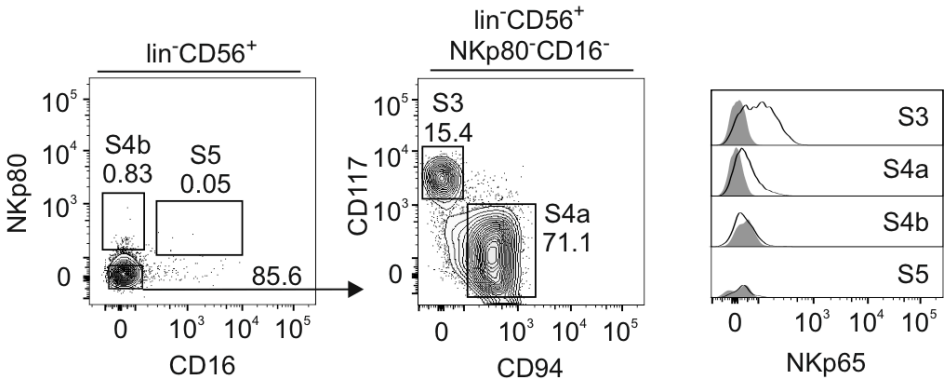

Figure 30: NKp65 expressing ILC3-like cells can be recapitulated *in vitro*.
Representative flow cytometric analyses of *in vitro* differentiated innate lymphocytes (ivILC) at day 28 in culture pre-gated for lin^-CD56^+ (left). NK cell developmental stages were dissected by NKp80, CD16, CD117 and CD94 expression (left, middle) and NKp65 surface expression analyzed on stage 3 (S3, $CD117^{high}CD94^-$), stage 4a (S4a, $CD117^{int}CD94^+$), stage 4b (S4b, $NKp80^+CD16^-$) and stage 5 (S5, $NKp80^+CD16^+$) cells using OMAR1-bio plus SA-PE (black lines, right). Isotype stainings are shown as shaded histograms.

4.3.1.2 NKp65 expression and the trajectory of *in vitro* NK cell and ILC3 development

Monitoring the frequencies of S3 and S4a cells over time, exemplarily shown for one donor, revealed that frequencies of $CD117^{int}CD94^+$ S4a cells expand at the expense of $CD117^{high}CD94^-$ S3 cells (Figure 31A), indicative of a developmental pathway from S3 to S4a as also suggested by Caligiuri et al.. Analyzing NKp65 expression over time on these subsets showed that NKp65 was first expressed by $CD117^{high}CD94^-$ S3 cells (day seven). Conversely, $CD94^+$ S4a cells, although already present at day seven, were $NKp65^-$ and acquired NKp65 expression at later time points (from day 14 on) (Figure 31B).

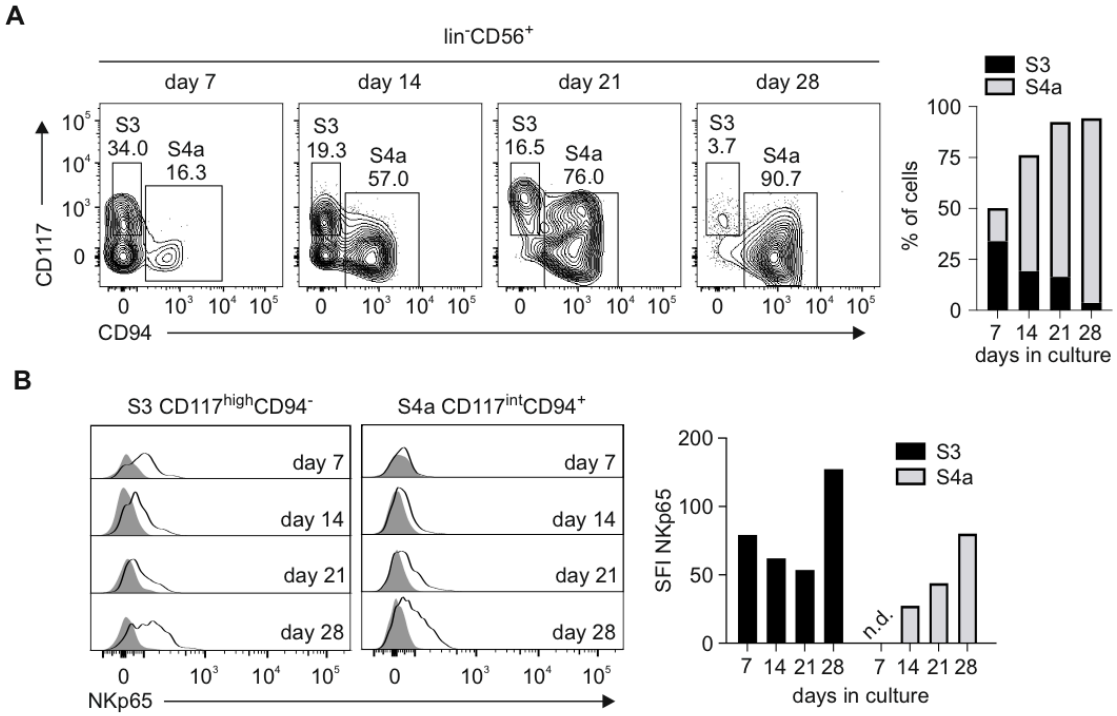

Figure 31: NKp65 expression in the trajectory of *in vitro* NK cell and ILC3 development.
Flow cytometric analyses of *in vitro* differentiated stage 3 (S3) and stage 4a (S4a) cells at day 7, 14, 21 and 28 in culture. Cells were pre-gated for lin$^-$CD56$^+$ cells and S3 and S4a cells segregated by CD117 and CD94 expression. **A**, Percentages of S3 and S4a cells among lin$^-$CD56$^+$ cells at different time points, shown as contour plots (left) and bar diagram (right). **B**, Assessment of NKp65 expression on S3 and S4a cells gated as in **A** by OMAR1-bio plus SA-PE and respective isotype control staining, shown as histogram overlays (left) of NKp65 (black line) and isotype staining (grey shaded) or as specific fluorescence intensity (SFI) in a bar diagram (right).

As seen for NKp65 expression, also the distribution of S3 and S4a cells was inter-individually variable, with some donors showing higher proportions of CD94$^+$ cells, whereas others had a more stable CD117^{high} phenotype as exemplarily shown for one such donor in Figure 32A. Although the frequencies of the different cell types varied, NKp65 expression was detected on both subsets (Figure 32B). The long-term persistence (up to 67 days) of S3 cells, suggests that these cells belong to a stable lineage rather than being a NK cell precursor. This assumption was further corroborated by comparison of flow cytometric analyses at day 15 and 53. At day 15 the CD117$^-$CD94$^-$ population is to some extent intermingled with the S3 and S4a populations, whereas at day 53 the vast majority of cells had developed into two distinct populations of S3 and S4a cells, respectively (Figure 32). Therefore, S3 cells might be considered as *in vitro* differentiated ILC3 (ivILC3) well in line with a study by Tang et al. describing the differentiation of ivILC3 with equal phenotype in an *in vitro* coculture system with El08.1D2 cells (Ahn et al., 2013).

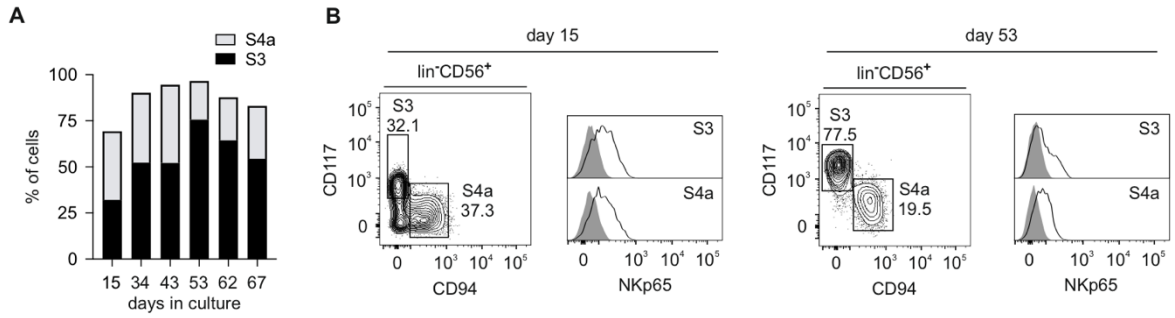

Figure 32: Long-term persistence of NKp65$^+$ stage 3 cells *in vitro*.
Analyses of *in vitro* differentiated stage 3 (S3) and stage 4a (S4a) cells at day 15, 34, 43, 53, 62 and 67 in culture by flow cytometry. Cells were pre-gated for lin$^-$CD56$^+$ cells and S3 and S4a cells segregated by CD117 and CD94 expression. **A**, Percentages of S3 and S4a cells among lin$^-$CD56$^+$ cells at different time points. **B**, Gating of S3 and S4a cells exemplarily shown at days 15 and 53 and analysis of NKp65 expression on these populations assessed by OMAR1-bio plus SA-PE staining (black line). Shaded histograms represent the respective isotype control stainings. Same results were observed for *in vitro* differentiated cells derived from CD34$^+$ hematopoietic stem cells of at least four independent human donors.

4.3.2 Phenotypic characterization of *in vitro* generated NKp65 expressing cells

The presence of S4a cells in the *in vitro* cultures demonstrates that the conducted conditions provide an environment allowing for their development from CD34$^+$ HSPC. Presuming that S3 cells are precursors of S4a cells, long term cultures should finally contain mainly S4a cells. Instead, although varying in frequencies, CD117^{high}CD94$^-$ S3 cells developed consistently for every donor and mostly persisted in culture even after several weeks. Hence, the sustained presence of CD117^{high}CD94$^-$ cells indicates that this population corresponds to a stable lineage, according to their phenotype most likely ILC3, rather than to a precursor subset of NK cells. In order to corroborate their phenotyping as ivILC3, the TF expression profile as well as the cytokine response of the CD117^{high}CD94$^-$ population was further analyzed.

4.3.2.1 Analysis of the transcription factor expression profile of *in vitro* differentiated NKp65$^+$ cells

In order to further characterize the phenotype of NKp65-expressing ivILC they were analyzed for transcription factor (TF) expression by flow cytometry (Figure 33). Segregation of S3 and S4a cells and analysis of RORγt and EOMES expression revealed that in contrast to reports of tonsillar stage S4a lymphocytes expressing RORγt (Freud et al., 2016), S4a ivILC were RORγt$^-$EOMES$^+$ (Figure 33A). Stage S3 ivILC markedly expressed RORγt but were EOMES$^-$ further confirming their ILC3 character (Figure 33B). Additionally, whereas EOMES$^+$ ILC from human tonsils were NKp65$^-$ (Figure 18), EOMES$^+$ ivILC markedly expressed NKp65, as did RORγt$^+$ S3 cells (Figure 33B).

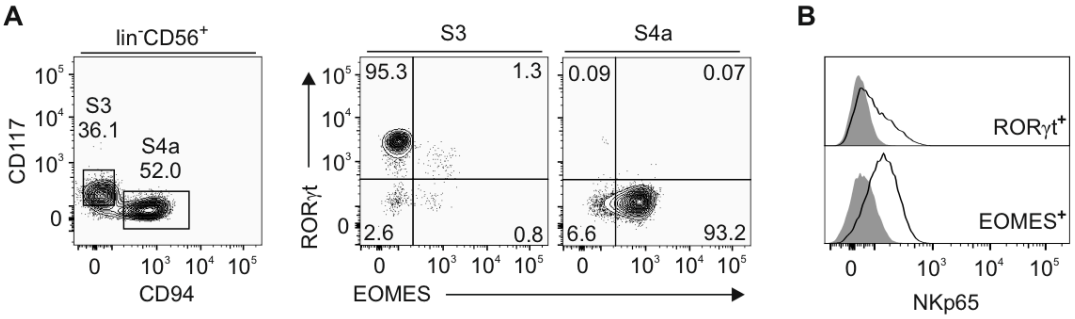

Figure 33: *In vitro* generated EOMES$^+$ and RORγt$^+$ cells express NKp65, respectively.
Representative flow cytometric analyses of permeabilized *in vitro* differentiated cells at day 30 in culture. **A**, Cells were pre-gated for lin$^-$CD56$^+$ and stages S3 and S4a analyzed for RORγt and EOMES expression. **B**, NKp65 expression on RORγt$^+$ S3 and EOMES$^+$ S4a cells gated as in (**A**) was assessed by OMAR1-bio plus SA-APC staining (black line), respective isotype stainings are shown as shaded histograms.

4.3.2.2 Cytokine response of *in vitro* innate lymphocytes

Besides the analysis of surface markers and intracellular signature TFs, the specific response of ILC to certain cytokines was conducted for their characterization. Hence, ivILC were stimulated with either ILC subset-specific cytokines e.g. IL-1β/IL-23 (ILC3) or IL-12/IL-18 (cNK) or with phorbol 12-myristate 13-acetate (PMA) and Ionomycin and subsequently assessed for intracellular cytokine production via flow cytometry. To discriminate between ILC3-like S3 and S4a NK cells, cells were gated for lin$^-$ CD56$^+$CD117^{high}CD94$^-$ (S3) and lin$^-$ CD56$^+$CD117^{low}CD94$^+$ (S4a), respectively (Figure 34A).

ILC3-like S3 cells exclusively responded to IL-1β and IL-23 stimulation by production of IL-22 and to some extent GM-CSF, whereas no IFN-γ production was observed. Stimulation with the NK cell activating cytokines IL-12 and IL-18 did not stimulate ILC3-like S3 cells to produce any of the cytokines analyzed (Figure 34B). Additionally, stimulation with PMA and Ionomycin (P/I) induced production of IL-22 and GM-CSF but not IFN-γ. In contrast, S4a cells did only marginally respond to IL-1β and IL-23, with all analyzed cytokines being produced by less than 5% of the cells. Instead, IL-12 and IL-18 stimulation led to strong IFN-γ response, and to a lesser extent to GM-CSF production. The expression of IL-22 was not observed for the S4a population even in the presence of P/I, which strongly induced IFN-γ and GM-CSF expression (Figure 34B).

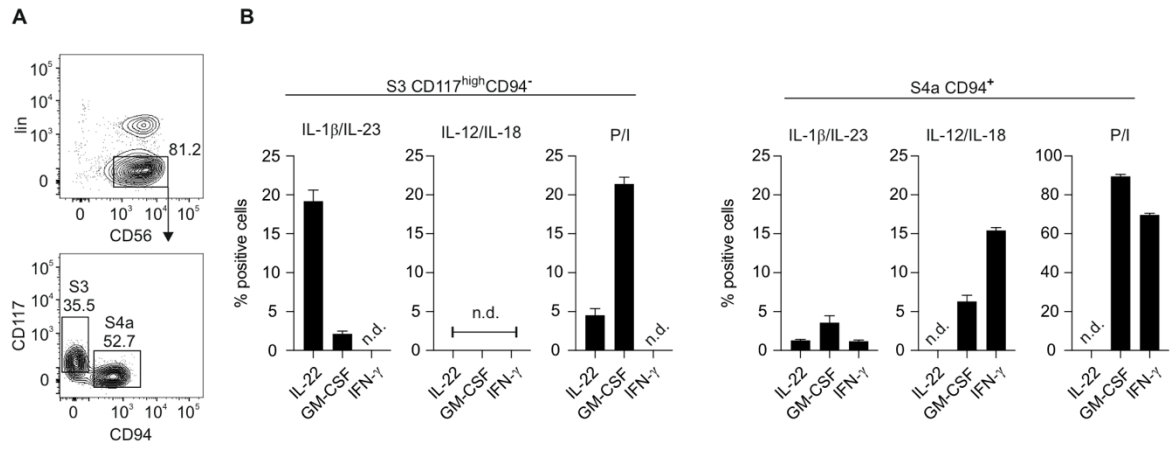

Figure 34: *In vitro* differentiated innate lymphoid cells (ivILC) respond to cytokines according to their phenotype.
A, **B**, In vitro ILC at day 41 in culture were stimulated for 4.5 h with IL-1β/IL-23, IL-12/IL-18 or PMA/Ionomycin (P/I) prior to permeabilization and analyses of intracellular IL-22, GM-CSF or IFN-γ production via flow cytometry. **A**, To dissect cells in stage 3 (S3) from cells in S4a, as shown in the contour plot, cells were gated for lin$^-$CD56$^+$CD117^{high}CD94$^-$ (S3) and lin$^-$CD56$^+$CD94$^+$ (S4a). **B**, Cytokine production is shown for S3 (left) and S4a (right) cells as percentage of positive cells among the respective subset. Bars represent mean ± s.d. of technical triplicates.

In summary these data demonstrate that based on the specificity of their response to signature cytokines CD94$^-$CD117^{high} S3 cells can be characterized as ivILC3, whereas the CD94$^+$CD117^{low} population shows NK cell character, well in line with the phenotypic analyses based on the expression of surface markers and TFs. Additionally, these data reveal that ivILC are functionally active.

4.3.3 NKp65 expression is downregulated during *in vitro* NK cell development

The observation that NKp65 expression marks an immature phenotype of developing NK cells (EOMES$^+$ S4a cells) was further investigated by intracellular transcription factor staining. The T-box transcription factors EOMES and T-bet were shown to be critically involved in the development and maturation of NK cells. During peripheral maturation NK cells upregulate T-bet expression and downregulate EOMES (Simonetta et al., 2016). Hence, cytokine producing CD56^{bright} NK cells express higher levels of EOMES and lower levels of T-bet than the cytotoxic CD16$^+$CD56^{dim} population. Terminally differentiated NK cells with a CD57$^+$CD56^{dim} phenotype express the highest levels of T-bet and the lowest levels of EOMES (Figure 35A). Therefore, the maturation state of NK cells can be valued based on T-bet and EOMES expression. Flow cytometric analyses of ivILC (day 40) using these markers and the mAb OMAR1 to detect NKp65 expression revealed highest expression of NKp65 on the least mature EOMES$^+$T-bet$^-$ subset, intermediate levels on the EOMES$^+$T-bet$^+$ population and low levels on the most mature EOMES$^-$T-bet$^+$ subset (Figure 35B). Thus, downregulation of NKp65

expression was accompanied by downregulation of EOMES and upregulation of T-bet expression, e.g. NK cell maturation. However, even after up to 60 days in culture, only a minute population showed characteristics of mature NK cells as marked by NKp80 (data not shown), indicating a lack of certain essential signals in the *in vitro* system.

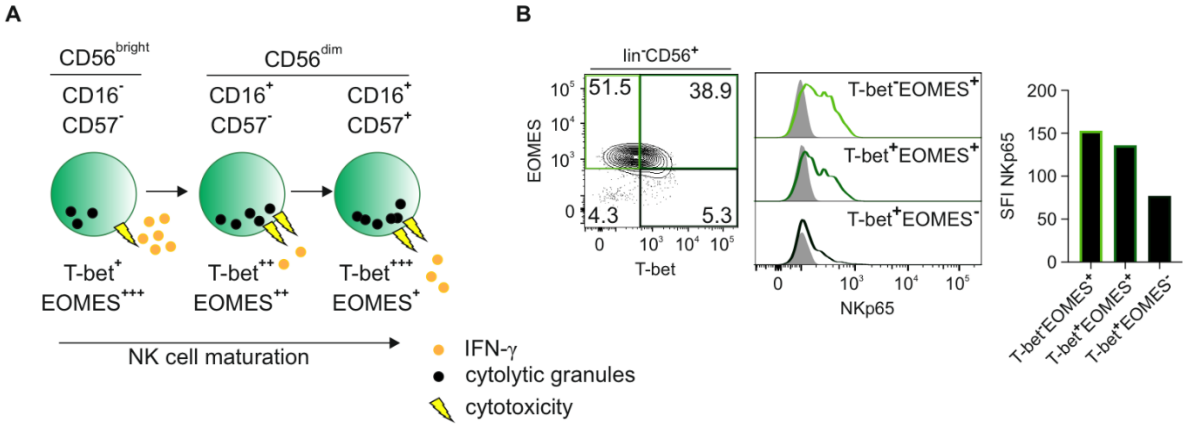

Figure 35: NKp65 expression is downregulated upon *in vitro* NK cell maturation.
A, Schematic depiction of NK cell maturation based on expression of T-bet and EOMES, adapted from (Simonetta et al., 2016). **B**, Flow cytometric analysis of permeabilized *in vitro* differentiated innate lymphocytes at day 40 in culture, pre-gated for lin$^-$CD56$^+$live cells. Maturation stages of NK cells were distinguished based on T-bet and EOMES expression and NKp65 expression analyzed by OMAR1-bio plus SA-BV421 staining (solid lines in histograms), grey shaded histograms represent isotype control stainings. NKp65 expression is also depicted as specific fluorescence intensity (SFI) in a bar diagram. Shown are data from one representative of two independent experiments with cells derived from three independent donors.

4.4 Notch dependency of *in vitro* NK cell development

4.4.1 Notch signaling is critically important for the development of NKp80$^+$ cells

Notch signaling is critical for T cell development and has also been reported to be involved in the development of ILC and NK cells (Radtke et al., 2013). The OP9-feeder cell system is frequently used to study T cell development in the presence or absence of Notch signaling (Schmitt and Zuniga-Pflucker, 2002), making use of OP9 cells transduced with the Notch ligands delta like canonical Notch ligand (DLL) 1 and 4.

To unravel the role of Notch signaling in ivILC development, CD34$^+$ HSPC were cultured on OP9 cells transduced with DLL1 (OP9-DLL1) or mock transduced cells (OP9-mock) in the presence of IL-7, stem cell factor (SCF), Fms-like tyrosine kinase 3 ligand (Flt3-L) and IL-15. Initiating cultures on the OP9-DLL1 feeder cell line, did not lead to sufficient development of ivILC (data not shown). Accordingly, CD34$^+$ HSPC were first cultured on OP9-mock feeder cells and developing ILC were subsequently transferred to OP9-DLL1 feeder cells. ivILC conducted to this procedure were then monitored for NKp65 expression and regarding their

developmental stage by flow cytometry using the previously described surface markers and signature TFs. In experiments shown in the previous section OP9-mock cells were used exclusively. As shown in (Figure 30) the frequencies of NKp80 expressing cells in these cultures were sparse. In contrary, ivILC that were cultured for several weeks on OP9-mock cells and subsequently transferred to OP9-DLL1 cells, not only acquired NKp80 expression (stage 4b), but also developed into even more mature NKp80^{+}CD16^{+} stage 5 cells (Figure 36A). In a parallel control experiment with OP9-mock cells ivILC remained in the NKp80^{-} stages S3 and S4a (Figure 36B).

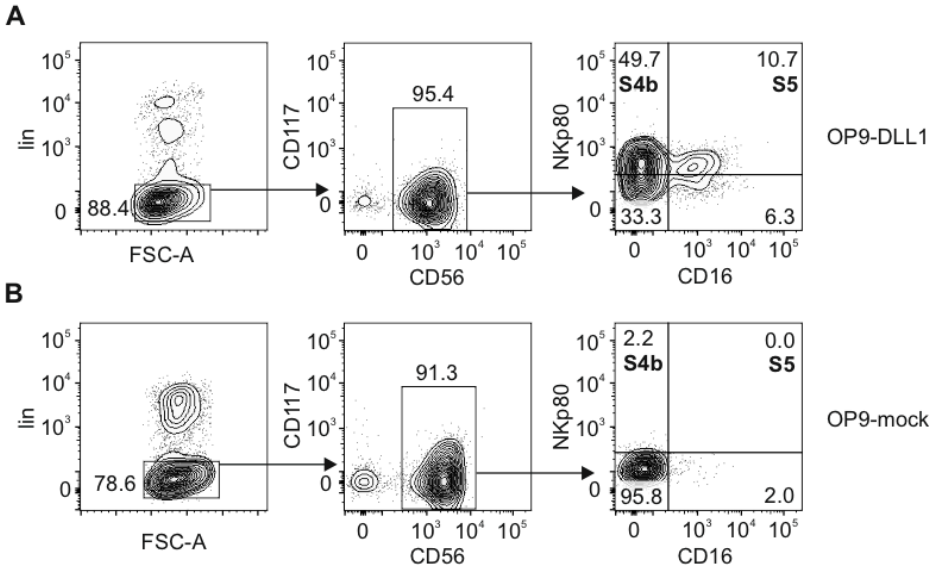

Figure 36: *In vitro* development of NKp80^{+} NK cells is dependent on Notch signaling.
A, **B**, Flow cytometric analyses of *in vitro* differentiated innate lymphocytes for NKp80 and CD16 expression. Cells were cultivated for 28 days on OP9-mock cells and subsequently either transferred to OP9-DLL1 cultures (**A**) or sustained on OP9-mock cells (**B**) for additional seven days prior to flow cytometric analysis. Shown is one representative of three independent experiments with cells generated from three independent donors.

Flow cytometric analyses of NK cell development based on the expression of T-bet and EOMES further revealed that in cocultures with OP9-DLL1 cells the majority of cells were in the most mature EOMES^{-}T-bet^{+} stage (65.2%), whereas in control cultures with OP9-mock cells only 6.1% exhibited this phenotype and the majority of cells persisted in the less mature EOMES^{+}T-bet^{-} stage (Figure 37A). Moreover, in OP9-DLL1 cocultures, NKp80 was markedly expressed by cells of every subset analyzed. In OP9-mock cocultures, despite of a minute increase in the EOMES^{-}T-bet^{+} stage, NKp80 expression of ivILC was neglectable (Figure 37 A, B). In conclusion, the presence of Notch ligands severely promotes NK cell maturation and is critically essential for NKp80 expression.

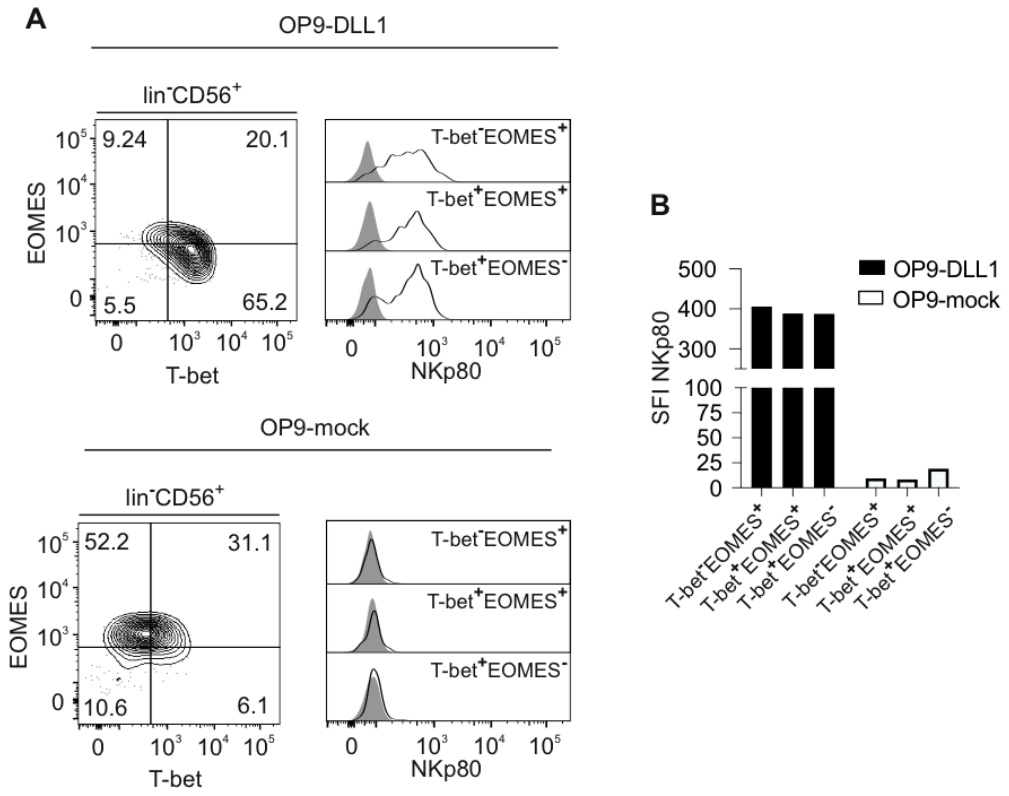

Figure 37: NKp80 expression is critically dependent on Notch signaling *in vitro*.
Flow cytometric analyses of permeabilized *in vitro* differentiated innate lymphocytes for EOMES, T-bet and NKp80 expression. Cells were cultivated for 28 days on OP9-mock cells and subsequently either transferred to OP9-DLL1 cultures (**A**, upper panel) or sustained on OP9-mock cells (**A**, lower panel) for additional seven days. **A**, Pre-gated for lin$^-$CD56$^+$ live cells, cells were separated into different NK cell maturation stages based on the expression of EOMES and T-bet. NKp80 expression for each subset is depicted as solid black line in histogram overlays with the respective isotype control staining shown as shaded histograms. **B**, Bar diagram of specific fluorescence intensity (SFI) of NKp80 expression on NK cell maturation stages gated as in **A**. Shown is one representative of three independent experiments with cells generated from three independent donors.

4.4.2 Downregulation of NKp65 expression upon Notch ligand induced NK cell maturation

Whereas NKp80 expression was enhanced on ivILC upon coculture with OP9-DLL1 cells, flow cytometric analyses of NKp65 expression revealed that NKp65 expression was reduced on all EOMES and/or T-bet expressing developmental subsets (Figure 38A) with the most severe effects observed for EOMES$^-$T-bet$^+$ cells. Of note, Notch induced downregulation of NKp65 expression was accompanied by reduced frequencies of NKp65+ cells among the different subsets (Figure 38B), suggesting that upon development into NKp80 expressing NK cells, ivILC lose NKp65 expression.

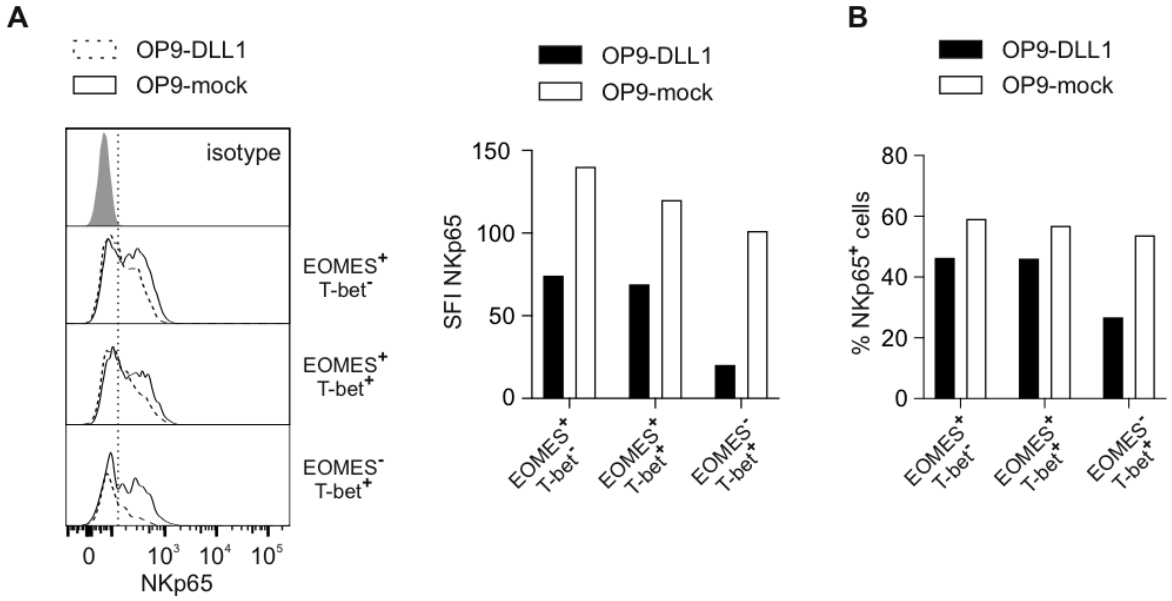

Figure 38: NKp65 expression is downregulated upon Notch induced NK cell development.
A, **B**, After induction of in vitro innate lymphocytes (ivILC) development in cocultures with OP9-mock feeder cells for 28 days, ivILC were transferred to cocultures with either OP9-DLL1 or sustained on OP9-mock feeder cells for additional seven days prior to permeabilization and flow cytometric analysis of phenotypic surface markers, T-bet, EOMES and NKp65 expression. **A**, Cells were gated for lin$^-$CD56$^+$ and segregated into different maturation stages based on EOMES and T-bet expression. NKp65 expression was analyzed on cells from OP9-DLL1 (dashed line) or OP9-mock cocultures by OMAR1-bio plus SA-BV421 staining. One representative isotype staining is shown as grey shaded histogram (**A**, **left**). NKp65 expression depicted as bar diagram of specific fluorescence intensity (SFI) of the different subsets (**A**, **right**). **B**, Percentages of NKp65$^+$ cells among the different NK cell maturation stages gated as in **A**. One representative of three independent experiments with cells derived from three different donors is shown.

4.4.3 NKp65$^+$ cells differentiate into NKp80$^+$ mature NK cells in the presence of Notch ligands

To investigate whether the NKp65 expressing S4a cells actually are precursors of NKp80 expressing mature NK cells, NKp65 expressing cells developed on OP9-mock cells were FACSorted (Figure 39) and subsequently seeded on OP9-mock or OP9-DLL1 cells.

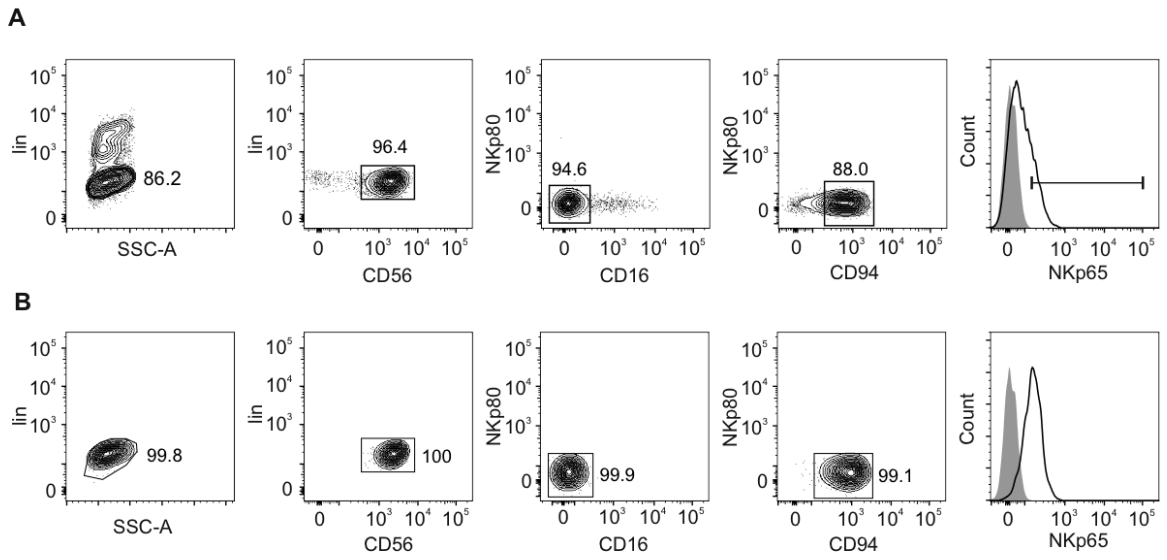

Figure 39: FACS-based purification of *in vitro* differentiated NKp65$^+$ innate lymphoid precursor cells.
A, Flow cytometric analysis of *in vitro* differentiated innate lymphoid cell precursor cells before FACsorting of NKp65$^+$ cells. Lin$^-$NKp80$^-$CD16$^-$CD56$^+$CD94$^+$NKp65$^+$ cells were FACsorted as indicated. **B**, Flow cytometric analysis of FACsorted NKp65$^+$ precursor cells. **A**, **B**, Cells were stained for NKp65 expression using OMAR1-bio plus SA-PE. Numbers in contour plots indicate the respective percentages of gated cells.

After five days in coculture these cells were analyzed for NKp80, NKp65 and CD16 expression by flow cytometry. As also seen for the bulk cultures (Figure 36), NKp65 expressing cells effectively developed into mature NKp80$^+$ S4b and NKp80$^+$CD16$^+$ S5 cells in the presence of the Notch ligand DLL1, whereas no NKp80 expressing cells developed in OP9-mock cocultures (Figure 40A). Induction of NKp80 and final NK cell maturation was not only observed in cocultures with OP9-DLL1 cells, but also in cocultures with OP9-DLL4 cells, expressing the delta like canonical ligand 4. Whereas NKp80 is upregulated in the presence of Notch-ligands, NKp65 expression is reduced (Figure 40B), which is most likely due to a loss of NKp65 expression during NK cell maturation.

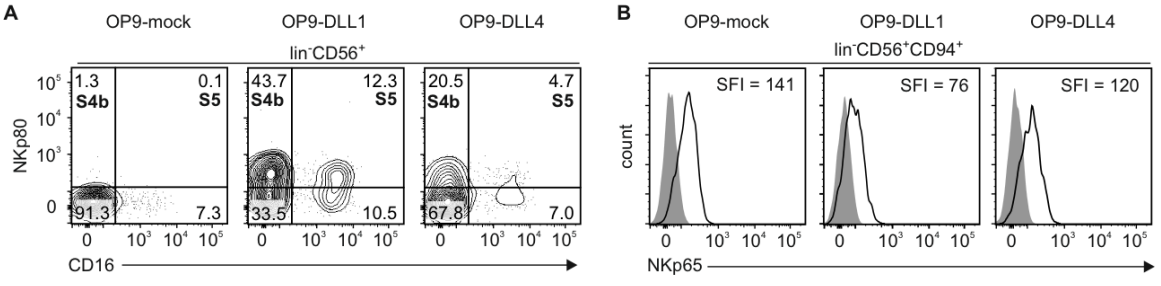

Figure 40: NKp65$^+$ lymphocytes differentiate into NKp80$^+$ NK cells in presence of Notch ligands.
A, **B**, Flow cytometric analyses of sorted NKp65$^+$ precursor cells (Fig. 23) after five days in culture on OP9-mock, -DLL1 or -DLL4 feeder cells, respectively. **A**, Pre-gated for lin$^-$CD56$^+$ live cells, cells were segregated into different NK cell maturation stages 4b (NKp80$^+$CD16$^-$) and S5 (NKp80$^+$CD16$^+$). **B**, NKp65 expression was assessed on lin$^-$CD56$^+$CD94$^+$ cells using OMAR1-bio plus SA-PE (solid line; SFI indicated). Isotype control stainings are shown as shaded histograms. Depicted is one representative out of two independent experiments.

4.4.4 NKp65^{+} stage 3 cells persist in presence of Notch signaling

The long-term persistence of NKp65 expressing stage 3 cells, in cultures with OP9-mock cells (Figure 32) led to the assumption that they do not represent NK cell precursors but are *in vitro* generated ILC3. This was further emphasized by their ILC3-like surface marker and transcription factor expression profile, as well as by their response to ILC3 signature cytokines (Figure 33 and Figure 34). Since in the conducted *in vitro* differentiation system NK cell development was shown to be dependent on Notch signaling, the persistence of S3 cells or accordingly ivILC3 in OP9-mock cocultures might be ascribed to the lack of Notch ligands. Therefore, after inducing ivILC development on OP9-mock cells, ivILC were transferred to cocultures with OP9-DLL1 cells. During incubation for several weeks, ivILC were analyzed by flow cytometry. Although NKp80 expressing NK cells were induced in these cocultures (Figure 41A), S3 cells/ivILC3 persisted over a time period of 55 days (Figure 41B). Hence, S3 cells were also stable in an environment enabling NK cell maturation, further corroborating their notion as ivILC3.

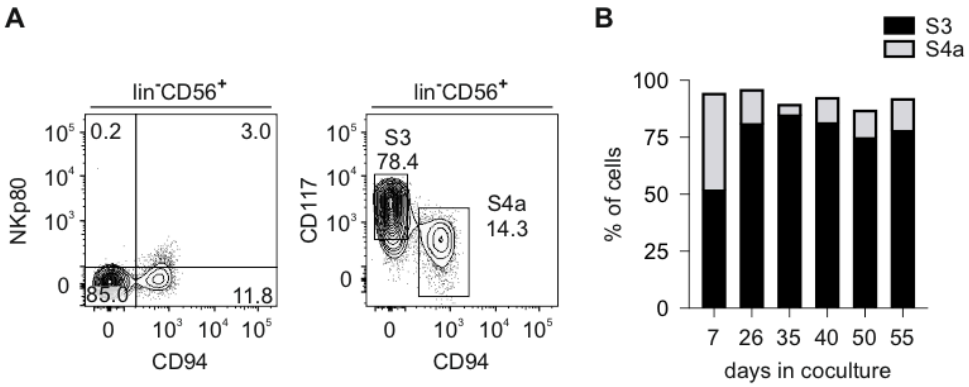

Figure 41: ivILC3 persist in an environment which supports NK cell maturation.
A, **B**, Flow cytometric analyses of *in vitro* differentiated lymphocytes (ivILC) cocultured with OP9-DLL1 cells at different time points. Cells were gated for lin^{-}CD56^{+} and the different developmental stages segregated by NKp80, CD94 and CD117 expression. Cells were cocultured for 34 days with OP9-mock cells prior to transfer to cocultures with OP9-DLL1 cells and cultivation for additional 55 days. **A**, Exemplary contour plot at day 55 of coculture. **B**, Bar diagram depicting the percentages of S3 (CD117^{high}CD94^{-}) and S4a (CD117^{low}CD94^{+}) cells among lin^{-}CD56^{+} cells at different time points of analysis.

4.5 Functional assessment of NKp65 on *in vitro* generated innate lymphocytes

4.5.1 NKp65 triggers cytotoxicity of *in vitro* generated human innate lymphocytes

In a previous study Spreu et al. reported that NK-92MI cells kill KACL-expressing cells in an NKp65-dependent manner (Spreu et al., 2010). Hence, ivILC were assayed for cellular cytotoxicity against different KACL expressing target cells. In order to obtain mainly NKp65$^+$ S3/ivILC3 and S4a cells and to prevent the development of S4a cells into more mature NKp65$^-$ stages, ivILC were generated on OP9-mock cells. To address cytotoxicity, KACL expressing target cells were labeled with a cell tracer (CellTrace^{TM} Far Red) and cocultured with ivILC in different effector to target cell (E:T) ratios. To assess NKp65 specific lysis, cells were incubated in presence of F(ab')$_2$ fragments of OMA1, an anti-KACL antibody blocking NKp65/KACL interaction (Bauer et al., 2015), or the respective isotype control (IgG2a F(ab')$_2$). The percentage of killed cells was then assessed by flow cytometry by counting the remaining Far Red$^+$ cells in cocultures and control cultures with target cells only.

First, susceptibility of U937 cells, a cell line endogenously expressing KACL and other ligands of activating NK cell receptors (Bauer et al., 2015; Welte et al., 2006), to NKp65-mediated cytotoxicity was addressed. NKp65 and KACL expression was verified via flow cytometry on ivILC and U937 cells, respectively prior to the experiment (Figure 42A). Killing assays in the presence and absence of OMA1 F(ab')$_2$ demonstrated that killing of U937 by ivILC occurs in a partially KACL-dependent manner. Especially at lower E:T ratios cytotoxicity was significantly reduced in presence of OMA1 F(ab')$_2$ (Figure 42B). NKp65-KACL dependence of U937 killing by ivILC was further corroborated by the observation that cytolysis correlated with the varying levels of NKp65 expression by ivILC established from different donors (Figure 42C). Whereas ivILC with high (SFI = 43, donor D#30) or intermediate (SFI = 34, D#32) expression efficiently lysed U937 cells in a NKp65-KACL dependent manner, ivILC with low NKp65 expression (SFI = 16, D#31) killed U937 cells independently of presence or absence of OMA1 F(ab')$_2$ (Figure 42C). Of note, not only NKp65-KACL dependent killing, but also killing capacity in general differed among the ivILC established from different donors.

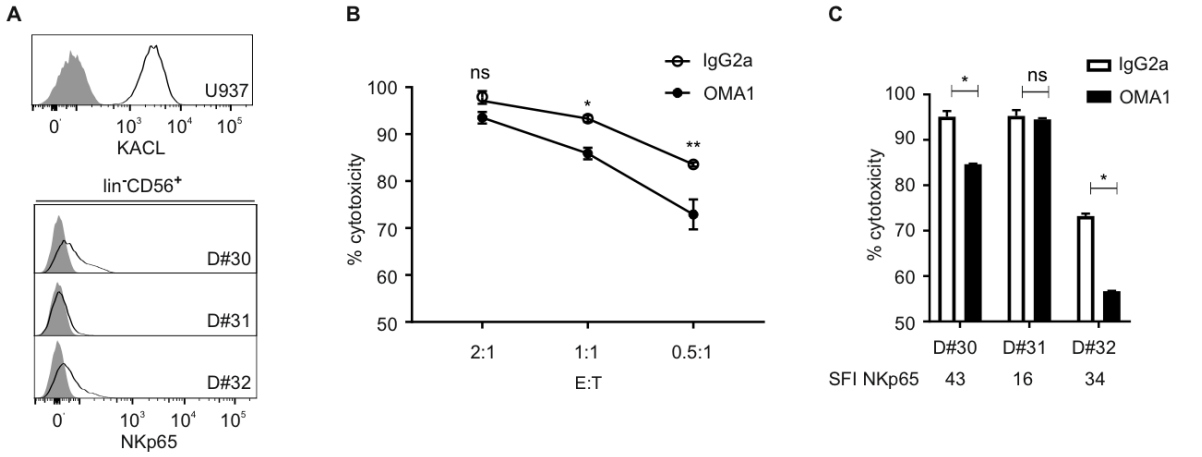

Figure 42: NKp65-mediated lysis of KACL$^+$ U937 cells by ivILC.
A, Flow cytometric analyses of KACL expression on U937 (upper panel) or NKp65 expression on in vitro differentiated lin$^-$CD56$^+$ innate lymphocytes (ivILC) from three different donors. KACL expression was assessed by OMA6-bio plus SA-PE staining and NKp65 expression by OMAR1-bio plus SA-PE staining (black lines), respectively. Isotype control stainings are shown as grey shaded histograms. **B**, Cytotoxicity in presence of F(ab')$_2$ fragments of the blocking anti-KACL mAb OMA1 or of the respective isotype control at different E:T ratios. **C**, Cytotoxicity of ivILC from three different donors against U937 (E:T = 1:1) in presence of OMA1 F(ab')$_2$ fragments or the respective isotype control. NKp65 expression levels (SFI) are indicated below. **B**, **C**, Depicted are means of technical triplicates ± s.d.. Statistical significance was calculated using two-way ANOVA with Tukey's post hoc test (ns, not significant; *P < 0.05; **P < 0.01).

Since U937 cells do also express ligands for other activating NK cell receptors (Welte et al., 2006), ivILC killed U937 target cells also to a high extent in a NKp65-independent manner. Therefore, NKp65-dependent cellular cytotoxicity was also assayed using NKR cells, a human T cell line mainly resistant to NK cell lysis (Howell et al., 1985). KACL expression was first analyzed on NKR cells transduced with KACL (NKR/KACL) or a control plasmid (NKR/mock) (Neuss et al., 2018) by flow cytometry, demonstrating high KACL expression on NKR/KACL cells, whereas mock transduced cells were KACL$^-$ (Figure 43A). Using these cells in killing assays with ivILC revealed that while control-transduced NKR cells were barely killed, transduction of KACL rendered NKR cells highly susceptible to ivILC-mediated cytotoxicity demonstrating that NKp65/KACL interaction promotes cellular cytotoxicity (Figure 43B). NKp65-KACL dependence of NKR/KACL killing by ivILC was further corroborated by the blockade of cytotoxicity in presence of anti-KACL OMA1 F(ab')$_2$ fragments.

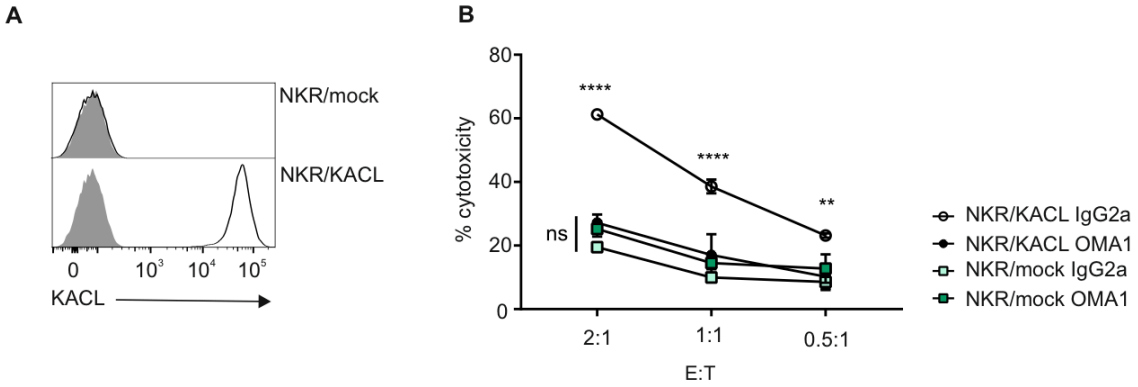

Figure 43: NKp65-mediated cytotoxicity by innate lymphocytes against NKR/KACL cells.
A, Histogram overlays of KACL (black line) or isotype (grey shaded) stainings assessed on NKR/mock and NKR/KACL cells by flow cytometric analyses using OMA6 or IgG2a plus Goat anti mouse-APC secondary antibodies. **B**, Cytotoxicity of ivILC against NKR/KACL or NKR/mock cells in presence of OMA1 F(ab')$_2$ fragments or respective isotype control at different E:T ratios. Depicted are means of triplicates ± s.d. of one representative of three independent experiments with ivILC established from three unrelated donors. Statistical significance was calculated using two-way ANOVA with Tukey's post hoc test (*P < 0.05; **P < 0.01; ****P < 0.0001).

4.5.2 Mechanistic analysis of NKp65 dependent killing

4.5.2.1 NKp65 dependent cytotoxicity can mainly be attributed to CD94$^+$ cells

The notion that target cell killing differed for cells derived from different donors, encouraged a more detailed analysis of the underlying mechanism of killing. ivILC used as effector cells were a heterogenous population of cells in different developmental stages. Therefore, the diverse cytotoxic potential of cells originating from different donors might arise from the inter-individual variability of percentages of different cell subsets within the bulk *in vitro* cultures (Figure 31 and Figure 32). Although classical ILC subsets ILC1, ILC2 and ILC3 are mainly cytokine producers without cytotoxic potential, for the ILC3 like CD94$^+$ stage 4a precursors in human NK cell development a cytotoxic potential has been indicated (Freud et al., 2016).

To unravel if the different *in vitro* generated subsets show varying cytotoxic potential they were segregated into S3 and S4a cells based on CD94 expression by MACS-technology and analyzed for purity as well as NKp65 expression by flow cytometry (Figure 44A, B). MACS-purification resulted in >95% pure fractions of CD94$^+$ (99.8% purity) and CD94$^-$ (95.7% purity) cells. Subsequently the CD94$^+$ and CD94$^-$ fraction were assessed for their cytotoxicity against U937 cells in presence or absence of the blocking OMA1 F(ab')$_2$ fragments as described before. Although both subsets showed cytotoxicity against U937 cells, the cytotoxic potential of CD94$^+$ cells was ~2-fold higher as compared to the CD94$^-$ subset (Figure 44C). Strikingly, a slight although not significant reduction in cytotoxicity in presence of OMA1 F(ab')$_2$ was exclusively

observed for the CD94$^+$ fraction, indicating that NKp65-KACL dependent killing is only conducted by CD94$^+$ cells whereas cytotoxicity by CD94$^-$ cells is NKp65 independent.

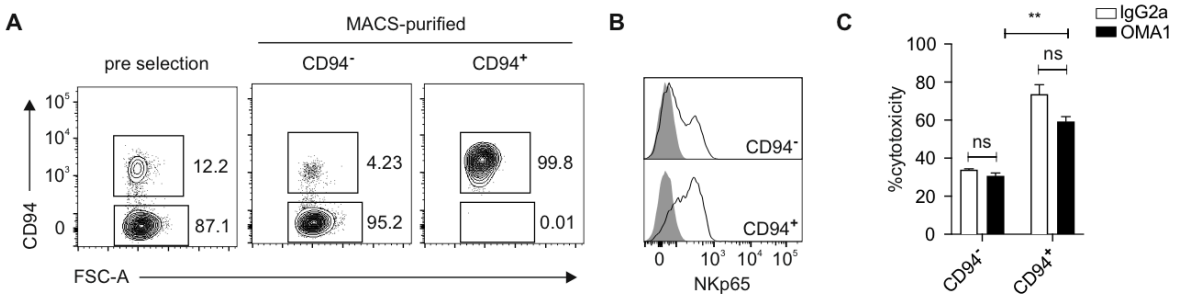

Figure 44: NKp65 dependent cytotoxicity is mainly mediated by CD94$^+$ cells.
A, **B**, Flow cytometric analyses of ivILC before and after MACS-purification of CD94$^+$ and CD94$^-$ cells. **A**, Purity is indicated by numbers in contour plots that represent percentages of the respective subset. **B**, NKp65 expression on the purified CD94$^+$ or CD94$^-$ cells was assessed using OMAR1-bio plus SA-PE (black lines). Respective isotype stainings are shown in grey. **C**, Cytotoxicity of ivILC against U937 cells in presence of OMA1 F(ab')$_2$ fragments or isotype control (E:T ratio = 0.5:1). Depicted are means of technical triplicates ± s.d.. Statistical significance was calculated using two-way ANOVA with Tukey's post hoc test (ns, not significant; **P < 0.01).

4.5.2.2 NKp65 dependent killing is at least in part perforin dependent, whereas there is no evidence for a caspase-8 dependency

NK cells unleash killing activities by either lytic granule-dependent or independent mechanisms. In lytic granule-dependent killing, target cells are lysed by an interplay of the membrane-disrupting protein perforin, and proteases known as granzymes. The second, caspase-8 dependent pathway involves the engagement of death receptors (e.g. Fas/CD95) on target cells by their cognate ligands (e.g. FasL) on the NK cells (Smyth et al., 2005). In order to unravel the underlying mechanism of NKp65 dependent cytotoxicity of ivILC against KACL expressing target cells, killing was analyzed in presence of specific inhibitors of the perforin/granzyme or caspase-8 mediated pathways.

Lytic-granule dependent killing was assessed by incubating ivILC with Concanamycin-A (CMA), an inhibitor reported to prevent granzyme/perforin mediated killing. After incubation with CMA, ivILC were cocultured with CellTracer^{TM} Far Red labelled KACL or mock transduced NKR target cells. The percentage of killed cells was then assessed by flow cytometry by counting the remaining Far Red$^+$ cells in cocultures and control cultures with target cells only. As shown before, NKR/KACL cells were more efficiently killed than NKR/mock cells. CMA significantly reduced killing of both cell lines, demonstrating that target cells are at least in part lysed by the perforin/granzyme pathway (Figure 45A). Cytotoxicity was not completely abrogated although CMA was used in concentrations reported to efficiently block perforin/granzyme mediated killing (Anft et al., 2020). In presence of CMA, ivILC lysed

NKR/mock cells independently of the E:T ratio (Figure 45A, right), whereas a slight but not significant dependency on the E:T ratio for NKR/KACL killing was observed even in the presence of CMA (Figure 45A, left).

Another pathway of target cell lysis conducted by NK cells is death receptor mediated induction of apoptosis. A central role for caspase-8 (casp-8) in this mechanism has been reported, rendering death by apoptosis sensitive to casp-8 inhibitors (iCasp-8) such as Z-IETD-FMK (Prager et al., 2019; Thoren et al., 2012). To study the dependency of ivILC mediated killing on casp-8, NKR/KACL target cells were incubated with iCasp-8 prior to assessing killing by flow cytometry as described before. No evidence was found for a casp-8 dependency, since both cell lines (NKR/mock and NKR/KACL) were lysed irrespectively of Z-IETD-FMK (Figure 45B).

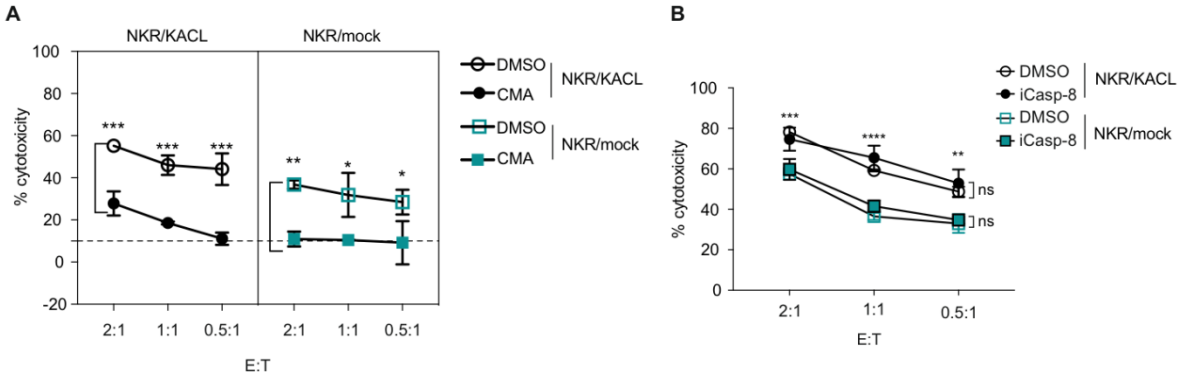

Figure 45: Cytotoxicity of *in vitro* differentiated innate lymphocytes can partially be circumvented by Concanamycin A (CMA).
A, **B**, Cytotoxicity of ivILC against NKR/KACL or NKR/mock cells in presence or absence of 50 nM CMA (**A**) or 10 µM caspase-8 inhibitor Z-IETD-FMK (iCasp-8) (**B**) at different E:T ratios. Target cells were labeled with CellTracer™ Far Red prior to coculture with ivILC. After 24 h in culture, percentage of cytotoxicity was assessed by counting remaining target cells in cocultures and control cultures with target cells only by flow cytometry. Depicted are means of technical triplicates ± s.d. of one representative of three independent experiments with ivILC established from three donors. Statistical significance was calculated using two-way ANOVA with Tukey's post hoc test (ns, not significant; *P < 0.05; **P < 0.01; ***P < 0.001; ****P < 0.0001). **A**, Stars indicate statistically significant differences between CMA and control treated samples. **B**, Stars above the symbols represent significant differences between NKR/KACL and NKR/mock cells, whereas not significantly different changes between iCasp-8 treated and non-treated samples are indicated at the right side of the diagram.

4.6 Regulation of NKp65 surface expression

As stated in the previous chapter, NKp65 was found to be exclusively expressed on NCR^+ILC3, as well as on a subset of NK cell precursors (S4a) which were found in human tonsils and could be recapitulated *in vitro*. The restricted expression of NKp65 on these rare subsets as well as the extraordinary high affinity to its ligand KACL (Li et al., 2013; Spreu et al., 2010) indicates that NKp65 expression is tightly regulated. Regulation of protein expression is a complex process that is controlled by the interplay of transcriptional, post-transcriptional, and post-translational mechanisms. Measuring total mRNA levels has been widely used to assess protein expression although numerous studies concluded that the correlation is poor (de Sousa Abreu et al., 2009; Schwanhausser et al., 2011). However, in a preliminary study by Dr. Isabel Vogler the transcript levels of KLRF2, the gene encoding for NKp65, as well as surface expression levels of NKp65 on ILC3 isolated from human tonsils and the cell line NK-92 were analyzed. NK-92 cells which showed high NKp65 surface expression were also found to be rich in transcripts, whereas lower surface expression on tonsillar ILC3 was reflected in significantly lower transcript levels, suggesting that NKp65 is primarily regulated at the transcriptional level.

4.6.1 Transcriptional regulation of NKp65

4.6.1.1 The KLRF2 core promotor – a TATA-less promoter

In an effort to investigate the transcriptional regulation of NKp65 expression, the promoter region of the KLRF2 gene was analyzed. Basal transcriptional activity is usually facilitated by the core promoter which is generally considered as the region from -40 to +40 base pairs (bp) relative to the transcriptional start site (TSS) that contains core promoter elements such as the TATA-box. Hence, after extracting the TSS of KLRF2 from the public Ensembl database (release 101) (Yates et al., 2020), the core promoter region -40 to +40 bp of the KLRF2 promoter was computationally screened for core promoter elements using the Elements Navigation Tool (ElemeNT v2) (Sloutskin et al., 2015) and the YAPP Eukaryotic Core Promoter Predictor (http://www.bioinformatics.org/yapp/cgi-bin/yapp.cgi) (Figure 46). Computational analysis did not reveal any TATA-box motifs in an appropriate distance to the TSS which is generally considered to be ~30 bp (Smale and Kadonaga, 2003). Instead the KLRF2 core promoter contains an Initiator (Inr) motif surrounding the TSS (-2 to +5 bp) as well as a ‘downstream promoter element’ (DPE) motif (+29 to +33 bp) in suitable spacing. It is well known that these two motifs, presuming that they are in an appropriate distance to each other, can synergistically regulate transcription (Kutach and Kadonaga, 2000). Hence, based on

this computational analysis the KLRF2 core promoter can be classified as a focused, TATA-less promoter.

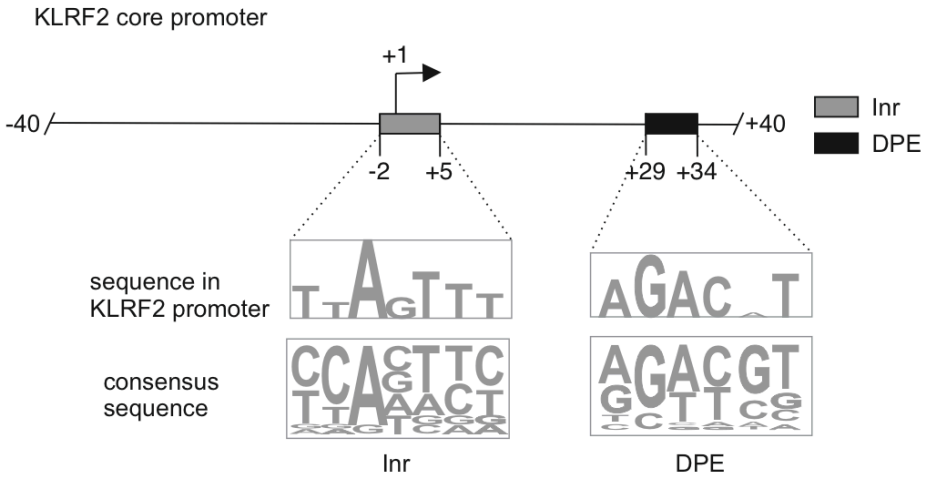

Figure 46: Computational analysis of the KLRF2 core promoter.
The KLRF2 core promoter defined as the region spanning -40 to +40 base pairs (bp) relative to the transcriptional start site (TSS, +1) was computationally analyzed for core promoter elements using the YAPP Eukaryotic Core Promoter Predictor and the ElemeNT database (Sloutskin et al., 2015). Shown as boxes are the identified synergistic Initiator (Inr, grey) and downstream promoter element (DPE, black) motifs, with the consensus sequences and the respective binding site within the KLRF2 promoter (extracted from the Ensembl database release 101 (Yates et al., 2020)).

4.6.2 The KLRF2 proximal promoter contains an activating region

Further computational analyses of the KLRF2 promoter (up to 1 kb upstream of the TSS) indicated a multitude of putative TF binding sites. Therefore, in a first approach the promoter was broadly screened for activating regions. To this end, in a preliminary work by Dr. Björn Bauer (Steinle laboratory) the putative promoter region (spanning -1005 to +108 bp relative to the TSS) and subsequent 5`-deletions were cloned from NK-92MI genomic DNA and analyzed for their activity using the Dual-Glo^{TM} luciferase assay system. Accordingly, NK-92MI cells were co-transfected by electroporation with *Firefly* luciferase vector constructs of the different promoter deletions or the empty vector and the *Renilla* luciferase vector for internal normalization. Luciferase activity was measured 24 h after transfection, normalized to *Renilla* luciferase activity and analyzed relative to the basic (empty) vector, arbitrarily set as 1 (Figure 47). Compared to the empty vector, promoter insert raised the luciferase reporter activity by ~4-fold. Deletions from -1005 to -351 did not lead to a reduction in promoter activity. Therefore, the region spanning -351 to +108 bp relative to the TSS could be defined as the proximal promoter. Whereas deletions from position -1005 to -351 showed no major change in

luciferase activity, comparing the constructs -351 and -145 revealed a significant reduction, implying the location of activating promoter elements within this region.

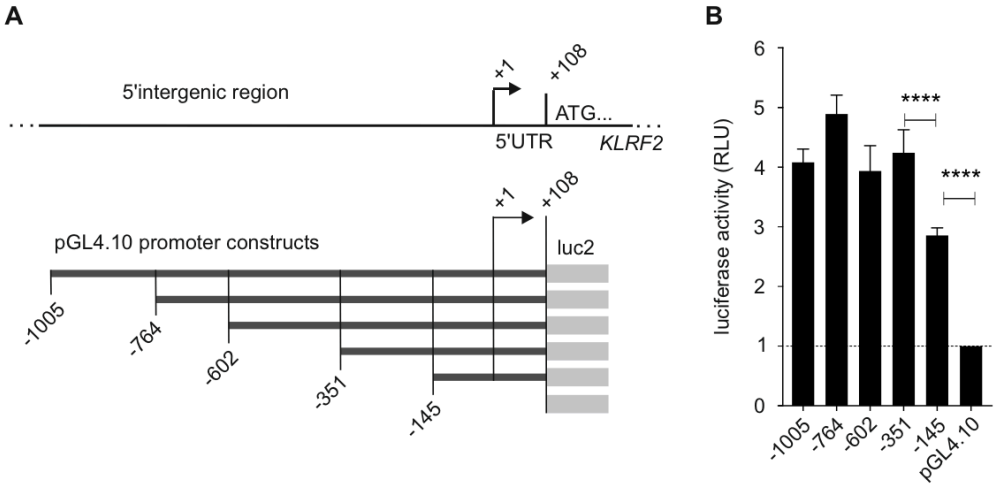

Figure 47: KLRF2 proximal promoter activity depends on an activating region -145 to -351 base pairs (bp) upstream of the transcriptional start site (TSS).
A, Schematic depiction of the genomic assembly of the KLRF2 promoter with indicated 5' intergenic region, TSS (+1), 5'-untranslated region (5'-UTR) and start codon ATG (+109 to +111 bp) (top). pGL4.10 constructs with the KLRF2 promoter (-1005 to +108 bp) or 5' truncated constructs derived thereof with indicated TSS (+1) and luciferase gene (grey box) (bottom). **B**, NK-92MI cells were transiently transfected with pGL4.10 constructs and luciferase activity measured after 24 h, normalized to *Renilla* luciferase activity and set relative to the control vector (set as 1). Means ± s.d. of three independent experiments. Significance was determined by one-way analysis of variance (ANOVA) with Tukey's post hoc test (****P < 0.0001). Data was generated by Dr. Björn Bauer, Steinle laboratory.

4.6.2.1 The KLRF2 proximal promoter activity depends on two regions containing activating promoter elements

Based on this preliminary study by Dr. Björn Bauer (Steinle laboratory), identifying an activating region from -351 to -145 bp relative to the TSS, a more detailed analysis of the KLRF2 proximal promoter was conducted by analyzing incremental 5' deletions (Figure 48). Luciferase assays comparing the previously examined constructs and additional incremental 5' deletions confined the previously described activating region to a stretch of 67 bp reaching from -297 to -230 bp relative to the TSS (activating region ii). This region was identified, since a significant change in luciferase activity was seen comparing the -297 and -230 constructs, while differences between the -230 construct and the -145 construct were not significant (Figure 48B). A further decrease in luciferase activity was observed with continuing deletion of bp, indicative of additional activating elements in the promoter region spanning position -145 to -105 (activating region i). Strikingly, ongoing shortening of the promoter region (-61 and -32) led to an abrogation of promoter activity, albeit both constructs contained the computationally

discerned core promoter elements Inr and DPE. These data emphasize the importance of upstream regulatory elements in the proximal promoter for KLRF2 transcriptional regulation.

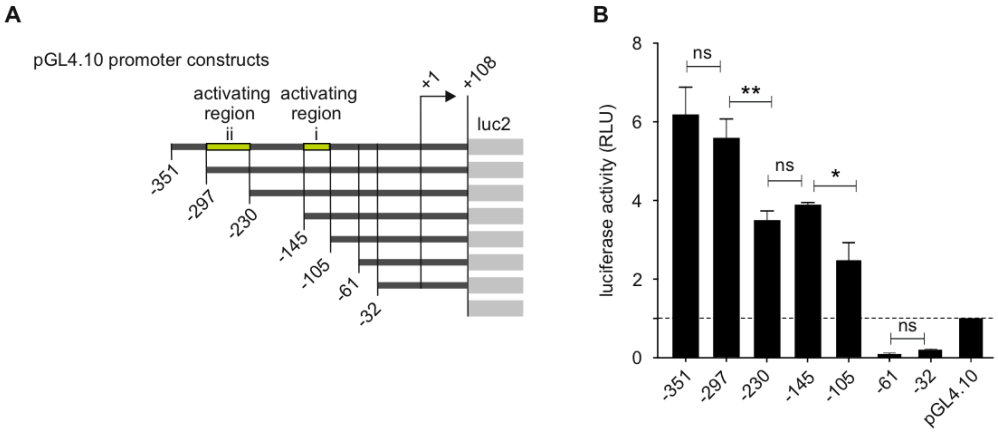

Figure 48: KLRF2 proximal promoter contains two regions with activating elements.
A, Schematic depiction of the pGL4.10 constructs with the KLRF2 proximal promoter (-351 to +108 bp) or 5' truncated constructs derived thereof with indicated TSS (+1) and luciferase gene (grey box). **B**, NK-92MI cells were transiently transfected with pGL4.10 constructs and luciferase activity measured after 24 h, normalized to *Renilla* luciferase activity and set relative to the control vector (set as 1). Means ± s.d. of three independent experiments. Significance was determined by one-way analysis of variance (ANOVA) with Tukey's post hoc test (ns, not significant; *P < 0,1; **P < 0.01). The -351, -145, -61 and -32 constructs were created by Dr. Björn Bauer (Steinle laboratory), whereas the luciferase assays shown here are part of the present study.

4.6.2.2 *In silico* sequence analysis for putative transcription factor binding sites in the KLRF2 promoter

A preliminary study by Dr. Isabel Vogler revealed rapid downregulation of NKp65 expression on tonsillar ILC3 when cultured *in vitro* that could be circumvented by the supplementation with IL-7 (Figure 49).

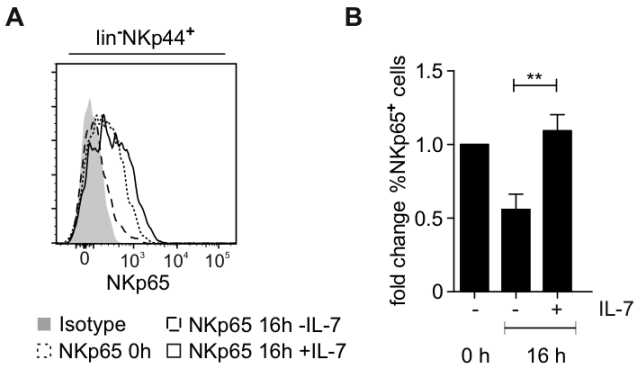

Figure 49: Sustained NKp65 expression *in vitro* requires IL-7 signaling.
Flow cytometric analyses of NKp44-enriched tonsillar lymphocytes for NKp65 surface expression (OMAR1-bio plus SA-PE) after *in vitro* culture for 16 h. **A**, NKp65 expression before (0 h; dotted line) or after culture in presence (black line) or absence (dashed line) of IL-7. One representative out of four independent experiments with a total of n = 6 unrelated donors. **B**, Percentage of NKp65-expressing cells among NKp44$^+$ tonsillar lymphocytes after culture in presence or absence of IL-7 set relative to the percentage of NKp65$^+$ cells at the begin of culture. Compiled data with means ± s.d. from four independent experiments with a total of n = 6 unrelated donors. Significance was determined by one-way analysis of variance (ANOVA) with Tukey's post hoc test (**P < 0.01). Data generated by Dr. Isabel Vogler and Dr. Stefan Leibelt, Steinle laboratory.

The IL-7 receptor signals via JAK1 and JAK3 to mediate phosphorylation of STAT1, STAT3 and STAT5 and activates the more complex PI3K pathway which leads to phosphorylation of numerous PI3K-responsive signaling factors, including kinases, which can activate numerous TFs. The most prominent TFs regulated by the PI3K pathway belong to the families of Forkhead box (FOX) and cAMP-responsive element binding (CREB) proteins (Mantamadiotis, 2017). Therefore, the two activating regions i (-145 to -105) and ii (-297 to -230) of the KLRF2 promoter were computationally screened for TF binding sites using the MatInspector software (Cartharius et al., 2005) and the results analyzed regarding TFs downstream of the PI3K and JAK/STAT signaling pathways. The *in silico* analysis of the two activating regions i and ii revealed 13 and 25 putative transcription factor binding sites, respectively (Table 21 and Table 22). Within activating region i one STAT5 binding site -117 to -125 bp upstream of the TSS was identified with high similarity to the reported STAT5 consensus sequence (Figure 50B). Among the 25 TFs with putative binding sites in the activating region ii, six could be allocated to the PI3K signaling pathway, e.g. the Forkhead domain factors FOXA2, FOXJ1, FOXI1 and FOXP1 (Chang et al., 2003), the 'nuclear factor interleukin 3 regulated protein' (E4BP4) (Tong et al., 2010) as well as the octamer binding protein Oct-1 (POU2F1) (Karvande et al., 2018) (Figure 50A).

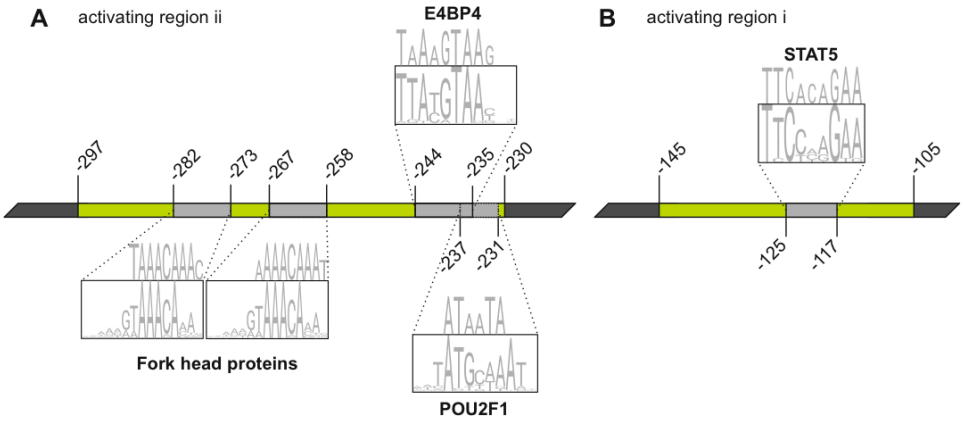

Figure 50: *In silico* sequence analysis of the KLRF2 promoter for putative transcription factor (TF) binding sites.
A, **B**, The two identified activating regions spanning -297 to -230 (**A**) and -145 to -105 bp (**B**) relative to the transcriptional start site (TSS) were analyzed for potential TF binding sites using the MatInspector software (Cartharius et al., 2005). Activating regions are marked in green and potential binding sites in grey. Numbers indicate the position relative to the TSS. Black boxes contain the consensus TF binding sites extracted from (Fornes et al., 2020), grey capitals above the black boxes indicate the respective site within the KLRF2 promoter (sequences extracted from the Ensembl database release 101 (Yates et al., 2020)) with matching nucleotides shown as large, and non-matching nucleotides as small letters. **A**, Activating region ii with two potential binding sites for Forkhead proteins, and one for E4BP4 and POU2F1, respectively. **B**, Activating region ii with one putative STAT5 binding site.

4.6.2.3 STAT5 is critically involved in the transcriptional regulation of NKp65

In an effort to validate an involvement of STAT5 in the transcriptional regulation of NKp65, KLRF2 promoter activity of constructs with point mutations specifically targeting the putative STAT5 binding site (Figure 51A) were assayed in NK-92MI cells using the Dual-Glo™ luciferase assay system as described before. Mutation of the consensus binding sequence of STAT5 resulted in a ~3-fold drop of transcriptional activity as compared to the -351 bp construct and reduced promoter activity to the level of the -105 construct that is devoid of the STAT5 binding site (Figure 51B). These data indicate a dependency of KLRF2 promoter activity on the putative STAT5 binding site located -117 to -125 bp downstream of the TSS.

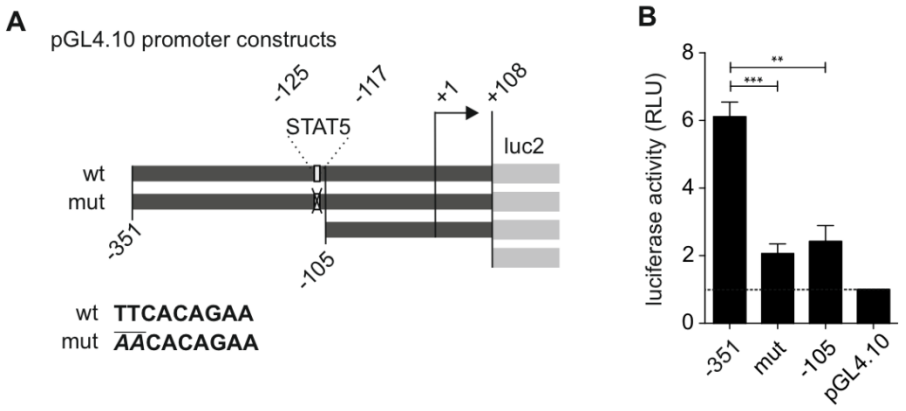

Figure 51: KLRF2 promoter activity depends on a STAT5 binding site.
A, pGL4.10 constructs with the KLRF2 proximal promoter (-351 to +108 bp) or constructs derived thereof with mutations (mut) in the putative STAT5 binding site (white box; at -117 to -125 bp relative to the transcriptional start site, marked as +1) or a 5' truncated promoter (-105 to +108 bp). Sequence of the STAT5 response element is shown below with mutated nucleotides marked by an overline. **B**, NK-92 cells were transiently transfected with pGL4.10 constructs and luciferase activity measured after 24 h, normalized to *Renilla* luciferase activity and set relative to the control vector arbitrarily set as 1. Means ± s.d. of three independent experiments. Significance was determined by one-way analysis of variance (ANOVA) with Tukey's post hoc test (**P < 0.01; ***P < 0.0001).

Direct binding of STAT5 to this specific site in the KLRF2 promoter (-117 to -125) was assessed in pulldown assays with lysates from NK-92MI cells using biotinylated oligonucleotides comprising the putative STAT5 binding site and mutants thereof (Figure 52). Oligonucleotides representing the STAT5 binding site, but not the respective mutants, precipitated STAT5 from cellular lysates as shown in the immunoblot analysis with antibodies against STAT5 (Figure 52B).

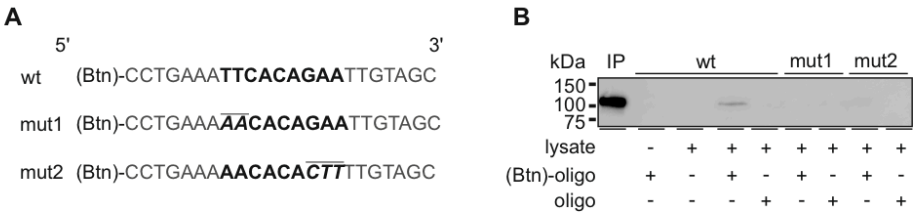

Figure 52: STAT5 binds to the predicted binding site in the KLRF2 promoter.
A, Sequence of biotinylated (Btn) oligomers including the putative STAT5 binding (black, bold type) and some flanking nucleotides (grey) of the respective site in the KLRF2 promoter. Mutants (mut1, mut2) thereof, with mutated nucleotides indicated by an overline. **B**, Cellular lysates from NK-92MI cells incubated with biotinylated oligonucleotides shown in **A** coupled to streptavidin-conjugated beads. Precipitated proteins were separated by SDS-PAGE and STAT5 detected by immunoblotting. Cellular lysates prior to precipitation are shown in the first lane (IP) and controls with non-biotinylated oligonucleotides or streptavidin-conjugated beads only as indicated. Representative result out of two independent experiments.

The crucial role of STAT5 in regulating NKp65 expression was further investigated with primary cells by flow cytometric analyses of NKp65 expression on MACS-purified tonsillar NKp44^{+}ILC3 cultivated in presence of IL-7 and a STAT5 inhibitor (iSTAT5). After 8 h, NKp65 expression on cells treated with iSTAT5 was 2-fold reduced as compared to control treated cells (Figure 53A, B). Additional analysis of the levels of KLRF2 transcripts by qPCR revealed a ~3-fold reduction, underlining that STAT5 is regulating NKp65 expression at the transcriptional level (Figure 53C).

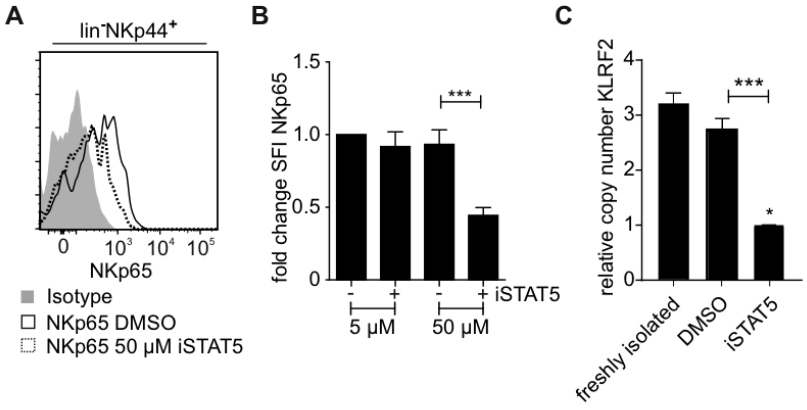

Figure 53: NKp65 expression requires STAT5 signaling.
A, **B**, Flow cytometric analyses of NKp44-enriched tonsillar innate lymphocytes for NKp65 expression (OMAR1-bio plus SA-APC) cultured with IL-7 and a STAT5 inhibitor (iSTAT5). **A**, Representative histograms of NKp65 expression in presence (dashed line) or absence (solid line) of 50 µM iSTAT5 and (**B**) -fold change in NKp65 surface expression (SFI) averaged from independent experiments with a total of three donors. **C**, Abundance of KLRF2 transcripts in NKp44-enriched tonsillar cells after 8 h culture in presence or absence of 50 µM iSTAT5. Relative levels of KLRF2 transcripts were determined by qPCR and normalized to inhibitor-treated samples marked by an asterisk. Means of triplicates ± s.d. of one representative out of three independent experiments. Significance was determined by one-way analysis of variance (ANOVA) with Tukey's post hoc test (***$P < 0.0001$).

Altogether, these data demonstrate the presence of a functional STAT5 response element in the KLRF2 promoter allowing for a direct transcriptional control of NKp65 expression by IL-7 signaling.

4.6.2.4 Transcriptional regulation of NKp65 might also depend on FOX proteins.

The computational analysis of the activating region ii indicated several putative binding sites for TFs that are associated with IL-7 and the PI3-Kinase signaling pathway. Therefore, in a first approach, successive microdeletions (mΔ1-5) in the KLRF2 promoter constructs, spanning the predicted FOX protein binding sites within the activating region ii in the KLRF2 promoter (Figure 54A) were screened in NK-92MI cells by Dual-Glo™ luciferase assays. Irrespective of the position of the microdeletion all constructs showed equal luciferase activities with no significant differences to the -230 construct, demonstrating an activating function of the entire region and pointing to an involvement of FOX proteins in the regulation of promoter activity (Figure 54B). If one of the four predicted FOX proteins (FOXA2, FOXJ1, FOXI1 and FOXP1) is binding to the KLRF2 promoter and directly regulating its activity has not been further investigated within this study.

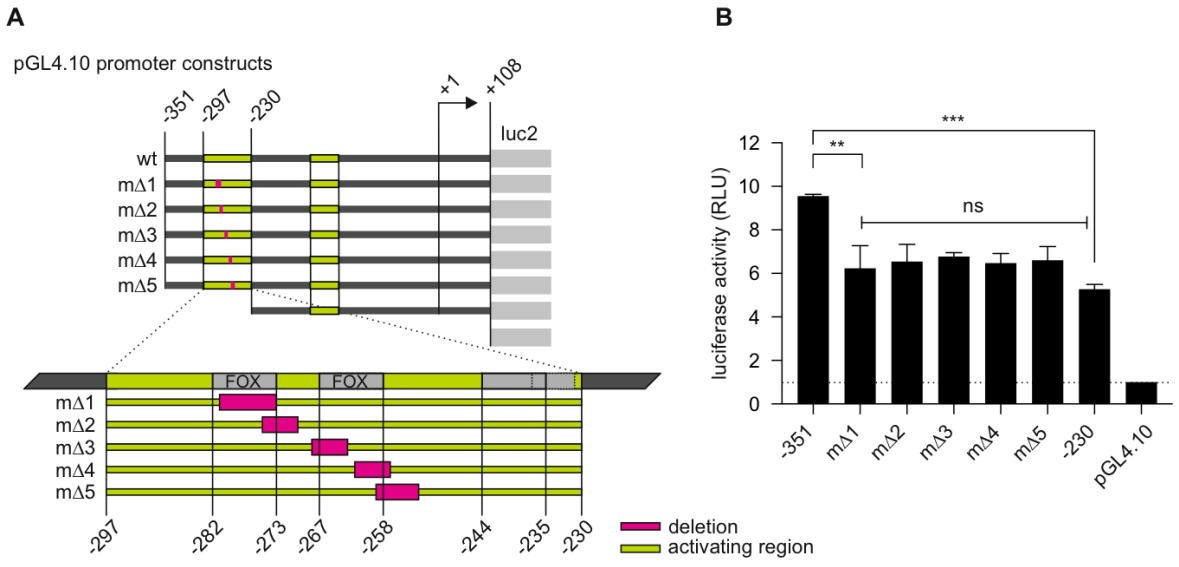

Figure 54: The second activating region (ii) in the KLRF2 promoter contains a broad area with activating promoter elements.
A, Schematic depiction of the pGL4.10 constructs with the KLRF2 promoter (-351 to +108 bp) or constructs derived thereof with micro deletions (mΔ1-5, shown as pink boxes) spanning the putative Forkhead box (FOX) protein binding sites (grey boxes) or a 5' truncated promoter devoid of the entire activating region ii (-230 to +108 bp). **B**, NK-92MI cells were transiently transfected with pGL4.10 constructs and luciferase activity measured after 24 h, normalized to *Renilla* luciferase activity and set relative to the control vector arbitrarily set as 1. Means ± s.d. of three independent experiments. Significance was determined by one-way analysis of variance (ANOVA) with Tukey's post hoc test (ns, not significant; **P < 0.01; ***P < 0.0001).

However, since the activating region ii was found to be fairly rich in putative binding sites for TFs downstream of the PI3-Kinase signaling cascade, NKp65 expression on MACS-purified NKp44^{+}ILC3 was analyzed after cultivation in presence of IL-7 and the PI3K inhibitor Ly294002 (iPI3K) by flow cytometry. Presence of iPI3K resulted in a 2-fold reduction of NKp65 surface expression (Figure 55A, B). Analyses of the relative copy numbers of KLRF2 by qPCR revealed that diminished surface expression was accompanied by reduced transcript levels (Figure 55C).

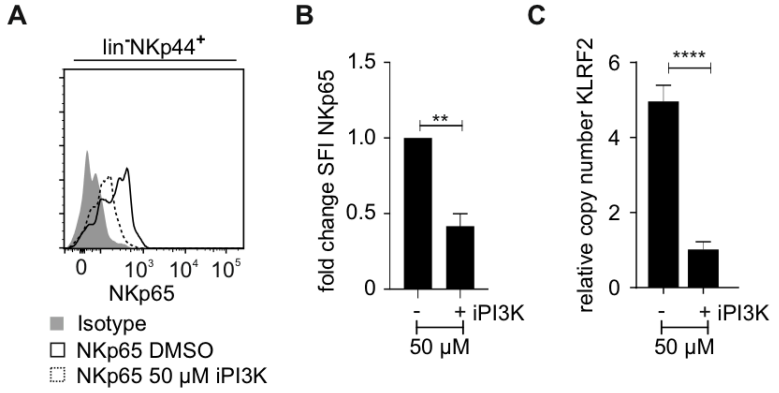

Figure 55: PI3-Kinase inhibitors impair NKp65 expression.
A, **B**, Flow cytometric analyses of NKp44-enriched tonsillar innate lymphocytes for NKp65 expression (OMAR1-bio plus SA-APC) cultured with IL-7 and the PI3-Kinase inhibitor Ly294002 (iPI3K). **A**, Representative histograms of NKp65 expression in presence (dashed line) or absence (solid line) of 50 µM iPI3K (isotype control shown in grey) and (**B**) -fold change in NKp65 surface expression (specific fluorescence intensity, SFI) averaged from independent experiments with a total of two unrelated donors. **C**, Abundance of KLRF2 transcripts in NKp44-enriched tonsillar cells after 8 h culture in presence or absence of 50 µM iPI3K. Relative levels of KLRF2 transcripts were determined by qPCR and normalized to inhibitor-treated samples marked by an asterisk. Means of triplicates ± s.d. of one representative out of two independent experiments. **B**, **C**, Statistical significance was analyzed by two-tailed unpaired Student's *t*-test (**P < 0.01; ****P < 0.0001).

4.6.3 Post-transcriptional regulation of NKp65 expression

The expression of many proteins is determined by a multifaceted process encompassing transcriptional, post-transcriptional and post-translational regulation. The expression of cell surface receptors is frequently regulated on the post-transcriptional level by ligand-induced downregulation, a process that plays an important role in acute attenuation of signaling events (Shankaran et al., 2007).

4.6.3.1 Ligand induced downregulation of NKp65 surface expression

To unravel whether NKp65 expression is regulated by ligand-induced downregulation, NK-92MI cells transduced with plasmids encoding for C-terminally FLAG-tagged NKp65 (NK-92MI/NKp65) were cocultured with CEM/KACL or CEM/mock transductants and subsequently analyzed for NKp65 expression by flow cytometry. Cells cultured in the presence

of CEM/KACL cells showed a ~2-fold reduction of NKp65 surface expression as compared to control cultures with mock transduced CEM cells or single cultures of NK-92MI/NKp65 cells (Figure 56A, B). KACL-induced downregulation of NKp65 expression was not only observed for the NK-92MI/NKp65 cell line but also on ivILC that were cultured with NKR/KACL cells (Figure 56C), emphasizing that KACL induced NKp65 downregulation is a directed process and independent of the cell type.

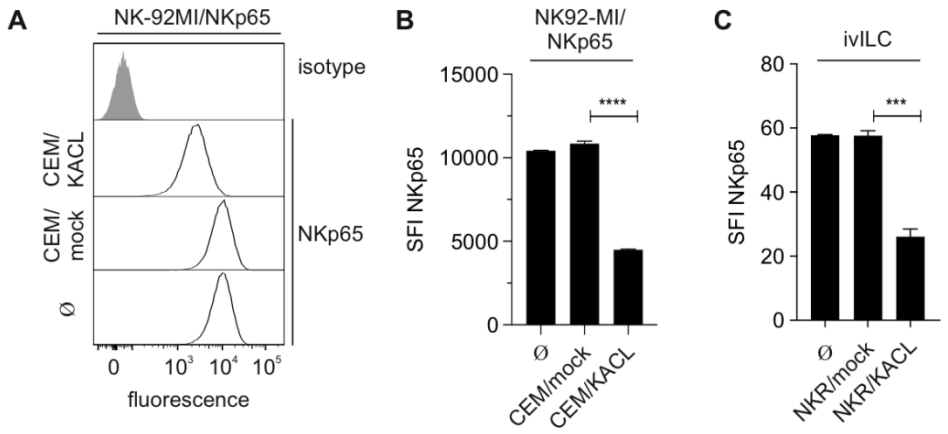

Figure 56: Stimulation of NKp65 with its ligand KACL leads to receptor downregulation.
A, **B**, Flow cytometric analyses of NK-92MI/NKp65 cells gated as $CD56^+$ cells for NKp65 expression (OMAR1-bio plus SA-APC) after 3 h cultivation with CEM/KACL, CEM/mock or without target cells (Ø). **A**, Representative histograms of NKp65 expression (black lines) and isotype control staining (grey shaded). **B**, NKp65 expression shown as means of triplicates ± s.d. of specific fluorescence intensity (SFI). **C**, Flow cytometric analyses of *in vitro* differentiated innate lymphocytes (ivILC) gated as lin^-CD56^+ cells for NKp65 expression (OMAR1-bio plus SA-PE) after 20 h cultivation with NKR/KACL, NKR/mock or without target cells (Ø). SFI of NKp65 expression shown as means of triplicates ± s.d.. **A-C**, Data are representative of two independent experiments, statistically significant differences determined by one-way analysis of variance (ANOVA) with Tukey's post hoc test (***$P < 0.001$; ****$P < 0.0001$) are indicated.

After coculturing NK-92MI/NKp65 and CEM/KACL cells a minute fraction of the previously $NKp65^-$ CEM/KACL cells bound the NKp65 specific mAb 12C10 (Figure 57A), an antibody that is not interfering with NKp65-KACL interaction. Strikingly, NKp65 on CEM/KACL cells was not detected with the blocking antibody OMAR1 and was reduced in presence of Batimastat (BB94) a chemical compound frequently used to inhibit metalloproteinase dependent shedding of surface molecules (Rasmussen and McCann, 1997) (Figure 57A). Additionally, NKp65 could not be detected on CEM/mock cells from cocultures with NK-92MI/NKp65 cells, except for a neglectable background staining detected with both antibodies (Figure 57B). These data indicate that NKp65 detected on the surface of CEM/KACL cells is actively bound to KACL and might has been transferred by cleavage from the cell surface of NK-92MI/NKp65 cells in a process involving metalloproteinases.

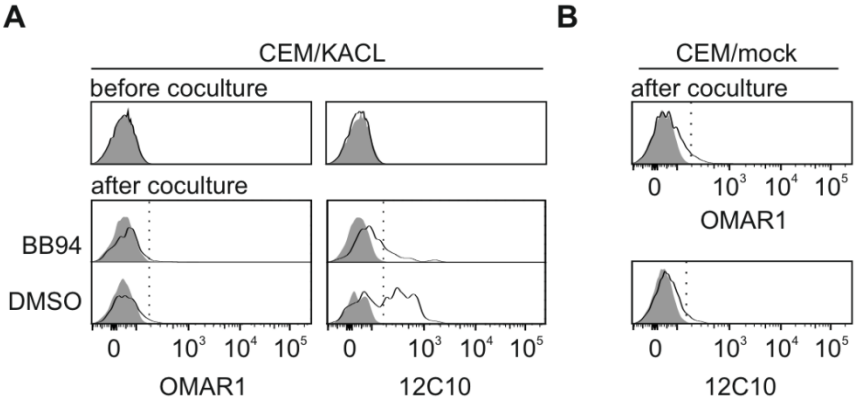

Figure 57: NKp65 is transferred to KACL-expressing cells upon ligand-receptor interaction.
A, **B**, Flow cytometric analyses of CEM/KACL (**A**) and CEM/mock (**B**) cells (gated as $CD56^-$) before and after 3 h cultivation with NK-92MI/NKp65 cells in presence or absence (DMSO) of 10 µM Batimastat (BB94) as indicated. For CEM/mock cocultures only DMSO controls are shown. Surface staining of NKp65 was assessed either by OMAR1-bio plus SA-APC or 12C10 plus APC-conjugated Goat anti-Mouse (GaM) antibodies (solid lines). Respective isotype control stainings (IgG1-bio plus SA-APC and IgG1 plus GaM-APC) are shown as shaded histograms.

4.6.3.2 NKp65 is shed by metalloproteinases upon ligation of KACL

To unravel if NKp65 is shed by metalloproteinases upon ligand binding, supernatants of NK-92MI/NKp65 and CEM/KACL cocultures were analyzed for the presence of truncated forms of NKp65. Making use of the C-terminal FLAG-tag, soluble NKp65 was precipitated from supernatants using anti-FLAG magnetic beads. Eluted proteins were deglycosylated by PNGaseF treatment and subjected to immunoblot analysis. In a previous report, deglycosylated membrane bound NKp65 immunoprecipitated from NK-92MI/NKp65 cells resulted in a distinct signal at ~24 kDa (Bauer et al., 2017). In supernatants of NK-92MI/NKp65 and CEM/KACL cocultures, a signal below 15 kDa was detected that diminished upon BB94 treatment of the cocultured cells (Figure 58A), indicating that NKp65 is shed by metalloproteinases upon binding to its ligand KACL. In order to validate that the precipitated protein is a truncated form of NKp65 and to determine the amount of shed protein, supernatants of NK-92MI/NKp65 and CEM/KACL cells cultured for three hours in presence or absence of BB94 were subjected to a NKp65 specific sandwich-ELISA using the mAbs 12C10 and OMAR1 (Figure 58B). In absence of any stimulus supernatants of NK-92MI/NKp65 cells contained ~150 pg/ml soluble NKp65 (sNKp65). Incubation with CEM/KACL cells raised the amount of sNKp65 to ~400 pg/ml, an increase that could be inhibited by BB94 treatment, entirely. Of note, even in presence of BB94 shedding of NKp65 was not prohibited entirely (Figure 58B). Nevertheless, these data indicate that NKp65 shedding is ligand induced and at least in part dependent on metalloproteinases.

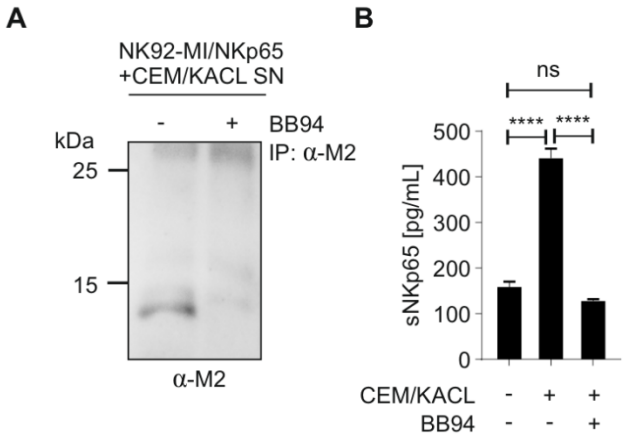

Figure 58: NKp65 is shed from the cell surface upon ligation of KACL.
NK-92MI cells transduced with FLAG-tagged NKp65 (NK-92MI/NKp65) were cultured with CEM/KACL cells in presence or absence of 10 µM Batimastat (BB94) as indicated. After 3 h, cleared supernatants (SN) were analyzed by immunoblotting (**A**) and ELISA (**B**). Shown is one representative of two independent experiments, respectively. **A**, After immune precipitation (IP) of FLAG-tagged NKp65 from SN using anti-FLAG (α-M2) magnetic beads, eluted protein was deglycosylated by PNGaseF treatment and probed with the anti-FLAG mAb α-M2 in immunoblotting. **B**, Soluble NKp65 (sNKp65) in SN was determined using a NKp65 specific sandwich-ELISA. Amounts of sNKp65 are shown as mean of triplicates ± s.d.. Statistical significance was determined by one-way analysis of variance (ANOVA) with Tukey's post hoc test (ns, not significant; ****P < 0.0001).

4.6.3.3 NKp65 shedding is augmented by PMA/Ionomycin stimulation

Metalloproteinases can be grouped into two families, the classical matrix metalloproteinases (MMPs) and 'a disintegrin and metalloproteinase' (ADAM) proteins (Malemud, 2006). Whereas MMPs are largely implicated in destruction of extracellular matrix, ADAMs have been mainly described as membrane-tethered proteases involved in ectodomain shedding of transmembrane proteins (Edwards et al., 2008; Lu et al., 2011). ADAM dependent shedding can be augmented by a variety of stimuli including PMA and Ionomycin treatment (Edwards et al., 2008). Therefore, the dependency of NKp65 shedding on PMA/Ionomycin (P/I) stimulation was analyzed. To this end, NK-92MI/NKp65 cells were cultured with or without PMA/Ionomycin in presence or absence of BB94 for 2 h and subsequently analyzed for NKp65 surface expression by flow cytometry. Additionally, the respective supernatants were assayed for sNKp65 by ELISA and immunoblotting.

Flow cytometric analyses of NKp65 surface expression using OMAR1 revealed high NKp65 expression in absence of P/I, irrespective of BB94 treatment. Stimulation with P/I for 2 h reduced NKp65 expression ~2-fold in absence of BB94, whereas supplementation with BB94 partially circumvented the effect (Figure 59A, B).

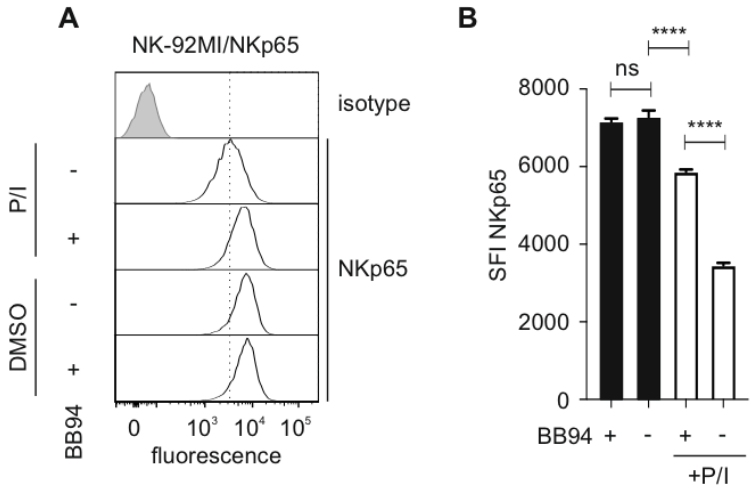

Figure 59: NKp65 shedding is induced by PMA/Ionomycin (P/I) stimulation.
Flow cytometric analyses of NK-92MI/NKp65 cells for NKp65 expression (OMAR1-bio plus SA-PE) after 2 h cultivation with P/I or DMSO in presence or absence of Batimastat (BB94) as indicated. Shown is one representative out of three independent experiments. **A**, Representative histograms of NKp65 expression (solid lines) or isotype control staining (grey shaded). **B**, Specific fluorescence intensity (SFI) of NKp65 expression shown as means of triplicates ± s.d.. Statistical significance was calculated using two-way ANOVA with Tukey's post hoc test (ns, not significant; ****P < 0.0001).

In order to validate that diminished NKp65 expression upon P/I treatment was due to ectodomain-shedding and to elucidate whether NKp65 is also proteolytically processed intracellularly, NK-92MI/NKp65 cells were stimulated with P/I and subsequently both, cell lysates and supernatants (SN) were analyzed. To this aim, FLAG-tagged NKp65 was immunoprecipitated from lysates and SN with anti-FLAG magnetic beads. Eluted proteins were deglycosylated with PNGaseF, followed by immunoblotting. Truncated forms of NKp65 (signals < 24 kDa) could only be detected in supernatants, whereas lysates contained the full-length protein (24 kDa), exclusively. Moreover, truncated protein was not detected in supernatants of BB94 treated samples (Figure 60A). Samples of the supernatants were also subjected to ELISA revealing that after 2 h in culture minimal amounts of soluble NKp65 were shed also in the absence of P/I and irrespective of BB94 treatment (Figure 60B, black bars). P/I induced an over 4-fold increase in sNKp65 that was circumvented by BB94 (Figure 60B, open bars). Together these data demonstrate that the NKp65 ectodomain is actively shed from the cell surface and indicates an involvement of metalloproteinases, most likely ADAMs, in this process.

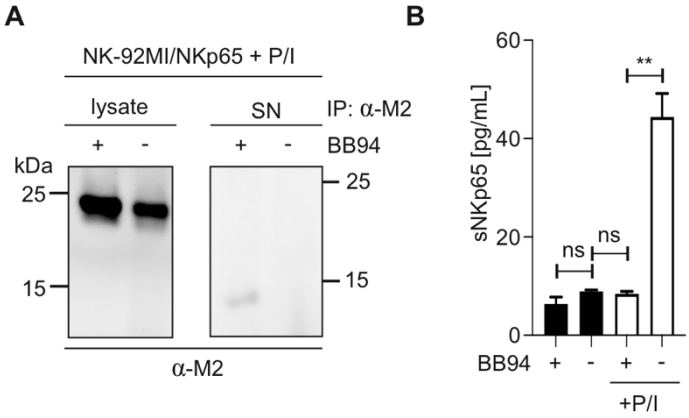

Figure 60: NKp65 is shed from the cell surface by metalloproteinases.
A, NK-92MI/NKp65 cell were stimulated with PMA/Ionomycin (P/I) and cultured with or without 10 µM Batimastat (BB94) for 2 h before FLAG-tagged NKp65 molecules in cell lysates (left) or culture supernatants (SN, right) were immunoprecipitated by anti-FLAG (α-M2) magnetic beads, deglycosylated (PNGaseF) and probed with the anti-FLAG mAb M2 in immunoblotting. **B**, The respective supernatants of NK-92MI/NKp65 cells from **A** were analyzed for soluble NKp65 (sNKp65) using a NKp65 specific sandwich-ELISA. Data are shown as means of triplicates ± s.d.. Statistical significance was calculated using two-way ANOVA with Tukey's post hoc test (ns, not significant; **P < 0.01). **A**, **B**, Representative experiments of at least three independent experiments are shown.

5. Discussion

5.1 Physiological expression of NKp65 and its role as a marker for ILC3

5.1.1 Sites of physiological NKp65 expression

Since its first description as an activating immunoreceptor in 2010 (Spreu et al., 2010), physiological expression of NKp65 remained elusive. Although, NKp65 was found to be expressed by the human NK cell line NK-92, only very low levels of KLRF2 transcripts were detected in NK cell-enriched lymphocytes. Screening various tissues for KLRF2 transcripts revealed that except for a slight enrichment in tonsil, placenta and small intestine, most tissues contained very low levels of KLRF2 transcripts (Figure 13). These data indicate NKp65 expression on a rare cell type which is mainly located at barrier sites. In 2016 Dr. Isabel Vogler (Steinle laboratory) generated monoclonal antibodies against NKp65 designated OMAR1 and 12C10, allowing for the detection of NKp65 surface expression on tonsillar NKp44$^+$ ILC3 (Figure 13). While lacking the expression of CD34 and the lineage markers CD3, CD14 and CD19, such NKp65$^+$NKp44$^+$ ILC3 express the characteristic surface markers for ILC3, CD127 and CD117 (Figure 17). Compared to NKp65$^-$ cells, NKp65$^+$ ILC3 show an enhanced expression of ILC3 related genes such as AHR, IL1R1 and CD117 also on transcriptional level, whereas classical NK cell markers such as CD16 and KIRs are downregulated (Figure 13). Further corroborating their ILC3 character, NKp65$^+$ ILC3 are marked by the expression of RORγt (Figure 18).

Although NKp65$^+$ ILC3 are readily detectable in the human tonsil, their function within this site remains unclear. Till now, there is no evidence for the expression of KACL, the ligand of NKp65, in the human tonsil (Spreu et al., 2010; Uhlen et al., 2015). However, tonsils are known as site of ILC development (Montaldo et al., 2014). For B cells it is well established, that they are activated and proliferate in the tonsil prior to migration through lymph and blood into various human tissues (Scadding, 1990). The tonsil is therefore considered a site of induction of humoral and cellular immune response (Olofsson et al., 1998). Hence, the tonsil might provide an environment for development of NKp65$^+$ ILC3 from which they migrate to colonize sites of the human body that harbor KACL-expressing cells, such as the skin (Spreu et al., 2010).

Although KLRF2 transcripts in tissue sections of the human skin are hardly detectable (Figure 13), preliminary analyses of enriched skin ILC3 revealed their expression of NKp65 which is confirmed within this work (Figure 26). However, detecting these cells is challenging since especially NCR$^+$ ILC3 are extremely rare in healthy human skin accounting for less than

2% of total lymphocytes (Villanova et al., 2014). Considering that the skin is mainly composed of non-lymphoid cells, NKp65 expressing cells constitute only a trickle of all skin cells, rationalizing the barely detectable KLRF2 transcripts within this tissue. However, the marginal appearance of NKp65$^+$ ILC3 in the human skin does not necessarily contradict their importance. Despite their low *in vivo* frequency, upon stimulation ILC release extremely high per cell quantities of cytokines corroborating their role as important immune regulators (Bonne-Annee et al., 2019; Vivier et al., 2018). Further, the extraordinary high affinity of NKp65 to its cognate ligand KACL which is selectively expressed by human keratinocytes might also compensate for their low frequency. An enrichment in skin and blood of psoriasis patients of NCR$^+$ILC3 has been described where they possibly initiate or contribute to disease (Teunissen et al., 2014; Villanova et al., 2014). Therefore, although very rare in healthy skin, an infiltration of diseased skin by NKp65$^+$ ILC3 is conceivable. Hence, studying a potential disease-modifying role of the high affinity NKp65/KACL interaction in inflammatory skin diseases such as psoriasis and atopic dermatitis is of demanding interest.

5.1.2 Inter-individually variable NKp65 expression

NKp65 expression on tonsillar ILC3 is heterogenous among different individuals, with some having high surface levels whereas in others NKp65 is barely detectable (Figure 16). These differences are not affiliated to variations in age or gender. As shown in this study, IL-7 signaling is essential for maintenance of NKp65 expression. Therefore, varying IL-7 levels might cause the observed inter-individual differences in NKp65 expression. In human tonsils, IL-7 is expressed by follicular dendritic cells (FDC) as well as squamous and vascular endothelial cells (Kroncke et al., 1996; Takakuwa et al., 2000). NKp65 expression was analyzed on ILC3 derived from surgically removed tonsils. The most common reasons for tonsillectomy are tonsil hypertrophy (TH) and chronic or acute inflammation (tonsillitis) (Zhang et al., 2003). Tonsil hypertrophy is manifested as an enlargement of the tonsil and not necessarily accompanied by inflammation, whereas chronic and acute tonsillitis describes the inflammation of the tonsils as a result of viral or bacterial infection (Reis et al., 2013; Ruco et al., 1995; Zhang et al., 2003). The epithelial surface of the human tonsil is maximized by the extension of the epithelium into deep tonsillar crypts. The reticulated squamous crypt epithelium is usually interspersed with different types of lymphocytes providing an environment for their intimate interaction (Perry, J Anat., 1994). Both, TH and tonsillitis are associated with a pronounced lymphocyte infiltration causing damage in the endothelial structure (Alatas and Baba, 2008; Ruco et al., 1995; Uğraş and Kutluhan, 2008). Considering that in human tonsils, IL-7 is

expressed by squamous and vascular endothelial cells (Kroncke et al., 1996; Takakuwa et al., 2000), diversification and damage of the epithelium in diseased tonsils might impact IL-7 production. Indeed, elevated levels of IL-7 mRNA have been reported for hypertrophic tonsils (Huang et al., 2020). As described in chapter 1.3.1 the amount of available IL-7 is not only determined by IL-7 producing cells, but also critically influenced by its local consumption via IL-7R expressing cells. Therefore, the elevated frequencies of LTi cells and T cells, both IL-7R expressing cells, in chronically inflamed tonsils (Chang et al., 2014) might compete with NKp65 expressing ILC3 for the available IL-7. Hence, the inter-individually different state of inflammation and tissue damage as well as amount of lymphocyte infiltration could critically determine the patients' individual IL-7 levels which in turn might impact NKp65 expression. In future research, capturing the individual IL-7 levels could provide evidence for a link between varying IL-7 levels and inter-individually different NKp65 expression.

Besides varying IL-7 levels, differences in NKp65 surface expression could also arise from single nucleotide polymorphisms (SNP). SNPs are defined as loci with alleles that differ in only a single nucleotide and are present in at least 1% of the population (Reed E. Pyeritz, 2018). However, the SNP database dbSNP of the National Center for Biotechnology Information (NCBI) also lists mutations with frequencies <1%. For KLRF2, the gene coding for NKp65, over 4,000 mutations are reported. Most of these are located in introns, are synonymous mutations or of extremely low frequency (<1%). Only two SNPs show frequencies over 1% and are nonsynonymous missense mutations, consequently resulting in an altered amino acid sequence. The SNP rs576601, a C to A change in the protein coding sequence with a minor allele frequency (MAF) of 0.316, alters the amino acid sequence at position 131 from proline to threonine (Figure 61). In the NKp65 protein structure, position 131 is located in the extracellular C-type lectin-like domain (Li et al., 2013). The second SNP (rs1797517) is a G to A change with a MAF of 0.233 which results in an amino acid change from valine to isoleucine within the stalk region of the protein at position 68.

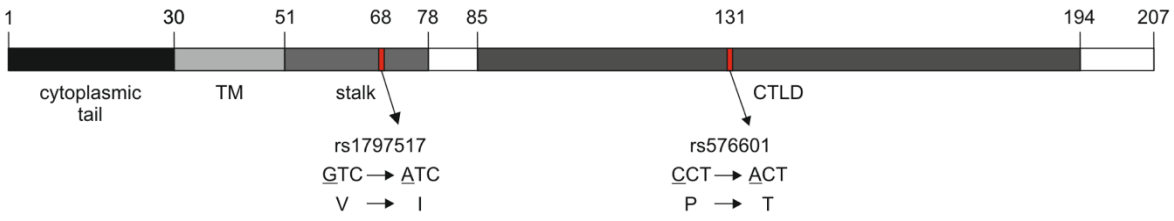

Figure 61: Schematic representation of the domain structure of NKp65 with indicated single nucleotide polymorphisms (SNP).
The different domains: cytosolic domain, transmembrane (TM) domain, stalk and C-type lectin-like domain (CTLD) are marked, as well as the two SNPs at position 68 and 131 (red boxes). The codons as well as the corresponding amino acids are indicated.

According to the position of the affected amino acid, both SNPs are prone to cause structural alterations which might lead to differences in protein expression. Since proline residues have a major impact on the proteins' conformation (MacArthur and Thornton, 1991), the SNP rs576601 causing a proline to threonine change is of special interest. Genotyping of the specific regions within the KLRF2 genomic sequence and correlating potential SNPs with NKp65 surface expression levels therefore might shed light on the inter-individually variable NKp65 expression.

5.1.3 NKp65 as a marker for ILC3

Since their discovery, a lot of research has been conducted to unambiguously define the different subsets of ILC. However, a specific marker for the identification of ILC3 and especially their demarcation from ILC3-like NK cells is still missing. The potential of NKp65 as a surface marker for ILC3 has already been suggested in 2016 (Steinle et al., 2016). In the same year, in a study published by Björklund et al. the heterogeneity of human ILC was delineated through single-cell RNA sequencing of tonsillar ILC (Bjorklund et al., 2016). Unbiased transcriptional clustering and analysis of transcriptional variation between the different subsets revealed KLRF2 as one of the most differentially regulated genes in ILC3 as compared to the other ILC subsets. While ILC1 and ILC2 were shown to be devoid of KLRF2 transcripts, some cells assigned to the NK cell cluster showed low levels of KLRF2 transcripts (Bjorklund et al., 2016) (Figure 62).

Figure 62: Violin plot depicting the distribution of KLRF2 gene expression among tonsillar ILC.
RNA seq data (GSE70580) were extracted from (Bjorklund et al., 2016) and analyzed using R-Studio. For analysis and assembly of the figure, the script allocated to the publication by Björklund et al. was used. The KLRF2 expression profile is shown as a violin plot with the average log_2(RPKM + 1) value encoded by the color and the distribution of data represented by its shape.

In this thesis, NKp65 expression was not detected on conventional NK cells which are defined based on a combination of classical NK cell markers such as NKp80, EOMES and CD94 (Figure 17, Figure 20). However, FACS based analyses of tonsillar lymphocytes also revealed NKp65 expression on a subset of $CD117^+CD94^+$ cells which are classified as stage 4a

NK cell precursor (Figure 23) (Freud et al., 2016). Despite the expression of CD94, stage 4a NK cells exhibit an ILC3-like phenotype, since they share most of their markers with ILC3 and are reportedly capable to produce IL-22 upon stimulation (Freud et al., 2016). Therefore, NKp65 is considered a specific marker of an ILC3-like phenotype. This is especially underlined, by the mutually exclusive expression of NKp65 on ILC3-like cells and its close relative NKp80 on mature NK cells (Figure 23, Figure 30). The detection of KLRF2 transcripts within the NK cell cluster by Björklund et al. does not necessarily argue against the notion of NKp65 as a marker for ILC3. Björklund et al. defined cells via their transcriptional profile and the congruous unbiased collocation to the respective cluster of related cells. The different cluster of cells were defined as ILC1, ILC2, ILC3 and NK cells based on the expression of 50 transcripts that most strongly define the respective cells. Consequently, even within one cluster a high heterogeneity of cells is delineated. Therefore, it is possible, that the NKp65 expressing $CD117^{+}CD94^{+}$ cells identified in this work, are allocated to the NK cell cluster in the study by Björklund and colleagues. Comparing transcriptional differences between KLRF2 expressing and KLRF2 negative cells within this cluster could support this assumption.

NKp65 not only demarcates ILC3 from mature NK cells, but also enables the distinction of NCR^{+} ILC3 from the closely related but functionally different subsets of other RORγt expressing ILC3 subsets, LTi cells and NCR^{-} ILC3 (Figure 19). So far, human NCR^{+} ILC3 were distinguished from LTi cells by analyzing NKp44 and CCR6 expression. Yet this is not a precise classification since CCR6 can also be expressed on NCR^{+} ILC3 (Killig et al., 2014) and $NKp44^{+}$ LTi cells have been described in human decidua (Vacca et al., 2015). The FACS based analysis shown in this work reveals that NKp65 is exclusively expressed by NCR^{+} ILC3, while NCR^{-} ILC3 as well as LTi cells are $NKp65^{-}$ (Figure 19). Interestingly, the analysis of KLRF2 transcripts in the ILC3 cluster defined by Björklund et al. which delineates all different subtypes of ILC3 including LTi cells, reflects a heterogenous expression among ILC3 (Figure 62) which is also suggestive of a subset-specific NKp65 expression.

In conclusion, NKp65 is exclusively expressed on cells with an ILC3-phenotype and is especially useful in demarcating ILC3 from NK cells and NCR^{+} ILC3 from highly related LTi cells and NCR^{-} ILC3. In this regard, NKp65 is superior to other commonly used markers, since it can solely identify these rare cells without the need of additional markers due to its highly specific expression.

5.1.4 NKp65 in NK cell development

As described in the previous section, NKp65 is expressed by a subset of $CD94^+CD117^+$ cells (Figure 23), which correspond to stage 4a NK cells in the model of NK cell development proposed by Freud and colleagues (Figure 21). Stage 4a cells share markers with NK cells such as CD94 and CD56 but also have ILC3 characteristics, e.g. the capability to produce IL-22 upon stimulation and the expression of CD117, CD161, and to some extent CD127 and RORγt (Freud et al., 2016). Whether these RORγt expressing cells are progenitors of NK cells or 'bona fide' ILC3 is highly debated. The fact that NK cells also develop independently of RORγt in RORγt deficient mice (Luci et al., 2009) and that at least murine NK cells are *Rorc isoform 2* (*Rorc2*, the gene encoding for RORγt in mice) fate-map negative (Satoh-Takayama et al., 2008; Vonarbourg et al., 2010) argues against a transitional $ROR\gamma t^+$ stage. In humans, RORγt independent NK cell development was reported in a study, demonstrating normal NK cell numbers in the PB of a patient with RORγt deficiency (Okada et al., 2015). On the other hand, several studies describe development of fully mature NK cells from human $ROR\gamma t^+$ precursors after *in vitro* culture or transfer into humanized mice (Freud et al., 2016; Scoville et al., 2016). However, these data do not exclude that S4a cells are arising from upregulation of NK cell markers caused by plasticity of ILC3 towards NK cells, a process that has been described to occur upon *in vitro* stimulation of ILC3 with IL-12 and IL-15 (Raykova et al., 2017) and *in vivo* at sites of inflammation (Bernink et al., 2013). In the current model of NK cell development stated by Freud et al. (Figure 7), ILC3 are segregated from stage 3 NK cells of their initial model (Figure 21) by the expression of NKp44, and NK cells are defined by a mixture of different markers including CD94 and NKp80. Thereby they unlink the highly RORγt expressing ILC3 from the trajectory of NK cell development. However, $ROR\gamma t^+CD117^+$ S4a NK cells are still placed in a linear developmental pathway (Figure 7). In this work, dissecting tonsillar lymphocytes into the various NK cell precursor and ILC subsets shows NKp65 expression exclusively on ILC3 and a small population of $CD117^+$ S4a NK cells (Figure 25). Among these populations, NKp65 expression is higher on ILC3 as compared to $CD117^+$ S4a NK cells (Figure 25 B). Considering NKp65 as a marker for ILC3 like cells, this would indicate, that $CD117^+$ S4a NK cells originate from plasticity of ILC3 towards a NK cell phenotype which is accompanied by downregulation of NKp65 expression. This hypothesis is supported by the notion that *ex vivo* sorted $CD117^+$ NK cells and ILC3 can give rise to each other when cultured *in vitro*, whereas $CD117^-$ NK cells maintain their phenotype (Chen et al., 2018). Based on the data from this work a revised model of NK cell development is proposed in which NKp65 might

serve as a marker to segregate the tangled pathways of ILC3 and NK cell development (Figure 63). This model suggests that NK cells arise via two distinct pathways. A direct and RORγt independent one giving rise to 'bona fide' NK cells, and a second one in which NK cells arise from plasticity of NKp65^{+}RORγt^{+} ILC3 towards a NK cell phenotype, traversing a plastic NKp65^{+}RORγt^{+}CD94^{+} stage. NK cells derived from the latter one, should therefore be considered 'ex ILC3' rather than 'bona fide' NK cells. In this model, NKp65 expression distinguishes CD94^{+} S4a NK cells which are placed in the linear NK cell development and are NKp65 negative, from the plastic CD94^{+}NKp65^{+} cells derived from plasticity of ILC3, designated intermediate ILC (int-ILC). Both pathways finally give rise to NKp80 expressing NK cells (Figure 63). Of note, the basic concept of a bidirectional pathway of NK cell development has also been suggested by others (Chen et al., 2018; Vonarbourg and Diefenbach, 2012).

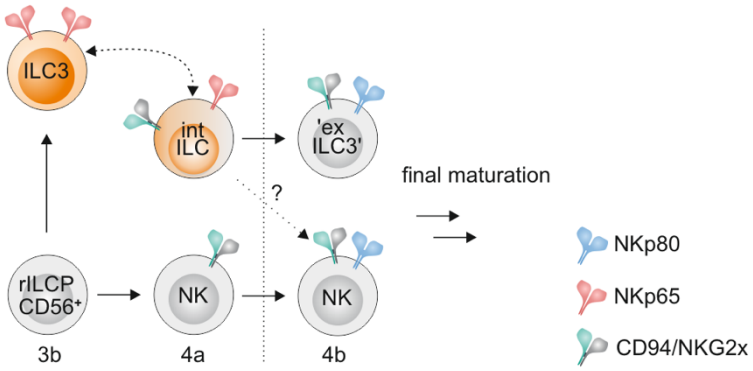

Figure 63: Proposed bidirectional model of NK cell development.
In the proposed model of NK cell development, NK cells derive from two different pathways involving precursor and intermediate cells which can be distinguished based on the expression of NKp65. The pathways branch at the CD56^{+} stage 3b which represents the restricted innate lymphoid cell (ILC) precursor (rILCP). In the linear pathway, NK cell development traverses the CD94^{+}NKp65^{-} stage 4a prior to development into stage 4b cells which are marked by the expression of NKp80. In an alternative pathway, rILCP first give rise to NKp65 expressing ILC3 which subsequently transdifferentiate into NKp65^{+} intermediate ILC ('int-ILC') which can give rise to NKp80 expressing 'ex ILC3'. Int-ILC might also give rise to stage 4b NK cells that are indistinguishable from cells derived from the linear pathway, as indicated by the dashed arrow and the question mark. Solid black lines represent developmental transitions, dashed lines indicate reversible transdifferentiation.

Support for this model is provided by the monitoring of NKp65 expression during *in vitro* differentiation of ILC from CD34^{+} HSPC as shown in this work. For visualization of the proposed developmental trajectory Figure 64 depicts the flow cytometric analysis of *in vitro* differentiated cells over a time span of 28 days based on Figure 31. Cells are segregated into ILC3, S4a NK cells and int-ILC by expression of CD94, CD117 and NKp65 and individual pathways are indicated by green and orange arrows.

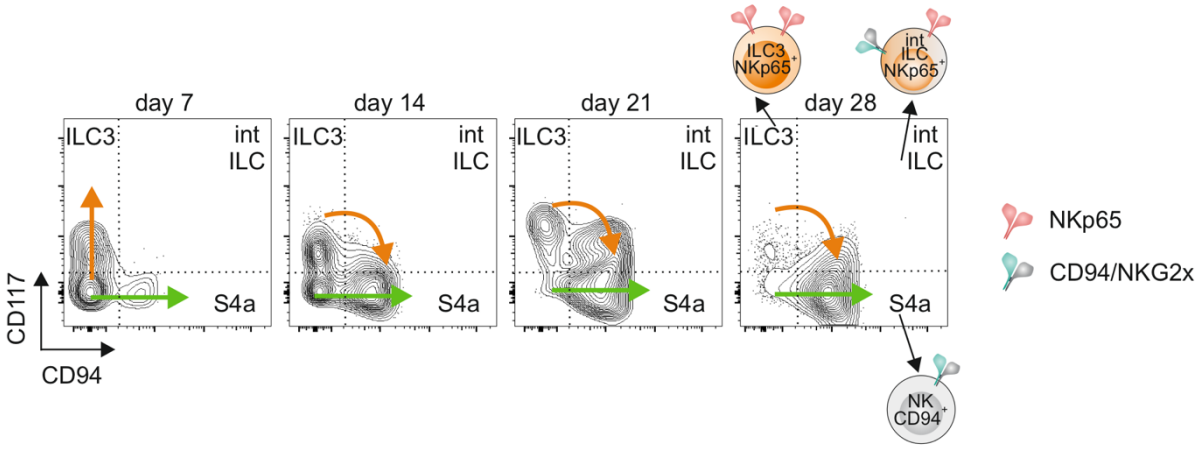

Figure 64: Depiction of the proposed developmental pathway of NK cell development during *in vitro* differentiation.
Flow cytometric analyses of *in vitro* differentiated ILC3, stage 4a (S4a) cells and intermediate ILC (int-ILC) at day 7, 14, 21 and 28 in culture. Cells were pre-gated for lin$^-$CD56$^+$ cells and ILC3, S4a cells and int-ILC segregated by CD117 and CD94 expression. In the respective contour plots, the different pathways of NK cell development are indicated by green and orange arrows.

After seven days, *in vitro* cultures of CD34$^+$ HSPC seeded on OP9-mock cells in presence of IL-7, IL-15, SCF and Flt3-L contain NKp65$^+$ ILC3 and NKp65$^-$CD94$^+$ S4a cells but lack NKp65$^+$CD94$^+$ int-ILC which emerge first at day 14 in culture (Figure 31 and Figure 64). Since mature NK cells express CD94 but are devoid of NKp65 expression (Figure 20), a transitional upregulation of NKp65 on cells that have already acquired CD94 expression seems unlikely. Therefore, the chronological order of emergence of CD94$^+$NKp65$^-$ S4a cells, prior to NKp65$^+$ int-ILC provides support for the notion that CD94$^+$NKp65$^-$ S4a cells are precursors in a direct pathway of NK cell development. NK cell development via the NKp65$^+$ int-ILC stage is corroborated by the accumulation of int-ILC at the expense of ILC3 from day 14 to day 28. Upon cultivation with OP9-DLL1 cells, NKp65$^+$ int-ILC subsequently mature into NKp80 expressing stage 4b and finally CD16$^+$ expressing stage 5 NK cells (Figure 40), demonstrating that the non-linear pathway via an intermediate stage also gives rise to mature NK cells. Although providing an environment in which NK cell maturation is feasible, NKp65$^+$ ILC3 as well as NKp65$^+$ int-ILC persist even in long term cultures arguing against them being part of an irreversible linear NK cell developmental pathway (Figure 41).

To finally validate the proposed model some further experiments are essential. Firstly, the direct developmental pathway via the NKp65$^-$CD94$^+$ NK cell precursor has to be validated by sorting of these cells and subsequent *in vitro* differentiation as shown for the NKp65$^+$ int-ILC (Figure 40). Further, slight phenotypic differences for *in vitro* generated and *ex vivo* tonsillar ILC have been observed in that NKp65$^+$ int-ILC are EOMES$^+$ (Figure 33) whereas NKp65$^+$ cells derived from human tonsil are solely RORγt$^+$ (Figure 18). Hence, the development of *ex*

vivo sorted NKp65^{+} ILC3, NKp65^{+} int-ILC and NKp65^{-} S4a cells into NK cells should also be addressed. An adjacent functional assessment as well as transcriptional profiling using RNA sequencing of NK cells derived via the different pathways could further provide information whether these cells differ in phenotype and/or their immunological role. Lastly, studying the differentiation of *ex vivo* sorted precursor cells in an appropriate humanized mouse model is inevitable to delineate *in vivo* NK cell development.

5.1.5 The role of Notch signaling during *in vitro* NK cell and ILC development

In order to investigate the role of NKp65 in NK cell development, OP9-mock cells have been used as feeder cells for *in vitro* differentiation studies, initially. Using these cells, ivILC robustly develop into NKp65 expressing cells whereas NKp80 and CD16 expressing cells barely emerge (Figure 30), suggesting a lack of certain signals for NK cell maturation. Since OP9 cells are devoid of the Notch ligands DLL1 and DLL4 (Schmitt and Zuniga-Pflucker, 2002) and a role of Notch signaling has already been reported for NK cell maturation (Felices et al., 2014), the involvement of Notch signaling during *in vitro* ILC differentiation was addressed and put into context of NKp65 and NKp80 expression in this work. The evolutionary conserved Notch signaling pathway is essentially required for embryonic development and regulates tissue homeostasis and maintenance of cells also in adult life (D'Souza et al., 2008). The human Notch signaling system consists of four Notch receptors (Notch 1-4) and five Notch ligands of the Jagged (Jagged 1 and Jagged 2) and the delta-like (DLL1, DLL3 and DLL4) protein families. Ligand binding by the Notch receptor leads to a conformational change which enables several sequential proteolytic events, resulting in the cleavage and release of the Notch intracellular domain (NICD). NICD subsequently translocates to the nucleus where it binds to the DNA binding protein 'Recombining binding protein suppressor of hairless' (RBPJ) and in concert with other factors acts as a transcriptional activator for a plethora of genes (Guruharsha et al., 2012). Both, cleavage of the NICD and binding to RBPJ are essential steps during this pathway and therefore often targeted in functional studies of Notch signaling (Gridley and Groves, 2014). In humans, Notch signaling is essential for early NK cell lineage-priming of HSC but leads to a developmental block at the non-cytotoxic CD56^{bright} stage if provided continuously as in cells transduced with the active NICD (Bachanova et al., 2009; Haraguchi et al., 2009). Contrarily, stimulation of CD56^{bright} cells isolated from PB with Notch ligands induces CD16 and KIR upregulation and enhances NK cell functions. Therefore, a temporal diverging need for Notch signaling during NK cell development has been suggested in which Notch signaling is essential in initial NK cell development, becomes detrimental at intermediate

stages and is again important for final NK cell maturation and acquisition of cytotoxic potential (Felices et al., 2014).

Due to their lack of DLL1 and DLL4 expression, OP9-mock cells are considered Notch ligand deficient cells. Considering the requirement of Notch signaling to initiate NK cell development (Haraguchi et al., 2009) as well as its critical role in generation of ILC3 (Kyoizumi et al., 2017), the development of NKp65^{+} ILC3 and S4a NK cells on OP9-mock cells (Figure 30) is at first sight counterintuitive. But, although being devoid of delta-like ligands, OP9-mock cells express the Notch ligands Jagged 1 and Jagged 2 (Schmitt and Zuniga-Pflucker, 2002), which at least under the conditions tested in this study, appear to be sufficient in inducing NK cell and ILC3 development. However, cells differentiated on OP9-mock cells do not acquire markers of mature NK cells such as NKp80 and CD16 (Figure 30), suggesting a developmental block at an immature stage. This is well in line with the reported accumulation of cells in the non-cytotoxic CD56^{bright} stage as a result of *in vitro* differentiation of precursors with continuous active Notch signaling (Bachanova et al., 2009). However, transferring ivILC from OP9-mock onto OP9-DLL1 cells, leads to induction of NKp80 expression and also further development into CD16 expressing cells (Figure 36 A). Albeit all Notch ligands induce the same signaling pathway, the functional outcomes have been shown to differ depending on the Notch receptor ligand combination (Pan et al., 2005). One among many possible reasons for these differences are alterations in the strength and duration of the signal which is determined by the availability as well as nature of the respective ligand (Bray, 2016). In the system used in this study, replacing OP9-mock with OP9-DLL1 cells results in both, the presence of a different ligand (DLL1 in addition to Jagged 1 and Jagged 2) as well as higher ligand proposition due to overexpression of DLL1 upon transduction. A lower level of Notch 1 activation elicited by Jagged 1 as compared to DLL1 has been reported to differentially regulate the expression of certain genes resulting in altered developmental processes (Petrovic et al., 2014). In concert with the higher availability of ligands this might explain why NKp80 expression is induced by OP9-DLL1 cells but lacking in cocultures with OP9-mock cells. Of note, although ivILC developed on OP9-mock cells were mainly NKp80 and CD16 negative, their TF expression profile mimicked the profile of CD56^{bright} (EOMES^{+}T-bet^{-}) and CD56^{dim} (EOMES^{+}T-bet^{+}) populations of human NK cells which *in vivo* are NKp80^{+}. This acquisition of a NK cell maturation-associated phenotype despite lacking NKp80 expression has also been observed by Freud and colleagues following cocultures of primary stage 3 or stage 4a NK cells with DCs (Freud et al., 2016) and indicates that Notch signaling directly impacts NKp80 expression also independently of NK cell maturation. Considering that NKp80 is not induced on the Jagged 1

and Jagged 2 expressing OP9-mock cells, but upregulated in presence of OP9-DLL1 and, although less pronounced, also with OP9-DLL4 cells, indicates specificity for delta like ligands (DLLs) in regulation of NKp80 expression. However, it is also possible that the observed effects are a consequence of differences between the OP9-mock and OP9-DLL1 or -DLL4 cells, other than the expression of DLLs, which might originate from the transduction process. Experiments using recombinant DLL1 or DLL4 protein or the application of blocking antibodies could provide further support for a specific effect of DLLs in promoting NKp80 expression. Additionally, analyzing the NKp80 promoter for binding sites of Notch related transcription factors such as RBPJ could provide evidence for NKp80 being transcriptionally regulated by Notch signaling.

Although promoting final *in vitro* NK cell maturation, OP9-DLL1 cells did not support differentiation from $CD34^+$ HSPC within a period of three weeks under the conditions tested in this study (data not shown). Contrarily, within the same period robust ivILC development was observed in cocultures with OP9-mock cells (Figure 28). These results suggest that *in vitro* NK cell development initially requires moderate Notch signaling provided by Jagged 1/2, followed by strong signals via DLL1 for final maturation, whereas strong Notch signaling in the beginning of the culture hinders NK cell differentiation. This is well in line with the temporarily different requirement of Notch signaling during human NK cell development as reported by Felices et al. and might be due to a pronounced T cell development in presence of distinct Notch signaling via DLL1 (Schmitt and Zuniga-Pflucker, 2002) which competes for NK cell development at early stages.

In contrast to NKp80 which is induced upon presence of Notch ligands, NKp65 expression is downregulated (Figure 38). This emphasizes the mutually exclusive expression of NKp80 on conventional NK cells and NKp65 on ILC3 and ILC3-like cells. The reduced NKp65 surface expression as result of transferring ivILC from OP9-mock to OP9-DLL1 cells is accompanied by a reduced frequency of NKp65 expressing cells. Assessing NK cell maturation based on the expression of the TFs EOMES and T-bet revealed the lowest NKp65 expression and frequency of NKp65 expressing cells among the most mature $EOMES^-T\text{-}bet^+$ subset. The decrease in NKp65 expression is exclusive for cocultures of ivILC and OP9-DLL1 cells, whereas in the absence of DLL1 also $EOMES^-T\text{-}bet^+$ cells stably express NKp65 (Figure 38). The development of FACS sorted $NKp65^+$ int-ILC into NKp80 expressing cells, observed only in cocultures with OP9-DLL1 or -DLL4 (Figure 40), excludes that the reduction in frequencies of $NKp65^+$ cells in bulk cultures is caused by an outgrowth of $NKp65^-$ or a selective loss of

NKp65$^+$ cells. These data once more demonstrate that acquiring a NK cell phenotype is accompanied by downregulation of NKp65 with concurrent NKp80 upregulation.

5.2 Cytotoxicity of NKp65 expressing ivILC

To cope with changes in the tissue microenvironment by rapid calibration of cytokine secretion and response to pathogens and tissue damage, ILC are endowed with a broad variety of receptors. Besides the intensively studied cytokine receptors, some subsets of ILC also express the germline-encoded NCRs NKp30, NKp46 and NKp44 (Colonna, 2018; Simoni and Newell, 2018). So far, NCRs have mainly been studied in the context of NK cell responses and only little is known about their implication in the immunobiology of helper like ILC (Barrow et al., 2019). Additionally, reports on a direct activation and immunorecognition of ILC3 through receptor-mediated cell-cell interactions are sparse. In this study, NKp65$^+$ *in vitro* generated ILC were shown to directly kill KACL expressing target cells via NKp65-KACL interaction. NKp65-KACL interaction promotes cellular cytotoxicity against the endogenously KACL expressing U937 cells (Figure 42) as well as KACL transduced NKR cells which are naturally devoid of KACL expression (Figure 43). The dependency of target cell killing on NKp65-KACL interaction is evidenced by the significantly reduced cytotoxicity in presence of the anti-KACL mAb OMA1 which blocks NKp65-KACL interaction (Bauer et al., 2015). Likewise, transduction of KACL renders NKR cells susceptible to ivILC-mediated cytotoxicity whereas control transduced cells are barely killed. Additionally, the extent of KACL-dependent cytotoxicity against U937 cells correlates with the varying NKp65 expression levels on ivILC derived from different donors. However, especially U937 cells are also lysed independently of NKp65 as suggested by the remaining cytotoxicity even in presence of the blocking antibody OMA1. This is most likely caused by their reported expression of other ligands for activating NK cell receptors (Welte et al., 2006) that might trigger cytotoxicity by ivILC. At an E:T-ratio of 0.5:1, even in presence of OMA1 over 70% of U937 cells are lysed (Figure 42) which is in clear contrast to about 15% lysis observed for NKR cells under the same conditions (Figure 43). This corroborates the assumption of an involvement of other NK cell activating receptors in NKp65 independent killing as, in contrast to U937 cells, NKR cells are known to be mostly devoid of NK cell activating ligands and therefore considered resistant to NK cell mediated killing (Tremblay-McLean et al., 2019). The cytotoxic potential against KACL expressing target cells is attributed to the CD94$^+$ cell subset of NKp65$^+$ ivILC (Figure 44), which is well in line with the reported non-cytotoxic nature of ILC3. However, recent reports indicate that

ILC3 can convert into ILC1-like cytotoxic cells in the presence of inflammatory cytokines which is suggested to occur *in vivo* for example during Crohn's disease (Bernink et al., 2013; Takayama et al., 2010). Moreover, *in vitro*, ILC3 acquire features of NK cells including cytotoxic potential upon stimulation with IL-12 and IL-15 (Raykova et al., 2017) and cytotoxic potential has been described for *ex vivo* stage 4a NK cell developmental precursors (Freud et al., 2016). The cytotoxic subset of NKp65 expressing cells presented in this work, expresses classical NK cell markers such as CD56 and CD94, but is devoid of NKp80 expression (Figure 30) and therefore not considered mature NK cells. Hence, NKp65 endows $CD94^+$ ILC3-like cells which might develop in result of certain stimuli also *in vivo*, to specifically lyse KACL expressing target cells. Cells with a related phenotype are also present in human skin (Figure 26), where they are spatially adjacent to KACL expressing target cells and might contribute to skin immunobiology.

5.2.1 NKp65 expressing ivILC kill KACL expressing target cells via a so far unknown mechanism

NK cells unleash their killing activity by the cytotoxic granule-dependent granzyme/perforin pathway or by engagement of death receptors that initiate caspase cascades resulting in apoptosis (1.2.1) (Prager and Watzl, 2019). Lytic granule mediated killing is a rapid process mostly induced upon a single contact, whereas death receptor dependent killing is much slower and requires multiple cell-cell contacts gradually activating caspase-8 (Zhang et al., 2016). Significant NKp65-dependent cytolysis of KACL expressing target cells requires prolonged over-night incubation suggesting that killing is death receptor mediated. However, KACL expressing cells are lysed by $NKp65^+$ ivILC irrespective of the presence of the casp-8 inhibitor Z-IETD-FMK in concentrations which were shown to effectively protect cells from NK cell-induced Fas- or TRAIL-mediated apoptosis (Özören et al., 2000; Thoren et al., 2012). Due to the lack of a suitable positive control demonstrating the functionality of the used compound, an involvement of casp-8 in NKp65-mediated killing cannot be excluded, entirely. Moreover, for both, Fas (Feng et al., 2004) and TRAIL-induced (Petak et al., 2003) cell death, casp-8 independent mechanisms have been described. Hence, to reliably exclude killing via death receptors, specific blocking antibodies against Fas, TRAIL or their respective ligands should be exerted.

The dependency on cytolytic granules was addressed by incubation of ivILC with CMA prior to the assessment of cytolytic capacity in a killing assay with KACL or mock transduced NKR cells. CMA is a vacuolar type H^+-ATPase inhibitor that blocks the acidification of lytic granules leading to inactivation of cathepsin L, which prevents the conversion of immature

perforin into its active form (Kataoka et al., 1994; Konjar et al., 2010). CMA treatment significantly reduced ivILC-mediated killing of both, KACL expressing and KACL deficient target cells. However, protection of target cells was only partial, suggesting that the cytolytic potential of ivILC is not solely dependent on cytolytic granules. Moreover, lysis of NKR/KACL cells is in contrast to NKR/mock cells slightly, albeit not significantly, dependent on the E:T ratio (Figure 45A). Considering an exclusive dependency of target cell killing on the perforin/granzyme pathway, lysis upon CMA treatment should not depend on the E:T ratio as observed for cytotoxicity against NKR/mock cells (Figure 45A, right).
In conclusion, in this study the mechanism of the NKp65-mediated killing of KACL expressing target cells could not be unraveled, entirely. There is no evidence for an involvement of casp-8, whereas although insignificant, an involvement of cytolytic granules is suggested.

5.3 Transcriptional regulation of NKp65 expression

5.3.1 The KLRF2 promoter

The genetic basis for phenotypic variations between different species is a major objective of evolutionary genetic research. It has become clear that organismal diversity is not only controlled by the number of genes, but also critically depends on variations in gene expression patterns (Levine and Tjian, 2003). In eukaryotes gene expression is controlled by a broad array of different mechanisms including chromatin condensation, methylation of DNA, transcriptional initiation, alternative splicing of RNA as well as translational and posttranslational control. Among these categories transcriptional initiation most commonly appears to be the critical determinant of gene expression. Transcriptional initiation is controlled by promoters, which are considered equally important for gene function as the coding sequence (Wray et al., 2003). Hence, studying the structure, function and regulation of promoters can explain tissue and species-specific gene expression. Therefore, in this work the KLRF2 promoter was studied in order to explain the tissue specific and cell type restricted expression of NKp65.

5.3.1.1 The KLRF2 core promoter is a TATA-less, focused promoter

Computational analysis of the KLRF2 promoter reveals the lack of any TATA-box motifs in an appropriate distance to the transcriptional start site (TSS) and is therefore considered a so-called TATA-less promoter. Since the majority of TATA-less genes are described to be constitutively expressed (Azizkhan et al., 1993) and NKp65 expression is tissue and cell type

specific, a TATA-box motif within the KLRF2 core promoter was expected. However, also gene expression of the related murine Nkrp1c – a member of the NKRP1-family and restrictively expressed by NK cells, NKT cells and activated T cells – is regulated by a TATA-less promoter (Aust et al., 2009; Ljutic et al., 2003). Furthermore, the NK cell specific NKG2A (Plougastel and Trowsdale, 1998) and murine 2B4 (Chuang et al., 1999), both expressed in a tissue-specific manner, are regulated by TATA-less promoters.

Transcriptional initiation in TATA-less promoters is often directed by other core promoter motifs such as Inr and DPE (Juven-Gershon and Kadonaga, 2010), which both are predicted within the KLRF2 core promoter in a distance allowing for their synergistic effect (Figure 46) (Kutach and Kadonaga, 2000). Computational analysis of promoter elements based on position weight matrices, as also adopted here, does not necessarily reflect their transcriptional activity, since sequence motifs are of short and redundant nature and are therefore often found in multiple locations of the genome (Pedersen et al., 1999). However, in computational analyses a synergistic combination like the Inr and DPE motifs are less likely to occur by chance than single elements, emphasizing the validity of the analysis. The presence of these core promoter motifs indicates that KLRF2 gene expression is regulated by focused transcription initiation, which in contrast to dispersed initiation is initiated at a single nucleotide or within a narrow region of nucleotides. In general, the transcription of most regulated genes is controlled by focused promoters while transcription of constitutively expressed genes is directed by dispersed promoters (Juven-Gershon and Kadonaga, 2010). Although computational analysis of promoter elements is widely used, the results have to be considered indicative and an actual involvement of the predicted sites has to be validated in functional studies. In order to evaluate KLRF2 promoter activity the putative promoter and sequential 5'-deletions thereof were cloned in front of a luciferase reporter gene and transfected into NK-92MI cells. NK-92MI cells endogenously expresses NKp65 (Spreu et al., 2010) and therefore provide all the necessary factors that might drive its expression. Strikingly, luciferase assays using promoter constructs from -61 to +108 or -32 to +108 bps lead to a near abrogation of promoter activity, albeit both constructs contain the computationally predicted core promoter elements (Figure 48). This indicates a requirement of upstream regulatory elements which either promote accessibility of the core promoter elements or provide docking sites for essential components of the transcriptional machinery.

5.3.1.2 The proximal promoter critically directs KLRF2 gene expression

The analysis of the core promoter emphasized the importance of upstream regulatory elements in the proximal or distal promoter for transcriptional regulation of KLRF2 gene

expression. In a preliminary study by Dr. Björn Bauer (Steinle laboratory), luciferase assays using the putative promoter region (spanning -1005 to +108 bp relative to the TSS) and successive 5‘-truncated promoter constructs revealed that deletions from position -1005 to -351 have no significant impact on promoter activity. Consequently, this region does not contain any regulatory *cis*-elements and the transcriptional regulation of *KLRF2* can be considered dominated by the proximal rather than the distal promoter region. In this work, by probing further incremental deletions two major activating regions within the proximal promoter were identified designated activating regions ii and i. In silico analysis of putative TF binding sites within these regions revealed a high number of putative binding sites (Table 21 and Table 22), discussed in the next section.

5.3.2 Transcription factors regulating NKp65 expression

Transcription factors are mostly modular proteins containing a DNA binding domain and domains that interact with other TFs, transcriptional regulators or components of the transcriptional machinery. These interacting proteins, although often not directly bound to the DNA can regulate transcription for example by compaction or opening of chromatin, thereby allowing, or permitting access of other transcriptional regulators. Hence, transcriptional regulation requires binding of TFs and other regulatory proteins in a combinatorial manner to assemble a multiprotein complex which facilitates highly regulated tissue- and cell type specific gene expression (Spitz and Furlong, 2012).

For *in silico* analysis of the activating regions for putative TF binding sites the MatInspector software was utilized. MatInspector predicts binding sites based on sequence motifs by position weight matrices (PWM). PWMs represent the nucleotide distribution of each position within the binding site, equally (Cartharius et al., 2005). This is superior to an alignment of the entire consensus sequence, since it allows for mismatches while accounting for the fact that some positions are more highly conserved than others (Stormo, 2000). The resulting matrix scores are the sum of each individual matrix value and delineate the similarity to the consensus sequence (Cartharius et al., 2005). Transcription factor binding sites (TFBs) are short, degenerated sequence motifs comprising usually around 5 to 15 bps. The evolutionary selected degeneracy of TFBs is beneficial since it enables distinct levels of activity for the same TF upon different promoters (Stormo, 2000). These characteristics of TFBs cause potential binding sites to occur very frequently in the human genome. Prediction of binding sites solely based on sequence motifs is insufficient to explain *in vivo* binding of TFs since it does not account for determinants beyond sequence specificity such as chromatin accessibility (Bulyk,

2003). However, *in silico* analyses of TFBs provide an informative basis for further functional assessment. Taking these restrictions of computational TFB analysis into account, it is not surprising that although the activating regions within the KLRF2 promoter are of short size (67 and 40 bps) a multitude of putative TFBs was predicted (Table 21 and Table 22). Based on the observation that IL-7 is essential for maintenance of NKp65 expression, in a first approach the high number of TFBs was constricted to TFBs for TFs that are targets of IL-7 downstream signaling. The TFs related to IL-7 signaling can be assigned to one of the two IL-7 signaling pathways, the PI3K or the JAK/STAT5 pathway (Figure 8). Putative binding sites for TFs assigned to the PI3K pathway are enriched within the activating region ii, whereas activating region i contains a response element for STAT5 (Figure 50).

5.3.2.1 The implication of Forkhead proteins

The predicted TFs associated with the PI3K pathway are the members of the Forkhead box (FOX) protein family FOXA2, FOXJ1, FOXI1 and FOXP1, as well as E4BP4 and Oct-1. Analyzing different microdeletions revealed that the entire section from -282 to -258 confers to the activating function of region ii. Since the putative binding sites for E4BP4 and Oct-1 are positioned outside this section they are considered not to be involved in the transcriptional regulation of NKp65. In the area from -282 to -258 two binding sites for FOX proteins were predicted (Figure 50). The huge family of human FOX proteins includes 50 different proteins, categorized into 19 subfamilies designated A-S. Irrespective of their subclass all FOX proteins share a highly conserved 110 amino acid winged-helix domain (Forkhead domain) which provides DNA binding. Classification into subfamilies is based on differences outside this conserved region (Lam et al., 2013). Considering that all FOX proteins share the DNA binding Forkhead domain it is not surprising, that they also bind to the same canonical Forkhead target sequence RYAAAYA (with R = A/G and Y = T/C). Although for some members of the FOX protein family a higher affinity to slightly different target sequences or flanking nucleotides have been described (Nakagawa et al., 2013), FOX proteins generally show extensive overlap in binding to the same genomic region (Chen et al., 2015). Therefore, although computational analysis predicted specific binding sites for FOXP1, FOXJ1, FOXI1 and FOXA2 all centered around one of the two canonical FOX protein binding motifs, theoretically every member of the FOX protein family can bind to these specific regions in the KLRF2 promoter. Microdeletions within either of the two FOX protein binding sequences reduces luciferase activity to the level of the construct lacking the entire activating site ii (Figure 54). This suggests that in order to drive transcription, both sites have to be occupied by an appropriate TF. The

proximity of the two binding sites, with a distance of only six nucleotides provides the possibility of a direct homo- or heterotypic protein interaction, which is required for the functional activity of some FOX proteins (Li et al., 2016).

At least *in vitro*, any given FOX protein can potentially bind to the consensus sequences present in the KLRF2 promoter. This complicates the identification of a specific FOX protein by simple methods such as pulldown assays or specific mutation of the respective site. However, the observed downregulation of NKp65 expression on *ex vivo* ILC3 upon treatment with the PI3K inhibitor Ly294002 (Figure 55) might provide information since not every member of the FOX protein family is equally affected by PI3K signaling. So far, only FOXA2 and the members of the FOXO subfamily have been described as direct targets of Act, a kinase downstream of the PI3K signaling pathway (Wolfrum et al., 2003; Zanella et al., 2013). However, the presence of two putative FOX protein binding sites, precisely matching the reported consensus sequence as well as the reduction in luciferase activity after deleting these sites, suggests a critical role of FOX protein in regulating promoter activity. In future studies, the discrete binding of FOX proteins to the predicted sites must be validated preferably in primary cells using Chromatin Immunoprecipitation (ChIP) assays. Alternatively, the impact of a certain FOX protein could be addressed by its overexpression or knock-down by siRNA or genetic modification.

5.3.2.2 NKp65 expression is transcriptionally regulated by STAT5

The *in silico* mapping of TFBs within the second activating region in the KLRF2 promoter revealed a STAT5 binding motif as the only IL-7 signaling related site. Treating cells with an inhibitor of STAT5 (iSTAT5) leads to downregulation of NKp65 surface expression which is accompanied by reduced KLRF2 transcript levels and indicates regulation on transcriptional level (Figure 53). STAT5 can influence gene expression either directly by binding to the pursuant site within the promoter or indirectly via TF intermediates that are STAT5 targets themselves. The STAT5 binding motif within the KLRF2 promoter has high similarity to the STAT5 consensus sequence and STAT5 is directly recruited to this specific site as shown in a pulldown assay (Figure 52). In this *in vitro* analysis STAT5 is precipitated by synthetic oligomers that do not reflect the naturally occurring state in which accessibility of DNA for TFs is determined by the chromatin structure. *In vivo* binding of STAT5 to the KLRF2 promoter therefore had to be validated in a ChIP assay which was done by Dr. Stefan Leibelt (data not shown). The functional relevance of STAT5 in the transcriptional regulation of NKp65 is underlined by the severe reduction of promoter activity upon mutation of two nucleotides within

the STAT5 response element (Figure 51). Abrogation of STAT5 binding to this mutated site was shown in a pulldown assay using the respective mutated oligomers (Figure 52). Mutation of only two nucleotides within the construct containing the entire proximal promoter nearly abrogates luciferase activity. This was surprising, since this construct contains the second activating region ii. Consequently, the activating function of this region is critically dependent on the presence of an intact STAT5 binding site and does not mediate transcriptional activity by itself. TFs that typically operate in conjunction with other factors, are the so-called pioneer TFs which promote transcriptional activation by chromatin remodeling resulting in accessibility of the DNA for other TFs. Pioneer TFs therefore often provide tissue specificity (Zaret and Carroll, 2011). One example for a pioneer TF is FOXA2 which has been described to act as chromatin remodeler during early liver development (Cirillo et al., 2002) and was predicted to bind within the activating region ii in the KLRF2 promoter (Figure 54). Besides remodeling chromatin, TFs bound to the activating region ii can also promote transcription by direct protein-protein interaction with STAT5 or by recruitment or replacement of STAT5 activating or repressing factors. A multitude of different proteins including transcriptional or epigenetic regulators, kinases and phosphatases have been reported to modulate STAT5 activity thereby providing cell type and tissue specificity (Able et al., 2017). Since translocation to the nucleus and binding to the DNA requires STAT5 phosphorylation, kinases and phosphatases critically regulate STAT5 transcriptional activity (Able et al., 2017; Gouilleux et al., 1994). Additionally, STAT5 interacts with proteins of the general transcription machinery such as p300 that binds the carboxy-terminal transactivation domain of STAT5 and enhances its transcriptional activity (Pfitzner et al., 1998). Repressors of STAT5 are for example the corepressor ‘silencing mediator for retinoic acid receptor and thyroid hormone receptor’ (SMRT) or ‘Sac-3 domain-containing protein’ (SHD1). Both were shown to physically interact with STAT5 and to repress its transcriptional activity (Khuda et al., 2004; Nakajima et al., 2001). A concerted transcriptional regulation including both activating sites within the KLRF2 promoter might explain why although STAT5 is expressed in various human tissues and cells (Rani and Murphy, 2016), NKp65 expression is restricted to ILC3. Based on the data gained from these analyses a model for the transcriptional regulation of NKp65 is proposed (Figure 65). In this model IL-7 signaling in ILC3 leads to activation of the JAK/STAT and the PI3K pathways resulting in the activation of STAT5 as well as other TFs, most likely FOX proteins, that bind to their respective site within the KLRF2 promoter. Binding of TFs to the activating region ii leads to chromatin opening, attraction of STAT5 activators and/or replacement of STAT5 repressors thereby

enhancing STAT5 transcriptional activity and consequently promoting KLRF2 gene transcription (Figure 65).

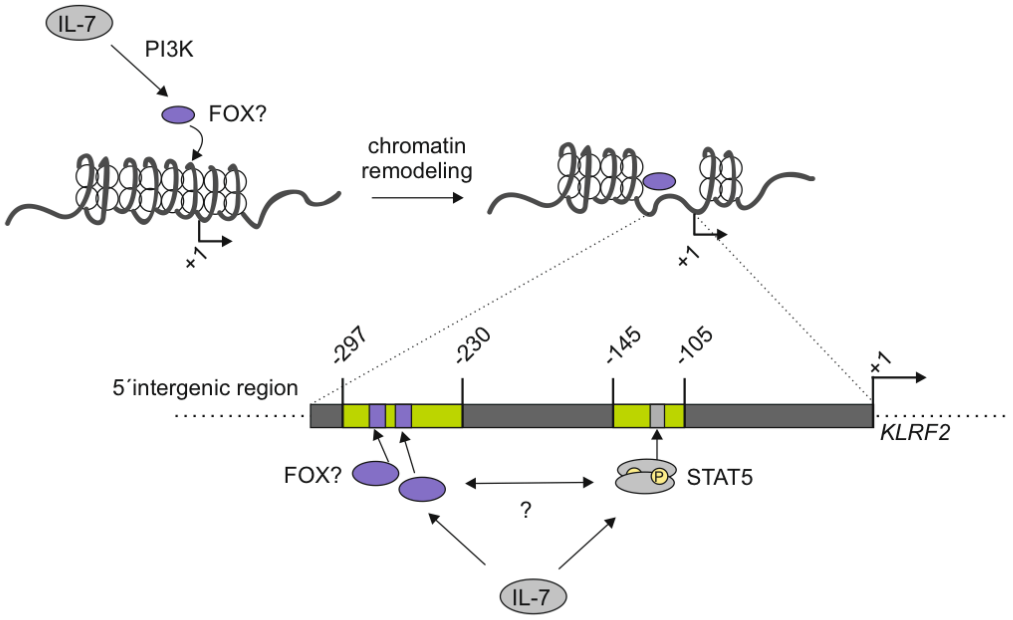

Figure 65: Proposed model of transcriptional regulation of NKp65 expression.
In the absence of IL-7 condensed chromatin obviates accessibility of response elements residing in the KLRF2 proximal promoter region. Stimulation of cells with IL-7 activates the PI3K and JAK/STAT pathways leading to the activation of different transcription factors (TFs) such as Forkhead box (FOX) proteins and STAT5. In a first step of transcriptional activation FOX proteins might act as pioneering factors by direct binding to the condensed chromatin and regulation of chromatin opening. In the open chromatin formation, the STAT5 binding site residing in the proximal promoter region is accessible. Binding of STAT5 dimers to the response element results in activation of transcription which might be further supported by direct interaction with FOX proteins or other TFs attracted during this process.

To further support the proposed model, promoter constructs with mutation of both, the FOX binding sites and the STAT5 binding site could be analyzed using luciferase assays. Further, the investigation of NKp65 surface expression on ILC3 after concomitant stimulation with PI3K and STAT5 inhibitors could provide evidence for a concerted dependency of NKp65 expression on both signaling pathways.

5.3.3 The IL-7/STAT5 pathway regulates NKp65 expression

This work provides evidence for a regulation of NKp65 expression via the IL-7/STAT5 pathway. The exclusive expression of NKp65 on IL-7R expressing ILC3 and their dependency on IL-7 signaling for development and maintenance of effector functions (Diefenbach et al., 2014) constitutes an interesting link. The rapid reduction of NKp65 expression on ILC3 upon IL-7 withdrawal (Figure 49) or inhibition of STAT5 (Figure 53) suggests that NKp65 expression requires perpetual STAT5 signaling. As stated in the introduction (1.3) IL-7 is generally considered to be constitutively expressed and mostly unaffected by external stimuli

which would allow for constant signaling that is necessary for sustained NKp65 expression. IL-15 also signals via the JAK/STAT5 pathway and a compensatory role of IL-15 for IL-7 mediated processes has been reported (Robinette et al., 2017). However, IL-15 is mainly produced upon external stimuli and its expression is restricted due to tight posttranscriptional regulation (Waldmann and Tagaya, 1999). Whereas signaling by γc-dependent cytokines usually leads to up regulation of the respective cytokine receptor (Depper et al., 1985), IL-7Rα is generally down regulated in response to IL-7 which has especially been shown for T cells (Mazzucchelli and Durum, 2007). Contrarily, IL-7Rα expression on ILC3 was shown to be more stable (Martin et al., 2017), allowing for enduring IL-7 signaling and maintenance of NKp65 expression via STAT5. Lastly, also the tissue distribution of NKp65 expressing cells suggests an involvement of IL-7 in the regulation of NKp65 expression. Whereas NKp65 expressing cells are absent from the peripheral blood (Figure 20) in which IL-7 levels are reportedly low (Lundstrom et al., 2012), NKp65 expressing cells are accumulated in tissue that is fairly rich in IL-7 such as the human tonsil (Figure 17), lymph nodes and the intestine (Figure 13) (Mazzucchelli and Durum, 2007).

5.4 Shedding of NKp65

Additional to its regulation on the transcriptional level, NKp65 surface expression is post-translationally controlled by its proteolytic release. Proteolytic cleavage of NKp65 is inducible by stimulation with its ligand KACL and by treatment with PMA and Ionomycin (P/I) and can be inhibited by the treatment with the metalloproteinase inhibitor Batimastat (BB94). BB94 is a broad-spectrum metalloproteinase inhibitor and therefore affects both types of metalloproteinases, MMPs and ADAMs (Rasmussen and McCann, 1997). However, MMPs are usually attributed to cleavage of extracellular matrix proteins, whereas ADAMs are mainly described as sheddases of transmembrane proteins (Edwards et al., 2008; Lu et al., 2011), implicating an involvement of ADAMs rather than MMPs in NKp65 shedding. Ligand- or P/I-induced proteolytic cleavage of NKp65 leads to the release of a truncated soluble form of NKp65 (sNKp65) with a molecular weight below 15 kDa and reduces NKp65 surface expression (4.6.3.2 and 4.6.3.3). The amount of sNKp65 depends on the stimulus, ranging from 40 pg/ml after P/I stimulation to 400 pg/ml after ligand-stimulation. Therefore, stimulation with its ligand KACL promotes NKp65 shedding more efficiently, suggesting a conformational change which might promote accessibility of cleavage sites, as also reported for shedding of other transmembrane receptors such as Notch (Kopan, 2012). Ectodomain shedding is an

important post-translational process modifying the expression and functions of hundreds of membrane proteins (Lichtenthaler et al., 2018). Its importance in immunology is especially highlighted by the shedding of NKG2D ligands which is thought to be a major escape mechanism employed by tumor cells to circumvent NKG2D-mediated immune surveillance (Zingoni et al., 2020). Though, shedding also positively modulates immune responses as shown for CD16 shedding, which promotes NK cell survival and allows for binding and lysis of several target cells in a process called serial killing (Anft et al., 2020; Srpan et al., 2018). If proteolytic cleavage of the receptor is required for detachment of effector and target cell, shedding must occur while the receptor is still actively bound to the ligand. This would leave the target cell decorated with remaining receptor ectodomains at its cell surface. Detection of NKp65 on KACL expressing target cells after coincubation with NK-92MI/NKp65 effector cells as shown in this work (Figure 57), suggests that NKp65 shedding is required for cell detachment. The solely detection of NKp65 with an antibody that is not interfering with NKp65-KACL interaction excludes that NKp65 expression is induced in the target cells upon stimulation and that it is actively bound to KACL on the target cells' surface. The sensitivity of this process to BB94 treatment further demonstrates an involvement of metalloproteinases (Figure 57). Thus, as also seen for CD16 (Srpan et al., 2018), NKp65 shedding might support detachment of effector and target cell, thereby enabling serial interactions with other target cells. Considering the extraordinarily high affinity of NKp65 to its ligand KACL, NKp65 shedding might not only be required for detachment, but also for termination of the signaling cascade. This would prevent NKp65 expressing cells from dysregulated cell signaling which can promote tumorigenesis, chronic inflammation and other pathological alterations (Hunter, 2000).

Considering the possible role of NKp65 shedding in promoting serial killing of target cells, it would be of immediate interest to further study whether inhibition of shedding by metalloproteinase inhibitors actually reduces the capacity of NKp65 expressing cells to kill target cells. This could also be addressed by identification of the cleavage site and subsequent establishment of shedding resistant variants of NKp65. Such shedding resistant cells could further be analyzed in comparison to wild type cells via live cell imaging to visualize possible serial killing events.

6. References

Able, A.A., Burrell, J.A., and Stephens, J.M. (2017). STAT5-interacting proteins: a synopsis of proteins that regulate STAT5 activity. *Biology* **6**: 20.

Abt, M.C., Lewis, B.B., Caballero, S., Xiong, H., Carter, R.A., Susac, B., Ling, L., Leiner, I., and Pamer, E.G. (2015). Innate immune defenses mediated by two ILC subsets are critical for protection against acute Clostridium difficile infection. *Cell Host Microbe* **18**: 27-37.

Ahn, Y.O., Blazar, B.R., Miller, J.S., and Verneris, M.R. (2013). Lineage relationships of human interleukin-22-producing CD56+ RORgammat+ innate lymphoid cells and conventional natural killer cells. *Blood* **121**: 2234-2243.

Alatas, N., and Baba, F. (2008). Proliferating active cells, lymphocyte subsets, and dendritic cells in recurrent tonsillitis: their effect on hypertrophy. *Arch Otolaryngol Head Neck Surg* **134**: 477-483.

Andrade, F., Roy, S., Nicholson, D., Thornberry, N., Rosen, A., and Casciola-Rosen, L. (1998). Granzyme B directly and efficiently cleaves several downstream caspase substrates: implications for CTL-induced apoptosis. *Immunity* **8**: 451-460.

Anfossi, N., Andre, P., Guia, S., Falk, C.S., Roetynck, S., Stewart, C.A., Breso, V., Frassati, C., Reviron, D., Middleton, D.*, et al.* (2006). Human NK cell education by inhibitory receptors for MHC class I. *Immunity* **25**: 331-342.

Anft, M., Netter, P., Urlaub, D., Prager, I., Schaffner, S., and Watzl, C. (2020). NK cell detachment from target cells is regulated by successful cytotoxicity and influences cytokine production. *Cell Mol Immunol* **17**: 347-355.

Artis, D., and Spits, H. (2015). The biology of innate lymphoid cells. *Nature* **517**: 293-301.

Aust, J.G., Gays, F., Mickiewicz, K.M., Buchanan, E., and Brooks, C.G. (2009). The expression and function of the NKRP1 receptor family in C57BL/6 mice. *J Immunol*: 106-116.

Azizkhan, J.C., Jensen, D.E., Pierce, A.J., and Wade, M. (1993). Transcription from TATA-less promoters: dihydrofolate reductase as a model. *Crit Rev Eukaryot Gene Expr* **3**: 229-254.

Bachanova, V., McCullar, V., Lenvik, T., Wangen, R., Peterson, K.A., Ankarlo, D.E., Panoskaltsis-Mortari, A., Wagner, J.E., and Miller, J.S. (2009). Activated notch supports development of cytokine producing NK cells which are hyporesponsive and fail to acquire NK cell effector functions. *Biol Blood Marrow Transplant* **15**: 183-194.

Bal, S.M., Golebski, K., and Spits, H. (2020). Plasticity of innate lymphoid cell subsets. *Nat Rev Immunol* **20**: 552-565.

Barrow, A.D., Martin, C.J., and Colonna, M. (2019). The natural cytotoxicity receptors in health and disease. *Front Immunol* **10**: 909.

Bartel, Y., Bauer, B., and Steinle, A. (2013). Modulation of NK cell function by genetically coupled C-type lectin-like receptor/ligand pairs encoded in the human natural killer gene complex. *Front Immunol* **4**: 362.

Bauer, B., Spreu, J., Rohe, C., Vogler, I., and Steinle, A. (2015). Key residues at the membrane-distal surface of KACL, but not glycosylation, determine the functional interaction of the keratinocyte-specific C-type lectin-like receptor KACL with its high-affinity receptor NKp65. *Immunology* **145**: 114-123.

Bauer, B., and Steinle, A. (2017). HemITAM: a single tyrosine motif that packs a punch. *Sci Signal* **10**.

Bauer, B., Wotapek, T., Zoller, T., Rutkowski, E., and Steinle, A. (2017). The activating C-type lectin-like receptor NKp65 signals through a hemi-immunoreceptor tyrosine-based activation motif (hemITAM) and spleen tyrosine kinase (Syk). *J Biol Chem* **292**: 3213-3223.

Bauer, S., Groh, V., Wu, J., Steinle, A., Phillips, J.H., Lanier, L.L., and Spies, T. (1999). Activation of NK cells and T cells by NKG2D, a receptor for stress-inducible MICA. *Science* **285**: 727-729.

Bernink, J.H., Krabbendam, L., Germar, K., de Jong, E., Gronke, K., Kofoed-Nielsen, M., Munneke, J.M., Hazenberg, M.D., Villaudy, J., Buskens, C.J.*, et al.* (2015). Interleukin-12 and -23 control plasticity of CD127(+) group 1 and group 3 innate lymphoid cells in the intestinal lamina propria. *Immunity* **43**: 146-160.

Bernink, J.H., Peters, C.P., Munneke, M., te Velde, A.A., Meijer, S.L., Weijer, K., Hreggvidsdottir, H.S., Heinsbroek, S.E., Legrand, N., Buskens, C.J.*, et al.* (2013). Human type 1 innate lymphoid cells accumulate in inflamed mucosal tissues. *Nat Immunol* **14**: 221-229.

Bjorklund, A.K., Forkel, M., Picelli, S., Konya, V., Theorell, J., Friberg, D., Sandberg, R., and Mjosberg, J. (2016). The heterogeneity of human CD127(+) innate lymphoid cells revealed by single-cell RNA sequencing. *Nat Immunol* **17**: 451-460.

Blackwood, E.M., and Kadonaga, J.T. (1998). Going the distance: a current view of enhancer action. *Science* **281**: 60-63.

Bonne-Annee, S., Bush, M.C., and Nutman, T.B. (2019). Differential modulation of human innate lymphoid cell (ILC) subsets by IL-10 and TGF-beta. *Sci Rep* **9**: 14305.

Bottino, C., Castriconi, R., Moretta, L., and Moretta, A. (2005). Cellular ligands of activating NK receptors. *Trends Immunol* **26**: 221-226.

Bray, S.J. (2016). Notch signalling in context. *Nat Rev Mol Cell Biol* **17**: 722-735.

Brazil, D.P., Yang, Z.Z., and Hemmings, B.A. (2004). Advances in protein kinase B signalling: AKTion on multiple fronts. *Trends Biochem Sci* **29**: 233-242.

Brestoff, J.R., Kim, B.S., Saenz, S.A., Stine, R.R., Monticelli, L.A., Sonnenberg, G.F., Thome, J.J., Farber, D.L., Lutfy, K., Seale, P.*, et al.* (2015). Group 2 innate lymphoid cells promote beiging of white adipose tissue and limit obesity. *Nature* **519**: 242-246.

Bryksin, A.V., and Matsumura, I. (2010). Overlap extension PCR cloning: a simple and reliable way to create recombinant plasmids. *Biotechniques* **48**: 463-465.

Buettner, M., and Lochner, M. (2016). Development and function of secondary and tertiary lymphoid organs in the small intestine and the colon. *Front Immunol* **7**: 342.

Bulyk, M.L. (2003). Computational prediction of transcription-factor binding site locations. *Genome Biology* **5**: 201.

Burke, T.W., and Kadonaga, J.T. (1997). The downstream core promoter element, DPE, is conserved from Drosophila to humans and is recognized by TAFII60 of Drosophila. *Genes Dev* **11**: 3020-3031.

Burshtyn, D.N., Scharenberg, A.M., Wagtmann, N., Rajagopalan, S., Berrada, K., Yi, T., Kinet, J.P., and Long, E.O. (1996). Recruitment of tyrosine phosphatase HCP by the killer cell inhibitor receptor. *Immunity* **4**: 77-85.

Cantley, L.C. (2002). The phosphoinositide 3-kinase pathway. *Science* **296**: 1655-1657.

Carlyle, J.R., Mesci, A., Fine, J.H., Chen, P., Belanger, S., Tai, L.H., and Makrigiannis, A.P. (2008). Evolution of the Ly49 and Nkrp1 recognition systems. *Semin Immunol* **20**: 321-330.

Cartharius, K., Frech, K., Grote, K., Klocke, B., Haltmeier, M., Klingenhoff, A., Frisch, M., Bayerlein, M., and Werner, T. (2005). MatInspector and beyond: promoter analysis based on transcription factor binding sites. *Bioinformatics* **21**: 2933-2942.

Cella, M., Fuchs, A., Vermi, W., Facchetti, F., Otero, K., Lennerz, J.K., Doherty, J.M., Mills, J.C., and Colonna, M. (2009). A human natural killer cell subset provides an innate source of IL-22 for mucosal immunity. *Nature* **457**: 722-725.

Cella, M., Otero, K., and Colonna, M. (2010). Expansion of human NK-22 cells with IL-7, IL-2, and IL-1beta reveals intrinsic functional plasticity. *Proc Natl Acad Sci U S A* **107**: 10961-10966.

Chang, F., Lee, J.T., Navolanic, P.M., Steelman, L.S., Shelton, J.G., Blalock, W.L., Franklin, R.A., and McCubrey, J.A. (2003). Involvement of PI3K/Akt pathway in cell cycle progression, apoptosis, and neoplastic transformation: a target for cancer chemotherapy. *Leukemia* **17**: 590-603.

Chang, J.H., Kim, S., Koo, J., Lane, P.J.L., Yoon, S.O., Park, A.Y., Kim, K.-S., and Kim, M.-Y. (2014). The chronicity of tonsillitis is significantly correlated with an increase in an LTi cell portion. *Inflammation* **37**: 132-141.

Chen, L., Youssef, Y., Robinson, C., Ernst, G.F., Carson, M.Y., Young, K.A., Scoville, S.D., Zhang, X., Harris, R., Sekhri, P.*, et al.* (2018). CD56 expression marks human group 2 innate lymphoid cell divergence from a shared NK cell and group 3 innate lymphoid cell developmental pathway. *Immunity* **49**: 464-476.

Chen, X., Ji, Z., Webber, A., and Sharrocks, A.D. (2015). Genome-wide binding studies reveal DNA binding specificity mechanisms and functional interplay amongst Forkhead transcription factors. *Nucl Acids Res* **44**: 1566-1578.

Chuang, S.S., Lee, Y., Stepp, S.E., Kumaresan, P.R., and Mathew, P.A. (1999). Molecular cloning and characterization of the promoter region of murine natural killer cell receptor 2B4. *Biochim Biophys Acta* **1447**: 244-250.

Cirillo, L.A., Lin, F.R., Cuesta, I., Friedman, D., Jarnik, M., and Zaret, K.S. (2002). Opening of compacted chromatin by early developmental transcription factors HNF3 (FoxA) and GATA-4. *Mol Cell* **9**: 279-289.

Clark, M.R., Mandal, M., Ochiai, K., and Singh, H. (2014). Orchestrating B cell lymphopoiesis through interplay of IL-7 receptor and pre-B cell receptor signalling. *Nat Rev Immunol* **14**: 69-80.

Colonna, M. (2018). Innate lymphoid cells: diversity, plasticity, and unique functions in immunity. *Immunity* **48**: 1104-1117.

Constantinides, M.G., McDonald, B.D., Verhoef, P.A., and Bendelac, A. (2014). A committed precursor to innate lymphoid cells. *Nature* **508**: 397-401.

Cooper, M.A., Elliott, J.M., Keyel, P.A., Yang, L., Carrero, J.A., and Yokoyama, W.M. (2009). Cytokine-induced memory-like natural killer cells. *Proc Natl Acad Sci U S A* **106**: 1915-1919.

Cooper, M.A., Fehniger, T.A., Turner, S.C., Chen, K.S., Ghaheri, B.A., Ghayur, T., Carson, W.E., and Caligiuri, M.A. (2001). Human natural killer cells: a unique innate immunoregulatory role for the CD56(bright) subset. *Blood* **97**: 3146-3151.

Cortez, V.S., Fuchs, A., Cella, M., Gilfillan, S., and Colonna, M. (2014). Cutting edge: salivary gland NK cells develop independently of Nfil3 in steady-state. *J Immunol* **192**: 4487-4491.

D'Souza, B., Miyamoto, A., and Weinmaster, G. (2008). The many facets of Notch ligands. *Oncogene* **27**: 5148-5167.

Dadi, S., Chhangawala, S., Whitlock, B.M., Franklin, R.A., Luo, C.T., Oh, S.A., Toure, A., Pritykin, Y., Huse, M., Leslie, C.S.*, et al.* (2016). Cancer immunosurveillance by tissue-resident innate lymphoid cells and innate-like T cells. *Cell* **164**: 365-377.

Davis, D.M., Chiu, I., Fassett, M., Cohen, G.B., Mandelboim, O., and Strominger, J.L. (1999). The human natural killer cell immune synapse. *Proc Natl Acad Sci U S A* **96**: 15062-15067.

de Sousa Abreu, R., Penalva, L.O., Marcotte, E.M., and Vogel, C. (2009). Global signatures of protein and mRNA expression levels. *Mol Biosyst* **5**: 1512-1526.

Depper, J.M., Leonard, W.J., Drogula, C., Kronke, M., Waldmann, T.A., and Greene, W.C. (1985). Interleukin 2 (IL-2) augments transcription of the IL-2 receptor gene. *Proc Natl Acad Sci U S A* **82**: 4230-4234.

Diefenbach, A., Colonna, M., and Koyasu, S. (2014). Development, differentiation, and diversity of innate lymphoid cells. *Immunity* **41**: 354-365.

Diefenbach, A., and Raulet, D.H. (2001). Strategies for target cell recognition by natural killer cells. *Immunol Rev* **181**: 170-184.

Dikstein, R. (2011). The unexpected traits associated with core promoter elements. *Transcription* **2**: 201-206.

Doisne, J.M., Balmas, E., Boulenouar, S., Gaynor, L.M., Kieckbusch, J., Gardner, L., Hawkes, D.A., Barbara, C.F., Sharkey, A.M., Brady, H.J.*, et al.* (2015). Composition, development, and function of uterine innate lymphoid cells. *J Immunol* **195**: 3937-3945.

Drickamer, K., and Fadden, A.J. (2002). Genomic analysis of C-type lectins. *Biochem Soc Symp* **69**: 59-72.

Dzopalic, T., Bozic-Nedeljkovic, B., and Jurisic, V. (2019). Function of innate lymphoid cells in the immune-related disorders. *Hum Cell* **32**: 231-239.

Edwards, D.R., Handsley, M.M., and Pennington, C.J. (2008). The ADAM metalloproteinases. *Mol Aspects Med* **29**: 258-289.

Fathman, J.W., Bhattacharya, D., Inlay, M.A., Seita, J., Karsunky, H., and Weissman, I.L. (2011). Identification of the earliest natural killer cell-committed progenitor in murine bone marrow. *Blood* **118**: 5439-5447.

Fauriat, C., Long, E.O., Ljunggren, H.G., and Bryceson, Y.T. (2010). Regulation of human NK-cell cytokine and chemokine production by target cell recognition. *Blood* **115**: 2167-2176.

Felices, M., Ankarlo, D.E.M., Lenvik, T.R., Nelson, H.H., Blazar, B.R., Verneris, M.R., and Miller, J.S. (2014). Notch signaling at later stages of NK cell development enhances KIR expression and functional maturation. *J Immunol* **193**: 3344-3354.

Feng, H., Zeng, Y., Graner, M.W., Whitesell, L., and Katsanis, E. (2004). Evidence for a novel, caspase-8-independent, Fas death domain-mediated apoptotic pathway. *J Biomed Biotechnol* **2004**: 41-51.

Fornes, O., Castro-Mondragon, J.A., Khan, A., van der Lee, R., Zhang, X., Richmond, P.A., Modi, B.P., Correard, S., Gheorghe, M., Baranasic, D.*, et al.* (2020). JASPAR 2020: update of the open-access database of transcription factor binding profiles. *Nucl Acids Res* **48**: D87-D92.

Fort, M.M., Cheung, J., Yen, D., Li, J., Zurawski, S.M., Lo, S., Menon, S., Clifford, T., Hunte, B., Lesley, R.*, et al.* (2001). IL-25 induces IL-4, IL-5, and IL-13 and Th2-associated pathologies in vivo. *Immunity* **15**: 985-995.

Freud, A.G., and Caligiuri, M.A. (2006). Human natural killer cell development. *Immunol Rev* **214**: 56-72.

Freud, A.G., Keller, K.A., Scoville, S.D., Mundy-Bosse, B.L., Cheng, S., Youssef, Y., Hughes, T., Zhang, X., Mo, X., Porcu, P.*, et al.* (2016). NKp80 defines a critical step during human natural killer cell development. *Cell Rep* **16**: 379-391.

Freud, A.G., Yokohama, A., Becknell, B., Lee, M.T., Mao, H.C., Ferketich, A.K., and Caligiuri, M.A. (2006). Evidence for discrete stages of human natural killer cell differentiation in vivo. *J Exp Med* **203**: 1033-1043.

Fuchs, A., Vermi, W., Lee, J.S., Lonardi, S., Gilfillan, S., Newberry, R.D., Cella, M., and Colonna, M. (2013). Intraepithelial type 1 innate lymphoid cells are a unique subset of IL-12- and IL-15-responsive IFN-gamma-producing cells. *Immunity* **38**: 769-781.

Garcia-Lora, A., Algarra, I., and Garrido, F. (2003). MHC class I antigens, immune surveillance, and tumor immune escape. *J Cell Physiol* **195**: 346-355.

Geremia, A., Arancibia-Carcamo, C.V., Fleming, M.P., Rust, N., Singh, B., Mortensen, N.J., Travis, S.P., and Powrie, F. (2011). IL-23-responsive innate lymphoid cells are increased in inflammatory bowel disease. *J Exp Med* **208**: 1127-1133.

Glatzer, T., Killig, M., Meisig, J., Ommert, I., Luetke-Eversloh, M., Babic, M., Paclik, D., Bluthgen, N., Seidl, R., Seifarth, C.*, et al.* (2013). RORgammat(+) innate lymphoid cells

acquire a proinflammatory program upon engagement of the activating receptor NKp44. *Immunity* **38**: 1223-1235.

Glimcher, L., Shen, F.W., and Cantor, H. (1977). Identification of a cell-surface antigen selectively expressed on the natural killer cell. *J Exp Med* **145**: 1-9.

Gouilleux, F., Wakao, H., Mundt, M., and Groner, B. (1994). Prolactin induces phosphorylation of Tyr694 of Stat5 (MGF), a prerequisite for DNA binding and induction of transcription. *EMBO J* **13**: 4361-4369.

Green, M.R., Sambrook, J., and Sambrook, J. (2012). Molecular cloning : a laboratory manual, 4th edn (Cold Spring Harbor, N.Y.: Cold Spring Harbor Laboratory Press).

Gridley, T., and Groves, A.K. (2014). Overview of genetic tools and techniques to study Notch signaling in mice. *Methods Mol Biol* **1187**: 47-61.

Guia, S., and Narni-Mancinelli, E. (2020). Helper-like innate lymphoid cells in humans and mice. *Trends Immunol* **41**: 436-452.

Guruharsha, K.G., Kankel, M.W., and Artavanis-Tsakonas, S. (2012). The Notch signalling system: recent insights into the complexity of a conserved pathway. *Nat Rev Genet* **13**: 654-666.

Haraguchi, K., Suzuki, T., Koyama, N., Kumano, K., Nakahara, F., Matsumoto, A., Yokoyama, Y., Sakata-Yanagimoto, M., Masuda, S., Takahashi, T.*, et al.* (2009). Notch activation induces the generation of functional NK cells from human cord blood CD34-positive cells devoid of IL-15. *J Immunol* **182**: 6168-6178.

Hazenberg, M.D., and Spits, H. (2014). Human innate lymphoid cells. *Blood* **124**: 700-709.

Hoorweg, K., Peters, C.P., Cornelissen, F., Aparicio-Domingo, P., Papazian, N., Kazemier, G., Mjosberg, J.M., Spits, H., and Cupedo, T. (2012). Functional differences between human NKp44(-) and NKp44(+) RORC(+) innate lymphoid cells. *Front Immunol* **3**: 72.

Howell, D.N., Andreotti, P.E., Dawson, J.R., and Cresswell, P. (1985). Natural killing target antigens as inducers of interferon: studies with an immunoselected, natural killing-resistant human T lymphoblastoid cell line. *J Immunol* **134**: 971-976.

Huang, Q., Hua, H., Li, W., Chen, X., and Cheng, L. (2020). Simple hypertrophic tonsils have more active innate immune and inflammatory responses than hypertrophic tonsils with recurrent inflammation in children. *J Otolaryngol Head Neck Surg* **49**: 35.

Hunter, T. (2000). Signaling - 2000 and beyond. *Cell* **100**: 113-127.

Huntington, N.D. (2014). The unconventional expression of IL-15 and its role in NK cell homeostasis. *Immunol Cell Biol* **92**: 210-213.

Hurst, S.D., Muchamuel, T., Gorman, D.M., Gilbert, J.M., Clifford, T., Kwan, S., Menon, S., Seymour, B., Jackson, C., Kung, T.T.*, et al.* (2002). New IL-17 family members promote Th1 or Th2 responses in the lung: in vivo function of the novel cytokine IL-25. *J Immunol* **169**: 443-453.

Jeffery, H.C., McDowell, P., Lutz, P., Wawman, R.E., Roberts, S., Bagnall, C., Birtwistle, J., Adams, D.H., and Oo, Y.H. (2017). Human intrahepatic ILC2 are IL-13 positive amphiregulin positive and their frequency correlates with model of end stage liver disease score. *PLoS One* **12**: e0188649.

Jiang, Q., Li, W.Q., Aiello, F.B., Mazzucchelli, R., Asefa, B., Khaled, A.R., and Durum, S.K. (2005). Cell biology of IL-7, a key lymphotrophin. *Cytokine Growth Factor Rev* **16**: 513-533.

Juelke, K., and Romagnani, C. (2016). Differentiation of human innate lymphoid cells (ILCs). *Curr Opin Immunol* **38**: 75-85.

Juven-Gershon, T., and Kadonaga, J.T. (2010). Regulation of gene expression via the core promoter and the basal transcriptional machinery. *Dev Biol* **339**: 225-229.

Kang, J., and Coles, M. (2012). IL-7: the global builder of the innate lymphoid network and beyond, one niche at a time. *Semin Immunol* **24**: 190-197.

Karvande, A., Kushwaha, P., Ahmad, N., Adhikary, S., Kothari, P., Tripathi, A.K., Khedgikar, V., and Trivedi, R. (2018). Glucose dependent miR-451a expression contributes to parathyroid hormone mediated osteoblast differentiation. *Bone* **117**: 98-115.

Kataoka, T., Takaku, K., Magae, J., Shinohara, N., Takayama, H., Kondo, S., and Nagai, K. (1994). Acidification is essential for maintaining the structure and function of lytic granules of CTL. Effect of concanamycin A, an inhibitor of vacuolar type H(+)-ATPase, on CTL-mediated cytotoxicity. *J Immunol* **153**: 3938-3947.

Kelley, J., Walter, L., and Trowsdale, J. (2005). Comparative genomics of natural killer cell receptor gene clusters. *PLoS Genet* **1**: 129-139.

Keren, A., Shemer, A., Ginzburg, A., Ullmann, Y., Schrum, A.G., Paus, R., and Gilhar, A. (2018). Innate lymphoid cells 3 induce psoriasis in xenotransplanted healthy human skin. *J Allergy Clin Immunol* **142**: 305-308

Khuda, S.E., Yoshida, M., Xing, Y., Shimasaki, T., Takeya, M., Kuwahara, K., and Sakaguchi, N. (2004). The Sac3 homologue shd1 is involved in mitotic progression in mammalian cells. *J Biol Chem* **279**: 46182-46190.

Killig, M., Glatzer, T., and Romagnani, C. (2014). Recognition strategies of group 3 innate lymphoid cells. *Front Immunol* **5**: 142.

Kim, B.S., Siracusa, M.C., Saenz, S.A., Noti, M., Monticelli, L.A., Sonnenberg, G.F., Hepworth, M.R., Van Voorhees, A.S., Comeau, M.R., and Artis, D. (2013). TSLP elicits IL-33-independent innate lymphoid cell responses to promote skin inflammation. *Sci Transl Med* **5**: 170ra116.

Kim, G.Y., Hong, C., and Park, J.H. (2011). Seeing is believing: illuminating the source of in vivo interleukin-7. *Immune Netw* **11**: 1-10.

Kim, H.Y., Lee, H.J., Chang, Y.J., Pichavant, M., Shore, S.A., Fitzgerald, K.A., Iwakura, Y., Israel, E., Bolger, K., Faul, J.*, et al.* (2014). Interleukin-17-producing innate lymphoid cells and the NLRP3 inflammasome facilitate obesity-associated airway hyperreactivity. *Nat Med* **20**: 54-61.

Kim, S., Poursine-Laurent, J., Truscott, S.M., Lybarger, L., Song, Y.J., Yang, L., French, A.R., Sunwoo, J.B., Lemieux, S., Hansen, T.H.*, et al.* (2005). Licensing of natural killer cells by host major histocompatibility complex class I molecules. *Nature* **436**: 709-713.

Kitamura, T. (1998). New experimental approaches in retrovirus-mediated expression screening. *Int J Hematol* **67**: 351-359.

Klose, C.S., and Diefenbach, A. (2014). Transcription factors controlling innate lymphoid cell fate decisions. *Curr Top Microbiol Immunol* **381**: 215-255.

Klose, C.S., Kiss, E.A., Schwierzeck, V., Ebert, K., Hoyler, T., d'Hargues, Y., Goppert, N., Croxford, A.L., Waisman, A., Tanriver, Y.*, et al.* (2013). A T-bet gradient controls the fate and function of CCR6-RORgammat+ innate lymphoid cells. *Nature* **494**: 261-265.

Klose, C.S.N., and Artis, D. (2020). Innate lymphoid cells control signaling circuits to regulate tissue-specific immunity. *Cell Res* **30**: 475-491.

Klose, C.S.N., Flach, M., Mohle, L., Rogell, L., Hoyler, T., Ebert, K., Fabiunke, C., Pfeifer, D., Sexl, V., Fonseca-Pereira, D.*, et al.* (2014). Differentiation of type 1 ILCs from a common progenitor to all helper-like innate lymphoid cell lineages. *Cell* **157**: 340-356.

Konjar, S., Sutton, V.R., Hoves, S., Repnik, U., Yagita, H., Reinheckel, T., Peters, C., Turk, V., Turk, B., Trapani, J.A.*, et al.* (2010). Human and mouse perforin are processed in part through cleavage by the lysosomal cysteine proteinase cathepsin L. *Immunology* **131**: 257-267.

Kopan, R. (2012). Notch signaling. *Cold Spring Harb Perspect Biol* **4**: a011213.

Kroncke, R., Loppnow, H., Flad, H.D., and Gerdes, J. (1996). Human follicular dendritic cells and vascular cells produce interleukin-7: a potential role for interleukin-7 in the germinal center reaction. *Eur J Immunol* **26**: 2541-2544.

Kruse, P.H., Matta, J., Ugolini, S., and Vivier, E. (2014). Natural cytotoxicity receptors and their ligands. *Immunol Cell Biol* **92**: 221-229.

Kutach, A.K., and Kadonaga, J.T. (2000). The downstream promoter element DPE appears to be as widely used as the TATA box in Drosophila core promoters. *Mol Cell Biol* **20**: 4754-4764.

Kuttruff, S., Koch, S., Kelp, A., Pawelec, G., Rammensee, H.G., and Steinle, A. (2009). NKp80 defines and stimulates a reactive subset of CD8 T cells. *Blood* **113**: 358-369.

Kyoizumi, S., Kubo, Y., Kajimura, J., Yoshida, K., Hayashi, T., Nakachi, K., Moore, M.A., van den Brink, M.R.M., and Kusunoki, Y. (2017). Fate decision between group 3 innate lymphoid and conventional NK cell lineages by Notch signaling in human circulating hematopoietic progenitors. *J Immunol* **199**: 2777-2793.

Lai, S.Y., Molden, J., and Goldsmith, M.A. (1997). Shared gamma(c) subunit within the human interleukin-7 receptor complex. A molecular basis for the pathogenesis of X-linked severe combined immunodeficiency. *J Clin Invest* **99**: 169-177.

Lam, E.W., Brosens, J.J., Gomes, A.R., and Koo, C.Y. (2013). Forkhead box proteins: tuning forks for transcriptional harmony. *Nat Rev Cancer* **13**: 482-495.

Lanier, L.L. (1998). NK cell receptors. *Annu Rev Immunol* **16**: 359-393.

Lanier, L.L. (2005). NK cell recognition. *Annu Rev Immunol* **23**: 225-274.

Lanier, L.L., Chang, C., and Phillips, J.H. (1994). Human NKR-P1A. A disulfide-linked homodimer of the C-type lectin superfamily expressed by a subset of NK and T lymphocytes. *J Immunol* **153**: 2417-2428.

Law, R.H., Lukoyanova, N., Voskoboinik, I., Caradoc-Davies, T.T., Baran, K., Dunstone, M.A., D'Angelo, M.E., Orlova, E.V., Coulibaly, F., Verschoor, S.*, et al.* (2010). The structural basis for membrane binding and pore formation by lymphocyte perforin. *Nature* **468**: 447-451.

Lee, T.I., and Young, R.A. (2000). Transcription of eukaryotic protein-coding genes. *Annu Rev Genet* **34**: 77-137.

Lenhard, B., Sandelin, A., and Carninci, P. (2012). Metazoan promoters: emerging characteristics and insights into transcriptional regulation. *Nat Rev Genet* **13**: 233-245.

Levine, M., and Tjian, R. (2003). Transcription regulation and animal diversity. *Nature* **424**: 147-151.

Li, J., Doty, A.L., Tang, Y., Berrie, D., Iqbal, A., Tan, S.A., Clare-Salzler, M.J., Wallet, S.M., and Glover, S.C. (2017). Enrichment of IL-17A(+) IFN-gamma(+) and IL-22(+) IFN-gamma(+) T cell subsets is associated with reduction of NKp44(+) ILC3s in the terminal ileum of Crohn's disease patients. *Clin Exp Immunol* **190**: 143-153.

Li, J., Figueira, S.K., Vrazo, A.C., Binkowski, B.F., Butler, B.L., Tabata, Y., Filipovich, A., Jordan, M.B., and Risma, K.A. (2014). Real-time detection of CTL function reveals distinct patterns of caspase activation mediated by Fas versus granzyme B. *J Immunol* **193**: 519-528.

Li, S., Morley, M., Lu, M., Zhou, S., Stewart, K., French, C.A., Tucker, H.O., Fisher, S.E., and Morrisey, E.E. (2016). Foxp transcription factors suppress a non-pulmonary gene expression program to permit proper lung development. *Dev Biol* **416**: 338-346.

Li, Y., Wang, Q., Chen, S., Brown, P.H., and Mariuzza, R.A. (2013). Structure of NKp65 bound to its keratinocyte ligand reveals basis for genetically linked recognition in natural killer gene complex. *Proc Natl Acad Sci U S A* **110**: 11505-11510.

Lichtenthaler, S.F., Lemberg, M.K., and Fluhrer, R. (2018). Proteolytic ectodomain shedding of membrane proteins in mammals-hardware, concepts, and recent developments. *EMBO J* **37**: e99456.

Lifton, R.P., Goldberg, M.L., Karp, R.W., and Hogness, D.S. (1978). The organization of the histone genes in Drosophila melanogaster: functional and evolutionary implications. *Cold Spring Harb Symp Quant Biol* **42 Pt 2**: 1047-1051.

Lim, A.I., Menegatti, S., Bustamante, J., Le Bourhis, L., Allez, M., Rogge, L., Casanova, J.L., Yssel, H., and Di Santo, J.P. (2016). IL-12 drives functional plasticity of human group 2 innate lymphoid cells. *J Exp Med* **213**: 569-583.

Lim, C.Y., Santoso, B., Boulay, T., Dong, E., Ohler, U., and Kadonaga, J.T. (2004). The MTE, a new core promoter element for transcription by RNA polymerase II. *Genes Dev* **18**: 1606-1617.

Liu, T., Wu, J., Zhao, J., Wang, J., Zhang, Y., Liu, L., Cao, L., Liu, Y., and Dong, L. (2015). Type 2 innate lymphoid cells: a novel biomarker of eosinophilic airway inflammation in patients with mild to moderate asthma. *Respir Med* **109**: 1391-1396.

Ljunggren, H.G., and Karre, K. (1985). Host resistance directed selectively against H-2-deficient lymphoma variants. Analysis of the mechanism. *J Exp Med* **162**: 1745-1759.

Ljutic, B., Carlyle, J.R., and Zuniga-Pflucker, J.C. (2003). Identification of upstream cis-acting regulatory elements controlling lineage-specific expression of the mouse NK cell activation receptor, NKR-P1C. *J Biol Chem* **278**: 31909-31917.

Long, E.O., Kim, H.S., Liu, D., Peterson, M.E., and Rajagopalan, S. (2013). Controlling natural killer cell responses: integration of signals for activation and inhibition. *Annu Rev Immunol* **31**: 227-258.

Lu, P., Takai, K., Weaver, V.M., and Werb, Z. (2011). Extracellular matrix degradation and remodeling in development and disease. *Cold Spring Harb Perspect Biol* **3**: a005058.

Luci, C., Reynders, A., Ivanov, I.I., Cognet, C., Chiche, L., Chasson, L., Hardwigsen, J., Anguiano, E., Banchereau, J., Chaussabel, D.*, et al.* (2009). Influence of the transcription factor RORγt on the development of NKp46+ cell populations in gut and skin. *Nat Immunol* **10**: 75-82.

Lundstrom, W., Fewkes, N.M., and Mackall, C.L. (2012). IL-7 in human health and disease. *Semin Immunol* **24**: 218-224.

MacArthur, M.W., and Thornton, J.M. (1991). Influence of proline residues on protein conformation. *J Mol Biol* **218**: 397-412.

Mace, E.M., Dongre, P., Hsu, H.T., Sinha, P., James, A.M., Mann, S.S., Forbes, L.R., Watkin, L.B., and Orange, J.S. (2014). Cell biological steps and checkpoints in accessing NK cell cytotoxicity. *Immunol Cell Biol* **92**: 245-255.

Mace, E.M., Gunesch, J.T., Dixon, A., and Orange, J.S. (2016). Human NK cell development requires CD56-mediated motility and formation of the developmental synapse. *Nat Commun* **7**: 12171.

Magri, G., Miyajima, M., Bascones, S., Mortha, A., Puga, I., Cassis, L., Barra, C.M., Comerma, L., Chudnovskiy, A., Gentile, M.*, et al.* (2014). Innate lymphoid cells integrate stromal and immunological signals to enhance antibody production by splenic marginal zone B cells. *Nat Immunol* **15**: 354-364.

Malemud, C.J. (2006). Matrix metalloproteinases (MMPs) in health and disease: an overview. *Front Biosci* **11**: 1696-1701.

Malik, S., and Roeder, R.G. (2000). Transcriptional regulation through Mediator-like coactivators in yeast and metazoan cells. *Trends Biochem Sci* **25**: 277-283.

Mantamadiotis, T. (2017). Towards targeting PI3K-dependent regulation of gene expression in brain cancer. *Cancers (Basel)* **9**: 60.

Marquardt, N., Beziat, V., Nystrom, S., Hengst, J., Ivarsson, M.A., Kekalainen, E., Johansson, H., Mjosberg, J., Westgren, M., Lankisch, T.O*., et al.* (2015). Cutting edge: identification and characterization of human intrahepatic CD49a+ NK cells. *J Immunol* **194**: 2467-2471.

Martin, C.E., Spasova, D.S., Frimpong-Boateng, K., Kim, H.O., Lee, M., Kim, K.S., and Surh, C.D. (2017). Interleukin-7 availability is maintained by a hematopoietic cytokine sink comprising innate lymphoid cells and T cells. *Immunity* **47**: 171-182.

Maston, G.A., Evans, S.K., and Green, M.R. (2006). Transcriptional regulatory elements in the human genome. *Annu Rev Genomics Hum Genet* **7**: 29-59.

Mazzucchelli, R., and Durum, S.K. (2007). Interleukin-7 receptor expression: intelligent design. *Nat Rev Immunol* **7**: 144-154.

Medema, J.P., Scaffidi, C., Kischkel, F.C., Shevchenko, A., Mann, M., Krammer, P.H., and Peter, M.E. (1997). FLICE is activated by association with the CD95 death-inducing signaling complex (DISC). *EMBO J* **16**: 2794-2804.

Melo-Gonzalez, F., and Hepworth, M.R. (2017). Functional and phenotypic heterogeneity of group 3 innate lymphoid cells. *Immunology* **150**: 265-275.

Mindt, B.C., Fritz, J.H., and Duerr, C.U. (2018). Group 2 innate lymphoid cells in pulmonary immunity and tissue homeostasis. *Front Immunol* **9**: 840.

Mjosberg, J., and Spits, H. (2016). Human innate lymphoid cells. *J Allergy Clin Immunol* **138**: 1265-1276.

Mjosberg, J.M., Trifari, S., Crellin, N.K., Peters, C.P., van Drunen, C.M., Piet, B., Fokkens, W.J., Cupedo, T., and Spits, H. (2011). Human IL-25- and IL-33-responsive type 2 innate lymphoid cells are defined by expression of CRTH2 and CD161. *Nat Immunol* **12**: 1055-1062.

Montaldo, E., Teixeira-Alves, L.G., Glatzer, T., Durek, P., Stervbo, U., Hamann, W., Babic, M., Paclik, D., Stolzel, K., Grone, J*., et al.* (2014). Human RORgammat(+)CD34(+) cells are lineage-specified progenitors of group 3 RORgammat(+) innate lymphoid cells. *Immunity* **41**: 988-1000.

Montaldo, E., Vacca, P., Vitale, C., Moretta, F., Locatelli, F., Mingari, M.C., and Moretta, L. (2016). Human innate lymphoid cells. *Immunol Lett* **179**: 2-8.

Monticelli, L.A., Sonnenberg, G.F., Abt, M.C., Alenghat, T., Ziegler, C.G., Doering, T.A., Angelosanto, J.M., Laidlaw, B.J., Yang, C.Y., Sathaliyawala, T*., et al.* (2011). Innate lymphoid cells promote lung-tissue homeostasis after infection with influenza virus. *Nat Immunol* **12**: 1045-1054.

Mora-Velandia, L.M., Castro-Escamilla, O., Mendez, A.G., Aguilar-Flores, C., Velazquez-Avila, M., Tussie-Luna, M.I., Tellez-Sosa, J., Maldonado-Garcia, C., Jurado-Santacruz, F., Ferat-Osorio, E*., et al.* (2017). A human Lin(-) CD123(+) CD127(low) population endowed with ILC features and migratory capabilities contributes to immunopathological hallmarks of psoriasis. *Front Immunol* **8**: 176.

Moretta, A., Bottino, C., Vitale, M., Pende, D., Cantoni, C., Mingari, M.C., Biassoni, R., and Moretta, L. (2001). Activating receptors and coreceptors involved in human natural killer cell-mediated cytolysis. *Annu Rev Immunol* **19**: 197-223.

Moro, K., Yamada, T., Tanabe, M., Takeuchi, T., Ikawa, T., Kawamoto, H., Furusawa, J., Ohtani, M., Fujii, H., and Koyasu, S. (2010). Innate production of T(H)2 cytokines by adipose tissue-associated c-Kit(+)Sca-1(+) lymphoid cells. *Nature* **463**: 540-544.

Murphy, K., Travers, P., Walport, M., and Janeway, C. (2012). Janeway's immunobiology, 8th edn (New York: Garland Science).

Nakagawa, S., Gisselbrecht, S.S., Rogers, J.M., Hartl, D.L., and Bulyk, M.L. (2013). DNA-binding specificity changes in the evolution of forkhead transcription factors. *Proc Natl Acad Sci U S A* **110**: 12349-12354.

Nakajima, H., Brindle, P.K., Handa, M., and Ihle, J.N. (2001). Functional interaction of STAT5 and nuclear receptor co-repressor SMRT: implications in negative regulation of STAT5-dependent transcription. *EMBO J* **20**: 6836-6844.

Natarajan, K., Sawicki, M.W., Margulies, D.H., and Mariuzza, R.A. (2000). Crystal structure of human CD69: a C-type lectin-like activation marker of hematopoietic cells. *Biochemistry* **39**: 14779-14786.

Neuss, S., Bartel, Y., Born, C., Weil, S., Koch, J., Behrends, C., Hoffmeister, M., and Steinle, A. (2018). Cellular mechanisms controlling surfacing of AICL glycoproteins, cognate ligands of the activating NK receptor NKp80. *J Immunol* **201**: 1275-1286.

Okada, S., Markle, J.G., Deenick, E.K., Mele, F., Averbuch, D., Lagos, M., Alzahrani, M., Al-Muhsen, S., Halwani, R., Ma, C.S.*, et al.* (2015). IMMUNODEFICIENCIES. Impairment of immunity to Candida and Mycobacterium in humans with bi-allelic RORC mutations. *Science* **349**: 606-613.

Olofsson, K., Hellstrom, S., and Hammarstrom, M.L. (1998). The surface epithelium of recurrent infected palatine tonsils is rich in gammadelta T cells. *Clin Exp Immunol* **111**: 36-47.

Orr, M.T., and Lanier, L.L. (2011). Inhibitory Ly49 receptors on mouse natural killer cells. *Curr Top Microbiol Immunol* **350**: 67-87.

Özören, N., Kim, K., Burns, T.F., Dicker, D.T., Moscioni, A.D., and El-Deiry, W.S. (2000). The caspase 9 inhibitor Z-LEHD-FMK protects human liver cells while permitting death of cancer cells exposed to tumor necrosis factor-related apoptosis-inducing ligand. *Cancer Research* **60**: 6259-6265.

Palmer, M.J., Mahajan, V.S., Trajman, L.C., Irvine, D.J., Lauffenburger, D.A., and Chen, J. (2008). Interleukin-7 receptor signaling network: an integrated systems perspective. *Cell Mol Immunol* **5**: 79-89.

Pan, Y., Liu, Z., Shen, J., and Kopan, R. (2005). Notch1 and 2 cooperate in limb ectoderm to receive an early Jagged2 signal regulating interdigital apoptosis. *Dev Biol* **286**: 472-482.

Pantelyushin, S., Haak, S., Ingold, B., Kulig, P., Heppner, F.L., Navarini, A.A., and Becher, B. (2012). Rorgammat+ innate lymphocytes and gammadelta T cells initiate psoriasiform plaque formation in mice. *J Clin Invest* **122**: 2252-2256.

Parham, P. (2005). MHC class I molecules and KIRs in human history, health and survival. *Nat Rev Immunol* **5**: 201-214.

Pedersen, A.G., Baldi, P., Chauvin, Y., and Brunak, S. (1999). The biology of eukaryotic promoter prediction - a review. *Comput Chem* **23**: 191-207.

Petak, I., Vernes, R., Szucs, K.S., Anozie, M., Izeradjene, K., Douglas, L., Tillman, D.M., Phillips, D.C., and Houghton, J.A. (2003). A caspase-8-independent component in TRAIL/Apo-2L-induced cell death in human rhabdomyosarcoma cells. *Cell Death Differ* **10**: 729-739.

Peter, M.E., and Krammer, P.H. (2003). The CD95(APO-1/Fas) DISC and beyond. *Cell Death Differ* **10**: 26-35.

Petrovic, J., Formosa-Jordan, P., Luna-Escalante, J.C., Abelló, G., Ibañes, M., Neves, J., and Giraldez, F. (2014). Ligand-dependent Notch signaling strength orchestrates lateral induction and lateral inhibition in the developing inner ear. *Development* **141**: 2313-2324.

Pfitzner, E., Jahne, R., Wissler, M., Stoecklin, E., and Groner, B. (1998). p300/CREB-binding protein enhances the prolactin-mediated transcriptional induction through direct interaction with the transactivation domain of Stat5, but does not participate in the Stat5-mediated suppression of the glucocorticoid response. *Mol Endocrinol* **12**: 1582-1593.

Plougastel, B., and Trowsdale, J. (1998). Sequence analysis of a 62-kb region overlapping the human KLRC cluster of genes. *Genomics* **49**: 193-199.

Prager, I., Liesche, C., van Ooijen, H., Urlaub, D., Verron, Q., Sandstrom, N., Fasbender, F., Claus, M., Eils, R., Beaudouin, J.*, et al.* (2019). NK cells switch from granzyme B to death receptor-mediated cytotoxicity during serial killing. *J Exp Med* **216**: 2113-2127.

Prager, I., and Watzl, C. (2019). Mechanisms of natural killer cell-mediated cellular cytotoxicity. *J Leukoc Biol* **105**: 1319-1329.

Puel, A., Ziegler, S.F., Buckley, R.H., and Leonard, W.J. (1998). Defective IL7R expression in T(-)B(+)NK(+) severe combined immunodeficiency. *Nat Genet* **20**: 394-397.

Radtke, F., MacDonald, H.R., and Tacchini-Cottier, F. (2013). Regulation of innate and adaptive immunity by Notch. *Nat Rev Immunol* **13**: 427-437.

Rani, A., and Murphy, J.J. (2016). STAT5 in cancer and immunity. *J Interferon Cytokine Res* **36**: 226-237.

Rasmussen, H.S., and McCann, P.P. (1997). Matrix metalloproteinase inhibition as a novel anticancer strategy: a review with special focus on batimastat and marimastat. *Pharmacol Ther* **75**: 69-75.

Raulet, D.H., Gasser, S., Gowen, B.G., Deng, W., and Jung, H. (2013). Regulation of ligands for the NKG2D activating receptor. *Annu Rev Immunol* **31**: 413-441.

Raulet, D.H., and Vance, R.E. (2006). Self-tolerance of natural killer cells. *Nat Rev Immunol* **6**: 520-531.

Raykova, A., Carrega, P., Lehmann, F.M., Ivanek, R., Landtwing, V., Quast, I., Lünemann, J.D., Finke, D., Ferlazzo, G., Chijioke, O.*, et al.* (2017). Interleukins 12 and 15 induce cytotoxicity and early NK-cell differentiation in type 3 innate lymphoid cells. *Blood Adv* **1**: 2679-2691.

Reed E. Pyeritz, R.E. (2018). Emery and rimoin's principles and practice of medical genetics and genomics : clinical principles and applications, 7th edition. edn (San Diego, CA: Elsevier).

Reis, L.G., Almeida, E.C., da Silva, J.C., Pereira Gde, A., Barbosa Vde, F., and Etchebehere, R.M. (2013). Tonsillar hyperplasia and recurrent tonsillitis: clinical-histological correlation. *Braz J Otorhinolaryngol* **79**: 603-608.

Roan, F., Stoklasek, T.A., Whalen, E., Molitor, J.A., Bluestone, J.A., Buckner, J.H., and Ziegler, S.F. (2016). CD4+ group 1 innate lymphoid cells (ILC) form a functionally distinct ILC subset that is increased in systemic sclerosis. *J Immunol* **196**: 2051-2062.

Robinette, M.L., Bando, J.K., Song, W., Ulland, T.K., Gilfillan, S., and Colonna, M. (2017). IL-15 sustains IL-7R-independent ILC2 and ILC3 development. *Nat Commun* **8**: 14601.

Rodig, S.J., Meraz, M.A., White, J.M., Lampe, P.A., Riley, J.K., Arthur, C.D., King, K.L., Sheehan, K.C., Yin, L., Pennica, D.*, et al.* (1998). Disruption of the Jak1 gene demonstrates obligatory and nonredundant roles of the Jaks in cytokine-induced biologic responses. *Cell* **93**: 373-383.

Roye, O., Delhem, N., Trottein, F., Remoue, F., Nutten, S., Decavel, J.P., Delacre, M., Martinot, V., Cesbron, J.Y., Auriault, C.*, et al.* (1998). Dermal endothelial cells and keratinocytes produce IL-7 in vivo after human Schistosoma mansoni percutaneous infection. *J Immunol* **161**: 4161-4168.

Ruco, L.P., Uccini, S., Stoppacciaro, A., Pilozzi, E., Morrone, S., Gallo, A., De Vincentiis, M., Santoni, A., and Baroni, C.D. (1995). The lymphoepithelial organization of the tonsil: an immunohistochemical study in chronic recurrent tonsillitis. *J Pathol* **176**: 391-398.

Ruiter, B., Patil, S.U., and Shreffler, W.G. (2015). Vitamins A and D have antagonistic effects on expression of effector cytokines and gut-homing integrin in human innate lymphoid cells. *Clin Exp Allergy* **45**: 1214-1225.

Salimi, M., Barlow, J.L., Saunders, S.P., Xue, L., Gutowska-Owsiak, D., Wang, X., Huang, L.C., Johnson, D., Scanlon, S.T., McKenzie, A.N.*, et al.* (2013). A role for IL-25 and IL-33-driven type-2 innate lymphoid cells in atopic dermatitis. *J Exp Med* **210**: 2939-2950.

Sancho, D., Gomez, M., and Sanchez-Madrid, F. (2005). CD69 is an immunoregulatory molecule induced following activation. *Trends Immunol* **26**: 136-140.

Satoh-Takayama, N., Lesjean-Pottier, S., Vieira, P., Sawa, S., Eberl, G., Vosshenrich, C.A., and Di Santo, J.P. (2010). IL-7 and IL-15 independently program the differentiation of intestinal CD3-NKp46+ cell subsets from Id2-dependent precursors. *J Exp Med* **207**: 273-280.

Satoh-Takayama, N., Vosshenrich, C.A., Lesjean-Pottier, S., Sawa, S., Lochner, M., Rattis, F., Mention, J.J., Thiam, K., Cerf-Bensussan, N., Mandelboim, O.*, et al.* (2008). Microbial flora drives interleukin 22 production in intestinal NKp46+ cells that provide innate mucosal immune defense. *Immunity* **29**: 958-970.

Sawa, S., Lochner, M., Satoh-Takayama, N., Dulauroy, S., Berard, M., Kleinschek, M., Cua, D., Di Santo, J.P., and Eberl, G. (2011). RORgammat+ innate lymphoid cells regulate intestinal homeostasis by integrating negative signals from the symbiotic microbiota. *Nat Immunol* **12**: 320-326.

Sawa, Y., Arima, Y., Ogura, H., Kitabayashi, C., Jiang, J.J., Fukushima, T., Kamimura, D., Hirano, T., and Murakami, M. (2009). Hepatic interleukin-7 expression regulates T cell responses. *Immunity* **30**: 447-457.

Scadding, G.K. (1990). Immunology of the tonsil: a review. *J R Soc Med* **83**: 104-107.

Schmitt, T.M., and Zuniga-Pflucker, J.C. (2002). Induction of T cell development from hematopoietic progenitor cells by delta-like-1 in vitro. *Immunity* **17**: 749-756.

Schwanhausser, B., Busse, D., Li, N., Dittmar, G., Schuchhardt, J., Wolf, J., Chen, W., and Selbach, M. (2011). Global quantification of mammalian gene expression control. *Nature* **473**: 337-342.

Scoville, S.D., Freud, A.G., and Caligiuri, M.A. (2019). Cellular pathways in the development of human and murine innate lymphoid cells. *Curr Opin Immunol* **56**: 100-106.

Scoville, S.D., Mundy-Bosse, B.L., Zhang, M.H., Chen, L., Zhang, X., Keller, K.A., Hughes, T., Chen, L., Cheng, S., Bergin, S.M.*, et al.* (2016). A progenitor cell expressing transcription factor RORγt generates all human innate lymphoid cell subsets. *Immunity* **44**: 1140-1150.

Serafini, N., Vosshenrich, C.A., and Di Santo, J.P. (2015). Transcriptional regulation of innate lymphoid cell fate. *Nat Rev Immunol* **15**: 415-428.

Shalapour, S., Deiser, K., Sercan, O., Tuckermann, J., Minnich, K., Willimsky, G., Blankenstein, T., Hammerling, G.J., Arnold, B., and Schuler, T. (2010). Commensal microflora and interferon-gamma promote steady-state interleukin-7 production in vivo. *Eur J Immunol* **40**: 2391-2400.

Shankaran, H., Resat, H., and Wiley, H.S. (2007). Cell surface receptors for signal transduction and ligand transport: a design principles study. *PLoS Comput Biol* **3**: e101.

Shikhagaie, M.M., Bjorklund, A.K., Mjosberg, J., Erjefalt, J.S., Cornelissen, A.S., Ros, X.R., Bal, S.M., Koning, J.J., Mebius, R.E., Mori, M.*, et al.* (2017). Neuropilin-1 is expressed on lymphoid tissue residing LTi-like group 3 innate lymphoid cells and associated with ectopic lymphoid aggregates. *Cell Rep* **18**: 1761-1773.

Simonetta, F., Pradier, A., and Roosnek, E. (2016). T-bet and Eomesodermin in NK cell development, maturation, and function. *Front Immunol* **7**: 241.

Simoni, Y., Fehlings, M., Kloverpris, H.N., McGovern, N., Koo, S.L., Loh, C.Y., Lim, S., Kurioka, A., Fergusson, J.R., Tang, C.L.*, et al.* (2017). Human innate lymphoid cell subsets possess tissue-type based heterogeneity in phenotype and frequency. *Immunity* **46**: 148-161.

Simoni, Y., and Newell, E.W. (2018). Dissecting human ILC heterogeneity: more than just three subsets. *Immunology* **153**: 297-303.

Sloutskin, A., Danino, Y.M., Orenstein, Y., Zehavi, Y., Doniger, T., Shamir, R., and Juven-Gershon, T. (2015). ElemeNT: a computational tool for detecting core promoter elements. *Transcription* **6**: 41-50.

Smale, S.T., and Kadonaga, J.T. (2003). The RNA polymerase II core promoter. *Annu Rev Biochem* **72**: 449-479.

Smyth, M.J., Cretney, E., Kelly, J.M., Westwood, J.A., Street, S.E., Yagita, H., Takeda, K., van Dommelen, S.L., Degli-Esposti, M.A., and Hayakawa, Y. (2005). Activation of NK cell cytotoxicity. *Mol Immunol* **42**: 501-510.

Spits, H., Artis, D., Colonna, M., Diefenbach, A., Di Santo, J.P., Eberl, G., Koyasu, S., Locksley, R.M., McKenzie, A.N., Mebius, R.E.*, et al.* (2013). Innate lymphoid cells - a proposal for uniform nomenclature. *Nat Rev Immunol* **13**: 145-149.

Spits, H., Bernink, J.H., and Lanier, L. (2016). NK cells and type 1 innate lymphoid cells: partners in host defense. *Nat Immunol* **17**: 758-764.

Spitz, F., and Furlong, E.E. (2012). Transcription factors: from enhancer binding to developmental control. *Nat Rev Genet* **13**: 613-626.

Spreu, J., Kienle, E.C., Schrage, B., and Steinle, A. (2007). CLEC2A: a novel, alternatively spliced and skin-associated member of the NKC-encoded AICL-CD69-LLT1 family. *Immunogenetics* **59**: 903-912.

Spreu, J., Kuttruff, S., Stejfova, V., Dennehy, K.M., Schittek, B., and Steinle, A. (2010). Interaction of C-type lectin-like receptors NKp65 and KACL facilitates dedicated immune recognition of human keratinocytes. *Proc Natl Acad Sci U S A* **107**: 5100-5105.

Srpan, K., Ambrose, A., Karampatzakis, A., Saeed, M., Cartwright, A.N.R., Guldevall, K., De Matos, G., Onfelt, B., and Davis, D.M. (2018). Shedding of CD16 disassembles the NK cell immune synapse and boosts serial engagement of target cells. *J Cell Biol* **217**: 3267-3283.

Steinle, A., Li, P., Morris, D.L., Groh, V., Lanier, L.L., Strong, R.K., and Spies, T. (2001). Interactions of human NKG2D with its ligands MICA, MICB, and homologs of the mouse RAE-1 protein family. *Immunogenetics* **53**: 279-287.

Steinle, A.L., Bauer, B., Vogler, I., and Leibelt, S. (2016). C-type lectin-like NKC-encoded immunoreceptors NKp80 and NKp65 are selectively expressed by human innate lymphocyte subsets, uniquely signal via hemITAMs and facilitate tissue-specific immunosurveillance via their genetically linked ligands AICL and KACL. *J Immunol* **196**: 202.227.

Stormo, G.D. (2000). DNA binding sites: representation and discovery. *Bioinformatics* **16**: 16-23.

Sun, J.C., and Lanier, L.L. (2011). NK cell development, homeostasis and function: parallels with CD8(+) T cells. *Nat Rev Immunol* **11**: 645-657.

Suzuki, K., Nakajima, H., Watanabe, N., Kagami, S., Suto, A., Saito, Y., Saito, T., and Iwamoto, I. (2000). Role of common cytokine receptor gamma chain (gamma(c))- and Jak3-dependent signaling in the proliferation and survival of murine mast cells. *Blood* **96**: 2172-2180.

Takakuwa, T., Nomura, S., Matsuzuka, F., Inoue, H., and Aozasa, K. (2000). Expression of interleukin-7 and its receptor in thyroid lymphoma. *Lab Invest* **80**: 1483-1490.

Takashima, A., Matsue, H., Bergstresser, P.R., and Ariizumi, K. (1995). Interleukin-7-dependent interaction of dendritic epidermal T cells with keratinocytes. *J Invest Dermatol* **105**: 50S-53S.

Takayama, T., Kamada, N., Chinen, H., Okamoto, S., Kitazume, M.T., Chang, J., Matuzaki, Y., Suzuki, S., Sugita, A., Koganei, K.*, et al.* (2010). Imbalance of NKp44(+)NKp46(-) and NKp44(-)NKp46(+) natural killer cells in the intestinal mucosa of patients with Crohn's disease. *Gastroenterology* **139**: 882-892.

Takeda, K., Cretney, E., Hayakawa, Y., Ota, T., Akiba, H., Ogasawara, K., Yagita, H., Kinoshita, K., Okumura, K., and Smyth, M.J. (2005). TRAIL identifies immature natural killer cells in newborn mice and adult mouse liver. *Blood* **105**: 2082-2089.

Tang, J., Nuccie, B.L., Ritterman, I., Liesveld, J.L., Abboud, C.N., and Ryan, D.H. (1997). TGF-beta down-regulates stromal IL-7 secretion and inhibits proliferation of human B cell precursors. *J Immunol* **159**: 117-125.

Teunissen, M.B.M., Munneke, J.M., Bernink, J.H., Spuls, P.I., Res, P.C.M., Te Velde, A., Cheuk, S., Brouwer, M.W.D., Menting, S.P., Eidsmo, L.*, et al.* (2014). Composition of innate lymphoid cell subsets in the human skin: enrichment of NCR(+) ILC3 in lesional skin and blood of psoriasis patients. *J Invest Dermatol* **134**: 2351-2360.

Thoren, F.B., Riise, R.E., Ousback, J., Della Chiesa, M., Alsterholm, M., Marcenaro, E., Pesce, S., Prato, C., Cantoni, C., Bylund, J.*, et al.* (2012). Human NK Cells induce neutrophil apoptosis via an NKp46- and Fas-dependent mechanism. *J Immunol* **188**: 1668-1674.

Tong, X., Muchnik, M., Chen, Z., Patel, M., Wu, N., Joshi, S., Rui, L., Lazar, M.A., and Yin, L. (2010). Transcriptional repressor E4-binding protein 4 (E4BP4) regulates metabolic hormone fibroblast growth factor 21 (FGF21) during circadian cycles and feeding. *J Biol Chem* **285**: 36401-36409.

Trabanelli, S., Gomez-Cadena, A., Salome, B., Michaud, K., Mavilio, D., Landis, B.N., Jandus, P., and Jandus, C. (2018). Human innate lymphoid cells (ILCs): toward a uniform immune-phenotyping. *Cytometry B Clin Cytom* **94**: 392-399.

Tremblay-McLean, A., Coenraads, S., Kiani, Z., Dupuy, F.P., and Bernard, N.F. (2019). Expression of ligands for activating natural killer cell receptors on cell lines commonly used to assess natural killer cell function. *BMC Immunol* **20**: 8.

Turner, J.-E., and Gasteiger, G. (2018). Innate lymphoid cells: key players in tissue-specific immunity. *Semin Immunopathol* **40**: 315-317.

Turner, J.E., Morrison, P.J., Wilhelm, C., Wilson, M., Ahlfors, H., Renauld, J.C., Panzer, U., Helmby, H., and Stockinger, B. (2013). IL-9-mediated survival of type 2 innate lymphoid cells promotes damage control in helminth-induced lung inflammation. *J Exp Med* **210**: 2951-2965.

Uğraş, S., and Kutluhan, A. (2008). Chronic tonsillitis can be diagnosed with histopathologic findings. *Eur J Gen Med* **5**: 95-103.

Uhlen, M., Fagerberg, L., Hallstrom, B.M., Lindskog, C., Oksvold, P., Mardinoglu, A., Sivertsson, A., Kampf, C., Sjostedt, E., Asplund, A.*, et al.* (2015). Proteomics. Tissue-based map of the human proteome. *Science* **347**: 1260419.

Uhlig, H.H., McKenzie, B.S., Hue, S., Thompson, C., Joyce-Shaikh, B., Stepankova, R., Robinson, N., Buonocore, S., Tlaskalova-Hogenova, H., Cua, D.J.*, et al.* (2006). Differential activity of IL-12 and IL-23 in mucosal and systemic innate immune pathology. *Immunity* **25**: 309-318.

Vacca, P., Montaldo, E., Croxatto, D., Loiacono, F., Canegallo, F., Venturini, P.L., Moretta, L., and Mingari, M.C. (2015). Identification of diverse innate lymphoid cells in human decidua. *Mucosal Immunol* **8**: 254-264.

Valitutti, S., Muller, S., Cella, M., Padovan, E., and Lanzavecchia, A. (1995). Serial triggering of many T-cell receptors by a few peptide-MHC complexes. *Nature* **375**: 148-151.

van de Pavert, S.A., and Mebius, R.E. (2010). New insights into the development of lymphoid tissues. *Nat Rev Immunol* **10**: 664-674.

van de Pavert, S.A., and Vivier, E. (2016). Differentiation and function of group 3 innate lymphoid cells, from embryo to adult. *Int Immunol* **28**: 35-42.

Vely, F., Barlogis, V., Vallentin, B., Neven, B., Piperoglou, C., Ebbo, M., Perchet, T., Petit, M., Yessaad, N., Touzot, F.*, et al.* (2016). Evidence of innate lymphoid cell redundancy in humans. *Nat Immunol* **17**: 1291-1299.

Villanova, F., Flutter, B., Tosi, I., Grys, K., Sreeneebus, H., Perera, G.K., Chapman, A., Smith, C.H., Di Meglio, P., and Nestle, F.O. (2014). Characterization of innate lymphoid cells in human skin and blood demonstrates increase of NKp44+ ILC3 in psoriasis. *J Invest Dermatol* **134**: 984-991.

Vitale, M., Falco, M., Castriconi, R., Parolini, S., Zambello, R., Semenzato, G., Biassoni, R., Bottino, C., Moretta, L., and Moretta, A. (2001). Identification of NKp80, a novel triggering molecule expressed by human NK cells. *Eur J Immunol* **31**: 233-242.

Vivier, E., Artis, D., Colonna, M., Diefenbach, A., Di Santo, J.P., Eberl, G., Koyasu, S., Locksley, R.M., McKenzie, A.N.J., Mebius, R.E.*, et al.* (2018). Innate Lymphoid Cells: 10 Years On. *Cell* **174**: 1054-1066.

Vivier, E., Nunes, J.A., and Vely, F. (2004). Natural killer cell signaling pathways. *Science* **306**: 1517-1519.

Vivier, E., Tomasello, E., Baratin, M., Walzer, T., and Ugolini, S. (2008). Functions of natural killer cells. *Nat Immunol* **9**: 503-510.

Vogler, I., and Steinle, A. (2011). Vis-a-vis in the NKC: genetically linked natural killer cell receptor/ligand pairs in the natural killer gene complex (NKC). *J Innate Immun* **3**: 227-235.

Vonarbourg, C., and Diefenbach, A. (2012). Multifaceted roles of interleukin-7 signaling for the development and function of innate lymphoid cells. *Semin Immunol* **24**: 165-174.

Vonarbourg, C., Mortha, A., Bui, V.L., Hernandez, P.P., Kiss, E.A., Hoyler, T., Flach, M., Bengsch, B., Thimme, R., Holscher, C.*, et al.* (2010). Regulated expression of nuclear receptor RORgammat confers distinct functional fates to NK cell receptor-expressing RORgammat(+) innate lymphocytes. *Immunity* **33**: 736-751.

Vosshenrich, C.A., Garcia-Ojeda, M.E., Samson-Villeger, S.I., Pasqualetto, V., Enault, L., Richard-Le Goff, O., Corcuff, E., Guy-Grand, D., Rocha, B., Cumano, A.*, et al.* (2006). A thymic pathway of mouse natural killer cell development characterized by expression of GATA-3 and CD127. *Nat Immunol* **7**: 1217-1224.

Waldhauer, I., and Steinle, A. (2008). NK cells and cancer immunosurveillance. *Oncogene* **27**: 5932-5943.

Waldmann, T.A., and Tagaya, Y. (1999). The multifaceted regulation of interleukin-15 expression and the role of this cytokine in NK cell differentiation and host response to intracellular pathogens. *Annu Rev Immunol* **17**: 19-49.

Walker, J.A., Clark, P.A., Crisp, A., Barlow, J.L., Szeto, A., Ferreira, A.C.F., Rana, B.M.J., Jolin, H.E., Rodriguez-Rodriguez, N., Sivasubramaniam, M.*, et al.* (2019). Polychromic reporter mice reveal unappreciated innate lymphoid cell progenitor heterogeneity and elusive ILC3 progenitors in bone marrow. *Immunity* **51**: 104-118

Walker, J.A., and McKenzie, A.N. (2013). Development and function of group 2 innate lymphoid cells. *Curr Opin Immunol* **25**: 148-155.

Wang, X., Peng, H., and Tian, Z. (2019). Innate lymphoid cell memory. *Cell Mol Immunol* **16**: 423-429.

Welte, S., Kuttruff, S., Waldhauer, I., and Steinle, A. (2006). Mutual activation of natural killer cells and monocytes mediated by NKp80-AICL interaction. *Nat Immunol* **7**: 1334-1342.

Wilhelm, C., Harrison, O.J., Schmitt, V., Pelletier, M., Spencer, S.P., Urban, J.F., Jr., Ploch, M., Ramalingam, T.R., Siegel, R.M., and Belkaid, Y. (2016). Critical role of fatty acid metabolism in ILC2-mediated barrier protection during malnutrition and helminth infection. *J Exp Med* **213**: 1409-1418.

Wojno, E.D., Monticelli, L.A., Tran, S.V., Alenghat, T., Osborne, L.C., Thome, J.J., Willis, C., Budelsky, A., Farber, D.L., and Artis, D. (2015). The prostaglandin D(2) receptor CRTH2 regulates accumulation of group 2 innate lymphoid cells in the inflamed lung. *Mucosal Immunol* **8**: 1313-1323.

Wolfrum, C., Besser, D., Luca, E., and Stoffel, M. (2003). Insulin regulates the activity of forkhead transcription factor Hnf-3β/Foxa-2 by Akt-mediated phosphorylation and nuclear/cytosolic localization. *Proc Natl Acad Sci U S A* **100**: 11624-11629.

Wray, G.A., Hahn, M.W., Abouheif, E., Balhoff, J.P., Pizer, M., Rockman, M.V., and Romano, L.A. (2003). The evolution of transcriptional regulation in eukaryotes. *Mol Biol Evol* **20**: 1377-1419.

Xu, W., Cherrier, D.E., Chea, S., Vosshenrich, C., Serafini, N., Petit, M., Liu, P., Golub, R., and Di Santo, J.P. (2019). An Id2(RFP)-reporter mouse redefines innate lymphoid cell precursor potentials. *Immunity* **50**: 1054-1068

Xu, W., and Di Santo, J.P. (2013). Taming the beast within: regulation of innate lymphoid cell homeostasis and function. *J Immunol* **191**: 4489-4496.

Yang, J., Cron, P., Good, V.M., Thompson, V., Hemmings, B.A., and Barford, D. (2002). Crystal structure of an activated Akt/protein kinase B ternary complex with GSK3-peptide and AMP-PNP. *Nat Struct Biol* **9**: 940-944.

Yates, A.D., Achuthan, P., Akanni, W., Allen, J., Allen, J., Alvarez-Jarreta, J., Amode, M.R., Armean, I.M., Azov, A.G., Bennett, R.*, et al.* (2020). Ensembl 2020. *Nucl Acids Res* **48**: D682-D688.

Yokoyama, W.M., and Plougastel, B.F. (2003). Immune functions encoded by the natural killer gene complex. *Nat Rev Immunol* **3**: 304-316.

Zaiss, D.M., Yang, L., Shah, P.R., Kobie, J.J., Urban, J.F., and Mosmann, T.R. (2006). Amphiregulin, a TH2 cytokine enhancing resistance to nematodes. *Science* **314**: 1746.

Zanella, F., Dos Santos, N.R., and Link, W. (2013). Moving to the core: spatiotemporal analysis of Forkhead box O (FOXO) and nuclear factor-kappaB (NF-kappaB) nuclear translocation. *Traffic* **14**: 247-258.

Zaret, K.S., and Carroll, J.S. (2011). Pioneer transcription factors: establishing competence for gene expression. *Genes Dev* **25**: 2227-2241.

Zelensky, A.N., and Gready, J.E. (2005). The C-type lectin-like domain superfamily. *FEBS J* **272**: 6179-6217.

Zhang, M.-Y., Zhu, G.-Q., Shi, K.-Q., Zheng, J.-N., Cheng, Z., Zou, Z.-L., Huang, H.-H., Chen, F.-Y., and Zheng, M.-H. (2016). Systematic review with network meta-analysis: comparative efficacy of oral nucleos(t)ide analogues for the prevention of chemotherapy-induced hepatitis B virus reactivation. *Oncotarget* **7**: 30642-30658.

Zhang, P.C., Pang, Y.T., Loh, K.S., and Wang, D.Y. (2003). Comparison of histology between recurrent tonsillitis and tonsillar hypertrophy. *Clin Otolaryngol Allied Sci* **28**: 235-239.

Zingoni, A., Vulpis, E., Loconte, L., and Santoni, A. (2020). NKG2D ligand shedding in response to stress: role of ADAM10. *Front Immunol* **11**: 447.

Abbreviations

ADAM	A disintegrin and metalloproteinase
ADCC	Antibody-dependent cellular cytotoxicity
AhR	Aryl hydrocarbon receptor
AICL	Activation-induced C-type lectin
Akt	Protein kinase B
APC	Antigen presenting cell
AREG	Amphiregulin
BB94	Batimastat
BM	Bone marrow
bp	Base pair
BRE	TFBII recognition element
Btn	Biotin
Casp-8	Caspase-8
CB	Cord blood
CCR	Chemokine receptor
CD	Cluster of differentiation
CHILP	Common helper innate lymphoid cell precursor
ChIP	Chromatin immunoprecipitation
CILP	Common innate lymphoid progenitor
CLEC	C-type lectin-domain family member
CLP	Common lymphoid progenitor
Clr	C-type lectin-related
CLSF	C-type lectin-like superfamily
CMA	Concanamycin A
cNK	Conventional natural killer cell
CREB	cAMP-responsive element binding
CTLD	C-type lectin-like domain
Da	Dalton
CTLR	C-type lectin-like receptor
DC	Dendritic cell
DCE	Downstream core element
DLL	Delta like ligand
DMSO	Dimethyl sulfoxide
DNA	Deoxyribonucleic acid
DPE	Downstream promoter element
EILP	Early innate lymphoid progenitor
ELISA	Enzyme-linked immunosorbent assay
EOMES	Eomesodermin
E:T	Effector to target ratio
ETP	Early tonsil progenitor
FACS	Fluorescence-activated cell sorting
FDC	Follicular dendritic cells
Flt3-L	Fms-like tyrosine kinase 3 ligand
FOX	Forkhead box
hemITAM	Hemi-immunoreceptor tyrosine-based activation motif
HSC	Hematopoietic stem cells
HSPC	Hematopoietic stem and progenitor cells
iCasp-8	Caspase-8 inhibitor
Id2	Inhibitor of DNA binding 2
IFN	Interferon
Ig	Immunoglobulin
Inr	Initiator
Int-ILC	Intermediate ILC
ILC	Innate lymphoid cell
ILC2P	Innate lymphoid cell type 2 precursor
ILCP	Innate lymphoid cell precursor

iPI3K	PI3K inhibitor
IS	Immunological synapse
iSTAT5	STAT5 inhibitor
ITIM	Immunoreceptor tyrosine-based inhibition motif
ivILC	*In vitro* innate lymphocytes
JAK	Janus family tyrosine kinase
KACL	Keratinocyte associated C-type lectin
kb	Kilobase
KLR	Killer cell lectin-like receptor
KIR	Killer cell immunoglobulin-like receptors
Lin	Lineage
LLT1	Lectin-like transcript 1
LN	Lymph node
LP	Lamina propria
LRC	Leukocyte receptor complex
LTi	Lymphoid tissue inducer
mAb	Monoclonal antibody
MACS	Magnetic-activated cell sorting
MAF	Minor allele frequency
MMP	Matrix metalloproteinase
MHC	Major histocompatibility class
MICA	MHC class I chain-related protein A
MNC	Mononuclear cells
MTE	Motif ten element
NFIL3	Nuclear factor IL-3 regulated protein
NCR	Natural cytotoxicity receptor
NICD	Notch intracellular domain
NK	Natural killer
NKC	Natural killer gene complex
NKP	Natural killer cell progenitor
NKR	Natural killer cell receptor
NRP1	Neuropilin 1
PAMP	Pathogen-associated molecular pattern
PB	Peripheral blood
PBMC	Peripheral blood mononuclear cells
PDK1	Phosphoinositide-dependent protein kinase 1
PH	Pleckstrin homology
P/I	PMA/Ionomycin
PI3K	Phosphatidylinositol-3 kinase
PIP2	Phosphatidylinositol-4, 5-biphosphate
PIP3	Phosphatidylinositol-3, 4, 5-triphosphate
PMA	Phorbol 12-myristrate 13-acetate
PP	Peyer`s patches
PRR	Pattern recognition receptor
PWM	Position weight matrix
RBPJ	Recombining binding protein suppressor of hairless
rILCP	Restricted innate lymphoid cell precursor
RORγt	Retinoic acid receptor-related orphan receptor gamma-t
SA	Streptavidin
SCF	Stem cell factor
SCID	Severe combined immunodeficiency disease
SFI	Specific fluorescence intensity
SH2	Src-homology domain 2
siLP	Small intestinal lamina propria
SLAM	Signaling lymphocytic activation molecule
SLT	Secondary lymphoid tissue
SN	Supernatant
SNP	Single nucleotide polymorphism
STAT5	Signal transducers and activators of transcription 5

T-bet	T-box transcription factor TBX21
Tcf-1	T cell factor 1
TF	Transcription factor
TFB	Transcription factor binding site
TM	Transmembrane
TRAIL	TNF-related apoptosis-inducing ligand
TLR	Toll like receptor
TSLP	Thymic stromal lymphopoietin
TSS	Transcriptional start site
ULBP	UL-16 binding protein
UTR	Untranslated region
α-LP	Alpha-lymphoid progenitor
γc	Common γ-chain

List of figures

List of tables

Appendix

Table 21: Transcription factors with putative binding sites within the activating region ii of the KLRF2 promoter.
Putative transcription factor (TF) binding sites were determined using the MatInspector software (Cartharius et al., 2005). The KLRF2 promoter sequence was extracted from the Ensembl database release 101 (Yates et al., 2020).

Matrix Family	Detailed Family Information	Matrix	Detailed Matrix Information
V$EVI1	EVI1-myeloid transforming protein	V$EVI1.03	Ecotropic viral integration site 1 encoded factor, amino-terminal zinc finger domain
V$CREB	cAMP-responsive element binding proteins	V$E4BP4.01	E4BP4, bZIP domain, transcriptional repressor
V$DMRT	DM domain-containing transcription factors	V$DMRT7.01	Doublesex and mab-3 related transcription factor 7
V$CDXF	Vertebrate caudal related homeodomain protein	V$CDX2.01	Cdx-2 mammalian caudal related intestinal transcription factor
V$EVI1	EVI1-myeloid transforming protein	V$EVI1.02	Ecotropic viral integration site 1 encoded factor, amino-terminal zinc finger domain
V$ZF10	C2H2 zinc finger transcription factors 10	V$PRDM14.01	PR domain zinc finger protein 14
V$BRNF	Brn POU domain factors	V$BRN2.01	Brn-2, POU-III protein class
V$OCT1	Octamer binding protein	V$OCT1.03	Octamer-binding transcription factor-1, POU class 2 homeobox 1 (POU2F1)
V$SORY	SOX/SRY-sex/testis determining and related HMG box factors	V$SOX12.01	SRY-related HMG-box gene 12
V$HAND	Twist subfamily of class B bHLH transcription factors	V$PARAXIS.01	Paraxis (TCF15), member of the Twist subfamily of Class B bHLH factors, forms heterodimers with E12
V$BRNF	Brn POU domain factors	V$BRN2.03	Brn-2, POU-III protein class
V$ABDB	Abdominal-B type homeodomain transcription factors	V$HOXD10.01	Homeobox D10
V$ABDB	Abdominal-B type homeodomain transcription factors	V$HOXD10.01	Homeobox D10
V$ABDB	Abdominal-B type homeodomain transcription factors	V$HOXC13.01	Homeodomain transcription factor HOXC13
V$FKHD	Fork head domain factors	V$FOXJ1.01	Forkhead box J1
V$BHLH	bHLH transcription factors expressed in muscle, intestine and stomach	V$MESP1_2.01	Mesoderm posterior 1 and 2
V$IRFF	Interferon regulatory factors	V$IRF4.01	Interferon regulatory factor (IRF)-related protein (NF-EM5, PIP, LSIRF, ICSAT)
V$ETSF	Human and murine ETS1 factors	V$PEA3.01	Polyomavirus enhancer A binding protein 3, ETV4 (Ets variant gene 4)
V$SATB	Special AT-rich sequence binding protein	V$SATB1.01	Special AT-rich sequence-binding protein 1, predominantly expressed in thymocytes, binds to matrix attachment regions (MARs)
V$CIZF	CAS interacting zinc finger protein	V$NMP4.01	NMP4 (nuclear matrix protein 4) / CIZ (Cas-interacting zinc finger protein)
O$VTBP	Vertebrate TATA binding protein factor	O$VTATA.01	Cellular and viral TATA box elements
V$FKHD	Forkhead domain factors	V$HNF3B.01	Hepatocyte nuclear factor 3beta (FOXA2)

Table 22: Transcription factors with putative binding sites within the activating region i of the KLRF2 promoter.
Putative transcription factor (TF) binding sites were determined using the MatInspector software (Cartharius et al., 2005). The KLRF2 promoter sequence was extracted from the Ensembl database release 101 (Yates et al., 2020).

Matrix Family	Detailed Family Information	Matrix	Detailed Matrix Information
V$PLZF	C2H2 zinc finger protein PLZF	V$PLZF.01	Promyelocytic leukemia zinc finger (TF with nine Krueppel-like zinc fingers)
V$SF1F	Vertebrate steroidogenic factor	V$SF1.01	SF1 steroidogenic factor 1
V$BCL6	POZ domain zinc finger expressed in B-Cells	V$BCL6.03	B-cell CLL/lymphoma 6, member B (BCL6B)
V$ESRR	Estrogen-related receptors	V$ESRRA.01	Estrogen-related receptor alpha
V$FAST	FAST-1 SMAD interacting proteins	V$FAST1.03	Forkhead box H1 (Foxh1)
V$STAT	Signal transducer and activator of transcription	V$STAT5.01	STAT5: signal transducer and activator of transcription 5
V$STAT	Signal transducer and activator of transcription	V$STAT5B.01	Signal transducer and activator of transcription 5B
V$DMRT	DM domain-containing transcription factors	V$DMRT3.01	Doublesex and mab-3 related transcription factor 3
V$LTSM	Localized tandem sequence motif	V$LTSM.03	LTSM elements with 8 bp spacer
V$SORY	SOX/SRY-sex/testis determining and related HMG box factors	V$SOX21.03	SRY (sex determining region Y)-box 21, dimeric binding sites
V$HNF1	Hepatic Nuclear Factor 1	V$HNF1.01	Hepatic nuclear factor 1
V$GATA	GATA binding factors	V$GATA2.02	GATA-binding factor 2
V$NKX6	NK6 homeobox transcription factors	V$NKX61.01	NK6 homeobox 1
V$PLZF	C2H2 zinc finger protein PLZF	V$PLZF.01	Promyelocytic leukemia zinc finger (TF with nine Krueppel-like zinc fingers)
V$SF1F	Vertebrate steroidogenic factor	V$SF1.01	SF1 steroidogenic factor 1
V$BCL6	POZ domain zinc finger expressed in B-Cells	V$BCL6.03	B-cell CLL/lymphoma 6, member B (BCL6B)
V$ESRR	Estrogen-related receptors	V$ESRRA.01	Estrogen-related receptor alpha
V$FAST	FAST-1 SMAD interacting proteins	V$FAST1.03	Forkhead box H1 (Foxh1)
V$STAT	Signal transducer and activator of transcription	V$STAT5.01	STAT5: signal transducer and activator of transcription 5
V$STAT	Signal transducer and activator of transcription	V$STAT5B.01	Signal transducer and activator of transcription 5B
V$DMRT	DM domain-containing transcription factors	V$DMRT3.01	Doublesex and mab-3 related transcription factor 3
V$LTSM	Localized tandem sequence motif	V$LTSM.03	LTSM elements with 8 bp spacer

Acknowledgements

An dieser Stelle möchte ich mich bei allen bedanken, die mir während meiner Doktorarbeit beigestanden und mich auf unterschiedliche Art und Weise unterstützt haben.

Ich möchte mich zunächst bei Herrn Prof. Dr. Robert Tampé bedanken, der es mir durch seine Betreuung ermöglichte meine Doktorarbeit am Institut für Molekulare Medizin anzufertigen und mich auf diesem Weg in allen Belangen unterstützt hat. Weiterhin danke ich Prof. Dr. Rolf Marschalek für die Begutachtung meiner Arbeit.

Herrn Prof. Dr. Alexander Steinle danke ich für das spannende Forschungsprojekt und die Möglichkeit dieses am Institut für Molekulare Medizin bearbeiten zu können.

Ein besonderer Dank gilt Prof. Dr. Andreas Krueger für die wertvollen fachlichen sowie persönlichen Ratschläge und das Korrekturlesen meiner Doktorarbeit.

Mein Dank gilt weiterhin allen jetzigen und ehemaligen Kollegen der AG Steinle und der AG Krueger, die zum Gelingen meiner Doktorarbeit beigetragen haben. Ich danke euch für den wissenschaftlichen Austausch und den enormen Zusammenhalt.

Insbesondere bedanke ich mich bei Christina für Ihre Unterstützung in allen Laborangelegenheiten und den starken Rückhalt in schwierigen Zeiten. Sebastian danke ich für seine grenzenlose Hilfsbereitschaft und das kritische Lektorat meiner Doktorarbeit. Außerdem danke ich Sarah für die unermüdliche Motivationsarbeit, zahlreiche wissenschaftliche Diskussionen, Ihre Loyalität und das Korrekturlesen meiner Arbeit. Ganz besonders bedanke ich mich bei Björn für die zahlreichen fachlichen aber vor allem persönlichen Ratschläge und für die vielen motivierenden Gespräche. Herzlichst bedanke ich mich außerdem bei Heike, die mich fast auf meinem gesamten Weg begleitet hat für ihr stets offenes Ohr, für Ihre Fürsorge, Unterstützung und Ihre Freundschaft.

Ich danke weiterhin meinen Freunden für die Unterstützung im Verlauf der Doktorarbeit vor allem in Form aufmunternder Gespräche. Zuletzt möchte ich mich bei meinen Eltern und meinen Geschwistern bedanken. Meine Dankbarkeit für die Unterstützung, die ich durch euch erfahren habe, lässt sich nicht in Worte fassen.

Erklärung

Ich erkläre hiermit, dass ich mich bisher keiner Doktorprüfung im Mathematisch-Naturwissenschaftlichen Bereich unterzogen habe.

Frankfurt am Main, den _____ _____

(Ines Kühnel)

Versicherung

Ich erkläre hiermit an Eides statt, dass ich die vorgelegte Dissertation mit dem Titel „Function and expression of the human immunoreceptor NKp65 on innate lymphocytes" selbstständig angefertigt und mich keiner anderen Hilfsmittel als der in ihr angegebenen bedient habe, insbesondere, dass alle Entlehnungen aus anderen Schriften mit Angabe der betreffenden Schrift gekennzeichnet sind.

Ich versichere, die Grundsätze der guten wissenschaftlichen Praxis beachtet, und nicht die Hilfe einer kommerziellen Promotionsvermittlung in Anspruch genommen zu haben.

Frankfurt am Main, den _____ _____

(Ines Kühnel)